Deterministic hydrological, hydraulic and hydrogeological modeling for real-time decision support systems : application to the Paillons catchment, France

Paguedame Game

To cite this version:

Paguedame Game. Deterministic hydrological, hydraulic and hydrogeological modeling for real-time decision support systems : application to the Paillons catchment, France. Civil Engineering. Université Côte d'Azur, 2023. English. NNT : 2023COAZ4117 . tel-04433795v2

HAL Id: tel-04433795

https://hal.univ-cotedazur.fr/tel-04433795v2

Submitted on 8 Feb 2024

HAL is a multi-disciplinary open access archive for the deposit and dissemination of scientific research documents, whether they are published or not. The documents may come from teaching and research institutions in France or abroad, or from public or private research centers.

L'archive ouverte pluridisciplinaire **HAL**, est destinée au dépôt et à la diffusion de documents scientifiques de niveau recherche, publiés ou non, émanant des établissements d'enseignement et de recherche français ou étrangers, des laboratoires publics ou privés.

UNIVERSITÉ
CÔTE D'AZUR

ÉCOLE DOCTORALE
SCIENCES
FONDAMENTALES
ET APPLIQUÉES

THÈSE DE DOCTORAT

Modélisation hydrologique, hydraulique et hydrogéologique déterministes pour les systèmes d'aide à la décision en temps réel

Application au bassin versant des Paillons, France

Paguédame Ibrahim GAME
Polytech'Lab UPR UCA 7498, Université Côte d'Azur, France

Présentée en vue de l'obtention du grade de docteur en Science de l'Ingénieur **d'**Université Côte d'Azur
Dirigée par: Philippe Audra

Soutenance le: 4 décembre 2023

Devant le jury, composé de:
Philippe Gourbesville, Prof., UCA - Nice
Olivier Fouché-Grobla, Asst. Prof., Le CNAM, Paris
Philippe Audra, Prof., UCA - Nice
Yang Josh Tsun-Hua, Assoc. Prof., NYCU, Hsinchu

POLYTECH NICE-SOPHIA
POLYTECH'LAB

MÉTROPOLE
NICE CÔTE D'AZUR

MÉTROPOLE
NICE CÔTE D'AZUR
eau et assainissement

Modélisation hydrologique, hydraulique et hydrogéologique déterministes pour les systèmes d'aide à la décision en temps réel

Application au bassin versant des Paillons, France

Jury:

Rapporteurs
Olivier Fouché-Grobla, Asst. Professeur, Le Conservatoire National des Arts et Métiers (CNAM) - Paris
Yang Josh Tsun-Hua, Associate Professor, National Yang Ming Chiao Tung University - Hsinchu

Examinateurs
Philippe Gourbesville, Professeur, Polyecth'Lab – Université Côte d'Azur - Nice
Philippe Audra, Professeur, Polyecth'Lab – Université Côte d'Azur -Nice

Acknowledgments

Several years ago, I nurtured a dream of embarking on a journey of exploration and knowledge acquisition through higher education. This journey has taken me across countries, from Togo to the United States, then to the United Kingdom, and finally to France. Having initially grounded my academic pursuits in the fields of Physics and Chemistry, I aspired to specialize in environmental engineering. Thanks to unwavering determination and the unwavering support of my mentors, colleagues, friends, and family spanning various nations, I successfully realized my aspirations.

The pivotal moment arrived in 2018 when I enrolled in the Euroaquae Master's program in hydro-informatics in Europe. This marked a turning point in my academic journey. Following my graduation from Euroaquae, I seized the opportunity to participate in this PhD project within the AquaVar framework, under the guidance of Prof. Philippe Gourbesville and Prof. Philippe Audra. Reflecting on the past three years, I am profoundly thankful to my mentors and all those who contributed to my journey toward this significant achievement.

I extend my special gratitude to Dr. Masoud Ghulami for his invaluable assistance during the early stages of this research project. His contributions were instrumental in shaping the initial versions of the models, and his experience with the AquaVar project greatly enhanced my understanding of the Var's modeling system. My heartfelt thanks also go to Asst. Prof. Olivier Fouché, who played a vital role as a member of the thesis committee, enriching the study.

Throughout my PhD journey, I had the privilege of collaborating with local experts and managers who shared insights to enhance the quality of my project. Their support facilitated data collection and access to reports from Nice Metropolis water services. I extend my sincere appreciation to all who contributed to the development of AquaPaillons, including Félix Billaud, Guillaume Masselis, Pierre Roux, Jessica Fragni, Nathalie Le Nouveau, and their colleagues from the former Eau d'Azur and Nice metropolis.

Most of the modeling work was made possible through the generosity of the Danish Hydraulic Institute (DHI), who provided essential software tools and license dongles. The French Meteorological service, Météo-France, contributed significantly by providing real-time weather information for research purposes.

I am deeply grateful to my colleagues and partners within the laboratory, as well as the staff of Polytech Nice and the University Côte d'Azur, who provided both technical assistance and a supportive work environment. Their guidance and expertise were invaluable. I extend my thanks to colleagues such as Mingyan Wang, Hao-Ming Hsu, Dr. Lian Guey Ler, Charlene Monaco and Hezouwe Amaou Tallé, whose personal and professional qualities made our collaborative work environment positive and productive.

Lastly, I would like to express my heartfelt gratitude to my family, both here and abroad, particularly my girlfriend and stepdaughter, who remained steadfast in their support, even during the sleepless nights and packed weekends devoted to advancing this research project.

Abstract

In the southeastern region of France, floods and droughts affect the mountainous catchments including the Paillons and the Var on the east and west of Nice city, France. The Var valley is one of the main freshwater resource of the Nice metropolis (or Metropole Nice Côte d'Azur (MNCA)). The Paillons river is covered and crosses the dense urban centre. On the French Riviera, as in many Mediterranean coastal cities, urbanization and economic development are on the rise and can be deeply affected during extreme convective events such as the Alex storm recorded in October 2020 or the major flood of 2019. On top of that, demand for water resources is increasing.

This situation motivated the development of the AquaVar decision support system since 2014. Four main needs were to be met: represent the hydrological characteristics of the Var, be useful for predicting the impacts of future construction projects on the river and groundwater hydraulics, implement long-term scenarios for climate changes impacts, forecast the impacts of extreme hydrological events and consider pollutant leakage into the river or unconfined aquifer. To achieve those goals, three deterministic models were implemented. A hydrological model based on the DHI MIKE SHE was calibrated to represent complex hydrogeological processes in the entire catchment. Using observed or estimated discharges from the hydrological model, a hydraulic model was designed with the DHI MIKE 21FM to simulate surface flow and river-aquifer exchange in the lower Var valley. And the flow in the unconfined aquifer located in the lower Var valley was modeled with Feflow to accurately represent river-aquifer exchange. This tool successfully coupled hydrological, hydraulic and groundwater modules to optimize management of collected data and provide useful information for real-time management of water hazards and resources. To this date, the system has been used in several technical applications related to groundwater resources and extreme floods management in the Var catchment. However, other parts of the MNCA including the Paillons facing similar issues are not covered. Hence, the tool can be extended to the Paillons to address the risk of urban flooding and fill the gap in knowledge of the dynamics of the unconfined aquifer.

In this study, the surface and subsurface flow processes in the Paillons catchment are assessed with three deterministic models to meet the specific needs in the Paillons catchment. MIKE SHE represents the hydrological processes of the whole catchment. MIKEPlus's overland and river network modules model the surface flow processes and Feflow captures the groundwater dynamics. A modeling strategy was designed to achieve the assessment in 6-mn, hourly and daily time intervals. For MIKEPlus, the model is calibrated and validated with events selected in 2017 and 2019. Available video records were used to provide alternative real-time quantification of flood events. MIKE SHE was calibrated in 2011-2014 and validated in 2016-2020. Subsequently Artificial neural network (ANN) was applied to optimize MIKE SHE outputs. Feflow was assessed by varying the empiric parameters and using recharge and water depths from MIKE SHE simulations in 2009-2013 without any observed long-term data. To optimize the growth in video monitoring records, an image-based method is tested with Fudaa-LSPIV to estimate discharge and suggest the approach to be included in real-time management of floods in the Paillons.

The three deterministic models are the main parts of the AquaPaillons DSS. The study could confirm the application of AquaVar architecture and modeling process to the Paillons. Moreover, the AquaPaillons adds new quantification methods to the existing AquaVar architecture applied to the Paillons. Therefore, The tools could be used to reproduce flow events in real-time and forecast extreme events.

Key words: AquaPaillons project, AquaVar DSS, deterministic hydrological, hydraulic and groundwater models, Paillons catchment, MIKE SHE, MIKEPlus, Feflow, Fudaa-LSPIV, ANN.

Résumé

Dans la région sud-est de la France, les inondations et les sécheresses affectent les bassins versants montagneux, notamment les Paillons et le Var à l'est et à l'ouest de la ville de Nice, en France. La vallée du Var est l'une des principales ressources en eau douce de la métropole niçoise (ou Métropole Nice Côte d'Azur (MNCA)). La rivière des Paillons est couverte et traverse le dense centre urbain. Sur la Côte d'Azur, comme dans de nombreuses villes côtières méditerranéennes, l'urbanisation et le développement économique sont en hausse et peuvent être profondément affectés lors d'événements convectifs extrêmes tels que la tempête Alex enregistrée en octobre 2020 ou les inondations de 2019. De plus, la demande de ressources en eau augmente.

Cette situation a motivé le développement du système d'aide à la décision AquaVar depuis 2014. Quatre besoins principaux devaient être satisfaits: représenter les caractéristiques hydrologiques du Var, être utile pour prédire les impacts des futurs projets de construction sur l'hydraulique fluviale et souterraine, mettre en œuvre à long terme des scénarios d'impacts des changements climatiques, prévoir les impacts des événements hydrologiques extrêmes et envisager les fuites de polluants dans la rivière ou l'aquifère libre. Pour atteindre ces objectifs, trois modèles déterministes ont été mis en œuvre. Un modèle hydrologique basé sur le DHI MIKE SHE a été calibré pour représenter les processus hydrogéologiques complexes dans l'ensemble du bassin versant. À partir des débits observés ou estimés du modèle hydrologique, un modèle hydraulique a été conçu avec le DHI MIKE 21FM pour simuler les écoulements de surface et les échanges rivière-aquifère dans la basse vallée du Var. Et l'écoulement dans l'aquifère libre situé dans la basse vallée du Var a été modélisé avec Feflow pour représenter avec précision les échanges rivière-aquifère. L'outil AquaVar a couplé avec succès des modules hydrologiques, hydrauliques et hydrogéologique pour optimiser la gestion des données collectées et fournir des informations utiles pour la gestion en temps réel des risques et des ressources en eau. À ce jour, le système a été utilisé dans plusieurs applications techniques liées aux ressources en eaux souterraines et à la gestion des crues extrêmes dans le bassin versant du Var. Cependant, d'autres parties du MNCA, y compris les Paillons confrontés à des problèmes similaires, ne sont pas couvertes. Ainsi, l'outil peut être étendu aux Paillons pour répondre au risque d'inondation urbaine et combler le manque de connaissance de la dynamique de l'aquifère libre.

Dans cette étude, les processus d'écoulement de surface et souterrain dans le bassin versant des Paillons sont évalués avec trois modèles déterministes pour répondre aux besoins spécifiques du bassin versant. MIKE SHE représente les processus hydrologiques de l'ensemble du bassin versant. Les modules de réseau terrestre et fluvial de MIKEPlus modélisent les processus d'écoulement de surface et Feflow capture la dynamique des eaux souterraines. Une stratégie de modélisation a été conçue pour réaliser l'évaluation dans des intervalles de temps 6-mn, horaires et quotidiens. Pour MIKEPlus, le modèle est calibré et validé avec des événements sélectionnés en 2017 et 2019. Les enregistrements vidéo disponibles ont été utilisés pour fournir une quantification alternative en temps réel des événements d'inondation. MIKE SHE a été calibré en 2011-2016 et validé en 2016-2020. Un réseau de neurone artificiel (ANN) a été utilisé pour optimiser les résultats issus de MIKE SHE. Feflow a été évalué en faisant varier les paramètres empiriques et en utilisant la recharge et le niveau d'eau dans le cours d'eau calculés avec MIKE SHE entre 2009 et 2013 sans possibilité de comparaison effective avec des données observées sur le long terme. Afin d'optimiser la croissance des enregistrements de suivi vidéo des crues, une méthode basée sur l'image est testée avec Fudaa-LSPIV pour estimer le débit et proposer l'intégration de l'approche dans la gestion en temps réel des crues des Paillons.

Les trois modèles déterministes sont les pièces maîtresses du système AquaPaillons. L'étude pourrait confirmer l'application de l'architecture et du processus de modélisation AquaVar aux Paillons. En plus, AquaPaillons ajoute de nouvelles méthodes de quantification à l'architecture AquaVar existante appliquée aux Paillons. Finalement, les outils pourraient être utilisés pour reproduire les événements de débit en temps réel et prévoir les événements extrêmes.

Mots clés: Projet AquaPaillons, AquaVar DSS, modèles hydrologiques, hydrauliques et souterrains distribués déterministes, bassin versant des Paillons, MIKE SHE, MIKEPlus, Feflow, Fudaa-LSPIV, ANN.

Contents

Abbreviations

1D: one-dimensional

2D: two-dimensional

3D: three-dimensional

ANN: Artificial Neural Network

CR: Covered River

DEM: Digital Elevation Model

DSS: Decision Support Systems

DTM: Digital Terrain Model

HD: Hydrodynamic

LPR: Lower Paillons River

LSPIV: Large Scale Particle Image Velocimetry

MNCA: Métropole Nice Côte d’Azur

OR: Open River

PACA: Provence Alpes Côte d’Azur

PAPI: Programmes d’Actions de Préventions des Inondations

PPRI: Plan de Prévention des Risques Naturels d’Inondation

PGRI: Plan National de Gestion du Risque Inondation

SDAGE: Schéma Directeur d’Aménagement et de Gestion des Eaux

List of tables

List of figures

General Introduction

Study Background

In the southeastern region of France, floods and droughts affect the mountainous catchments including the Paillons and the Var on the east and west of Nice city, France. The Var valley is one of the main freshwater resource of the Nice metropolis (or Metropole Nice Côte d'Azur (MNCA)). The Paillons river is covered and crosses the dense urban centre. On the French Riviera, as in many Mediterranean coastal cities, urbanization and economic development are on the rise and can be deeply affected during extreme convective events such as the Alex storm recorded in October 2020 or the major flood of 2019. On top of that, demand for water resources is increasing (Abily et al., 2015; Chochon et al., 2022; Gourbesville & Ghulami, 2022; Salvan, 2017; Salvan et al., 2016; Wacheux, 2022). Therefore, the region needs an integrated modeling approach that provides reliable information to protect its people, functions, and assets.

This situation motivated the development of the AquaVar decision support system since 2014 (Du et al., 2016, 2018a; Gourbesville et al., 2018; Ma, Gourbesville, et al., 2020; Zavattero, 2019). Four main needs had to be met: represent the hydrological characteristics of the Var, be useful for predicting the impacts of future construction projects on the river and groundwater hydraulics, implement long-term scenarios for climate changes impacts, forecast the impacts of extreme hydrological events and consider pollutant leakage into the river or unconfined aquifer. To achieve those goals, three deterministic models were implemented. A hydrological model based on the DHI MIKE SHE was calibrated to represent complex hydrogeological processes in the entire catchment. Using observed or estimated discharges from the hydrological model, a hydraulic model was designed with the DHI MIKE 21FM to simulate surface flow and river-aquifer exchange in the lower Var valley. And the flow in the unconfined aquifer located in the lower Var valley was modeled with Feflow to accurately represent river-aquifer exchange. This tool successfully coupled hydrological, hydraulic and groundwater modules to optimize management of collected data and provide useful information for real-time management of water hazards and resources (Gourbesville et al., 2022). To this date, the system has been used in several technical applications related to groundwater resources and extreme floods management in the Var catchment (Ma & Gourbesville, 2020). However, other parts of the MNCA including the Paillons facing similar issues are not covered. Hence, the tool can be extended to the Paillons to address the risk of urban flooding and fill the gap in knowledge of the dynamics of the unconfined aquifer.

This research project aims to achieve two objectives. The first objective is to explore the requirements to extend AquaVar DSS to AquaPaillons. In fact, the Paillons has specific features that require additional components into the DSS. After reviewing the AquaVar DSS, the Paillons could include video monitoring information along with the modeling framework. The second objective is to use a new modeling strategy to improve knowledge of the global water cycle of the Paillons catchment.

AquaPaillons Project

To develop a similar tool for the Paillons catchment, the local water authority, MNCA Eau & Assainissement, started this research project. The main issue with the Paillons is flooding. In 2000, 2014, and 2019 major flood events caused damages to infrastructures in the Lower Paillons River (LPR) and its valley. Existing monitoring systems are used to manage water-related issues, but gaps and errors in collected information are present. The unconfined aquifer is used by some neighborhoods for drinking and by a few industries. Its dynamics are not well known due to lack of monitoring information (Tennevin et al., 2017).

Unlike the Var river, the LPR is partially covered. Within the riverbed, two retention storages exist. On the left bank, an underground road can be flooded and reduce flood risk in urban Nice. In fact, in urbanized areas where space is limited, covered river and underground roads are used to create more space on the surface for urban development, on one hand. On the other hand, they are useful for flood reduction and making urban spaces safer. The steep tributaries of the river and densely urbanized floodplains present a challenge for runoff water management. Approximately 16 km^2 area is channeled into the urban drainage network. Sediment deposition is a significant problem for the LPR, while erosion is prevalent in its steep tributaries. The riverbed channelization further exacerbates these issues. The region's geological layers partly consist of limestone, which provide irrigation and industry with groundwater (Le Gouz de Saint Seine, 1995; Tennevin et al., 2017). Extreme events from September to February are common. Every year, the river is dredged to reduce flood risk and to replenish the nearby beach which is exposed to winter coastal erosion. Consequently, a flexible model that can integrate frequent and localized changes in the riverbed geometry will be an efficient tool for real-time flood modeling.

Therefore, the AquaPaillons modeling tool should be able to:

- represent the real hydrological, hydraulic, and hydrogeological characteristics of the Paillons;
- forecast the impacts of extreme meteorological events in the catchment;
- be used for forecasting the effects of future developments on groundwater hydraulics and river;
- implement long-term scenario simulation to investigate the reaction of catchment to climate changes;
- consider pollutant transport in the river to cover the situation of the intrusion of sea water leakage of pollutants into the river or unconfined aquifer.

Accounting for the needs of the Paillons, this study identified 3 deterministic distributed models:

- A hydrological model will reproduce the complex processes in the catchment including rainfall-runoff, infiltration and evapotranspiration, alluvial groundwater dynamics and producing the upstream boundaries for the flood model and recharge and river water levels for the groundwater model;
- A flood model will be built with a focus on the LPR to simulate the surface flow movement in open and closed channels;
- A groundwater model will be constructed to simulate the flow in the unconfined alluvial aquifer and the coupling with the river hydraulic model will provide more accurate and detailed representation of the exchanges between the river and the aquifer in the Paillons.

Moreover, to optimize the growth in video records, an image-based estimation of river discharge will be tested on one hand. On the other hand, the outputs from MIKE SHE will be optimized using ANN to absorb uncertainties in inputs and catchment description that deterministic models cannot cover.

Objectives of the research

Previous studies (Archambaud & Berthet, 2021; Le Gouz de Saint Seine, 1995; Pline, 1991; SIP et al., 2016; Tennevin et al., 2017) assessed the hydrogeological processes or their impacts of the Paillons catchment and suggest further investigation. A flood warning system has existed since 1987, but gaps and errors pose a serious challenge. Modeling based on upstream observations is limited to when upstream observations are available. Video monitoring is not used to provide another mean of quantification of flood and records are limited in time. A complex hydraulic environment lies downstream: covered river, floodable underground tunnel, dense urban area. The unconfined aquifer is used by some neighborhoods for drinking and by a few industries. Its dynamics are not well known due to lack of or sparse monitoring information. Therefore, a new modeling strategy centered on deterministic modeling will provide the needed information to fill the gaps and improve knowledge of the global water cycle in the Paillons.

The research question focuses on how to model complex runoff processes and groundwater flow for real-time decision support system in the context of water hazards and resources management. A particular emphasis is given to strategies for long-term simulations for model evaluation.

The specific research's objectives are to:

- Collect and analyze all the information related to the hydrological, hydraulic, and hydrogeological characteristics of the Paillons in order to improve the knowledge of the global water cycle;
- Develop a numerical modeling system to represent the runoff and groundwater flow dynamics of the Paillons in the long-term and for extreme events;

- Based on the needs in the Paillons, the simulation should be handled with 3 different time intervals (6-mn, hourly and daily). The calibrated model will have the ability to forecast future scenarios in 6-mn, hourly and daily scale or to produce the realistic boundary conditions for the other components of the DSS focused on the inundation areas;
- Evaluate an optimization of outputs of the hydrological model with ANN;
- Test an image-based estimation of discharge from video records;
- Evaluate scenarios of groundwater extractions.

Thesis structure

According to the research's objectives, this work is divided into 5 consecutive chapters related to specific subjects explained above. The thesis begins with the discussion about AquaVar DSS and the strategy to extend it to the Paillons. The next chapter is more focused on describing the characteristics of the Paillons and analyzing the collected information. In the third chapter, the different models are built, and data requirement and interpolation methods are presented. The fourth chapter explores results and uncertainty analysis of surface hydraulics and image-based modeling. After that the results and uncertainty analysis of rainfall-runoff and groundwater flow modeling are discussed in the fifth chapter. Finally, the last section relates to the conclusion and future prospects, where the achievements of this research are summarized and recommendations for integrating the Paillons in the AquaVar DSS are presented.

The reader should be aware of the fact that parts of the research papers published by the author (Game et al., 2022, 2023a, 2023b) before submitting this thesis report were integrated into these chapters with little or no modifications.

Chapter I. Strategy of integrating AquaPaillons into AquaVar Decision Support System

Introduction

Decision Support Systems (DSS) are define by researchers as human-computer systems tailored to use information from various sources and provide alternative solutions to improve decision making in different contexts (Ma, Gourbesville, et al., 2020; Yazdani et al., 2017; Zavattero, 2019; Zhai et al., 2020). The systems are supposed to process information coming in different formats and to deal with simple and complex problems. In the water sector, stakeholders face numerous challenges ranging from providing water resources for a growing population worldwide and mitigate extremes meteorological events in vulnerable inhabited areas. In addition, protecting the natural environment has become a pressing issue in the context of climate change and the depletion of Earth's resources by humankind. Since the 1950s, DSSs concepts and tools have been developing thanks to the progress in computer technologies. Applications of the systems have emerged in water management sectors like irrigation, flood, urban drainage, water supply, etc.

In the southeastern region of France, floods and droughts affect the mountainous catchments including the Paillons and the Var to the east and west of Nice city (Figure 1). The Lower Var Valley is one of the main freshwater resource of the Nice metropolis (or Metropole Nice Côte d'Azur (MNCA)). The Paillons river is covered and crosses the dense urban centre. On the French Riviera, as in many Mediterranean coastal cities, urbanization and economic development are on the rise and can be deeply affected during extreme convective events such as the Alex storm recorded in October 2020 or the major flood of 2019. On top of that, demand for water resources is increasing (Du et al., 2019; Gourbesville & Ghulami, 2022; Ma et al., 2016; Ma, Gourbesville, et al., 2020; Salvan et al., 2016; Wacheux, 2022). Therefore, the region needs an integrated modeling approach that provides reliable information to protect its people, functions, and assets.

The AquaVar DSS tool has been developed since 2014 through 3 thesis research projects and several applications. This tool successfully optimized management of collected data and provided useful information for real-time management of water hazards and resources. However, other parts of the Nice metropolis including the Paillons facing similar issues are not covered. Hence, the tool can be extended to the Paillons to address the risk of urban flooding and fill the gap in knowledge of the dynamics of the unconfined aquifer. The extension to the Paillons will require addressing specific needs of the Paillons such modeling the covered river, the underground tunnel and considering a groundwater model without upstream boundary conditions. This chapter first reviewed the architecture of the AquaVar DSS is reviewed and then addressed the challenges and solutions of integrating the Paillons.

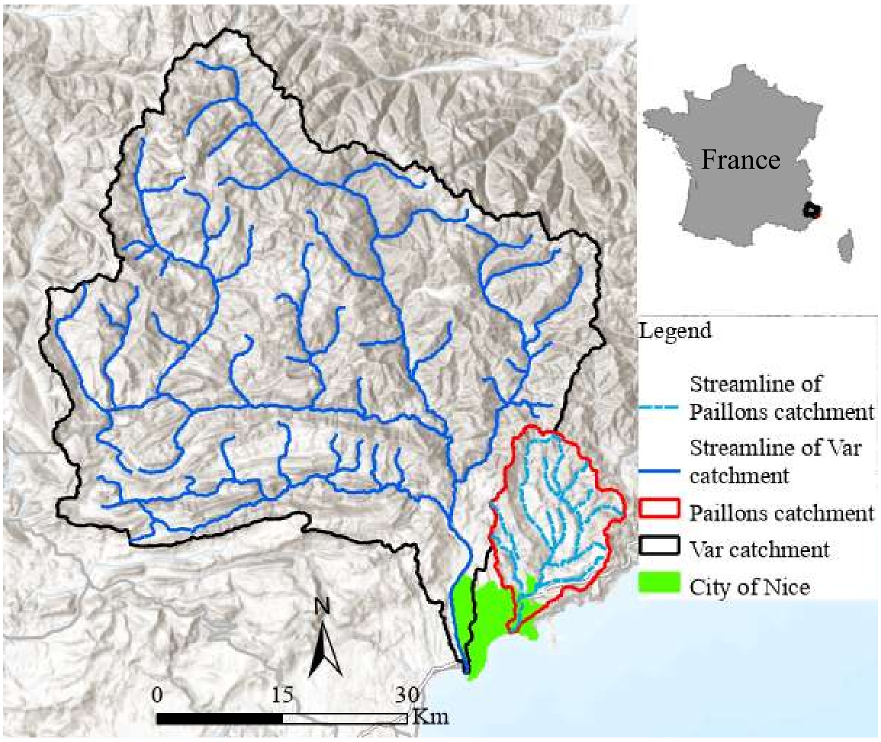

Figure 1 Locations of Var and Paillons catchments and their outlets in the city of Nice at the Mediterranean Sea.

1.1. Review of DSS systems and surface runoff/groundwater flow modeling tools

Decision support systems (DSS) for water resources and hazard management include tools and methods aimed at assisting decision-makers in dealing with complex challenges related to water resources and hazard management. From the literature on Google Scholar and Web of Science, these systems can be broadly categorized into several classes based on their functionalities and applications. Table 1 presents some of the methods and tools of DSSs for water resources and hazard management. The systems focus mostly on monitoring, modeling and data analysis for water quality, quantity, and hazard management. The choice of a specific DSS class depends on the nature of the water problem, the available information, and the objectives of the stakeholders. To provide comprehensive solutions for water resources and hazard management, many modern DSS may orchestrate multiple classes (Gourbesville et al., 2016; Wardropper & Brookfield, 2022; Zavattero, 2019). Indeed, this study targets an integrated system for hydrological processes in real-time.

Table 1 DSS methods and tools for water cycle challenges.

Water cycle challenges	Methods	Tools
• Flood , • Drought, • Quality, • Quantity, • Allocation, • Distribution, etc.	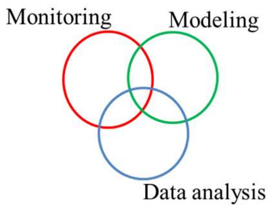 ➡ toward integrated methods	• Observation stations, • Surface water models, • Groundwater models, • Sewer models • Water distribution models ➡ toward integrated tools

In integrated hydrological DSS, hydrological models are essential tools for simulating and understanding the movement and distribution of water in catchments. These models are used for a range of purposes, including flood forecasting, water resource management, and environmental impact assessments (Abbott et al., 1986; Butts et al., 2004; Doummar et al., 2012; Downer & Ogden, 2004; Frana, 2012; Sun et al., 2023). Table 2 summarizes the different types of hydrological models published in the literature based on parameters, variables, data, features and processes.

Table 2 Different types of hydrological models (adapted from Devia et al., 2015).

Items	Model types	Modeling methods
Data-features-processes	Empirical	Uses observations and derived mathematical relations from inputs
	Conceptual	Uses simplified abstractions of the physical processes
	Physically-Based	Uses the fundamental physical laws governing water movement
Input-Output	Deterministic	Outputs depend on inputs
	Stochastic	Includes a degree of randomness in outputs
Space	Lumped	Applies spatially average characteristics
	Distributed	Divides a watershed into multiple grid cells or sub-basins Compute processes at each cell
Time	Static	Produces outputs for specific time periods
	Dynamic	Produces continuous outputs

A review of model utilities and application potentials in watershed management decision making over the past 40 years, by Sun et al.(2023), found 47 modeling tools linked to “Forest Hydrology Models”, “Distributed Hydrological Models”, and “Forest Watershed Decision Support Systems”. According to the author, Forest hydrology models represents models that are applicable to forests conditions whereas Forest watershed DSS focuses on DSS for catchments with large portions of forests (Figure 2). The models have been constantly evolving since the 1960s and many other tools can be found in different countries.

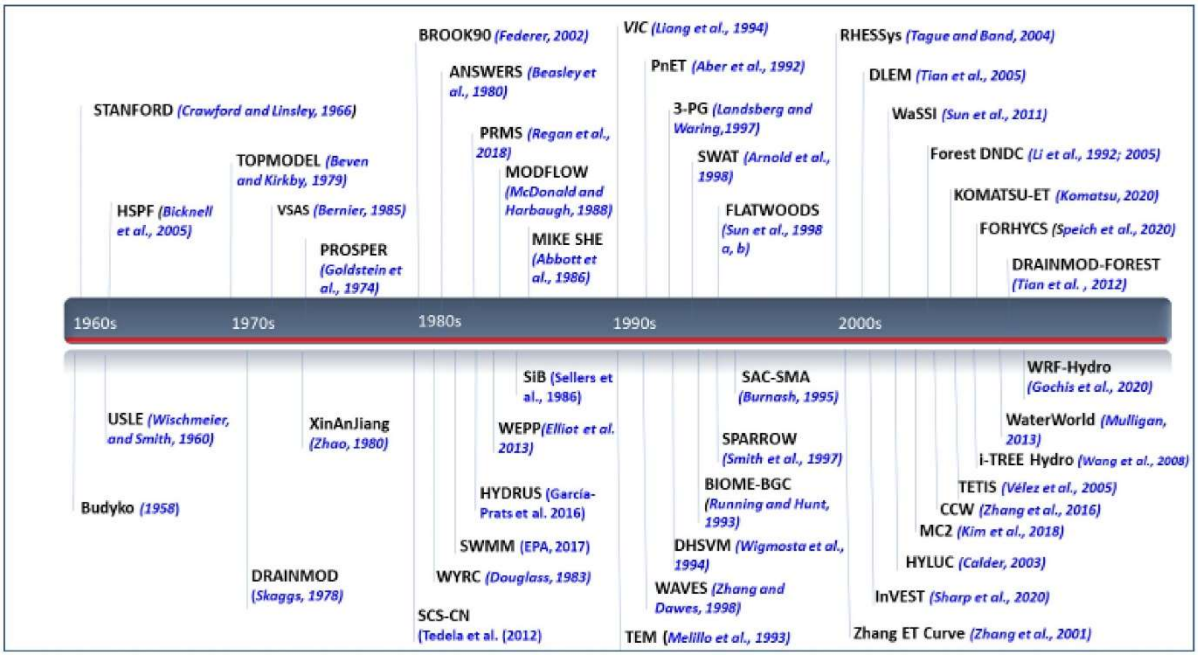

Figure 2 Examples of development of tools used in hydrological modeling since 1960s (Sun et al., 2023).

The models can also be classified as either deterministic or stochastic. The first are easier to derive simpler to use with output depending on inputs. The latter integrates a certain degree of randomness. However, deterministic models do not deal with all the uncertainties especially on long-term simulations. Fortunately joint stochastic-deterministic models can reduce uncertainties in hydrological modeling (Stojković et al., 2017).

The most widely used deterministic runoff model structures are the lumped models, such as the Soil Conservation Service (SCS) model, and the distributed models, such as the MIKE SHE. Lumped models are simpler and more computationally efficient, but they do not account for spatial variability in the catchment (Coron et al., 2017). Distributed models, on the other hand, are more complex and computationally expensive, but they can account for spatial variability in the catchment, making them more appropriate for larger or more complex watersheds (Khakbaz et al., 2012).

Calibration and validation of deterministic runoff models are essential steps to ensure that the model can accurately simulate the hydrological response of a catchment. The calibration techniques include trial and error method, the optimization of model parameters using optimization algorithms such as the non-linear least squares method, the Markov chain Monte Carlo, the artificial neural network (ANN) method, and the genetic algorithm (GA) method (Khakbaz et al., 2012; Liong et al., 2000; Shivhare et al., 2018). The validation techniques include comparing model predictions with observed data using statistical measures such as the Nash-Sutcliffe efficiency coefficient and the coefficient of determination (R-squared) (Ma, 2018; Zavattero, 2019).

1.2. Var catchment in context

Ma et al.(2020) synthetized the context, architecture, and applications of the AquaVar DSS. With a drainage area of 2800 km^2, the Var catchment is the largest catchment at the French Riviera. It has steep slopes mostly in the middle and upper sub-catchments. The elevation varies significantly from 0 m to 3100 m. The Var rises from spring at the Cavolle pass in the Maritime Alps and flows about 122 km to its outlet into the Mediterranean Sea between the cities of Saint-Laurent-du-Var and Nice. It is composed of 3 main tributaries, namely Tinée, Vésubie and Estéron. The geometry of 90% of the river is a result of natural erosion wearing away rocks and carving a network of valleys into a typical “V” shape cross-sections (Figure 3). The Var watershed is dominated by a typical Mediterranean climate with wet winters and dry summers. Annually, the catchment receives 815 mm of rain within 65 to 80 days. Apart from rainfall, snowmelt and flow from aquifers contribute to surface runoff in the Var. In spring, rainfall and snow melting generate the floods. In winter, floods are caused by extreme precipitations covering large portions of the catchment. The average annual discharge and the highest observed peak discharge over the period of 1985 – 2014 are 50 m^3/s and 3750 m^3/s (flood 1994) at Napoléon III Bridge near the outlet. An important groundwater resource is present in the downstream part of the Var, called the Lower Var Valley where the river runs on the last 22 km to the sea. In this valley, there are interactions between shallow aquifers, the rivers, and the underlying conglomerate bedrock. The unconfined alluvial aquifers constitute one of the main freshwater resource of the Nice metropolis. About 50 M m^3/year are extracted at public pumping stations (Ma, Gourbesville, et al., 2020).

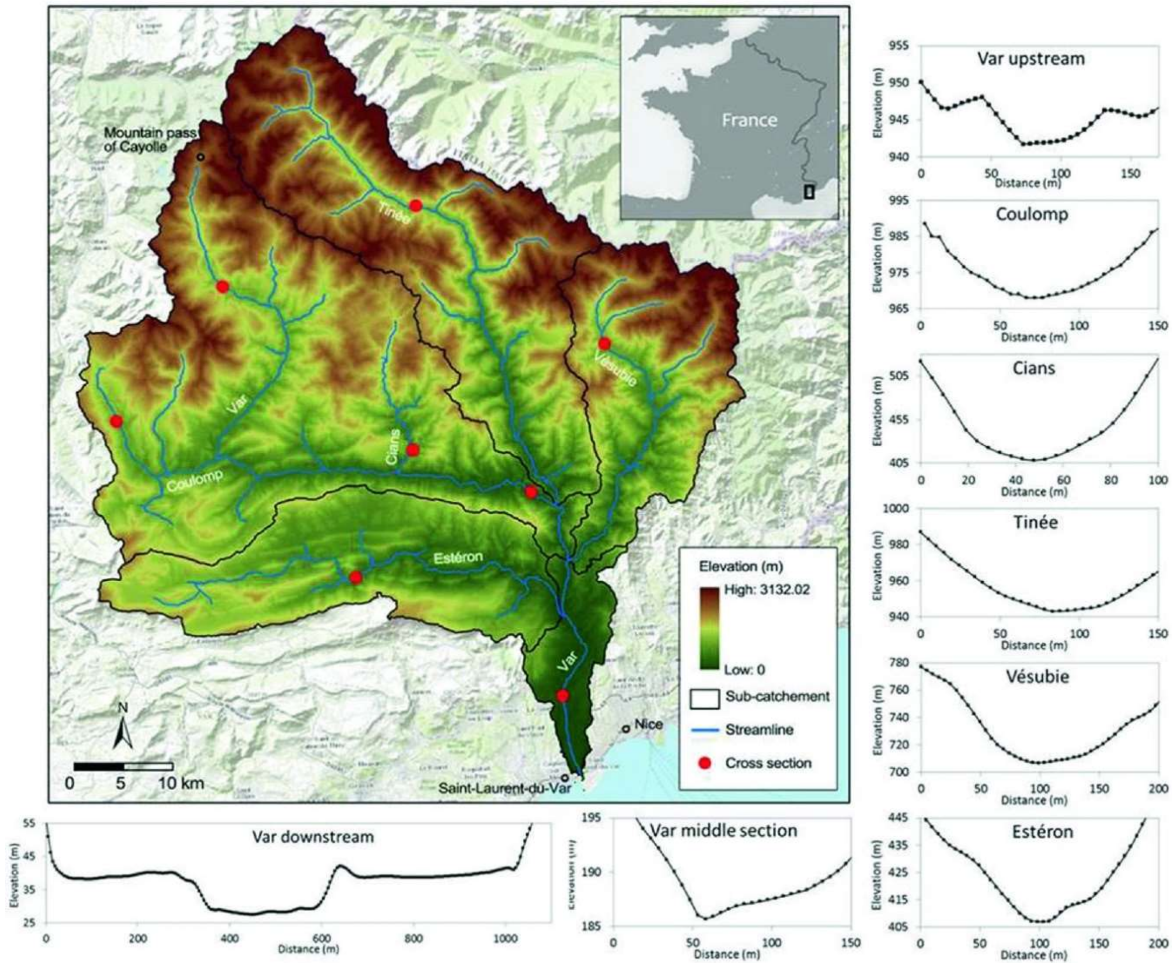

Figure 3 Var catchment at French Mediterranean region (Ma, Gourbesville, et al., 2020). Note the width scale differs for the different cross-sections.

Urbanization and economic development have been growing since the beginning of XIXth Century, in the Lower Var Valley (Gourbesville et al., 2022; Ma, Gourbesville, et al., 2020; Zavattero, 2019). The river floodplain has steadily shifted from its natural state to more artificialization. Urban expansions come with growing population and economic activities which require an increased extraction of groundwater. Artificialization resulted in reducing river embankments width from 600-1000 m to 150 – 280 m. When river cross-sections are reduced flow velocities increase. Rising velocities in a river exacerbate riverbed erosion and consequently the fall of the groundwater table. This situation makes pumping activities challenging. In 1967, the groundwater table fell below 8 m of its static level. That was the most serious shortage ever recorded sparking more attention to the reduction of riverbed erosions as the first effective measure to stabilize the groundwater table in the Lower Var Valley. In 1980s, the proposed solutions to reduce erosion and raise groundwater table consisted in the construction of 11 weirs at different locations. Presently, the upstream part of the Lower Var Valley is mostly industrial and agricultural. The downstream part is urbanized, and few pumping stations are located at the outflow (Figure 4).

As reported by Ma et al.(2020), to properly deal with the above mentioned challenges related to management of quantity and quality of the groundwater, local water authorities need a DSS tool which reliably represents underground physical processes. Another challenge faced by urban areas in the valley is flood hazard. The existing flood protection levees can hold flood of up to 75 years of return period. Considering the morphodynamic of the Var river and the abundant sediment deposition in some areas, the real capacity of the river is less than the designed capacity at many sections. Indeed, the management systems should also address flood processes to protect people and assets in the Lower Var Valley. Therefore, a DSS is a reasonable solution for nowcast and forecast of water information required for efficient decision making.

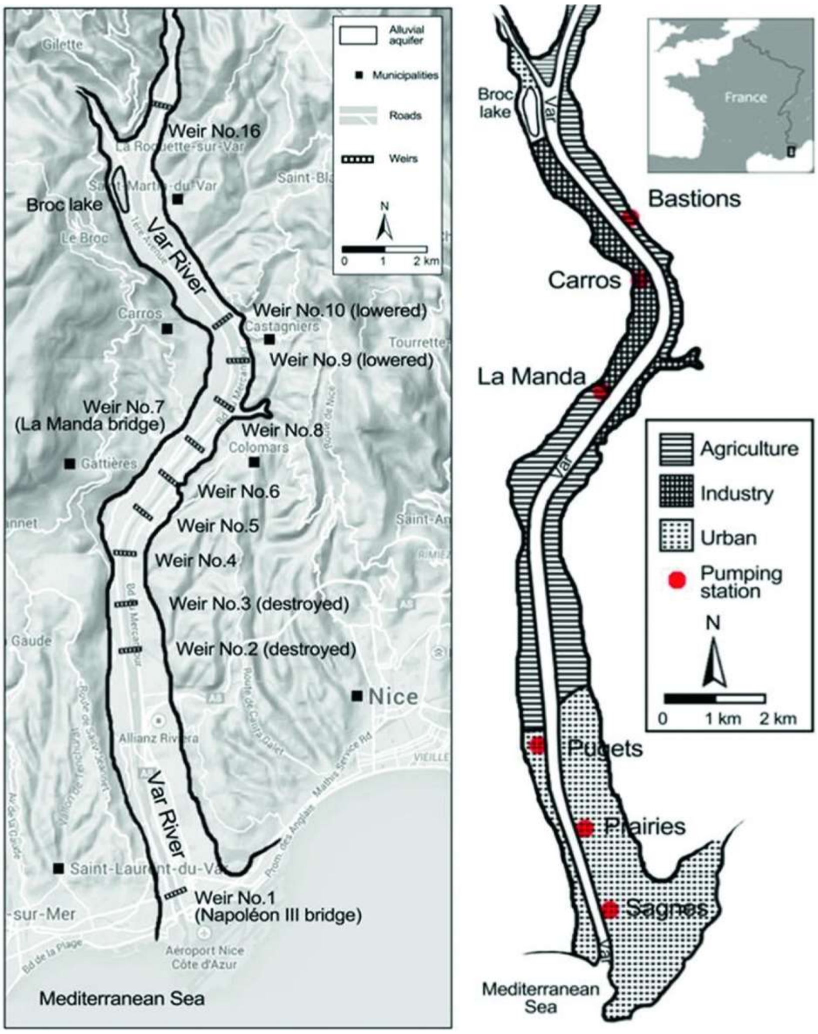

Figure 4 Artificial structures and economic activities in lower Var valley (Ma, Gourbesville, et al., 2020)

1.3. Aquavar DSS tool

The aim of the AquaVar project was to develop a DSS tool in the Var catchment with a focus on the Lower Var valley (Gourbesville et al., 2016; Ma et al., 2020; Gourbesville et al., 2022; Ma & Gourbesville, 2020; Zavattero, 2019; Du et al., 2018b). This tool handles global water cycle challenges such as drought, flood, pollution, and the impact of infrastructures. On one hand, it integrates three numerical models developed with the DHI software and coupled like in Figure 5 to provide forecast: MIKE SHE, MIKE 21FM and Feflow models. On the other hand, it is based on field data measurement network 78 stations for precipitation, 78 stations for temperature , at least 3 stations for water level in the river, 21 stations for groundwater level in the alluvial aquifer (and 5 stations in the conglomerate aquifer), and 1 station at Nice harbor for sea level (Zavattero, 2019).

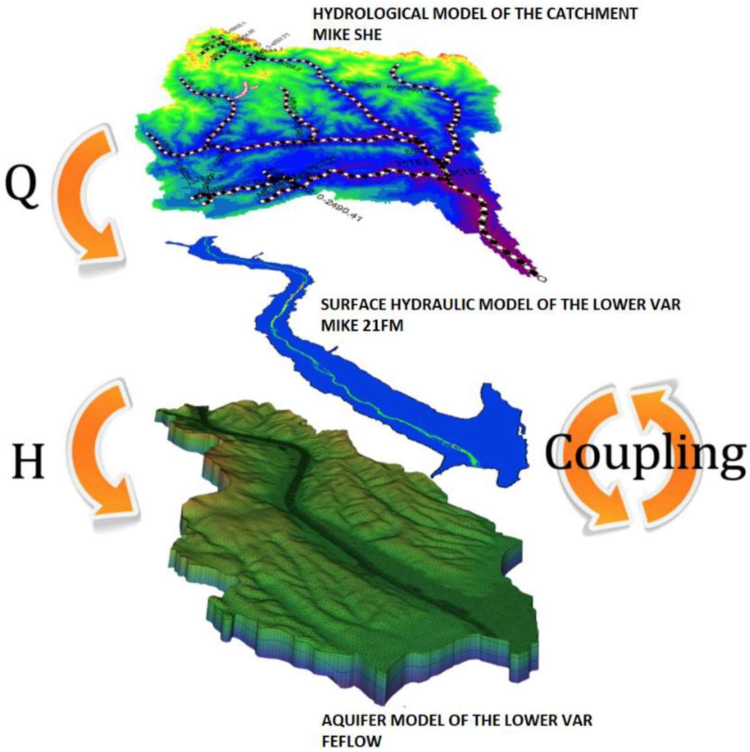

Figure 5 Coupling principle hydrological, hydraulic and groundwater models in the Lower Var River valley (Zavattero, 2019)

The numerical model starts with using MIKE SHE to compute runoff from precipitation over the whole Var catchment. Data required include topography, land-use, precipitation, evapotranspiration, temperature, and snow melting. Next, MIKE 21FM uses discharge provided by MIKE SHE as boundary conditions to reproduce surface hydraulics along the 22 km river stretch. Finally, Feflow calculates groundwater level and flow velocity in the unconfined aquifer. Additional information like physical data and groundwater extractions are needed.

A web platform (Figure 6) of the AquaVar DSS (Figure 7) is expected to represent the present and future of the water cycle in the Lower Var Valley. Measurements data and simulations of extreme events based on weather forecasts are the main display on the platform. Moreover, results of simulated scenarios should be available and additional scenarios can be simulated by the user. Possible scenarios are related to extreme hydrological events, accidental pollutions, morphological changes, river-aquifer exchange, etc. A database is required to store all data used to create the numerical models.

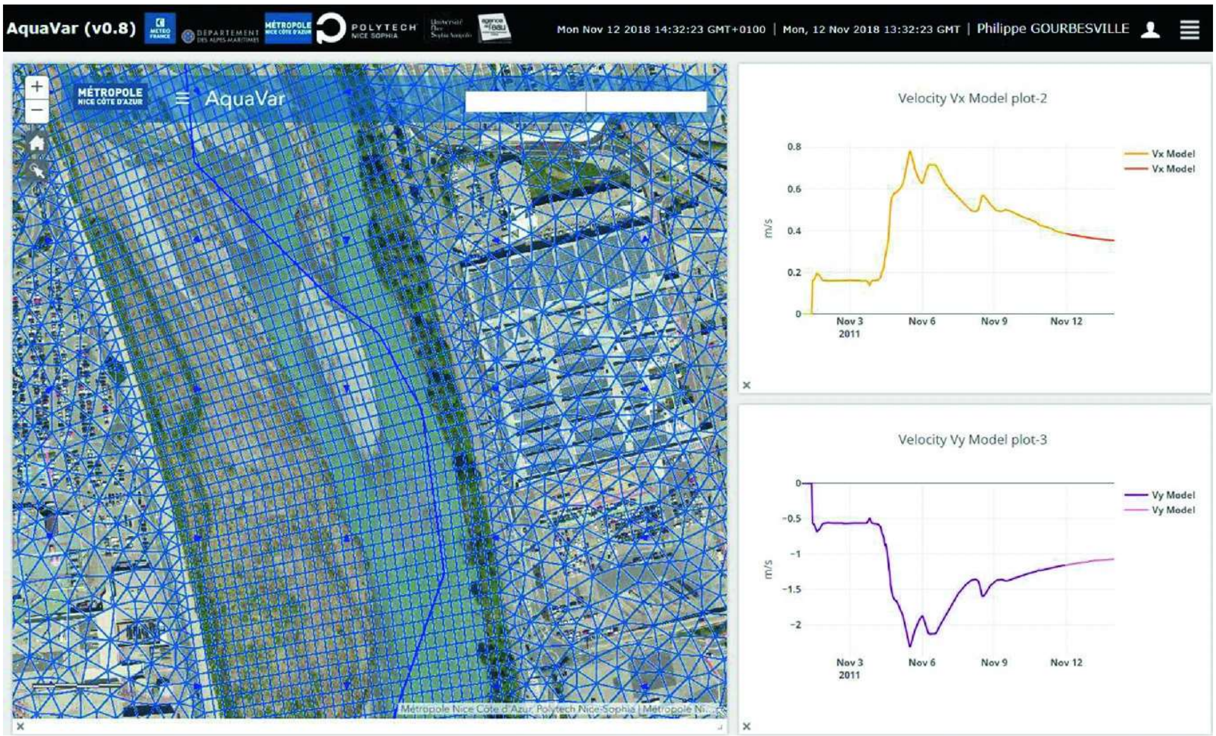

Figure 6 Example of AquaVar web interface (Ma, Gourbesville, et al., 2020)

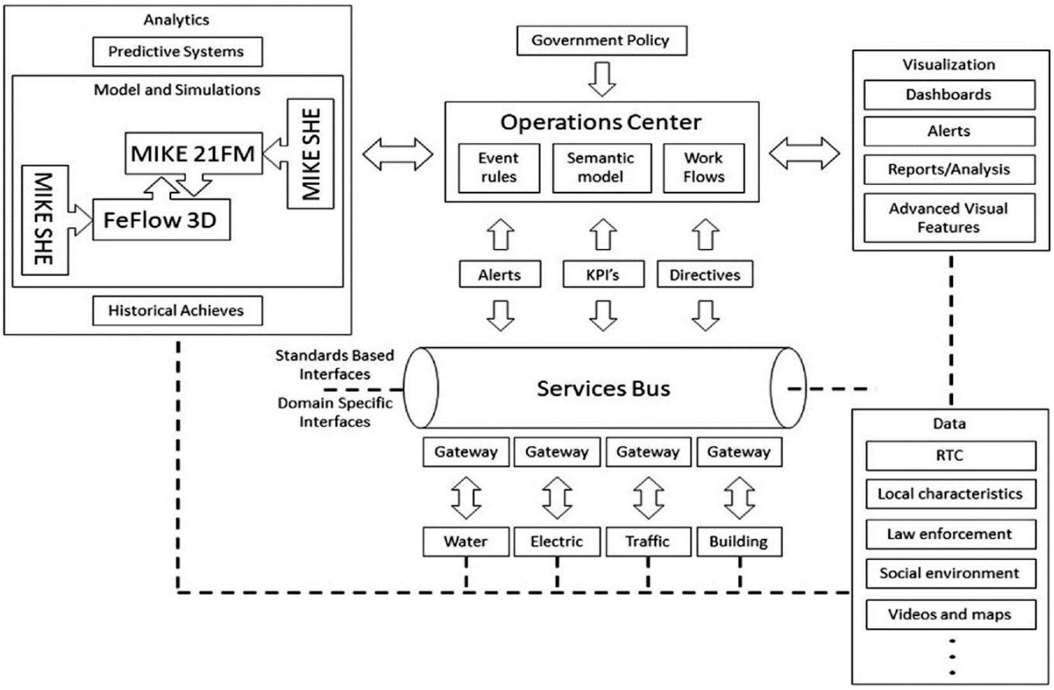

Figure 7 Designed architecture of AquaVar DSS (Ma, Gourbesville, et al., 2020)

The architecture is constituted of five main parts: Analytics for model and simulations, Operation Center for workflows and event rules, Visualization for dashboards and alerts, and Data for information storage. Numerous basic tools such as predefined alerts, Key Performance Indicators (KPIs) and directives are used to formalize data and transfer them among different parts in the service bus dedicated to the AquaVar DSS platform (Ma & Gourbesville, 2020).

The modeling system provides reliable representation of most of major hydrological and hydrogeological characteristics at any places in the catchment, and further supports the applications of surface hydraulics and groundwater flow simulations. The models have been applied to the period 2008 to 2014 (Figure 8 & Figure 9). The serious flood of November 2011 and the drought of summer 2012 were accurately reproduced. Of the 24 piezometers with automatic recorder for monitoring daily groundwater table, 6 piezometers have been applied for model validation (Figure 10). The results prove that the modeling system can characterize the dynamics of the groundwater movement by accounting for direct water recharge, exchange between river and aquifer exchange and groundwater extraction (Ma, Gourbesville, et al., 2020).

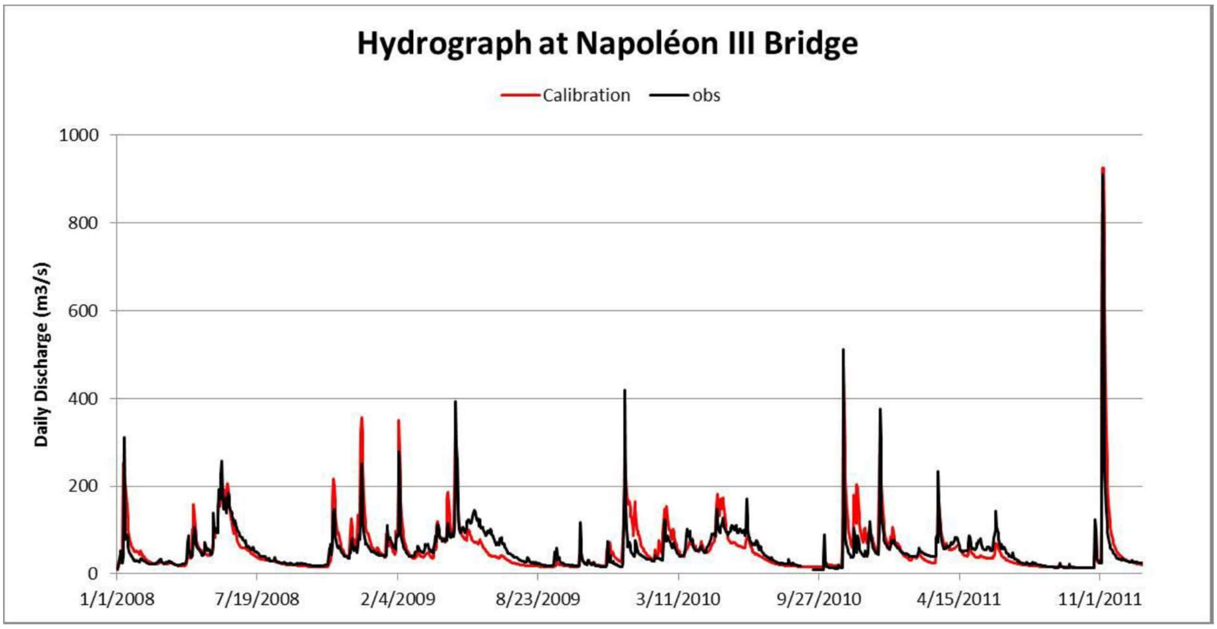

Figure 8 Comparison between daily calibration and observation discharges at Napoléon III Bridge (Ma, 2018).

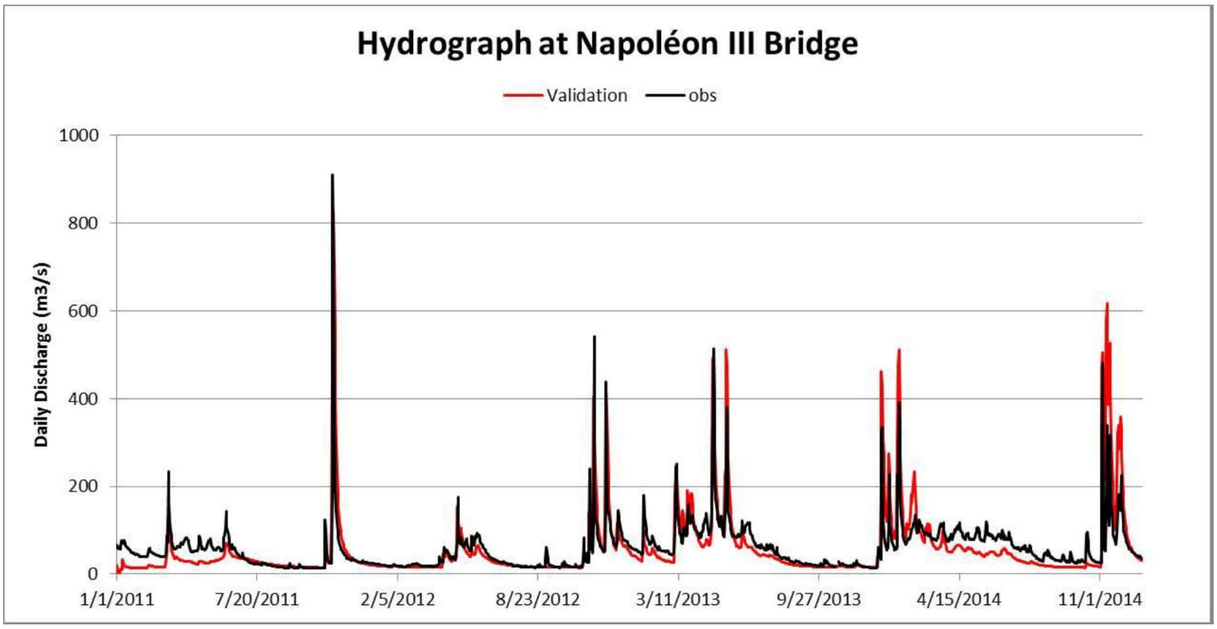

Figure 9 Comparison between daily validation and observation discharges at Napoléon III Bridge (Ma, 2018).

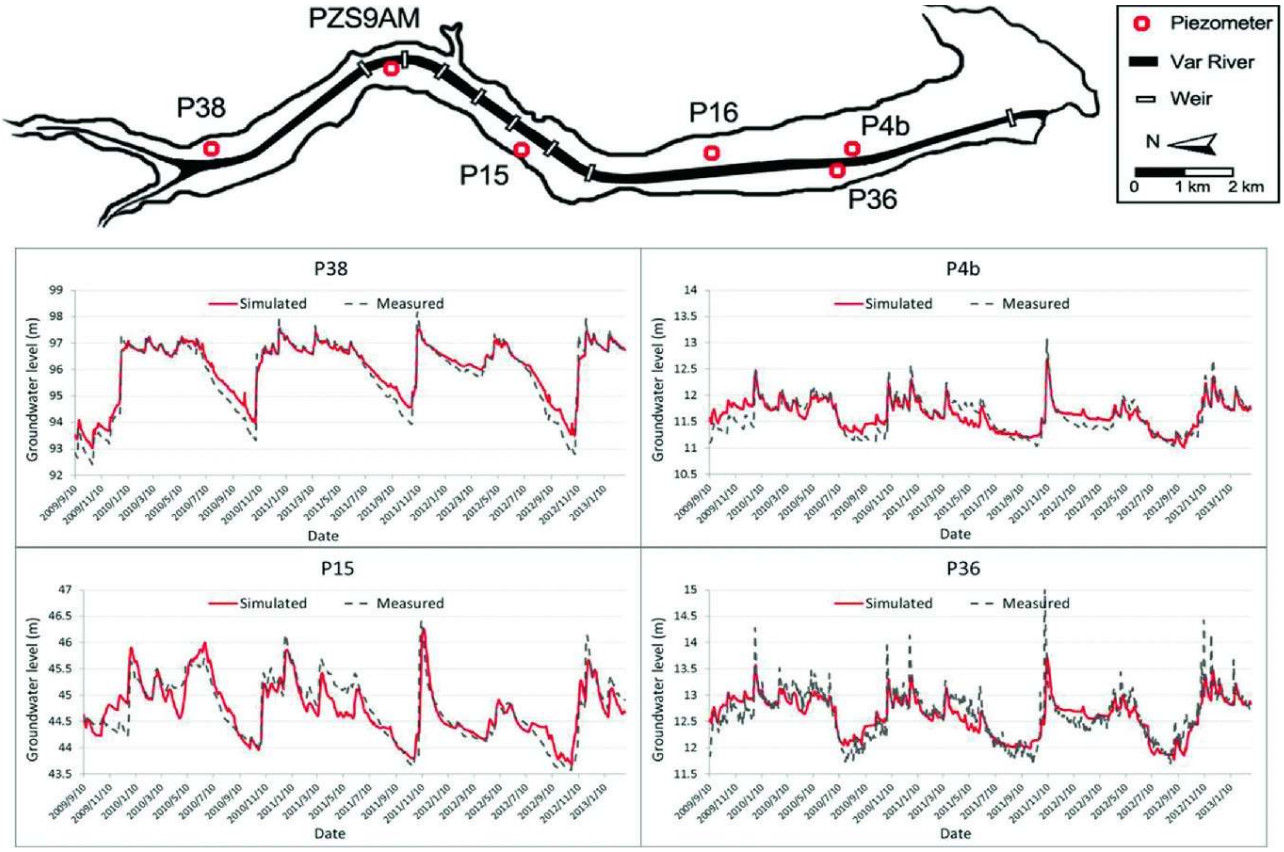

Figure 10 Modeling of groundwater table level using Feflow application in lower Var valley (Ma, Gourbesville, et al., 2020).

1.4. Description of the AquaVar modeling tools

The local government in the Lower Var Valley requests both real-time information of current processes and of the possibility to assess a future situation through modeling simulations. Continuous data collection is used to update the models in the AquaVar DSS. In order to provide sufficient information to well represent the physical processes at any locations in the catchment, three deterministic distributed models have been applied in the analytic system: MIKE SHE, MIKE 21FM and Feflow.

1.4.1. Hydrological model: MIKE SHE

1.4.1.1. MIKE SHE backgrounds

The creation of MIKE SHE was the result of collaborative efforts among three European water agencies: the British Institute of Hydrology in the UK, the Danish Hydraulic Institute (DHI) in Denmark, and SOGREAH in France. This collaboration was made possible under the financial support from the European Commission (Abbott et al., 1986). In fact, during the 1970s in Europe, a new generation of hydrological models emerged with the primary goal of providing more scientific information to optimize water resources management. These models aimed to estimate the impacts of increasing social activities, such as urbanization, changes in land-use, and infrastructural developments, on the natural environment. The key innovation in these new models was their physical distributed structure. In response to the demand for such advanced models, the Europe Hydrological System, also known as Système Hydrologique Européen (SHE), was developed. It was built to meet the specific requirements set by water resources managers. Interestingly, SHE successfully simulated hydrological processes in Europe and became the foundation for many subsequent deterministic hydrological models including SHETRAN, SHESED and MIKE SHE (Ewen et al., 2000).

The SHE model, proposed by Freeze and Harlan in 1969 (Abbott et al., 1986), was constructed based on a blueprint that divided the runoff process into various sub-processes, each individually simulated using corresponding equations. These deterministic formulas allowed for accurate representation of catchment physical processes (Freeze & Harlan, 1969). The Institute of Hydrology, UK, focused on simulating snow melting, interception during rainfall, and evapotranspiration. SOGREAH, France, handled both overland flow (surface water movement) and channel flow (stream water movement) in the model. Additionally, DHI was responsible for simulating soil water flow through unsaturated and saturated zones within the catchment (Abbott et al., 1986).

Following a series of validation tests to assess model quality, the first version of SHE became operational in 1982. Over time, DHI continued to develop and expand the SHE models, resulting in the creation of MIKE SHE. As of late, the MIKE SHE model has earned recognition as a high-performance system for accurately representing the water cycle in catchments. Moreover, it offers a comprehensive suite of pre- and post-processing tools, as well as a flexible combination of advanced and simplified solution techniques for various hydrological processes. The MIKE SHE simulation adeptly captures evapotranspiration, rainfall-runoff, overland flow, and soil flow (both unsaturated and saturated). The representation of these processes can vary in terms of spatial distribution and complexity, depending on the modeling objectives, available field measurements, and the decisions made by the modeler (Butts et al., 2004; Graham & Butts, 2005). One notable advantage of MIKE SHE over other hydrological software is its user-friendly interface, which allows users to intuitively construct the model description based on their previous modeling studies, such as the conceptual model of the watershed. Input data required for setting up MIKE SHE model can be specified in various formats, independent of the model domain and grid, including common GIS formats. During the simulation runtime, spatial data is mapped with numerical grids, facilitating changes in spatial discretization (Graham & Butts, 2005).

1.4.1.2. MIKE SHE architecture

As discussed by Ma (2018), deterministic distributed hydrological applications often face significant challenges in terms of data requirements and execution time, limiting their applicability. One effective approach to mitigate these issues involves simplifying the hydrological processes in the model simulation, which reduces the model's complexity and data needs. However, it is crucial for hydrological modelers to carefully assess and discuss the potential impacts on result accuracy when representing only the main processes in the model simulation. Ma (2018) suggested that the modeling approach used to represent catchment behavior should offer flexibility, allowing modelers to choose suitable simulation methods. This flexibility should not be restricted solely to fully deterministic approaches but should also include elements of stochastic methods.

The MIKE SHE model exemplifies this approach by integrating various simulation techniques to represent different natural processes. This integration provides modelers with the opportunity to optimize each component's function, particularly when applying the model to represent the hydrology system in large river basins or catchments with intricate hydrogeological conditions. The modeling structure of MIKE SHE primarily comprises eight main functions: "Rain and Snow", "Evapotranspiration", "Snow Melt", "Overland Flow", "Channel Flow", "Unsaturated Zone Flow", "Groundwater Flow" and "Sewer Flow", all aimed at effectively representing multiple hydrological processes within a catchment (Figure 11).

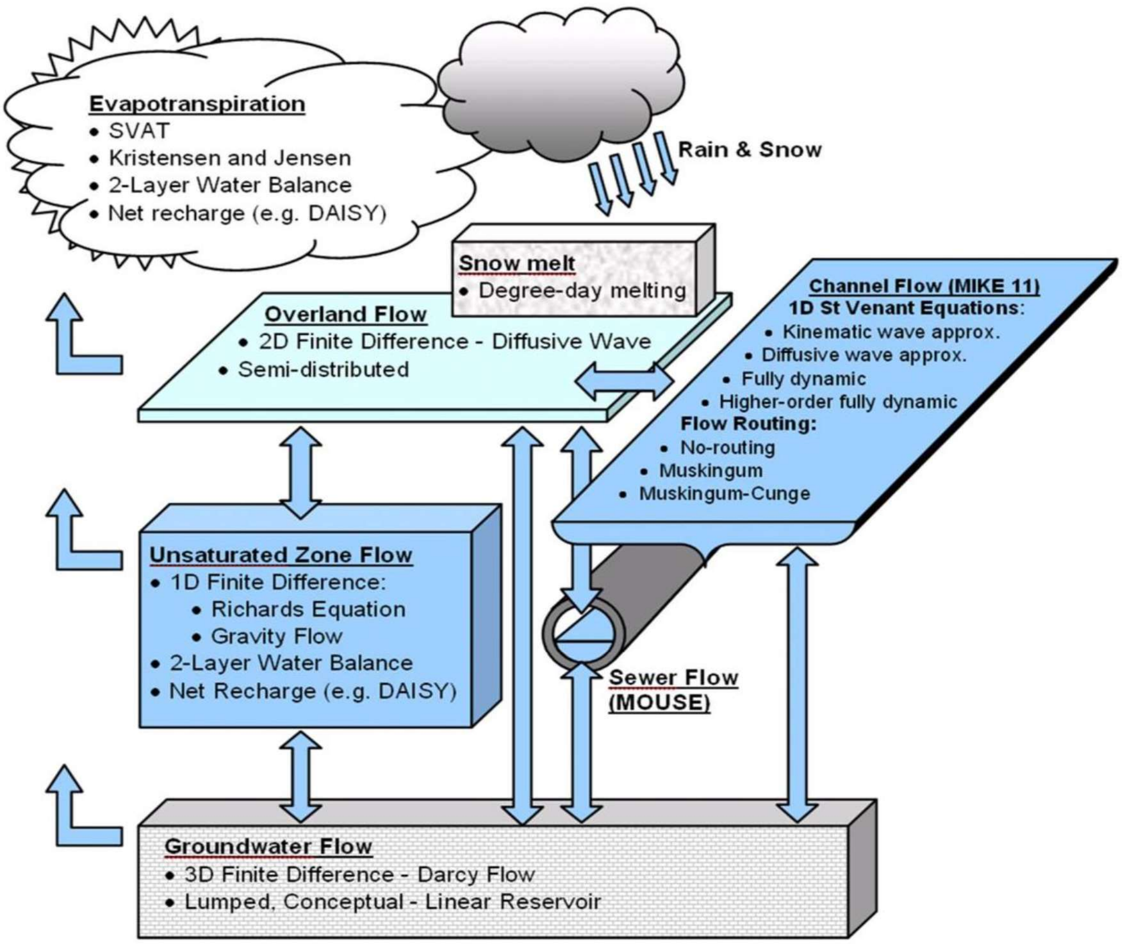

Figure 11 Representation of the processes in the MIKE SHE model (DHI, 2023d).

Rain and snow

Precipitation or rainfall is crucial factors in hydrological systems, serving as the starting point and primary inputs for hydrological processes, particularly in representing rainfall-runoff relationships. The accuracy of rainfall data significantly impacts simulation results (Ma, 2018). MIKE SHE offers three different formats to represent precipitation spatially: uniform, station based, and fully distributed. Depending on data availability and modeling objectives, precipitation rates can be described as constant value or as time series in the MIKE SHE Model.

The uniform rainfall method assumes a homogeneous rainfall situation in the study area at a specific simulation time. It is well suited for small catchment or where surveys data is limited. On the other hand, the station based method, which is appropriate for medium or large catchment with higher density of rain gauges, divides the catchment into several sub-catchments based on available gauging stations, and assumes uniform rainfall for each sub-catchment. Defining the area of sub-catchments can be done using various methods, with the Thiessen Polygons method being one of the most used.

The third method of rainfall representation in MIKE SHE, considered the most realistic, is the Fully Distributed approach. This method aims to describe the meteorological conditions of the catchment in a more accurate manner, leading to significant improvements in simulation results. However, applying this rainfall input is challenging as rainfall measurements in the catchment are often limited to a few locations. Therefore, this rainfall input is usually obtained through various interpolation methods. Moreover, MIKE SHE provides a tool called Precipitation Lapse Rate to correct rainfall variations based on elevation.

Evapotranspiration

In the MIKE SHE model, the computation of evapotranspiration incorporates both meteorological and vegetation data to assess the overall evapotranspiration and net rainfall. This estimation relies on several factors, including canopy interception from rainfall, canopy surface evaporation, soil surface evaporation, water uptake by plants, and plant transpiration. During the simulation, MIKE SHE offers three primary functions for calculating the actual evapotranspiration (AET):

- Soil Vegetation Atmosphere Transfer (SVAT)

The SVAT function is formulated with the underlying assumption of a two-layer system (soil and canopy) interconnected through a resistance network (Shuttleworth & Wallace, 1985). This function incorporates a solitary, partially transparent canopy layer positioned over the soil layer and computes the actual evapotranspiration (AET) solely based on standard meteorological and vegetation data. Importantly, it should be emphasized that this process is independent of Reference Evapotranspiration (Graham & Butts, 2005).

- Kristensen and Jensen Method

The primary ET model used in MIKE SHE is the Kristensen and Jensen Method, which is based on equations derived empirically by Kristensen & Jensen (1975), at the Royal Veterinary and Agricultural University (KVL), in the Kingdom of Denmark. This model employs specific equations to determine the relationship between Leaf Area Index (LAI), Root Depth, Reference Evapotranspiration, and Soil Moisture Status. Notably, the model assumes that precipitation does not occur as snow due to considering temperatures above 0°C.

To implement this function in MIKE SHE, it is required to have time series of root depth, LAI, Reference ET and other empirical parameters. Reference ET represents the value of evapotranspiration from a reference surface with an limitless water supply (Sekulić et al., 2017). It is mainly influenced by climate and can be calculated using meteorological data. If direct ET information is not available from gauging stations, it is recommended to use the FAO Penman-Monteith method to estimate the Reference ET value.

ET from Snow

$$\boldsymbol{ET_{snow}} = \boldsymbol{ET_{wetsnow}} + \boldsymbol{ET_{drysnow}} \qquad \text{Eq. 1}$$

With

$$\boldsymbol{ET_{wetsnow}} = \boldsymbol{ET_{ref}} * \Delta\boldsymbol{t}$$
$$\boldsymbol{ET_{drysnow}} = \boldsymbol{ET_{ref}} * \boldsymbol{Sf} * \Delta\boldsymbol{t}$$

where ET_{snow} (L) is the evapotranspiration from the snow cover area. The computation involves two distinct steps: initially, if there is wet snow storage present, the ET will draw water from it. The availability of water in wet snow storage is determined based on the Reference Evapotranspiration ET_{ref} (LT^{-1}). If the wet snow storage is insufficient or absent in the study area, the ET will derive water from the dry snow storage instead. This dependency on dry snow storage considers both the Reference Evapotranspiration ($ETref$) and the sublimation reduction factor (Sf) as defined in the Snow Melt function in MIKE SHE. If, at the time of calculation, there is an insufficient amount of snow storage, $ETsnow$ will be limited and reduce the snow storage to zero.

Evaporation from Canopy

$$\boldsymbol{E_{can}} = \mathbf{min}\,(\boldsymbol{I_{max}}, \boldsymbol{ET_{ref}} * \Delta\boldsymbol{t}) \qquad \text{Eq. 2}$$

with

$$\boldsymbol{I_{max}} = \boldsymbol{C_{int}} * \boldsymbol{LAI}$$

where E_{can} *(*LT^{-1}*), the canopy evaporation, is computed by comparing* I_{max} *(L) , the interception storage capacity, and amount of* ETr_{ef} *during the calculation time interval* Δt*.* C_{int} *(L) interception coefficient and LAI (-) are required to get value of* I_{max} *in the model simulation.*

Plant Transpiration

$$\boldsymbol{ET_{at} = f_1(LAI) * f_2(\theta) * RDF * ET_{ref}} \qquad \text{Eq. 3}$$

with

$$\boldsymbol{f_1(LAI) = C_2 + C_1 * LAI}$$

$$\boldsymbol{f_2(LAI) = 1 - \left(\frac{\theta_{FC} - \theta}{\theta_{FC} - \theta_W}\right)^{\frac{C_3}{E_p}}}$$

where ET_{at} *(*LT^{-1}*) represents transpiration from vegetation computed with 2 functions that account for the impacts of soil moisture content and LAI. The RDF (-) represents root distribution. Empirical parameters* C_1*,* C_2*, and* C_3 *are applied in the computation.* θ_{FC} *(-) is the volumetric moisture content at field capacity. And* θ_W*(-) is the volumetric moisture content at wilting point. The parameter of* θ *(-) is the actual volumetric moisture content at the simulation time step.*

Soil Evaporation

$$\boldsymbol{E_s = ET_{ref} * f_3(\theta) + [ET_{ref} - E_{at} - ET_{ref} * f_3(\theta)] * f_4(\theta) * [1 - f_1(LAI)]} \qquad \text{Eq. 4}$$

where soil evaporation E_S *(*LT^{-1}*) calculated from the upper part of the unsaturated zone corresponding to a basic amount of evaporation* $ET_{ref}f_3(\theta)$ *plus surplus evaporation from the excess soil water when soil saturation reaches field capacity.*

Furthermore, the extraction of evapotranspiration from the saturated zone occurs exclusively when vegetation roots come into contact with the water table (DHI, 2023d). Additionally, in order to incorporate the Kristensen and Jensen method into the MIKE SHE simulation, it is necessary to apply the Richards equation and gravity flow methods during the Unsaturated Zone Flow calculation (Graham & Butts, 2005).

- Two Layer Water Balance Method

In the MIKE SHE model, a simplified approach called the Two Layer Water Balance Method is introduced to streamline the simulation of the transpiration process in unsaturated flow. This method, proposed based on a formulation by Yan & Smith (1994), divides the unsaturated zone into two sections and facilitates the computation of actual evapotranspiration and the amount of water recharging the saturated zone (DHI, 2023d).

The computation of actual evapotranspiration using the Two Layer Water Balance Method is akin to the Kristensen and Jensen Method. It explicitly calculates from different storages within the MIKE SHE model:

$$\boldsymbol{ET_{actual} = ET_{snow} + ET_{canopy} + ET_{ponded} + ET_{UZ} + ET_{SZ}} \qquad \text{Eq. 5}$$

where ET_{actual} *(*LT^{-1}*) is calculated by summing up ET from various sources, including snow cover, canopy, ponded water bodies, unsaturated zone, and saturated zone. It uses the same data requirements as the Kristensen and Jensen calculation. However, unlike the Kristensen and Jensen method, the Two Layer Water Balance simulation does not consider flow dynamics.*

The Two Layer Water Balance method simplifies the representation of hydrological processes in wetland areas or swamp with shallow groundwater tables. It can also be applied to simulate areas with deeper and drier unsaturated zones, but in such cases, the model results require careful calibration. The upper layer is defined by the model starting from the ground surface and extending to the Evapotranspiration (ET) extinction depth specified by the modeler. Throughout the simulation process, whenever there are alterations in root depth or the water table level, the thickness of the upper unsaturated zone undergoes changes at different time steps. When the water table reaches the ground surface, the upper zone reaches zero thickness. If the water table is calculated to be below the ET extinction depth, the lower zone is considered in the calculation, extending from the bottom of the upper zone to the water table. Conversely, when the groundwater table overtops the ET extinction depth, the thickness of the lower zone is zero. It is important to note that the MIKE SHE model does not consider the storage of the unsaturated zone, and as a result, the two-layer water balance function assumes that all infiltrated water immediately recharges the saturated zone without considering any dynamic changes.

Snow Melt

The MIKE SHE model enables modelers to assess the effects of snow melting and freezing processes on stream flow within the catchment. To represent the snow melting process, the model employs a modified degree-day approach. The function of snow melting in MIKE SHE is designed to account for various influencing factors such as air temperature, radiation, and energy sources.

$$\boldsymbol{Mt_{otal}} = \boldsymbol{M_T} + \boldsymbol{M_R} + \boldsymbol{M_E} \qquad \text{Eq. 6}$$

Air temperature melting

$$\boldsymbol{M_T} = \boldsymbol{CT} * (\boldsymbol{T_{air}} - \boldsymbol{T_0}) \qquad \text{Eq. 7}$$

where M_T *(*LT^{-1}*) is the rate of melting due to the air temperature depends,* C_T *(mm/day/C) is the degree-day factor, the difference between air temperature* T_{air} *at the computation cell and the threshold melting temperature* T_0 *defined as 0°C for most cases.*

Radiation melting

$$\boldsymbol{M_R} = -\boldsymbol{C_{rad}} * \boldsymbol{R_{sw}} \qquad \text{Eq. 8}$$

where M_R *(*LT^{-1}*) is the radiation melting rate,* C_{rad} *(unit: mm/kJ/*m^2*) the radiation melting factor and* R_{sw} *(unit: kJ/*m^2*/hour) the amount of incoming solar radiation.*

Energy melting

$$\boldsymbol{M_E} = \boldsymbol{C_E} * \boldsymbol{P} * (\boldsymbol{T_{air}} - \boldsymbol{T_0}) \qquad \text{Eq. 9}$$

where M_E *(*LT^{-1}*) is the rate of melting due to energy in liquid rain,* C_E *(unit: mm/mm rain/C) is the energy melting coefficient.*

Additionally, the amount of snow melting caused by various factors was calculated using three different methods. The empirical coefficients C_T and C_R, which represent the time-varying and spatially distributed format, were employed to enable model calibration over the winter season as snow properties change. On the other hand, the parameter C_E remains a constant value throughout the entire model.

Overland Flow

Ponded water flowing downhill towards the river system generates surface runoff. This water accumulation results from the remaining rainfall after accounting for losses caused by infiltration, evapotranspiration, river flow spilling over banks, and water exchange between surface and underground. In MIKE SHE's overflow function, which employs the Finite Difference Method to solve 2D St.-Venant equations, the key inputs for the calculation involve topography, flow resistance, and losses due to evapotranspiration, infiltration, or other hydrological processes along the flow path.

The mass conservation equation:

$$\frac{\partial h}{\partial t}+\frac{\partial hu}{\partial x}+\frac{\partial hv}{y}=i \qquad \text{Eq. 10}$$

And the momentum equation:

$$\begin{cases}\frac{\partial hu}{\partial t}+\frac{\partial(hu^2+\frac{gh^2}{2})}{\partial x}+\frac{\partial huv}{\partial y}=gh\big(S_{0x}-S_{fx}\big)\\ \frac{\partial hv}{\partial t}+\frac{\partial huv}{\partial x}+\frac{\partial(hv^2+\frac{gh^2}{2})}{\partial y}=gh(S_{0y}-S_{fy})\end{cases} \qquad \text{Eq. 11}$$

where h (L) is the flow depth. u *and* v *are the flow velocities in x- and y-direction.* i *is the net input into overland flow.* S_O *is the slope of ground surface and* Sf *is the friction slope in x- and y-direction.*

Nonetheless, obtaining a dynamic solution for the 2D St.-Venant equations poses significant numerical challenges. In the MIKE SHE calculation, a simplification is employed by neglecting the momentum losses caused by local and convective acceleration, as well as lateral inflows perpendicular to the flow direction (DHI, 2023d). This reduction in equation complexity is widely recognized as the diffusive wave approximation.

$$\begin{cases}S_{fx}=S_{0x}-\frac{\partial h}{\partial x}=S_{0x}-\frac{\partial z_g}{\partial x}=-\frac{\partial z}{\partial x}\\ S_{fy}=S_{0y}-\frac{\partial h}{\partial y}=S_{0y}-\frac{\partial z_g}{\partial y}=-\frac{\partial z}{\partial y}\end{cases}\text{with } Z=Z_g+h \qquad \text{Eq. 12}$$

The use of the diffusive wave approximation enables substantial variations in flow depth between adjacent calculation grids to be accommodated, allowing for the simulation of backwater conditions. However, when simulating water movement characterized by low velocities and shallow depths, certain numerical challenges may arise.

In the MIKE SHE model, the Chézy law is employed to depict the connection between water depth and velocity. The resulting simplified equations, with Manning-Strickler coefficients K in both the x- and y-directions, are presented as follows:

$$\begin{cases}uh=K_x(-\frac{\partial z}{\partial x})^{\frac{1}{2}}(-\frac{\partial z}{\partial x})h^{\frac{5}{3}}\\ vh=K_{xy}(-\frac{\partial z}{\partial y})^{\frac{1}{2}}(-\frac{\partial z}{\partial y})h^{\frac{5}{3}}\end{cases} \qquad \text{Eq. 13}$$

Apart from the topography and Manning-Strickler coefficients required for the calculation, the overland flow function in MIKE SHE includes two additional parameters that need to be set during the modeling setup:

- Detention storage: This parameter controls the volume of water flowing over the ground surface. It ensures that overland flow occurs only when the water depth on the surface exceeds a specified threshold defined by the detention storage value.
- Initial water depth: This parameter represents the amount of water already present at the beginning of the simulation.

Furthermore, MIKE SHE offers a semi-distributed overland flow function that employs an empirical relationship among flow depth, surface elevation, and surface roughness. This function, based on the work of Crawford & Linsley (1966), is available in the MIKE SHE model and helps describe the characteristics of overland flow.

Channel Flow: Coupling with MIKE 11

The MIKE SHE overland function has the theoretical capability to accurately represent 2D surface flow as channel flow when provided with high-resolution topography input. However, in practice, obtaining such high-resolution topography data, especially for large catchments, is often challenging. Additionally, using high-resolution input for simulations increases the computational time significantly. To address these limitations, the MIKE SHE model couples with MIKE 11 to simulate channel flow. MIKE 11 assumes that the channel flow has a single direction and utilizes an implicit, finite difference scheme to solve the 1D St.-Venant equation, which represents unsteady flow in rivers and estuaries. This coupling allows MIKE SHE to achieve more accurate channel flow simulation and enables the simulation of hydraulic structures like weirs and gates.

The MIKE SHE/11 coupling is established through river links, which are located at the boundaries between adjacent grid cells (Figure 12). These river links form a network created by the MIKE SHE setup program based on the specified coupling reaches. While the entire river system is incorporated into the hydraulic model, water exchange occurs only within the coupling reaches (Vo, 2015). Since the river links are defined at the edges of grid cells, MIKE 11's river geometry details can be partially represented within MIKE SHE, depending on the resolution of the MIKE SHE model. Consequently, the accuracy of the river network reproduction improves with a more refined MIKE SHE grid resolution.

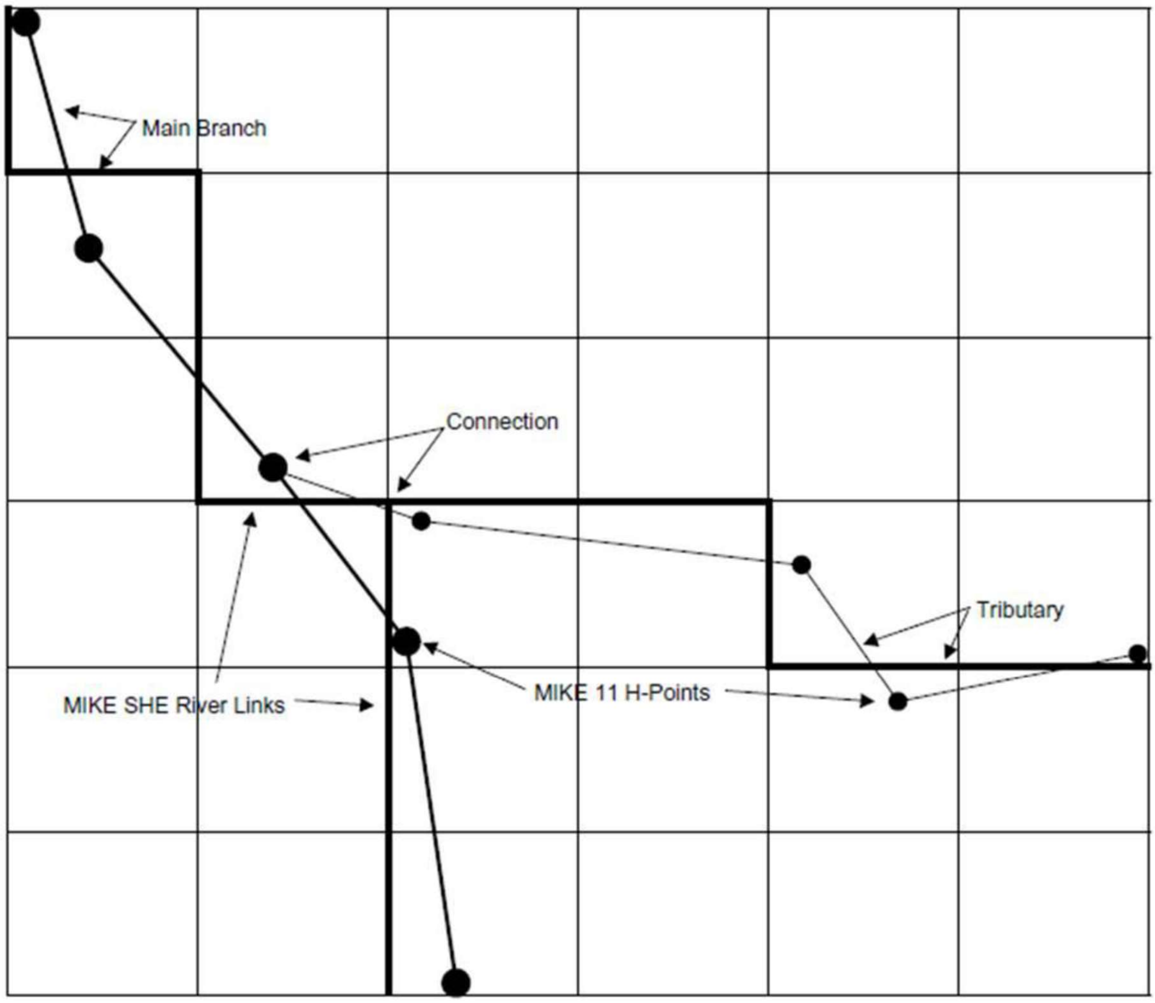

Figure 12 MIKE SHE and MIKE 11 coupling points and links (DHI, 2023d).

The water exchange can also be controlled using the function implemented in the MIKE SHE/11 coupling process. In situations where flooding is not permitted, the MIKE 11 river water levels at specific H-points are interpolated to the MIKE SHE river links. However, only the exchange flow originating from the overland and saturated zones in MIKE SHE will be considered during the calculation. On the other hand, when flooding is allowed, the MIKE 11 river water levels are interpolated to designated MIKE SHE grid cells. This interpolation helps determine whether ponded water exists on the cell surface. If there is ponded water present, the unsaturated or saturated exchange flows are calculated based on the water level above the cell. Furthermore, there is a scenario called "overbank spilling," which permits excess water from the open channel to flow to the MIKE SHE grid as overland flow.

Nonetheless, the integration between MIKE SHE and MIKE 11 through link reaches presents some limitations. One such limitation is that each MIKE SHE link can only be connected to a single coupling reach. This can lead to issues when dealing with intricate drainage or river networks with branches less than half a cell width apart, or when the length of a MIKE 11 branch is smaller than the MIKE SHE cell size. Problems may arise if the MIKE 11 cross-section is wider than the MIKE SHE cell size, as this would result in the river link's cross-section being reduced to the cell width. To address these challenges, activating the Flood code option or Direct Overbank Spilling options becomes necessary to accurately represent water flow in the flood plain.

Unsaturated Zone Flow

The flow within the unsaturated zone is a crucial aspect of MIKE SHE and numerous modeling applications. The unsaturated zone can be likened to a shallow, heterogeneous top layer of soil, characterized by cyclic fluctuations in soil moisture as water is exchanged among various hydrological processes like rainfall, evapotranspiration, and infiltration (Vo, 2015). Both vertical and horizontal pathways can describe the flow in the unsaturated zone, but due to gravity's predominant role in the infiltration process, the flow is primarily considered vertical. While this assumption is generally acceptable in many cases, it may be limiting in specific situations, such as very steep hill slopes or small-scale catchments where lateral and vertical flow intensities are approximately equal. In the case where lateral flow should be considered, other algorithms such the SWAT can used (Liu et al., 2016).

The hydrological process within the unsaturated zone can be broadly explained as follows: rainfall contributes to the topsoil moisture, with a portion of water extracted by evapotranspiration, and the rest recharges the groundwater reservoirs. In the MIKE SHE model, three options are available to represent the vertical movement of water through the unsaturated zone (Ma, 2018).

Richards Equation

The MIKE SHE unsaturated zone model predominantly adopts the complete Richards equation, named after L.A. Richards, who initially employed it in 1931. This equation necessitates the use of a tabular or functional representation for both the moisture-retention curve and effective conductivity. It is widely accepted as the default choice for the model's operation.

$$\frac{C\partial\Psi}{\partial t} = \frac{\partial}{\partial z}\left(K(\theta)\frac{\partial\Psi}{\partial z}\right) + \frac{\partial K(\theta)}{\partial z} - \boldsymbol{S} \qquad \text{Eq. 14}$$

where Ψ is the pressure head (L)function of θ the volumetric soil moisture (-)and $K(\theta)$ the unsaturated hydraulic conductivity (LT^{-1}). S and T are the root extraction (LT^{-1}) and time component (T^{-1}). C is the soil capacity (-).z is the gravitational component (L).

In MIKE SHE, the numerical solution for the full Richards Equation employs a fully implicit formulation. This means that the spatial derivatives in the equation are represented using their finite difference analogs at the time level (n+1). Additionally, the values of $C(\theta)$ and $K(\theta)$ are referenced at the time level (n+1/2).

Gravity Flow

In practical applications, simulating Richards Equation demands extended computational time. However, the MIKE SHE model offers a solution to this issue by incorporating the Gravity Flow function. By assuming that gravity flow predominates as the primary direction of flow in the unsaturated zone, this function conveniently disregards the effects of the pressure head term on vertical flow.

$$\frac{\partial \theta}{\partial t} = \frac{\partial q}{\partial z} - \boldsymbol{S(z)} \qquad \textbf{Eq. 15}$$

The Gravity Flow function in MIKE SHE solves the equation explicitly, starting from the top of the soil column and moving downward. The water depth on the overland is assumed to represent the available water for infiltration from the ground surface. The infiltration process is controlled by inputting information of conductivity-saturation relationship into the model by hydrological modelers.

Compared to the full Richards equation, gravity flow is much faster and more computationally stable. It finds widespread use in areas with coarse soil, where capillary pressure is low, or in cases where the focus is on studying evapotranspiration and infiltration processes, and the dynamics in the unsaturated zone are not a primary concern.

DHI has released comments regarding different methods used in MIKE SHE. The full Richards equation method provides the most accurate representation of dynamic unsaturated flow but is the most computationally intensive. The gravity flow method offers a suitable solution for assessing time-varying groundwater recharge based on actual precipitation and evapotranspiration when no dynamics are involved. The two-layer water balance method is more usually used when the groundwater table is superficial and groundwater recharge is principally shaped by evapotranspiration. Additionally, the MIKE SHE model accounts for flow through macropores, which are secondary, continuous pore domains in the unsaturated zone. This flow can be represented either by a simple bypass flow or a full macropore flow. In the case of the simple bypass flow function, the infiltration water is divided into two paths: one passing through the soil matrix and the other directly routed to the groundwater table. The latter is the bypass flow computed as a portion of the next rainfall at each computation time step for the unsaturated zone, and the actual bypass fraction depends on actual water content of the unsaturated zone and a user-specified maximum fraction. On the other hand, the full macropore flow method simulates macropore flow when the capillary head in the micropore domain exceeds a threshold matrix pressure head, indicating that the minimum pore size belongs to the macropore domain. In this case, water flow is presumed to be laminar and not impacted by capillarity, representing gravitational flow. To account for the close interaction between the unsaturated and saturated zones, MIKE SHE utilizes an iterative mass balance technique. This technique guarantees a realistic depiction of groundwater table fluctuations, particularly in situations with shallow soils. The coupling process is not resolved by a matrix with an implicit flux coupling, which allows flexibility in choosing different time steps for optimization of computational time (Bringas, 2016; DHI, 2023d).

Groundwater Flow: Saturated Zone Flow

The groundwater process holds immense importance within the hydrological systems of catchment areas worldwide. During the dry season, it becomes a vital resource for recharging stream flows. Moreover, the groundwater process interacts with various other hydrological processes in diverse ways. It is crucial, necessary, and effective to incorporate and integrate this process into the overall hydrological modeling to reduce uncertainties. In MIKE SHE, representing the groundwater process is achieved through simulating the saturated zone using either the Finite Difference Method or Linear Reservoir Method. This choice is made due to the complexity of the model functions integrated into the modeling system.

Finite Different Method

In this method, the flow in saturated zone is usually reproduced through 3D Darcy equation:

$$\frac{\partial}{\partial x}\left(K_{xx}\frac{\partial h}{\partial x}\right) + \frac{\partial}{\partial y}\left(K_{yy}\frac{\partial h}{\partial y}\right) + \frac{\partial}{\partial z}\left(K_{zz}\frac{\partial h}{\partial z}\right) - \mathbf{Q} = \mathbf{S}\frac{\partial h}{\partial t} \qquad \textbf{Eq. 16}$$

where h is the hydraulic head (L) and Q presents the source/sink terms. S is the specific storage coefficient (-). K_{xx}, K_{yy} and K_{zz} are the hydraulic conductivity in x-, y- and z-direction (LT^{-1}).

The equation in the MIKE SHE model is solved using an iterative implicit finite difference technique known as the Finite Difference Method. MIKE SHE offers two solution techniques: Successive Over-Relaxation (SOR) and Preconditioned Conjugate Gradient (PCG). Implementing the Finite Difference Method requires various data inputs related to the definition of the saturated area (Lower/Upper levels and Horizontal extent), hydraulic conductivity (in both horizontal and vertical directions), specific yield, initial and boundary conditions, and drainage. Although the Finite Difference Method yields more accurate results for simulating the saturated zone in MIKE SHE, it comes with a significant data requirement. Consequently, some parameters in the model may need to be estimated through hypotheses or under special conditions. This increased data uncertainty and the complexity of model setup can raise challenges.

Linear Reservoir Method

The possibility of employing the lumped conceptual approach, known as the Linear Reservoir Method, in the MIKE SHE saturated zone simulation can simplify the computational process and data requirements. This method relies on the relationship between storage and time, aiming to streamline the simulation process.

$$\boldsymbol{S} = \mathbf{kQ} \qquad \textbf{Eq. 17}$$

where S is the storage in the reservoir (L), Q is the outflow from reservoir (LT^{-1})and k stands for the time constant (T).

To compute the groundwater flow, this approach partitions the study area into multiple sub-catchments, each treated as an individual reservoir (Figure 13). In every sub-catchment, the saturated zone is depicted as a collection of interconnected, shallow interflow reservoirs, alongside distinct, deep aquifers that supply to the base flow in streams (Ma, 2018).

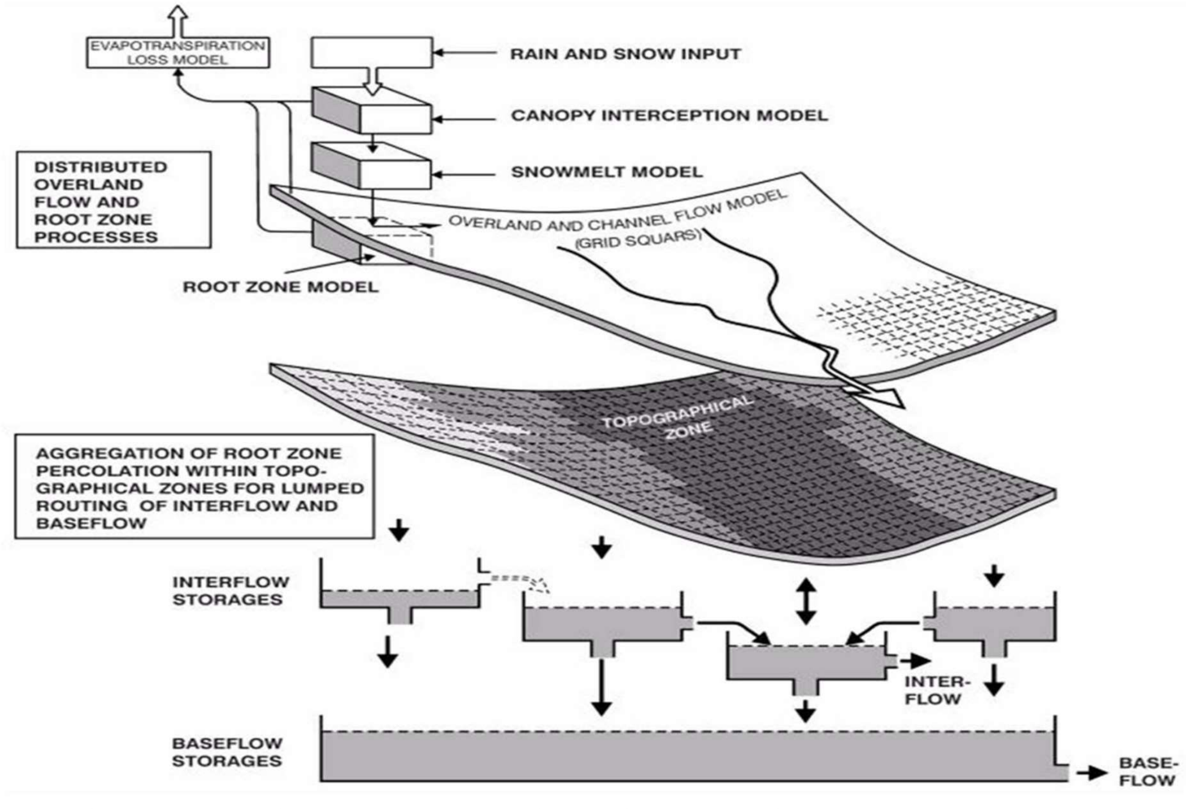

Figure 13 MIKE SHE model structure with the linear reservoir module (DHI, 2023d).

Furthermore, the flow exchange between each sub-catchment (reservoirs) can be represented as depicted in Figure 14. As a result, the required input data is simplified to include only the map information concerning the division of the model area into sub-catchments, interflow, and base flow reservoirs. The application of the Linear Reservoir Method in the saturated zone of MIKE SHE model simulation is intended to serve as a reliable and efficient tool in various fields, including:

- Assessing water balance and simulating runoff for ungauged catchments.
- Predicting hydrological effects resulting from land-use changes.
- Forecasting floods.
- Conducting long-term simulations, such as assessing the impact of climate changes.

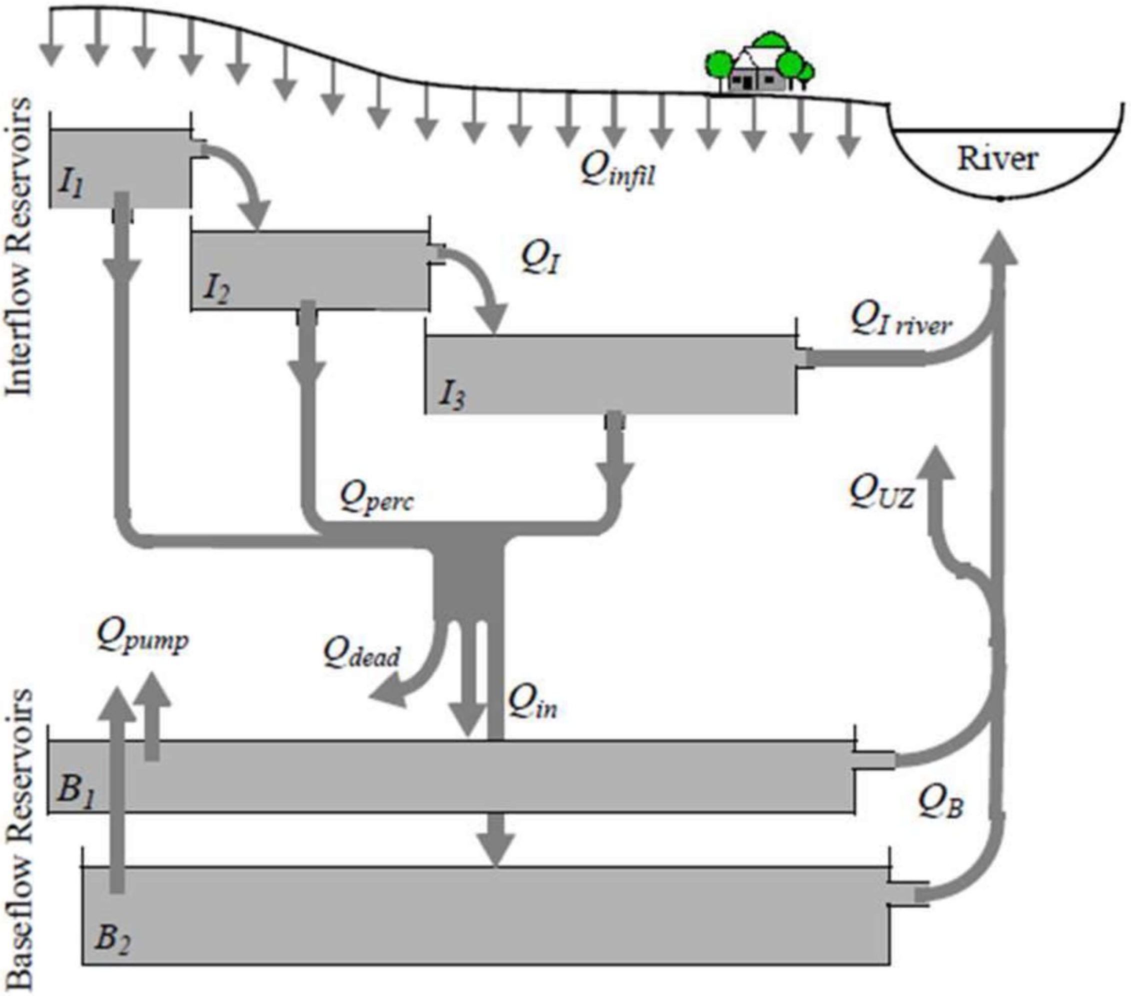

Figure 14 Flow diagram for the MIKE SHE linear reservoir module (DHI, 2023d).

1.4.1.3. Performances of MIKE SHE

The AquaVar Environmental DSS design places significant emphasis on hydrological modeling assessment as the initial step in the integrated modeling system. The selection of a suitable model at this stage is crucial for generating detailed and accurate representations of the complex catchment hydrological system. After extensive discussions and comparisons, the MIKE SHE model was chosen to fulfill these requirements (Ma, 2018). Notably, the MIKE SHE model has a strong track record of successful application in various countries by diverse organizations, including universities, research centers, and consulting engineering companies (Refsgaard, 1997). As mentioned earlier, the MIKE SHE model is capable of seamlessly integrating numerous hydrological processes within a catchment system.

It serves as a primary hydro-informatics tool for addressing water resources management issues and problems concerning the interaction between surface and groundwater, as well as environmental and ecological components.

1.4.2. Surface hydraulic model: MIKE 21FM

The 2D free surface flow model holds a central and crucial role in the development of the AquaVar DSS tool. This integrated modeling system requires a highly performing model to accurately represent the Lower Var River valley system (Zavattero, 2019). The MIKE 21FM model has been selected for this purpose due to its ability to simulate various physical and chemical processes, including hydrodynamic behavior, pollution transfer, and morphological changes. It serves as the core of the AquaVar DSS tool, as it receives boundary conditions from the Mike SHE hydrological flow results and provides boundary conditions for the Feflow groundwater flow model. MIKE 21FM is extensively used as a key hydro-informatics tool for addressing coastal management and river-related challenges, as well as environmental and ecological aspects.

Developed by the Danish Hydraulic Institute (DHI) for oceanographic, coastal, and estuarine applications, the MIKE 21FM model employs a flexible mesh approach, allowing for triangles or quadrangles as cells, in contrast to the older Mike 21 model. Its hydrodynamic module serves as the fundamental computational component for various modules within the MIKE 21FM modeling system, such as the Transport, ECO Lab, Mud Transport, and Sand Transport. Moreover, its usage has been extended to river modeling.

To simulate hydrodynamics in MIKE 21FM, the model employs a solution of 2D Shallow Water Equations (SWEs) (Eq. 18) using the finite volume numerical method. Unstructured grids define the topography, enabling the generation of unsteady two-dimensional flows in vertically homogeneous single-layer fluids. Overland flow is described using the kinematic wave approximations of the Saint-Venant system, which comprises two components, the conservation of mass and momentum integrated over the vertical:

$$
\begin{cases}
\dfrac{\partial h}{\partial x} + \dfrac{\partial p}{\partial x} + \dfrac{\partial q}{\partial y} = \mathrm{w} \\
\dfrac{\partial p}{\partial t} + \dfrac{\partial}{\partial x}\left(\dfrac{p^2}{h}\right) + \dfrac{\partial}{\partial y}\left(\dfrac{pq}{h}\right) + gh\dfrac{\partial z_w}{\partial x} + \mathrm{gp}\dfrac{\sqrt{p^2+q^2}}{C^2h^2} - \dfrac{1}{\rho_w}\left[\dfrac{\partial}{\partial x}(h\tau_{xx}) + \dfrac{\partial}{\partial y}(h\tau_{xy})\right] \\
\qquad + \dfrac{h}{\rho_w}\left(\dfrac{\partial p_a}{\partial x}\right) = 0 \\
\dfrac{\partial q}{\partial t} + \dfrac{\partial}{\partial y}\left(\dfrac{q^2}{h}\right) + \dfrac{\partial}{\partial x}\left(\dfrac{pq}{h}\right) + gh\dfrac{\partial z_w}{\partial x} + \mathrm{gp}\dfrac{\sqrt{p^2+q^2}}{C^2h^2} - \dfrac{1}{\rho_w}\left[\dfrac{\partial}{\partial x}(h\tau_{yy}) + \dfrac{\partial}{\partial y}(h\tau_{xy})\right] \\
\qquad + \dfrac{h}{\rho_w}\left(\dfrac{\partial p_a}{\partial y}\right) = 0
\end{cases}
\qquad \text{Eq. 18}
$$

where, h is the water depth [m], $w=R-I$ *is the mass source term [m/s] (with R the rainfall rate and I the infiltration rate),* zw *is the surface elevation [m],* $(p,q)=(hu,hv)$ *are the flux densities in directions x and y respectively [m²/s],* C *is the Chézy friction coefficient* $[m^{1/2}/s]$*,* g *is the gravity* $[m/s^2]$*,* pa *is the atmospheric pressure* $[kg/m/s^2]$*,* ρw *is the density of water* $[kg/m^3]$ *and* $\tau_{xx}, \tau_{yy}, \tau_{xy}$ *are the components of effective shear stress, determined by viscosity and velocity gradient.*

The time integration in this study explores two options for modeling pollutant transport in the Var River. The first option is a lower-order method, specifically the first-order explicit Roe scheme. The second option involves a higher-order approach using the second-order Runge-Kutta method. Regardless of the chosen method, the convection flux is computed using the Roe scheme (Roe, 1981), and a TVD slope limiter method is applied to minimize oscillations and achieve second-order accuracy in space (Darwish & Moukalled, 2003).

The research work utilizes three modules of the MIKE 21FM software: hydrodynamic, transport, and sediment transport (Zavattero et al., 2016). The main objectives of the study are to simulate extreme hydrological events, accidental pollution, and changes in morphology in the Var River.

A comprehensive review of surface water quality models has been conducted with a focus on their development in three stages (Zavattero, 2019). The analysis involves evaluating the suitability, accuracy, and methods employed by different models (Wang et al., 2013). From 1925 to 1965, water quality models primarily examined interactions among various components in river systems affected by point source pollution from human and industrial activities, including transmission, sediment oxygen, and algal photosynthesis. Subsequently, from 1965 to 1995, 2D and 3D models gained popularity due to their ability to realistically reproduce hydraulic phenomena, and a non-linear relationship was adopted. Notable models during this period include QUAL (Brown et al., 1987; Grenney et al., 1979), MIKE 11 (DHI, 1993), and WASP (Wool et al., 2020). After 1995, water quality models incorporated nutrients and toxic chemicals to account for the increase in organic compounds, heavy metals, and nitrogen compounds.

Currently, software tools like Mike 21, MIKE 21FM, or Telemac2D serve as valuable resources for pollution transport prevention. These software tools are employed in various ways, such as hydrodynamic-ecological simulations, trajectory and residence time analysis of biochemical pollutants, and oil spill modeling. However, it is essential to recognize that these tools may be controlled by different methods and could potentially produce varying results (Zavattero, 2019). To simulate pollutant transport using MIKE 21FM, two modules are essential: the hydrodynamic module, which forms the basis, and the second module, representing the behavior of pollutants in the water. Figure 15 illustrates the process involved in this simulation.

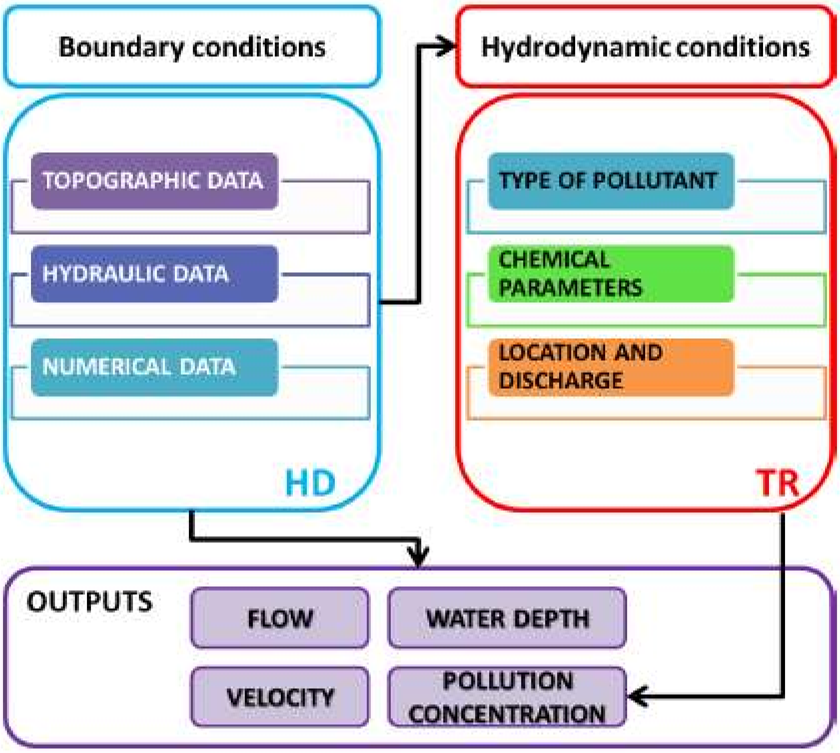

Figure 15 Modelling process for pollutants transport in MIKE21FM (Zavattero, 2019).

The 2D model considers both physical and chemical processes to describe the evolution of pollutants. These pollutants can be categorized as either conservative or non-conservative. Initially, the pollutant is characterized by its concentration, representing the mass per unit volume. Subsequently, two types of mechanisms are employed to illustrate the pollutant's transportation.

The first mechanism is known as advection transport, as explained by Gulliver in 2007. This process involves the transportation of the pollutant within the water body and is influenced by the water velocity, making the hydrodynamic aspect crucial in this regard. The second mechanism deals with dispersion transport, which is described using Fick's law. Unlike advection transport, dispersion transport does not require any motion and describes the evolution of the pollutant concentration (DHI, 2023c).

To achieve the simulation of pollutants, the advection-dispersion equation is used:

$$\partial_t(hc) + \partial_x(hcu) + \partial_y(hCv) = Kc(\partial_x^2 c + \partial_y^2 c) + C_{sce}S_{ce} \qquad \textbf{Eq. 19}$$

$$\frac{\partial c}{\partial t} = \mathbf{kc} \qquad \textbf{Eq. 20}$$

where, $c(x,y,t)$ is the concentration [kg/m³], (u, v)(x, y, t) are the velocity in directions x and y respectively [m/s], Kc is the diffusion coefficient [m²/s], $Csce$ is the initial concentration [kg/m³], Sce is the flux of pollutant [m/s], and k is the decay constant. The constituents decay linearly in time. In DHI software tools, the decay coefficient is indicated, per second, by the user.

The 2D tracer equation's solution in MIKE 21FM utilizes a finite volume method. The user has the flexibility to select the time integration method, such as the hydrodynamic option, to achieve higher precision in the results. In either approach, the TVD-MUSCL limiter method is employed (Darwish & Moukalled, 2003) to reduce oscillations and enhance accuracy.

1.4.3. Groundwater model: Feflow

The development of the Feflow software was carried out by DHI WASY (Diersch, 2005), with a focus on applications in groundwater and porous media modeling. This powerful software has the capability to simulate various processes, including fluid flow, groundwater age, contaminant transport, and heat transport, considering both fully and variably saturated conditions at different scales. The AquaVar project's Feflow model construction is extensively described by Du et al. (2016).

The fundamental equations governing saturated flow are the fluid continuity equation and the Darcy equation (Verruijt, 1970). The fluid continuity equation, also known as the conservation of mass equation, describes the transient and saturated groundwater flow through a small dice of porous medium in an unconfined aquifer (Figure 16). To simplify the conditions, two assumptions are made:

- The medium is considered porous, incompressible, and non-deformable.
- The fluid is assumed to have a constant density.

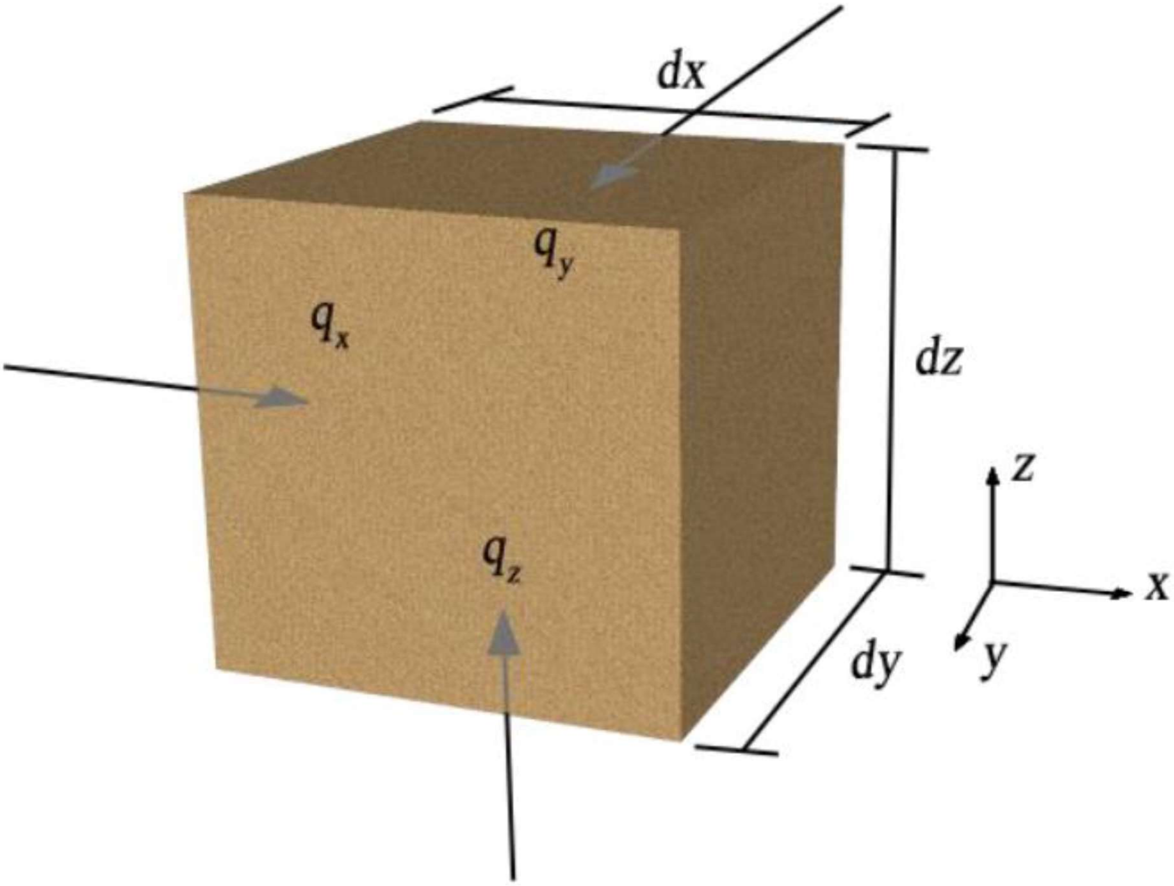

Figure 16 Representation of the derivation of the continuity equation for the saturated groundwater flow (Du et al., 2016).

In this instance, the change of the mass of water accumulated in the soil only rests on the flux that penetrates and exits from the soil. It is expressed as:

$$S_s \frac{\partial \psi_g}{\partial t} + \frac{\partial q_x}{\partial x} + \frac{\partial q_y}{\partial y} + \frac{\partial q_z}{\partial z} = 0 \qquad \text{Eq. 21}$$

or a vector form can be used:

$$S_s \frac{\partial \psi_g}{\partial t} + \nabla q = 0 \qquad \text{Eq. 22}$$

where, Ss is the specific storage [m^{-1}], ψg is hydraulic head of the groundwater [m]and q is the vector notion of the flux of groundwater flow [m/s].

The flux in the saturated area, as depicted in Figure 17, is determined using the Darcy equation. This equation, grounded in physical principles, enables the calculation of groundwater flow through a specific cross-section based on the hydraulic gradient.

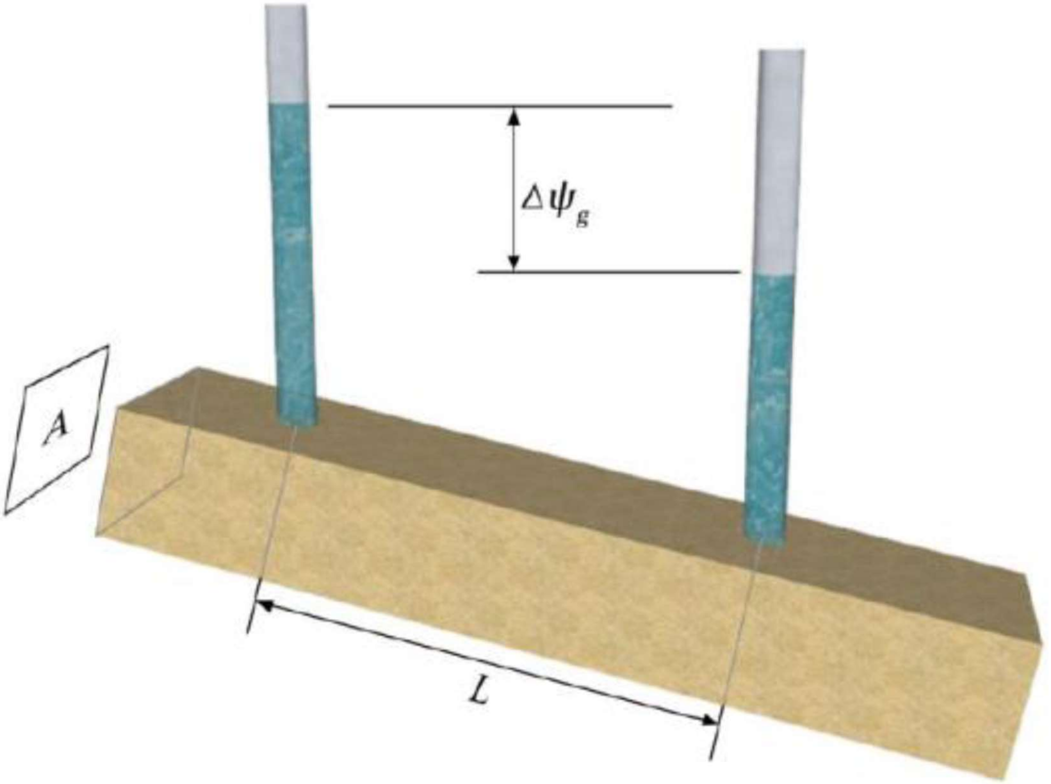

Figure 17 Representation of the Darcy's equation (Du et al., 2016)

For a given piece of soil with a length L and a cross-section A, Darcy equation is written in the form below:

$$Q = K\,A\,i = -K\nabla\psi_g \;= 0 \qquad \text{Eq. 23}$$

where, Q is the groundwater flow rate through the cross-section [m³/s], K is the hydraulic conductivity of the soil [m/s], A is the cross-section of the soil [m²], i is the hydraulic gradient [m/m], which is the ratio between the hydraulic drop $\Delta\psi_g$ and L the distance between two selected points in the soil.

Considering only the speed of the groundwater flow, the Darcy's equation can be streamlined:

$$q = K\,i = -K\frac{\nabla\psi_g}{L} \qquad \text{Eq. 24}$$

where, q is the velocity of groundwater flow (m/s).

For the saturated flow modeling, the governing equations are the fluid continuity and Darcy equations:

$$(S_sB + S_y).\frac{\partial\psi_g}{\partial t} + \nabla(\mathrm{Bq}) = B\varepsilon Q + P \qquad \text{Eq. 25}$$

where, S_s is the specific storage (m^{-1}). B is thickness of the unconfined aquifer (m). S_y is the dimensionless specific yield, also labeled drain/fillable porosity or effective porosity. ψ_g is hydraulic head of the groundwater (m). q is the vector notion of the flux of groundwater flow (m/s). Q is the specific mass supply per unit time per unit depth (s^{-1}). ε is total porosity of the porous media (dimensionless). P is accretion of the mass added into the system per unit area per unit time (m/s).

In the Feflow software, these two equations are adapted to accommodate variable saturation and solved using the finite element method (Diersch, 2005). The continuity equation includes porosity and external mass supply as additional factors. Meanwhile, the Darcy equation incorporates a hydraulic conductivity function of the saturation.

The numerical model's boundary is defined by the hydrogeological catchment, limited by the impermeable layer's edge or geological faults (Figure 18). The hydraulic conductivity of the alluvium is spatially distributed based on field measurements, while the other layers have uniform values. This model primarily considers river-aquifer exchanges, direct recharge/loss from rainfall/evapotranspiration, and groundwater extraction as the most influential source/sink terms affecting groundwater flow. Depending on the season, the first two terms can either replenish or deplete the aquifer, while groundwater extraction always leads to a subtraction of groundwater (Du, 2016).

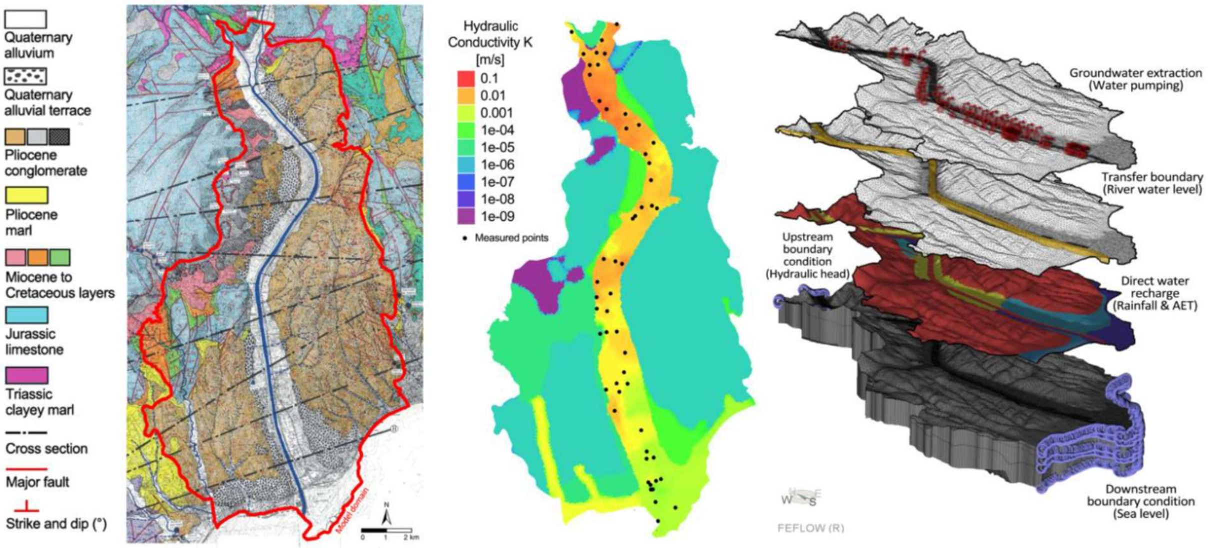

Figure 18 (a) Model domain and Geological map in the Lower Var valley; (b) map of selected hydraulic conductivities; (c) model boundary conditions (Du et al., 2016).

The 3D groundwater flow model is a crucial element in the AquaVar DSS tool's design, representing the final stage of the modeling process. Its role within the integrated modeling system is significant. To ensure accurate and detailed representation of the alluvial aquifer system in the Lower Var valley, it is essential to select a high-performance model.

The chosen model in this phase must be capable of effectively simulating various physical and chemical processes, including hydrodynamic behavior, pollution transfer, and salt intrusion. Among the hydro-informatics tools employed, the Feflow model stands as the last link in the AquaVar DSS tool's chain. Its boundary conditions are derived from the MIKE 21FM results.

In the pursuit of addressing groundwater resource-related inquiries, water table knowledge, and environmental and ecological components, the Feflow model has been widely applied as one of the primary analytical tools (Du et al., 2019).

1.4.4. Coupling for river-aquifer exchanges

River-aquifer exchange is not properly modeled by the selected individual models. To improve the representation of these interactions, groundwater models are coupled with surface water models ((Du et al., 2016; Zavattero, 2019)). In the DHI MIKE tools, piMIKE1D supports the coupling between an existing Feflow Fluid-Transfer BC and a river network file from MIKE 1D (Diersch, 2005). However, in the AquaVar system, a coupling interface was devised. This interface was specifically tailored to facilitate interactions between the MIKE 21FM (a 2D free surface flow model) and Feflow (a 3D saturated groundwater flow model) software tools. The constraint of using DHI software necessitated a comprehensive understanding of the underlying processes within both MIKE 21FM and Feflow, without altering their core code.

The concept behind this interface was to facilitate the exchange of data between these two models. This was achieved by introducing a source term (either positive or negative) in MIKE 21FM and providing boundary conditions from the surface model to Feflow. In practice, the coupling interface converted files from one model to another and calculated the direction and volume of these exchanges.

This coupling interface was developed using JavaScript, and it relied on a well-defined algorithm. To validate the functionality of this interface, various test cases were executed. Initial cases were designed to ensure the basic functioning of the interface, while a third case was simulated to validate the coupling methodology itself.

The algorithm effectively facilitated data exchange between the MIKE 21FM and Feflow models. It proficiently represented bidirectional river-aquifer exchanges and quantified the volume of water involved in these exchanges. However, during testing, certain limitations were identified. Firstly, the source term used in MIKE 21FM, which was based on the precipitation module, was treated as a lateral inflow, influencing the hydrodynamics. Secondly, the equations used in the Feflow model were rooted in the fluid continuity equation, focusing on transient, saturated groundwater flow and Darcy's law, with unsaturated flow not being considered in this configuration. Finally, the algorithm calculated the exchanged water volume using a simple equation reliant on hydraulic conductivity. This parameter was found to require calibration and added intricacy to the coupling interface.

In closing, this coupling interface was tailored to suit the needs of the DSS tool for the AquaVar project, offering valuable insights into DHI software tools.

1.4.5. Summary of calibrated parameters in AquaVar modeling system

The models used in AquaVar were calibrated by varying the values of a set of parameters for each model. The main parameters are summarized in Table 3, Table 5, Table 6 and Table 6. The calibration of hourly and daily versions of MIKE SHE was based on the sensitivity analysis of daily simulations due to the longer computation time for hourly simulation. Five modules of MIKE SHE are included in the simulations: Climate, River and Lakes, Overland, Saturated and Unsaturated zones. In addition the time step control parameters were also evaluated. A total of 33 parameters were calibrated. Slight differences appeared for parameters like degree day coefficient, leakage coefficient, surface Manning-Strickler coefficient, saturated hydraulic conductivity, horizontal hydraulic conductivity, and soil depth. The soil depth is distributed in 3 classes based on slope classification (0-10°, 10-40° and 40-90°). This hypothesis is motivated by the lack of knowledge of soil depth distribution in the Var catchment. Shallower soil depths are used for hourly simulation compared to daily simulations. The horizontal hydraulic conductivity of hourly simulations is slightly smaller than that of daily simulations, but the opposite trend is noted with surface Manning-Strickler coefficient. For saturated hydraulic conductivity, silt and loam soil types have large differences, almost 10 times difference between hourly and daily.

Calibration of the Feflow model of the Lower Var Valley focused on three parameters: specific yield, in-transfer and out-transfer rates. The specific yield varies between 0.05 and 0.2 while in-transfer and out-transfer rates are less than 0.0005 /m. The remaining parameters were left as initially assumed. Parameters like hydraulic conductivity of the alluvial zone were interpolated based on field measurements. The semi-distributed rainfall-runoff coefficients were assumed to be more than 0.6, leaving less than 0.4 for infiltration.

Moreover, the MIKE 21FM surface model was calibrated with mesh size, surface Manning and thresholds. The quadrangular mesh was set for the riverbed and triangular meshes for the floodplain and weir location due to the two one direction nature of flow in the riverbed. The surface Manning varied from 10 for the riverbed to 70 for the floodplain in drought periods. However, in the flood period the coefficient was assumed to be uniformly 25 all over the domain. In fact, floods tend to carry materials which will be deposited in the floodplain.

Table 3 Optimized parameters in hourly and daily MIKE SHE simulations in Var catchment (Ma, 2018).

Components	**Parameters**			**Units**	**Calibrated values (Hourly)**	**Calibrated values (Daily)**
Time step control	Max precipitation depth per time step	$P_{\text{Max depth}}$		mm	50	
	Max infiltration amount per time step	$P_{\text{Max infiltration}}$		mm	50	
	Input precipitation rates requiring its own time step	$P_{\text{Input rate}}$		mm/hour	5	
Climate	Degree-day coefficient	$C_{\text{Degree day}}$	Flat	m/°C/day	4	2
			Northwards		2	1
			Southwards		4	2
Rivers and Lakes	Bed resistance	M_{Bed}		$m^{1/3}/s$	20 to 27	
	Leakage coefficient	C_{Leak}		/s	7.50E-05	
Overland Flow	Manning-Strickler	M_{Forest}		$m^{1/3}/s$	8	4
		$M_{\text{Open Space}}$			10	5
		M_{Grass}			15	10
		$M_{\text{Agricultural}}$			20	
		$M_{\text{Artificial}}$			25	

Table 4 Optimized parameters in hourly and daily MIKE SHE simulations in Var catchment (Ma, 2018).

Components	Parameters			Units	Calibrated values	
Unsaturated Zone	Loam	Water content at saturation		-	0.48	
		Water content at field capacity		-	0.28	
		Water content at wilting point		-	0.14	
		Saturated hydraulic conductivity		m/s	6.00E-06	6.00E-05
	Silt	Water content at saturation		-	0.51	
		Water content at field capacity		-	0.31	
		Water content at wilting point		-	0.11	
		Saturated hydraulic conductivity		m/s	2.00E-05	8.00E-06
	Clay	Water content at saturation		-	0.56	
		Water content at field capacity		-	0.36	
		Water content at wilting point		-	0.22	
		Saturated hydraulic conductivity		m/s	5.00E-06	4.00E-06
	Sand	Water content at saturation		-	0.38	
		Water content at field capacity		-	0.18	
		Water content at wilting point		-	0.08	
		Saturated hydraulic conductivity		m/s	1.00E-03	
	ET Surface Depth	ET_{Depth}		m	0.1	
Saturated Zone	Horizontal hydraulic conductivity	$Ksz_{Horizontal}$		m/s	5.50E-03	6.50E-03
	Vertical hydraulic conductivity	$Ksz_{Vertical}$		m/s	5.50E-04	6.50E-04
	Specific Yield	Sy		-	0.20	
	Soil depth	Response Surface slope (°)	0-10	m	-8	-12
			10-40		-4	-5
			40-90		0	0

Table 5 Optimized parameters in daily Feflow simulation in Lower Var Valley (Du et al., 2018b).

Parameters		**Units**	**Calibrated values**
Specific storage	S_s	/m	1.00E-04
Specific yield	S_y	-	0.05 to 0.2 distributed
In-transfer rate	ϕ_{in}	/s	0 to 1.00E-04 distributed
Out-transfer rate	ϕ_{out}	/s	0 to 5.00E-04 distributed
Horizontal hydraulic conductivity	Quaternary Alluvium $Ksz_{Horizontal}$	m/s	4.00E-02 to 1.00E-09 interpolated
	Quaternary Alluvial terraces $Ksz_{Horizontal}$	m/s	1.00E-04
	Pliocene conglomerate $Ksz_{Horizontal}$		2.60E-06
	Pliocene marl $Ksz_{Horizontal}$		1.00E-09
	Layers from Miocene to Cretaceous $Ksz_{Horizontal}$		1.00E-09
	Jurassic limestone $Ksz_{Horizontal}$		1.00E-05
Rainfall-runoff coefficient	Industrial & dense urban area	-	0.9
	Dispersed urban area		0.8
	Mountainous forests		0.7
	Agricultural land		0.6

Table 6 Optimized parameters MIKE 21FM simulation on Lower Var Valley (Zavattero, 2019).

Parameters		**Units**	**Calibrated values**	
Mesh size (shape)	Riverbed	m	10 (quadrangular)	
	Weir locations		10 (triangular)	
	Floodplain		25 (triangular)	
Manning-Strickler coefficient			Flood period	Drought period
	M_{river}	$m^{1/3}/s$	25	25
	$M_{vegetation}$			10
	$M_{urban\ areas}$			70
	$M_{agricultural\ areas}$			20
Threshold values	Drying depth	m	5.00E-03	
	Wetting depth		5.00E-02	
	Flooding depth		1.00E-01	

According to Zavattero (2019), computing power is the biggest challenge of in setting up the AquaVar modeling system. Simulations are performed in a loop with updated data. Thus a short computation time is required. On a computer system 2 Intel i7-4790, 3.6 GHz, RAM 16 GB, the required computation for each model is evaluated (Table 7).

Table 7 Comparison of simulation and computing times (Zavattero, 2019).

Parameters	**MIKE SHE Hydrological model**	**MIKE 21FM Surface flow model**	**Feflow Groundwater flow model**
Cell size of the shortest mesh	25 m	10 m	25 m
Δt of simulation for flood event	0.5 h	2 seconds	0.25 h
Δt of simulation for drought event	6 h	5 seconds	1 hour
Computing time	5 mn	0.3 seconds	0.15 mn
Ratio flood event (simulation/computing time)	6	6	100
Ratio drought event (simulation/computing time)	72	16	400

In terms of computational capacity, the MIKE 21FM model emerges as the most restrictive due to the short mesh resolution and, consequently, the higher number of elements it encompasses (Zavattero, 2019). This computational workload underwent theoretical assessment, after which the three models were executed in four distinct configurations: flood events, drought events, as well as pollution events occurring within flood and drought periods. The computation duration for a 6-hour simulation of a flood event totals 2 h across all three models. For simulating a drought event, a 2-hour computation period adequately covers a simulation spanning 20 h. Based on these instances, the computational prowess of the current computer setup can be summarized as follows: for a computation time of T h, the monitoring system possesses the capability to simulate (or predict, if predictive precipitation data from MeteoFrance is used) a flood event spanning 3T h, or a drought event extending up to 10T h. In the context of pollutant transport, a computation time of T h empowers the monitoring system to simulate 2T h.

To encapsulate the frequency of simulations and time predictions, Figure 19 illustrates the frequency of simulations within the flood configuration, employing a computer characterized by the aforementioned attributes. For the flood scenario, a simulation is initiated every hour, and following five short simulations, an extended simulation is conducted. In contrast, for the drought or averaged scenario, simulations are commenced every 6 h, with a subsequent extended simulation after five short ones. This structured iterative approach enables the Decision Support System (DSS) tool to generate a forecasted state every 4 h in the context of the flood configuration and every 18 h for the drought configuration, all achieved through precisely managed loops of time.

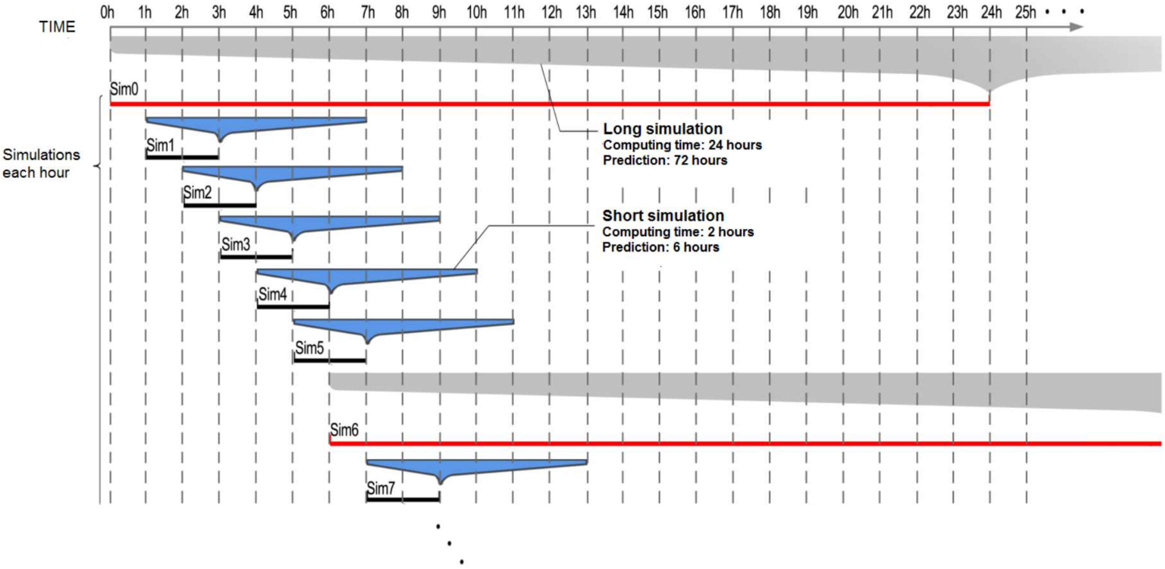

Figure 19 Simulations and time prediction frequencies (Zavattero, 2019).

1.5. Challenges *and solutions* of setting up AquaPaillons

To this date, the AquaVar DSS tool has been used in several technical applications related to groundwater resources and extreme floods management in the Var catchment (Ma & Gourbesville, 2020). However, other parts of the MNCA including the Paillons facing similar issues are not covered. Hence, the tool can be extended to the Paillons to address the risk of urban flooding and fill the gap in knowledge of the dynamics of the unconfined aquifer.

To develop a similar tool for the Paillons catchment, specificities of the study area must be considered. The main issue with the Paillons is flooding. In 2000, 2014, and 2019 major flood events caused damages to infrastructures in the Lower Paillons River (LPR) and its valley. Existing monitoring systems are used to manage water-related issues, but gaps and errors in collected information are present. The unconfined aquifer is used by some neighborhoods for drinking and by a few industries. Its dynamics are not well known due to lack of monitoring information (Tennevin et al., 2017). The surface hydraulic component of AquaVar is based on open channel modeling. Game et al. (2023) studied open channel modeling of the LPR. The study showed the possibility to reproduce flow processes and inundations maps by representing the covered portion of the river as open channels. However, in real-time, pressurized flow or clogging that may happen cannot be considered. Also, the geometry of the covered river (CR) is not respected, therefore the effect of the artificial underground waterways reaching maximum capacity is not integrated. Other challenges include the high computation time needed to accurately represent the riverbed with 2 m mesh size. With such fine resolution riverbed, more computing power is needed for the tool to be integrated into a real-time forecasting system. Maintenance of such tool like updating river geometry or recalibrating models will require even greater resources.

Unlike the Var river, the LPR is partially covered. Within the riverbed, two retention storages exist. On the left bank, an underground road can be flooded and reduce flood risk in urban Nice (Figure 20). In fact, in urbanized areas where space is limited, Covered River (CR) and underground roads are used to create more space on the surface for urban development, on one hand. On the other hand, they are useful for flood reduction and making urban spaces safer. The steep tributaries of the river and densely urbanized floodplains present a challenge for runoff water management. Approximately 16 km^2 area is channeled into the urban drainage network. Sediment deposition is a significant problem for the LPR, while erosion is prevalent in its steep tributaries. The riverbed channelization further exacerbates these issues. The region's geological layers consist mainly of marls and limestone, which provide irrigation and industry with groundwater (Le Gouz de Saint-Seine, 1995; Tennevin et al., 2017). Extreme events from September to February are common. Every year, the river is dredged to reduce flood risk and to replenish the nearby beach which is exposed to winter coastal erosion. Consequently, a flexible model that can integrate frequent and localized changes in the riverbed geometry will be an efficient tool for real-time flood modeling.

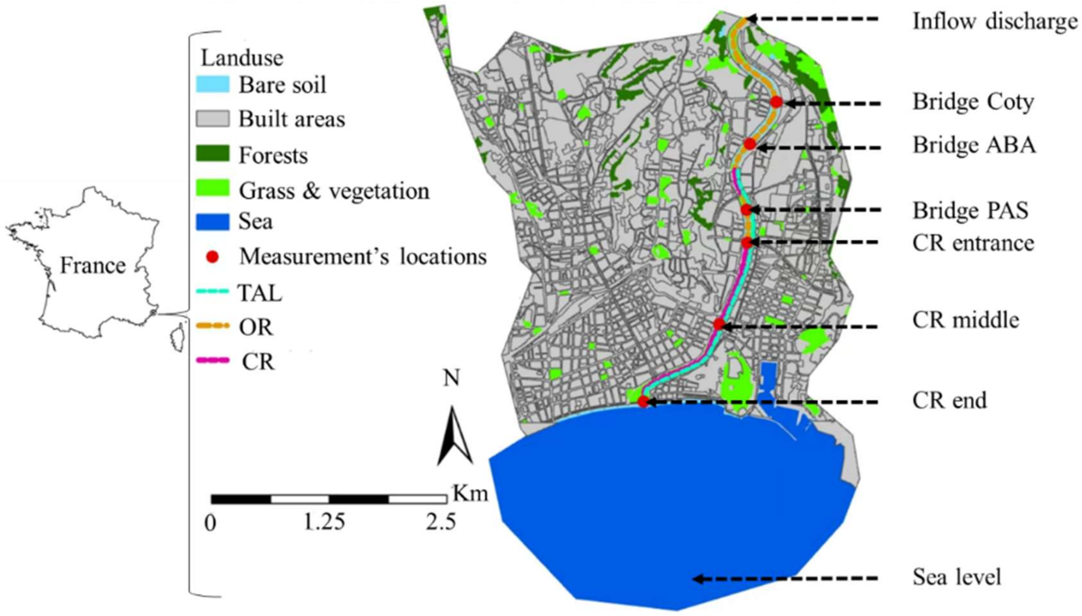

Figure 20 Lower Paillons River crossing the urban centre in Nice, France

Due to the need to extend AquaVar DSS to the LPR and the capabilities of DHI Mike tools to meet the specific modeling objectives for this river, the surface hydraulic model based on DHI MIKEPlus will be used for the LPR. The DHI MIKEPlus integrates modules for 1D and 2D surface models, collection systems and rainfall-runoff modeling. Coupling 1D-2D has been applied to river networks, urban drainages and urban flood zones. (Li et al., 2018; Salvan et al., 2018; Zavattero, 2019). Depending on the modeling objectives, each approach can generate useful information for management purposes. Input data required for the MIKEPlus includes topography, land-use, runoff, and weather information. The modeling results generated by this tool are used in flood management activities, and it can be coupled with hydrological and groundwater modeling tools like DHI Mike SHE and Feflow. This coupling enables the assessment of flood extents and river-aquifer exchanges. When monitored runoff data are not available or of low quality, hydrological modeling results are used as inputs to hydraulic models. Many parameters required for model set up can be retrieved from literature, and calibrated sets of parameters can be obtained for areas of interest (DHI, 2023a, 2023c, 2023b).

However, real-time validation of modeling results is only possible with available discharges and water depths estimates. With large gaps and errors in available records, other sources of information for validating measurements in real-time should be explored. Available videos records have not been used up to now to quantify flow characteristics and fill the gaps in records. In the context of growth in data collection, optimizing the use of available information is highly needed. While rainfall-runoff modeling is the central part of the DSS tool, the use of image-based estimates of floods can provide additional insights to the understanding of complex hydraulic processes in the Paillons.

1.6. Theoretical background of image-based estimation of river discharge in real-time

Image-based river discharge estimation is an alternative approach to improve the quantification of flood events in real-time (Ansari et al., 2023; Chahrour et al., 2021; Eltner et al., 2020; Farnoush & Maghrebi, 2023; Hauet et al., 2013; Lu et al., 2023; Tauro et al., 2019). This technic is not only useful in places where there is a lack of gauging stations, but also in places where growth and gaps in data collection are challenging. The principles of Particle Image Velocimetry (PIV) analyse the cross-correlation of image patterns to estimate flow. However, estimation of discharge from video images requires knowledge of water depths, the geometry of the river and estimates of average velocities.

Several assumptions are needed to estimate average velocities. A velocity index for a power law is used to link surface velocity to average velocities. This index depends on the shape of the vertical velocity profiles and the distance from the banks. An alternative method is the use of information entropy. In this case, velocity profiles are derived by maximizing the entropy function of surface velocity and two Lagrange multipliers. In contrast with PIV, a Eulerian method, the Particle Tracking Velocimetry (PTV) is a Lagrangian method which generates particle trajectories, velocities, and velocity gradients. But with 2D velocity distribution, the isovel pattern in the cross-section is assumed. With such assumptions, discharge quantification is possible with images of surface velocity and elevation (Chahrour et al., 2021).

Fudaa-LSPIV (Hauet et al., 2013) is a software for processing sequential images to estimate surface velocity fields and discharges through cross-sections by assuming a coefficient linking the surface velocity to the depth-averaged velocity for each calculation step; and interpolating the velocities towards the edges according to the hypothesis of the Froude number varying linearly towards zero at the edge. The discharge is then estimated based on the method of the median section. The tool uses the Large-Scale Particle Image Velocimetry (LSPIV) technique. It measures the 2D surface velocity field from visible tracers (plant debris, small floaters, etc.), bubbles or turbulence figures by cross-correlation statistical analysis of images. This method is derived from the PIV used in the laboratory, but for a study on large-scale objects such as rivers.

The main principles of LSPIV presented in Jodeau et al. (2022) include:

- Image Capture:

LSPIV involves cameras positioned strategically to capture images of the water surface. These cameras are typically mounted at an elevated location overlooking the region of interest.

- Image stabilization:

According to Jodeau et al. (2022) stabilization is employed to eliminate the impact of camera motion on the scene. The transition from one frame to another can be represented using a geometric transformation, encompassing rotation, translation, zooming, or more intricate models. The concept revolves around implementing the inverse transformation on the second image to effectively counteract the motion. The primary stages involve identifying key points within the two frames, aligning these points, determining the geometric transformation, and rectifying the motion. The user defines a “flow area” that is free of key points to perform stabilization on the river banks (Figure 21).

Jodeau et al. (2022) explained that prominent features within an image, such as "edges" or "corners," correspond to regions where there are significant fluctuations in intensity (gradients). The SURF library (Oyallon & Rabin, 2015) is harnessed for key point extraction. The approach involves isolating points in which intensity variations are pronounced in both horizontal and vertical directions. This selection is achieved by using the determinant of the Hessian matrix (second derivatives):

$$\mathbf{DoH} = \boldsymbol{det}\begin{pmatrix} \frac{\mathbf{d^2I(x,y)}}{\mathbf{dx^2}} & \frac{\mathbf{d^2I(x,y)}}{\mathbf{dxdy}} \\ \frac{\mathbf{d^2I(x,y)}}{\mathbf{dxdy}} & \frac{\mathbf{d^2I(x,y)}}{\mathbf{dy^2}} \end{pmatrix} \qquad \text{Eq. 26}$$

where I is the intensity of the pixel at the point of coordinate (x, y). The key points selected correspond to where the DoH is above an automatically defined threshold t_H.

Figure 21 Source image and defined flow area (Jodeau et al., 2022)

According to these authors, after obtaining the key points, the next step involves establishing correspondences between them across different frames. This task is accomplished using the SURF descriptor, which serves as a unique "ID" for each point. This descriptor encompasses essential information, including the point's scale (or "size"), its orientation, and the distribution of gradients within its local vicinity. The size of the point determines the extent of its neighborhood, while gradient directions are measured relative to the point's orientation. Due to these inherent attributes, the SURF descriptor remains unaffected by rotations, translations, and zooming, ensuring its robustness. Matching is carried out by pairing key points that share the same descriptor. The process of matching is illustrated in the accompanying image using red lines. Although the matching process is generally accurate, errors known as "false matches" can occur. To mitigate such errors, the ORSA method (Moisan & Stival, 2004) is employed. This approach relies on a stochastic process that incorporates constraints from epipolar geometry.

As stated in the user manual of Fudaa-LSPIV, now, two sets of matched points are obtained, signifying that the positions of each point on frames 1 and 2 are known. The current objective revolves around establishing the homography H that characterizes the relationship between positions X and X'. In the realm of image processing, linear transformations, such as affine or projective models, is typically considered. Linear transformations uphold properties like parallelism, angles, and ratios. In the case of affine models, only parallelism is maintained, while projective models encompass a broader range of transformations, sacrificing these properties. Despite its sensitivity, the projective model is optimal for representing perspective effects and capturing alterations in the camera's viewpoint. Each individual point serves as a control point, guiding the determination of coefficients within the homography matrix. The process involves estimating these coefficients using the Direct Linear Transform (DLT) method. Since the system lacks a unique solution, the "best solution" that aligns with the control points is selected (Jodeau et al., 2022).

The H matrix derived previously is used for image transformation. This approach adheres to a conventional framework in image processing, facilitating the management of spatial discretization within the image—where pixel indices are integers. The process involves determining the inverse matrix that converts X' to X, traversing pixels within the X' image (the image to be rectified), and applying the inverse transformation to the coordinates of the processed pixel (i,j), which are integers, to obtain the corresponding real coordinates (i',j'). Subsequently, a bicubic interpolation technique (using Hermitian splines in two dimensions) is employed. This interpolation method is used to ascertain the intensity value at the integer coordinates (i',j') based on the surrounding real values (Jodeau et al., 2022).

- Orthorectification:

An orthoimage is a depiction that has been adjusted to eliminate the impact of perspective and is proportionally scaled to correspond with the real world within a specific plane. In the context of LSPIV analyses, the objective is to orthorectify the surface plane of the flow, assuming that the flow is essentially flat. This plane can be mathematically described using X and Y coordinates as $Z=b_1X+b_2Y+b_3$. The longitudinal and transverse slopes on the scale of the capture are assumed negligible. In addition, the actual coordinate system is framed in relation to the river's plane (with the

XY plane running parallel to the river's plane). Thus, the plane equation is simplified to $Z=b_3$, where b_3 represents the free surface height in the real-world reference, denoted as h.

The process of constructing orthoimages involves the following 4 steps. The first step is to establish the region of interest within the real-world reference, specifically defining the (X,Y) coordinates for the four corners of the orthoimage. This task is performed within the Orthorectification menu. Then, the algorithm samples this designated region with a specified resolution to generate a grid. Each node within this grid serves as the central point for a pixel in the orthorectified image. For every grid node with coordinates (Xi, Yi), compute the corresponding coordinates (ii, ji) within the source image. These calculated coordinates (ii, ji) are represented as real numbers rather than integers. Associate each central pixel (Xi, Yi) with a grayscale intensity, determined by the pixel (ii, ji) in the source image. Given that the coordinates (ii, ji) are real values, a cubic convolution interpolation is employed to define the grayscale intensity based on neighboring pixels (Jodeau et al., 2022).

- Tracer Particles:

Tracer particles, often in the form of neutrally buoyant materials, are introduced into the flow. These particles move with the water, allowing their motion to be used as an indicator of fluid velocity (Jodeau et al., 2022).

- Particle Tracking:

Advanced image processing techniques are used to track the movement of tracer particles between image frames. This involves identifying and tracking individual particles' positions in consecutive images (Jodeau et al., 2022).

- Displacement Calculation:

The displacement of tracer particles between frames is used to calculate the fluid velocity vector at each measurement point. This is typically done using algorithms that consider the spatial and temporal scales of the flow (Jodeau et al., 2022).

An analysis of statistical cross-correlation is executed on the orthorectified images to ascertain the displacement of discernible tracers present on the surface. The Fudaa-LSPIV software employs a specialized algorithm optimized for extensive spatial scale applications, accommodating potentially lower image resolutions. The cross-correlation computation occurs between two images, separated by a time interval of Δt seconds, involving an interrogation window (referred to as IA or interrogation area). This IA is centered on a point a_{ij} within the first image and on a point b_{ij} within the subsequent image. The sizing of the interrogation window is adjustable within the Fudaa-LSPIV software. The correlation coefficient $R(a_{i,j}, b_{i,j})$ is computed through the following equation:

$$\mathbf{R}(\boldsymbol{a}_{\boldsymbol{i},\boldsymbol{j}}, \boldsymbol{b}_{\boldsymbol{i},\boldsymbol{j}}) = \frac{\sum_{i=1}^{M_i} \sum_{j=1}^{M_j} \left[(A_{i,j}-\overline{A_{i,j}})(B_{i,j}-\overline{B_{i,j}})\right]}{\left[\sum_{i=1}^{M_i} \sum_{j=1}^{M_j} (A_{i,j}-\overline{A_{i,j}})^2 \sum_{i=1}^{M_i} \sum_{j=1}^{M_j} (B_{i,j}-\overline{B_{i,j}})^2\right]^{1/2}} \qquad \text{Eq. 27}$$

where, M_i and M_j denote the dimensions of the interrogation window in terms of pixels, while A_{ij} and B_{ij} represent the pixel intensity distributions within the respective interrogation windows. This computation is selectively carried out solely for b_{ij} points situated within a user-defined search window (referred to as SA or Searching Area), thereby optimizing computational efficiency.

The assumption is made that the most likely displacement of the flow from point a_{ij} over the time interval Δt corresponds to the correlation maximum. This allows for the potential specification of a minimum required correlation level (Jodeau et al., 2022).

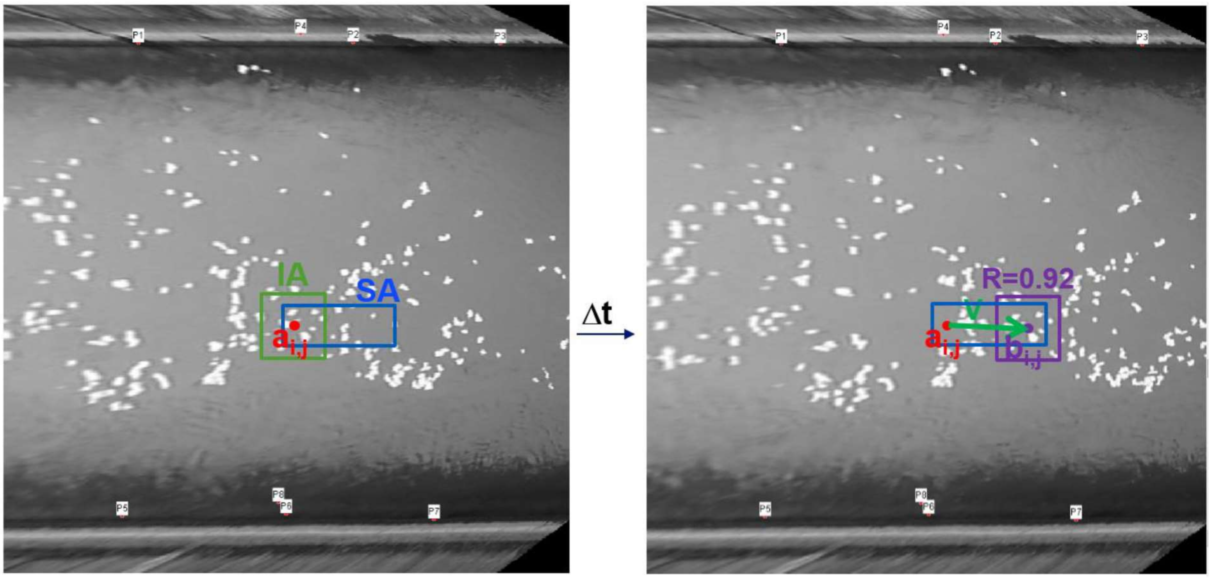

Figure 22 Searching area and area of interrogation in the Fudaa-LSPIV (Jodeau et al., 2022).

Given that the calculation's accuracy is limited to the nearest pixel, it becomes advantageous to implement sub-pixel interpolation. The model considers $b_{i,j}$ as the location of the correlation's peak. Within Fudaa-LSPIV, a refinement process using a one-dimensional Gaussian distribution is applied along the i and j axes. This method facilitates a displacement precision of approximately 0.2 pixels. The sub-pixel position of the correlation maximum is therefore calculated. The surface velocities are calculated from the displacements divided by Δt. The calculation is reproduced by iteration over the whole image for each node of the calculation domain. A surface 2D velocity field, "instantaneous" (between two successive images), is thus calculated. Fudaa-LSPIV allows the application of filters to eliminate aberrant velocities resulting from the statistical calculation. Filters on the smallest value of the correlation coefficient, on the amplitude and the direction of the flow velocities are integrated in the software. Finally, Fudaa-LSPIV permits to average the filtered instantaneous velocity fields to compute a velocity field averaged over the duration of the image sequence (Jodeau et al., 2022).

- Discharge calculation:

Considering the bathymetric profile of at least 1 cross-section incorporated in the assessment area, Fudaa-LSPIV can calculate the flow passing through this section. At a time step defined by the user, the bathymetric transect is interpolated, and a surface velocity is computed for each step from the closest LSPIV surface velocities (distance-weighted). The user also defines a coefficient linking the surface speed to the depth-averaged speed for each calculation step. The flow is then computed by using the method of the median section, with the interpolation of the surface velocities towards the edges executed according to the hypothesis of the Froude number varying linearly towards zero at the edge (Jodeau et al., 2022).

LSPIV is more suitable for surface flows where particles can be tracked optically. It may not capture three-dimensional flow information or complex flows near boundaries as effectively as other methods. It is well-suited for low- to moderate-velocity flows, such as those encountered in rivers, streams, and open channels. It may not be ideal for high-velocity or turbulent flows. Overall, LSPIV offers a non-intrusive, cost-effective, and efficient method for obtaining velocity information over a large area in natural water bodies, contributing to our understanding of fluid dynamics and hydrological processes (Jodeau et al., 2022).

Conclusion

The AquaVar DSS tool has been developed since 2014 through three thesis research projects and several applications. This tool successfully optimized management of collected data and provide useful information for real-time management of water hazards and resources. However, other parts of the Nice metropolis including the Paillons facing similar issues are not covered. Hence, the tool can be extended to the Paillons to address the risk of urban flooding and fill the gap in knowledge of the dynamics of the unconfined aquifer. The extension to the Paillons will require addressing specific needs of the Paillons. Large gaps and uncertainties may require the use of ANN through commercial software like NeuroShell 2 to further improve modeling results.

The DHI MIKEPLUS 1D-2D coupled overland and river network modules are suitable for the Lower Paillons River. MIKE SHE and Feflow will remain the parts that deal with rainfall-runoff and groundwater flow.

Exploring the use of video monitoring will provide additional information for real-time validation of modeling results and management of flood events.

Chapter II. The Paillons catchment and its lower valley in the Mediterranean region: state of the art, data & context

Introduction

In the last two decades, Nice Metropolis and its catchments have experienced at least 6 major extreme flood events. Local and national decision makers have declared these events to be natural disasters each time (examples: Nov. 2000, Jan. 2014, Nov 2019, etc.) (Tennevin et al., 2017). Since 1983, 73 disasters have been officially recorded in Nice (Observatoire des Territoires, 2021). This is not a localized problem as floods and droughts occur regularly around the globe and climate change is making these extreme weather events more intense (Abbass et al., 2022; Schwarz & Soubeyroux, 2022). The southeastern region of France, where Nice is located, is particularly exposed to extreme weather events such as the October 2020 Alex storm (Carrega & Michelot, 2021; Chochon et al., 2022; Gourbesville & Ghulami, 2022; Lanini et al., 2022; Payrastre et al., 2022; Pons et al., 2022).

In order to issue a disaster decree, decision makers rely on forecast data, field observations, and past experiences. Monitoring and modeling play a central role in water hazards management (Henriksen et al., 2018). The Paillons catchment has had a weather and flood monitoring system since 1983, but the growth in monitored data presents challenges such as gaps and errors. Every year, gauging stations break down after flood events and in some periods, erratic values are measured. The current real-time models used in the Paillons catchment are based on upstream runoff observations and water absorption capacities of the soil. But gaps in upstream monitoring make those models useless. Only few events have complete runoff records (Le Gouz de Saint Seine, 1995). To worsen the picture, few information exists on direct recharge to groundwater and interactions with surface runoff. To address these challenges, it is necessary to explore alternative modeling methods that can optimize the management of data growth and provide useful modeling results. Luckily, the growth in rainfall and temperature records at national level is an advantage. National meteorological data can be used to fill the gap in local station data. An integrated approach to provide runoff, groundwater flow and river-aquifer exchanges is indispensable. Every time a monitoring system fails to give runoff information, a modeling system comes to the rescue. Unfortunately, models also rely on observed input data. For example, meteorological data required as input to deterministic hydrological model has gaps and uncertainties. What is the best way to deal with all these challenges?

A clear understanding of the characteristics of a Mediterranean watershed is required to answer questions about the complexity of hydrological processes, the particular features of extreme events, and the role of climate change. Additionally, to address gaps or lack of gauged data, an appropriate modeling strategy is needed (Du et al., 2016, 2018b, 2019; Gourbesville et al., 2016, 2018; Ma et al., 2016; Salvan et al., 2018; Zavattero, 2019; Zavattero et al., 2016, 2018). The chosen strategy should consider the characteristics of the study area, including its economic and cultural significance, land-use, and hydrogeology. National and local weather data providers such as Meteo-France and Nice Metropolis, as well as spatial data, constitute the basis of the modeling system. National weather information is sparse, and quality assessed. Local weather data is raw and well distributed within the catchment. Spatial data is available at 5m, 1m and 25cm resolution. Last but not least, Paillons catchment and its lower valley has a context. It is worth rediscovering its characteristics. It is a vibrant economic zone. The land-use is dominated by forest; but downstream is densely urbanized. It is definitely interesting to know more about its hydrology, geology, and hydrogeology. The main river flowing through the city up to the sea has evolved. Channelized, it still exchanges water with aquifers. The alluvial and karstic aquifers provide water resources for drinking and economic activities. Previous studies and reports highlight the state of the art of runoff modeling in a steep catchment and context of the Paillons (Archambaud & Berthet, 2021; Emily, 2000b; Emily & Tennevin, 2009; Le Gouz de Saint Seine, 1995; Pietri, 1955; Pline, 1991; Sabbion, 2016; Tennevin et al., 2017, 2018, 2019).

Mediterranean catchments have unique hydrological characteristics that are shaped by the Mediterranean. These catchments are also characterized by steep terrain, rocky soils, and a high degree of land-use/land cover changes, which make them challenging to model. Many models have been developed that are specifically tailored for Mediterranean catchments. Examples such as TOPMODEL, SWAT, HEC-RAS, MIKE SHE, MIKE 21FM and Feflow have been used in various applications such as flood forecasting, water resources management, and climate change impact assessment (Audra et al., 2006; Du et al., 2016, 2018b, 2019; Emily, 2000b; Gourbesville et al., 2016, 2018; Le Gouz de Saint Seine, 1995; Ma et al., 2016; Pline, 1991b; Salvan, 2017; Salvan et al., 2018; Zavattero, 2019; Zavattero et al., 2016, 2018). Physically based models like the Danish Hydraulic Institute (DHI) MIKE framework (MIKE SHE, MIKE 21FM and Feflow) have an advantage that it can reproduce complex hydrological processes at high degree of precision with coarse to fine grid resolutions using basic physics (Downer & Ogden, 2004; Frana, 2012). The AquaVar project in the Var catchment located in the Mediterranean region is an example the application of MIKE framework to runoff and groundwater flow modeling for real-time decision support systems (Gourbesville et al., 2018). However, in an ungauged catchment like the Paillons, there is no study concerning the MIKE framework for modeling extended period processes of runoff and exchange with alluvial groundwater. Indeed, further research is needed to improve the model's capabilities and to better represent the complex hydrological processes in the Paillons catchment.

This section aims at using literature review and data analysis to improve runoff knowledge in the Paillons catchment and help decision makers with pertinent insights. This will include local and regional climate aspects, water cycle and historical events in Paillons' region, modeling strategy, and context and data in Paillons catchment. It prepares the ground for modeling phases for flood risk and water resources management.

2.1. Review methodology

Figure 23 illustrates a framework of literature and data search methodology inspired from previous studies (Abbass et al., 2022). This chapter analyzed 70 technical reports,8 thesis manuscripts, and 50 research articles published between 1955 and 2022 on runoff modeling and the Paillons catchment. Most of the technical reports cover data and context in the Paillons catchment. Two thesis focuses on runoff and groundwater modeling in the Paillons. Four thesis explore deterministic modeling of runoff and groundwater in the Var catchment. Studies on the Var are presented in Chapter 1. One thesis highlights modeling flash floods in urban catchments in Nice area. Fifty percent of research articles emphasis the advantages and limitations of runoff models. There are several case studies with deterministic models. Modeling tools such as Mike Zero integrated different components of the water cycle. In a growing data records era, integrated models can help optimize management of collected data while reproducing complex hydrological processes. Studies in the Mediterranean catchments discuss challenges involving steep areas, karstic zones, and urbanization.

Extracted data include model parameters that are not available as field measurements in the area of study. Rainfall data is provided by Meteo-France and Nice Metropolis (MNCA). We obtained records for twenty-eight national stations and ten local stations for the periods 1921-2021 and 1989-2020, respectively. Groundwater information is scarce. Data analysis involves finding the characteristics of each dataset: trends, ranges, averages, etc. We also discussed data quality and implications for deterministic hydraulic modeling.

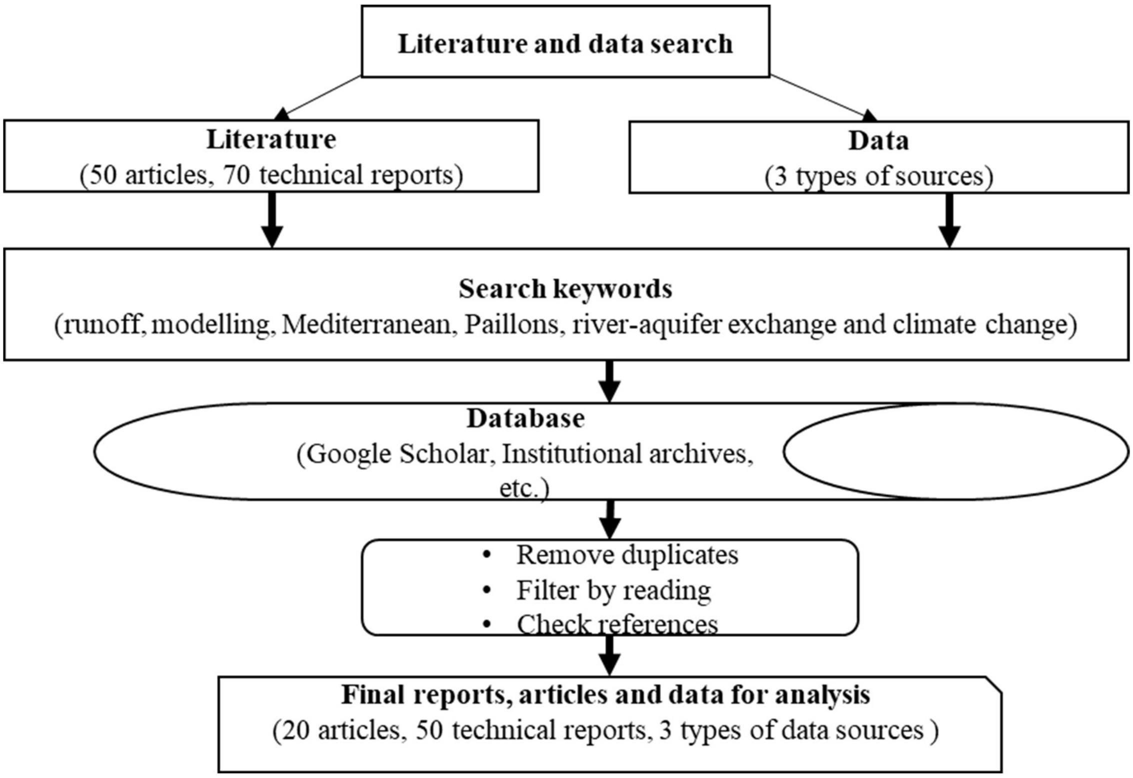

Figure 23 Framework for literature review and data analysis.

2.2. Previous studies in Paillons catchment and its lower valley

Prior investigations were conducted to evaluate the hydrology, the hydraulic and hydrogeology in the Paillons catchment and its lower valley (Archambaud & Berthet, 2021; Audra et al., 2006; Emily, 2000a; Le Gouz de Saint Seine, 1995; Pietri, 1955; Pline, 1991a; Sabbion, 2016; SIP et al., 2016; Tennevin et al., 2017, 2018, 2019a, 2019b). These studies relied on data analysis and numerical models. The aim was to improve the knowledge of surface runoff and subsurface flow processes, and guide management plans of flood risk and groundwater resources.

Le Gouz de Saint Seine (1995) carried out a study of the hydrology of the Paillons catchment by modeling rainfall-runoff and flood risk using physically-based distributed models related to the unit hydrograph approach. The review section gave information about historical events and the characteristics of the Paillons catchment. The models were developed to be used for estimating magnitude of flood for selected return periods based on design rainfall and forecasting floods based on observed or forecasted rainfall. This study used spline interpolation method to generate rainfall maps for daily simulations. For 6-mn simulations, kriging spatial interpolation was preferred. Runoff modeling focused on the main contributing sub-catchments. Due to data limitations, 40 rainfall episode were selected for model calibration and validation. A set of episodes were calibrated individually. Then another set was used for validation. There was no long periods simulations involving several years. For each event, an initial inflow discharge is assumed. Knowledge of baseflow in the Paillons is limited because the gauging stations are not precise enough to estimate low flow discharge and are sensitive to seasonal vegetation in the riverbed. An assumption is also made about the initial soil moisture content at the beginning of each episodes. The maximum observed discharge in the selected events was 165 m^3/s. Raw runoff data were smoothed to remove noise by averaging between t-18 mn and t+ 18 mn with t being the date. But the absolute maximal value of each event was preserved. The calibrated saturated hydraulic conductivity was 1.1 10^{-3} and 4.4 10^{-3} m/s for the two main subbasins. This modeling approach led to poor performance rates. The efficiency rate was less than 0.42. The author suggested running runoff simulation for at least several months to improve modeling results. Moreover, the flood risk assessments used the Bernoulli equations in stationary mode to estimate river capacity or overtopping thresholds at different locations. This approach does not apply in real-time events. Interestingly, the study was able to estimate flood return periods including the 10-year and 100-year floods at 260 and 800 m^3/s, respectively.

Research lead by Pline (1991) contributed in improving the knowledge about the unconfined alluvial aquifer of the lower Paillons Valley. This study proposed a reconstruction of the topography and the lithostratigraphy of the sedimentary basins. The alluvial zone is heterogeneous and can be divided into three layers vertically. A top layer with heterogenous permeabilities represent a shallow unconfined aquifer with depths ranging from 1 to 8 m. An intermediate zone or semi-confined and less permeable lies on top of the confined bottom alluvial layer. The piezometric level of the bottom layer is higher than the surface elevation. Any well in that layer is artesian as it brings groundwater to the surface without pumping. The overall depth of the alluvial formation varies between 1 and 70 m. The surveys carried out in Nice show varying permeability in the centre of Nice: silt (10^{-6}-10^{-7} m/s), gravel ($2x10^{-5}$ m/s); coastal deposits (10^{-3}-10^{-4} m/s). In the northern part of the city, higher permeabilities were measured between $5x10^{-4}$ and $2x10^{-4}$ m/s. The alluvial aquifer interacts with the karstic and conglomerate aquifers. The bedrock layer is made of impervious marls. Urbanization has dramatically decreased direct infiltration. However, river exchange with the unconfined aquifer is important.

Studies conducted by Archambaud & Berthet (2021) assessed the state of the art and the characteristics of the Paillons catchment with the aim of developing a new flood prevention plan. The initial phase of the study compared previous runoff modeling studies and focused on assessing the floods events of November and December 2019. The modeling results were not satisfactory due to challenges in defining initial conditions at the beginning of each flood event. Design rainfall events were used to estimate the 100-year flood magnitude of 794 m^3/s for the whole catchment.

Studies on the hydrogeology of the Paillons catchment lead by Tennevin et al. (Emily & Tennevin, 2009; Tennevin et al., 2017, 2018, 2019a, 2019b) provide useful information on geometry and characteristics of the geological layers. The permeability of the geological layers is indeed very variable, and results in an alternation of practically impermeable formations (clayey marls from Trias, Cenomanian and Priabonian), horizons with medium to low permeability (Senonians marly-limestone, Oligocene flysches and sandstones), and very rich groundwater units, generally limestone (Jurassic, Turonian and Lutetian). The distribution of underground flows and their final destination are governed by the geometry of aquifer reservoirs and by their relationship with the bordering impermeable units which condition the possibilities of deep water storage and the position of outlets. These situations are also regulated by the conditions of exchange that are established between the various reservoirs and with their immediate environment (rivers, coast). Due to its geological diversity and its great extension, the territory concerned by the study provides a wide range of hydrogeological structures: nummulitic aquifers (oligocene sandstone and eocene limestone), located exclusively in the northern and central sectors, at the right of the large synclines; the Jurassic and Cretaceous aquifers, which occupy the periphery and show a maximum development in the west, east and south sectors.

2.3. Regulations of water resources and hazard management in the Paillons catchment

As summarized in Zavattero (2019), to safeguard water resources and enhance flood risk mitigation, a range of tools have been devised across different scales in France in line with the European water policy (Figure 24). Specifically, in the Paillons catchment and its lower valley, where diverse water-related challenges exist, local governing bodies require a reliable mechanism to consolidate solutions aimed at attaining favorable quality and quantity conditions for all water bodies, while also addressing flood prevention measures. In fact, the local authorities have implemented a series of regulatory instruments, including the River contract, the Flood Prevention Program (FPP) [PAPI 2014], as well as the Plan for Flood Risk Prevention (PFPR) [PPRI 1999].

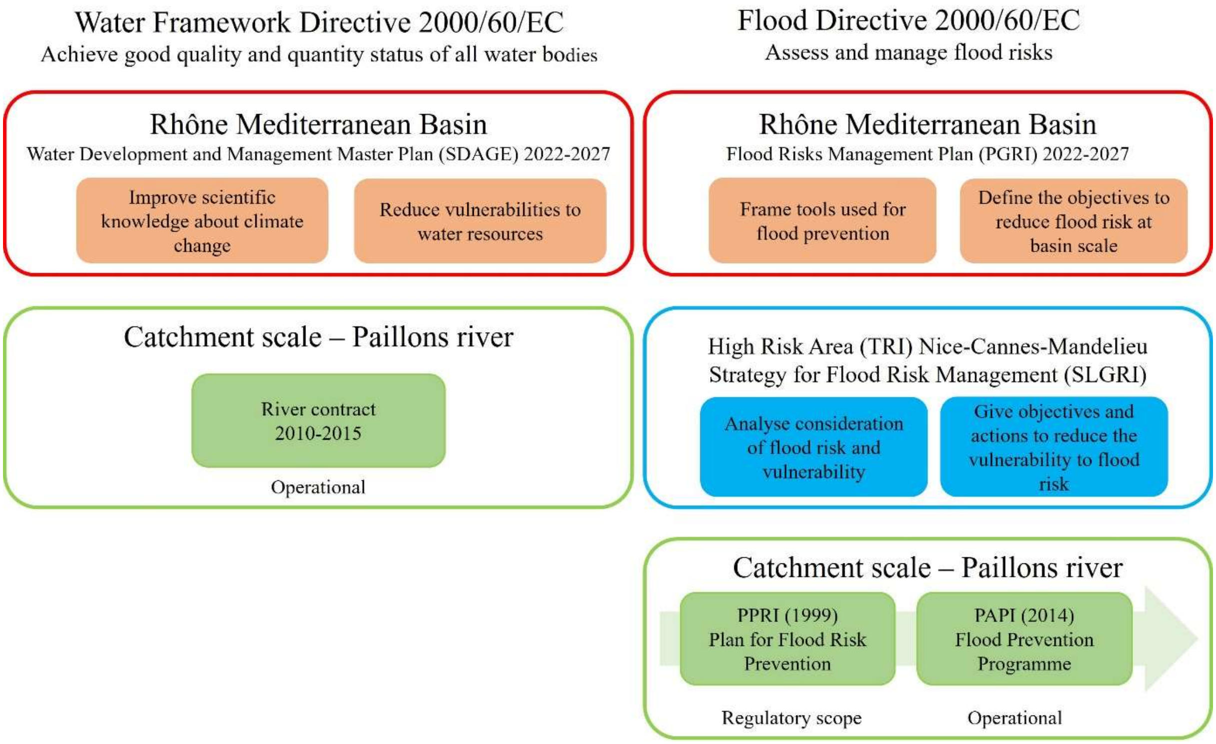

Figure 24 Different regulatory and operational tools used, in the Paillons catchment and its lower valley, to implement the European water policy (adapted from Zavattero (2019)).

The French water policy is shaped by a pair of European directives: the 2007 Flood Directive and the 2000 Water Framework Directive. These directives were formulated to propose approaches for addressing water-related challenges. The French legal framework has tailored its strategy to various levels, including the basin, catchment, and local scales (Zavattero, 2019). The Paillons catchment is located in the Rhône-Mediterranean Basin. To deal with the flood issue, a Flood Risks Management Plan (in French: Plan National de Gestion du Risque Inondation – PGRI) was implemented to reduce the vulnerability. For water resources, a Water Development and Management Master Plan (in French: Schéma Directeur d'Aménagement et de Gestion des Eaux (SDAGE)) has been updated for the period 2022 - 2027. In the Alpes-Maritimes department, a public institution such as SMIAGE was created to manage the water issues over the region. Several studies have been conducted to update the PFPR for the Paillons catchment.

To manage flooding risk, 2 tools were built in the Paillons: the Flood Prevention Program (PAPI) and the Plan for Flood Risk Prevention (PFPR). The latter is used as a regulatory framework, whereas the first one is an operational tool describing actions. The PFPR [PPRI 1999], being updated currently, provides recommendations for the development of communities in relation to the flood risk. This plan was built using a hydraulic study that provided flood hazard maps. The FPP [PAPI 2014] allowed improving resilience through preparedness programs and maintenance of existing and new flood protection infrastructure.

Consistent with the Water Framework Directive, a plan was designed in the River contract (Safege, 2009). The overall objective of this contract is to set up, in coherence with the Water Framework Directive and the future SDAGE, a global and sustainable management plan making it possible to make these human issues compatible with the preservation and sustainability of the resource and natural environments. It is a technical and financial contract between the French government, the local authorities and stakeholders (Zavattero, 2019). This operational tool permits supporting 62 actions distributed in 3 groups: essential actions (31) to be carried out to achieve good condition and regulatory compliance, actions (14) allowing the improvement of environments and local will actions (17).

2.4. Paillons catchment and its Mediterranean region in a changing climate

2.4.1. Past, present, and future climate aspects

The Paillons catchment is located in the Mediterranean region. The region is characterized by hot and dry summers, mild winters, and highly variable precipitation patterns, which are likely to be affected by climate change in several ways (Lionello et al., 2006). Higher temperatures are likely to lead to increased evapotranspiration (Rind et al., 1990), which will in turn lead to higher water demand and lower soil moisture, resulting in increased water stress for ecosystems and human populations. In fact, temperatures have been constantly rising by 0.3°C per decade in the Mediterranean region. Over the period 1959-2009, the region has shown an increase in average summer temperatures between +0.4°C and +0.5°C per decade. The hottest summer of this period was recorded in 2003. The rising trend of temperature has also been noted in winter, with an average increase in winter temperatures of +0.2°C per decade over the period 1959-2009.(DRIAS, 2023; Meteo−France, 2023a; Ribes et al., 2019; Schwarz & Soubeyroux, 2022).

In Provence-Alpes-Côte d'Azur (PACA), climate projections show continuous warming until the 2050s, whatever the scenario (Figure 25). Over the second half of the XXIst century, the evolution of the annual average temperature differs significantly depending on the scenario considered. The only one that stabilizes warming is the low emissions scenario (RCP2.6). According to the high emissions scenario (RCP8.5), warming could exceed 5.2°C by the end of the century. Average temperatures will increase in the PACA up to 2.1°C by 2030, 3.1°C in 2050 and 5.2°C in 2080. The summer would be the season most exposed to warming; spring, autumn and winter would also become subject to strong warming from 2080 (DRIAS, 2023; Meteo−France, 2023a).

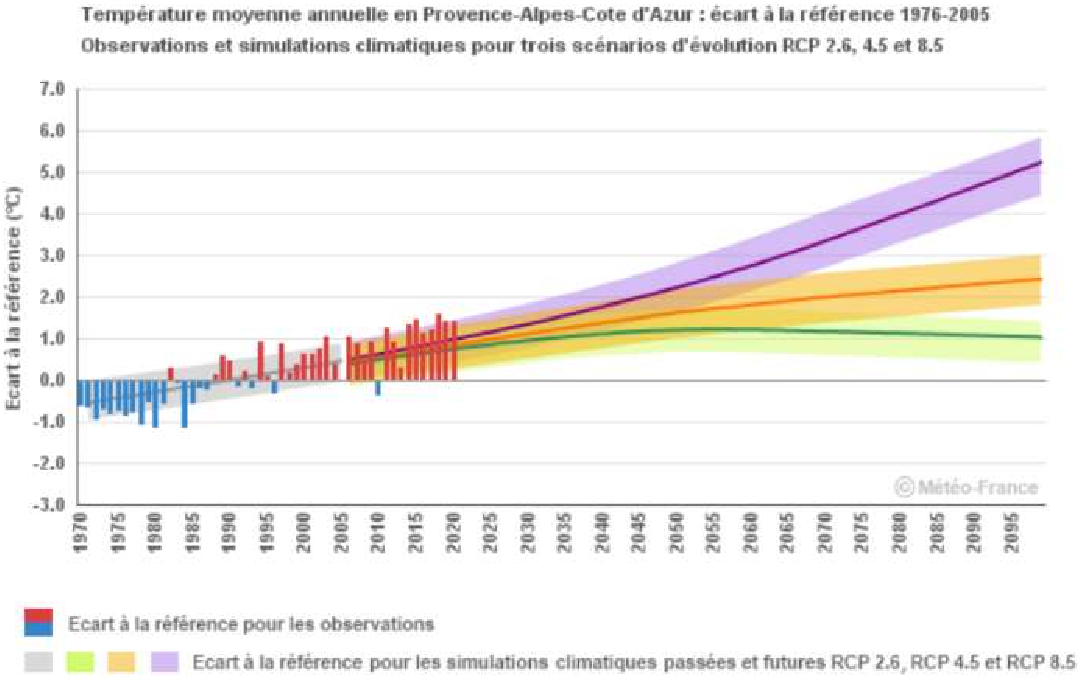

Figure 25 Average annual temperature in PACA (Meteo−France, 2023a).

The most extreme rainfall events (daily total over 200 mm) are frequent around the Mediterranean (Figure 26). The number of these events is also characterized by strong variations from one year to another. In Nice, annual rainfall has shown a slight decrease in totals since 1961 (Figure 27) (Meteo−France, 2023a; Ribes et al., 2019).

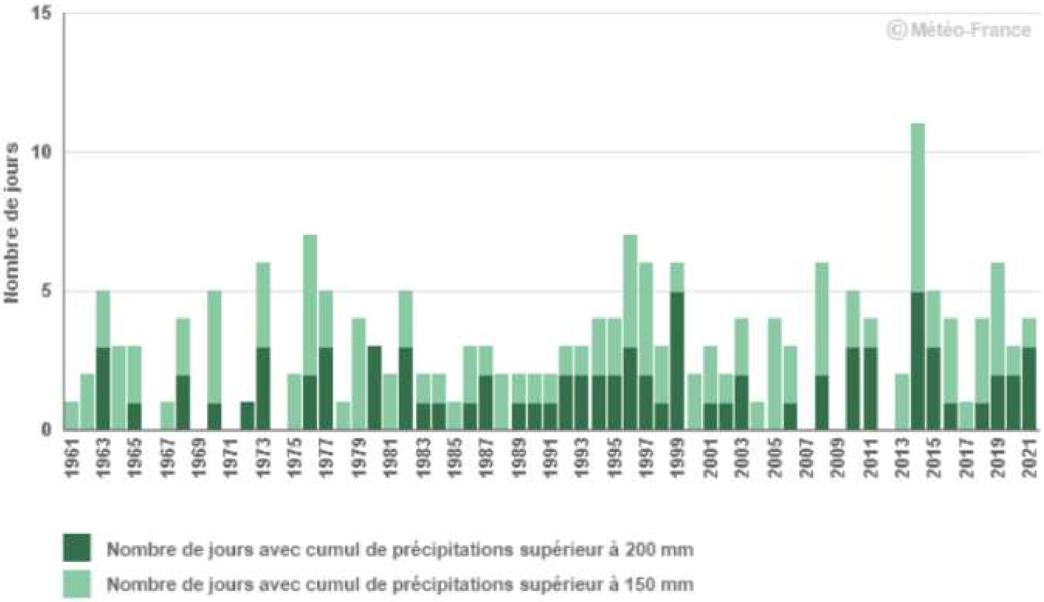

Figure 26 Number of days with cumulative precipitation greater than 200 mm (dark green) and 150 mm (light green) estimated with a network of 75 stations for monitoring extreme rainfall in the Mediterranean region (Meteo−France, 2023a).

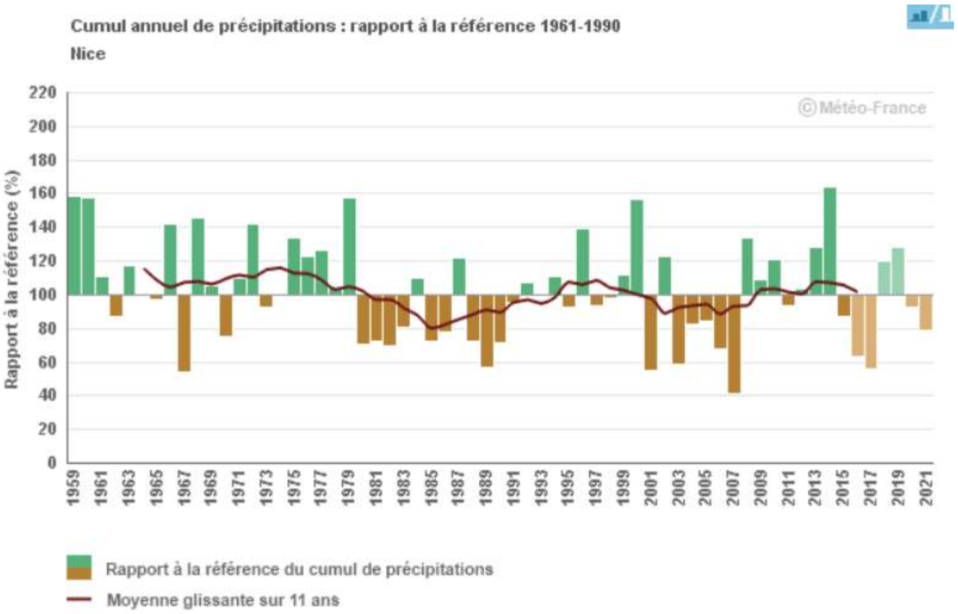

Figure 27 Maximum annual cumulative precipitation in Nice, compared to the reference 1961-1990 (Meteo−France, 2023a).

Regardless of this variability, climate projections indicate minor change in annual accumulations by the end of the XXIst century, for each emission scenario. On one hand, a more or less marked drop is expected in summer accumulations by the end of the century according to the scenarios of high emissions (RCP8.5) and moderate emissions (RCP4.5). On the other hand, little change is predicted in the low emissions scenario (RCP2.6) (Figure 28) (DRIAS, 2023; Meteo−France, 2023a).

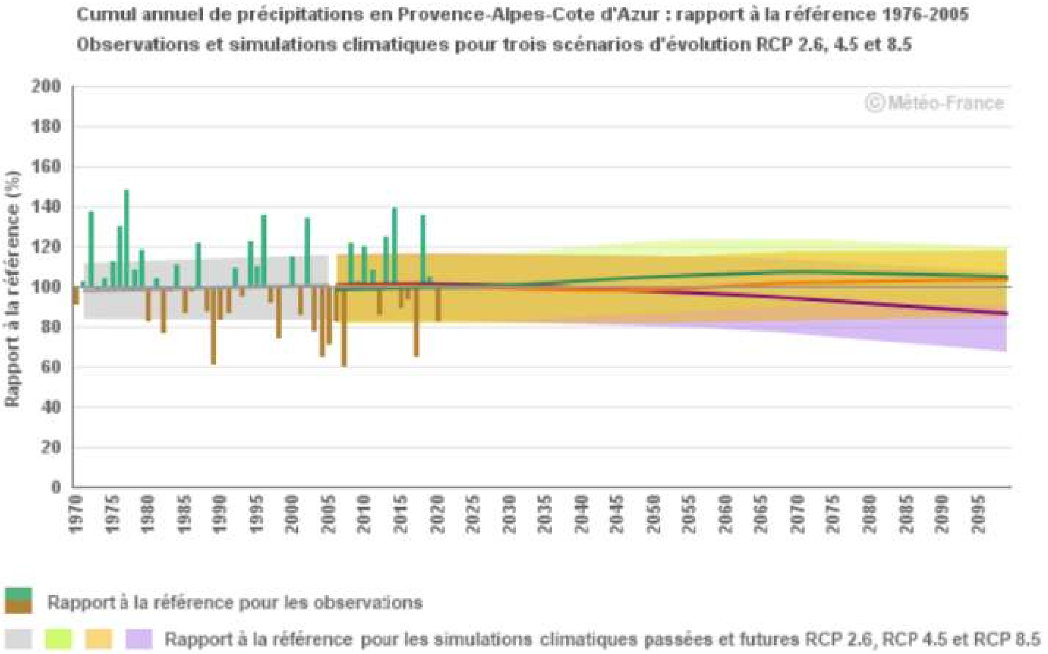

Figure 28 Climate change projections for annual precipitations in PACA, RCP2.6, RCP4.5 and RCP8.5 (Meteo−France, 2023a).

The projected future outcomes for precipitation in the PACA region vary in their forecasts. Nonetheless, most of the findings anticipate a notable reduction in the annual accumulated figures, particularly with a pronounced decline expected during the summer months. Such a trend could lead to heightened challenges in water resource management.

Comparison of the annual soil moisture cycle in PACA between the 1961-1990 climate reference period and the near (2021-2050) or distant (2071-2100) time horizons over the XXIst century (according to an SRES A2 scenario) shows significant drying in all seasons. In terms of potential impact for vegetation and non-irrigated crops, this change translates into an average lengthening of the dry soil period of the order of 2 to 4 months, while the period wet is reduced in the same proportions. It is noted that the average soil humidity at the end of the century could correspond to the extreme dry situations of today. The analysis of the annual percentage of the surface affected by soil drought since 1959 makes it possible to identify the years having experienced the most severe events such as 2017 and 2007. The evolution of the 10-year average shows the increase in the surface of droughts going from values of the order of 5% in the 1960s to more than 10% today (DRIAS, 2023; Meteo−France, 2023a).

In conclusion, the hydrological regime of Mediterranean catchments is likely to be altered, with potential impacts on the water resources availability, flood and drought risk and ecosystem services. Therefore, adaptation measures are necessary in the Mediterranean region to mitigate these impacts and to maintain sustainable water resources management. This justifies the urgency of better representing runoff and groundwater flow processes in the Paillons catchment.

2.4.3. Review of major extremes events

The Paillons catchment is part of the Alpes-Maritimes department, located in the southeast of France along the Mediterranean coast, which is known to experience a range of extreme meteorological events. The area is prone to high winds, heavy rainfall thunderstorms and storm surges that have caused significant damage and disruption (DRIAS, 2023; Meteo−France, 2023a; Observatoire des Territoires, 2021). It is worth noting that, while the Alpes-Maritimes department is not particularly prone to some of these hazards compared to other areas of the globe, the impacts of these events can be significant due to the high population density and the high economic value of the area.

The maximum 6-mn and hourly rainfall ever recorded are 22 mm and 115 mm on October 3rd, 2015. The highest daily record of 513 mm occurred on October 2nd, 2020. (Meteo−France, 2023b). Figure 29 maps out the daily rainfall distribution of 8 extreme events in the Alpes-Maritimes. The variability in most affected areas from one event to the other is noticeable. Any area of the region can potentially be affected by an extreme event. The Paillons catchment, located in the southeast of the Alpes Maritimes department has been more or less affected by each of these rainy events.

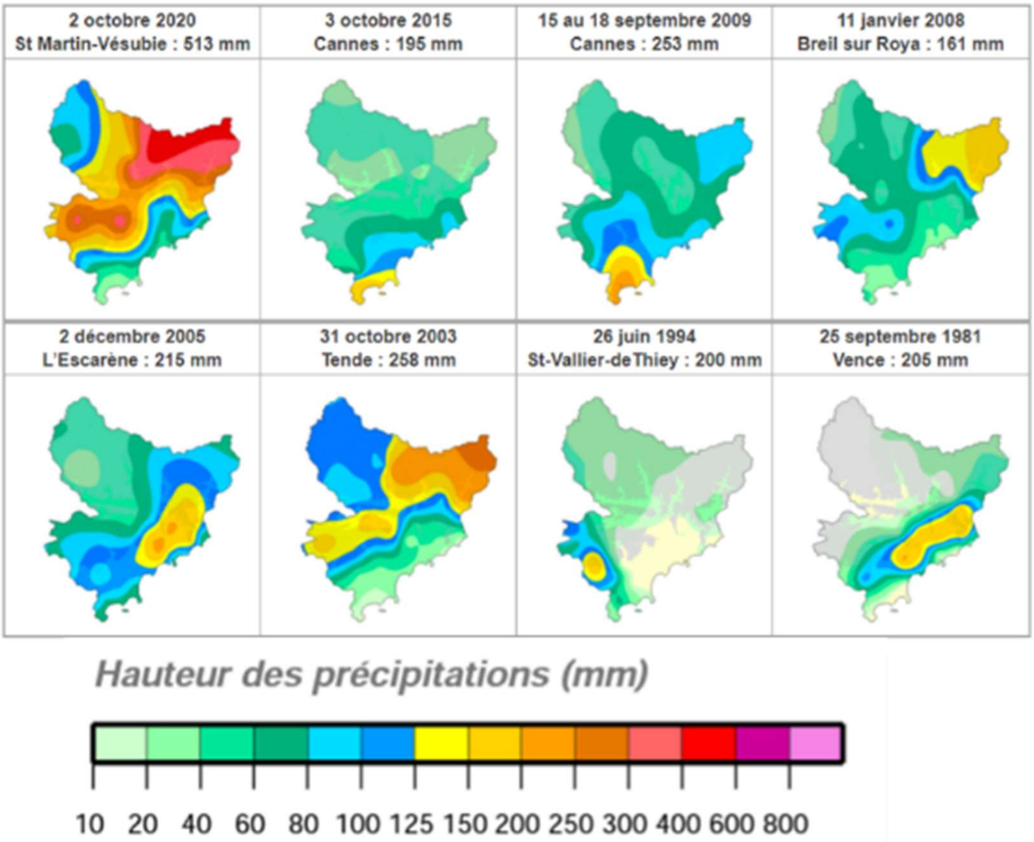

Figure 29 Cartography of the most remarkable daily rainy events in the Alpes-Maritimes (Meteo−France, 2023b).

The most significant floods of the Paillons river in Nice are: October 27th, 1882; November 10th, 1886; November 17th, 1940 ; April 25th, 1952; November 7th, 1957; October 14th, 1979; December 3rd, 2005; November 6th, 2000; January 17th, 2014; November 23rd, 2019, and December 20th, 2019. Since 1987, local water services have implemented monitoring systems that recorded some of these extreme rainfall events and their associated disasters. Figure 30 shows dates, extents and locations of damages caused by flood events in 1913, 1940, 1957, 1979, 1994, 2000 and 2019. The events in 1940 and 1957 have the largest flood extents. The river has been channelized and partly covered downstream over time. The most recent events mostly affected flood protection structures and bridges.

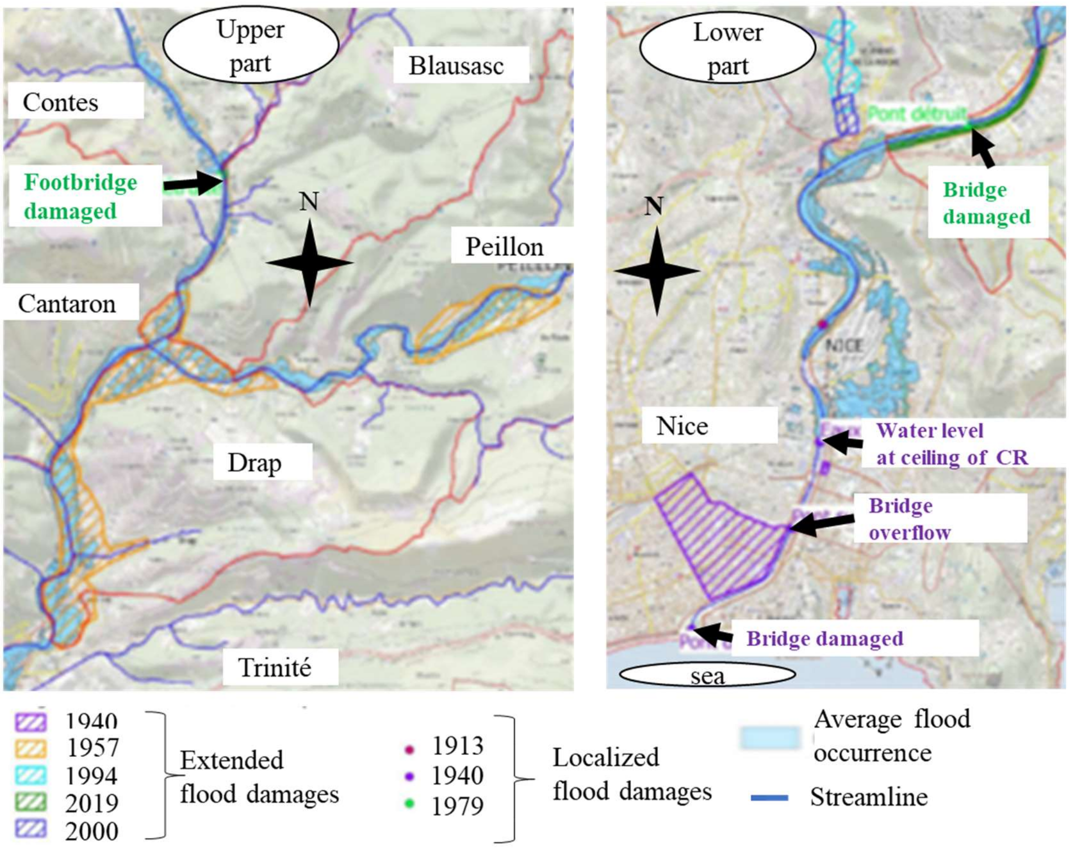

Figure 30 Map of flooded areas from 1913 to 2000 in Paillons river (adapted from Tennevin et al. (2017)). Water level at ceiling of covered river (CR) in 1940. The CR was later extended to the sea.

The flood event that occurred on November 6th, 2000 is one of the most important event of the last two decades which has available records. The flooding caused considerable damage to infrastructure and property, but no deaths (Figure 31). The event caused erosion of the banks along the watercourse, the creation of jams and localized overflows. Several sectors were concerned in the municipalities of Contes, Blausasc and Drap. A truck and a car were carried away by the waters in Contes. In Contes, two pedestrian footbridges were destabilized. The flood destroyed riprap at the "la Roseyre" industrial zone. A house was partly destroyed by erosion of the right bank. In Drap, the footbridge giving access to the Condamine building was destroyed and taken to the piles of the railway bridge. The downstream embankment of the RD2204 roundabout upstream of the Peille bridge was scoured over 8 m. The RD19 road in St-André-de-la-Roche was submerged, the right bank of the road damaged and many cellars flooded (Le Gouz de Saint Seine, 1995; Pline, 1991a; Tennevin et al., 2017).

Figure 31 Damages of flood of November 6th,2000 in the Paillons upper valley (www.cypres.org).

The flood of November 6th, 2000, was mainly caused by extreme rainfall of a return period estimated at 25-30 years. This event occurred in specific meteorological conditions. It was preceded by three significant rainfall episodes with two of more than 100 mm over a period of a month. A fourth episode cumulated 111 mm within 24 h. Moreover, high winds of 100 km/h generated tides of 4 to 5 m in the "Baie des Anges" and caused sea level to rise by 1 m. On November 5th,the rainfall started at 8:30 pm local time. The next day, November 6th,the event ended at 1 pm. Two rainfall stations recorded peak rainfall intensity of 6.2 mm and 5.2 mm within 6 mn.

There were discharge and water depths records available in printed pdf format documents (Figure 32 &Figure 33). Extraction from pdf document may have introduced additional uncertainties in data. ABA gauge did not exist until 2009 and PDE gauge was closed in 2007. At 4 of 8 gauges, complete time series of water depths show 2 m variation from baseflow on average. The smoothed peak discharge of 402 m^3/s at PDE in Nice was recorded at 11:06 am on November 6th. At TRI gauge located upstream of PDE, the recorded peak was 434 m^3/s which is higher than that of PDE. At PDR and LAC gauges, discharge was estimated at 88 and 156 m^3/s, respectively. The time to peak was estimated at 4 h. It should be noted that there are uncertainties in the rating curves used to calculate discharge in addition to uncertainties related to stage water depths measured at each gauging station. Moreover, 4 gauges did not have complete water depths records due to disfunctions.

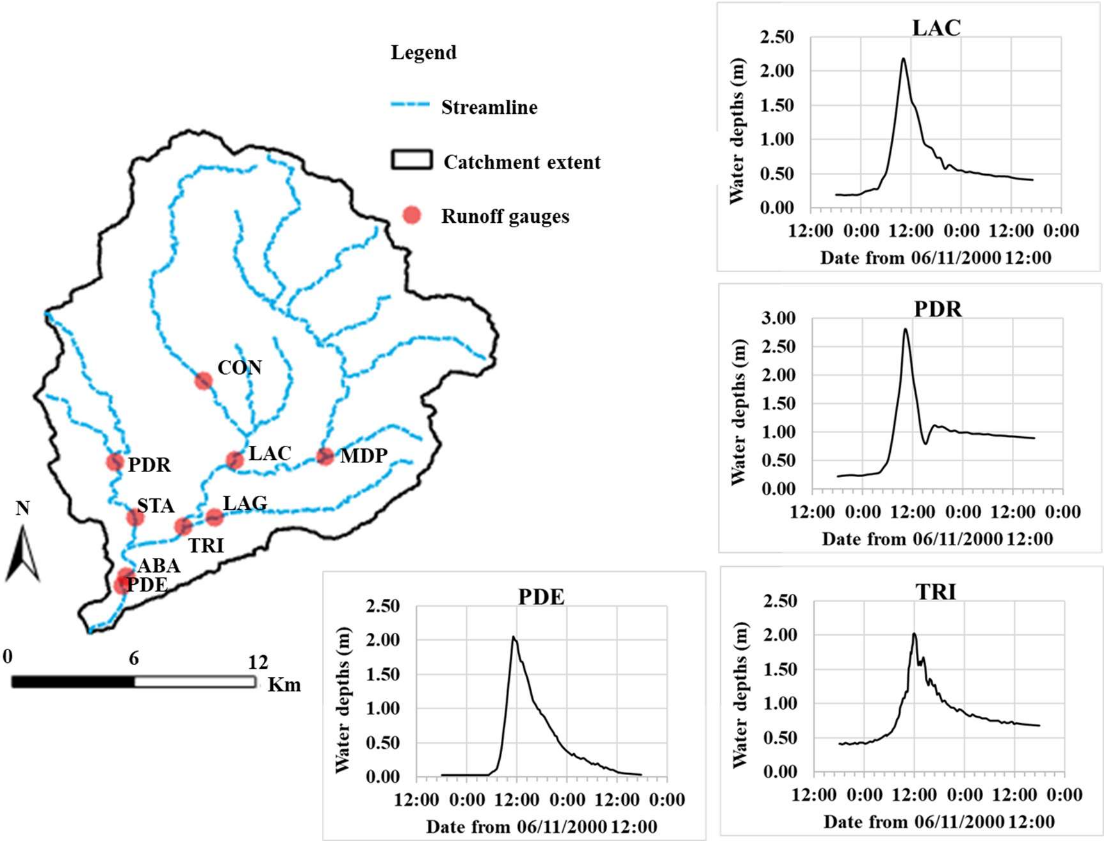

Figure 32 Water depths of flood event of November 6th, 2000, recorded at 4 gauges (PDE, TRI, PDR and LAC).

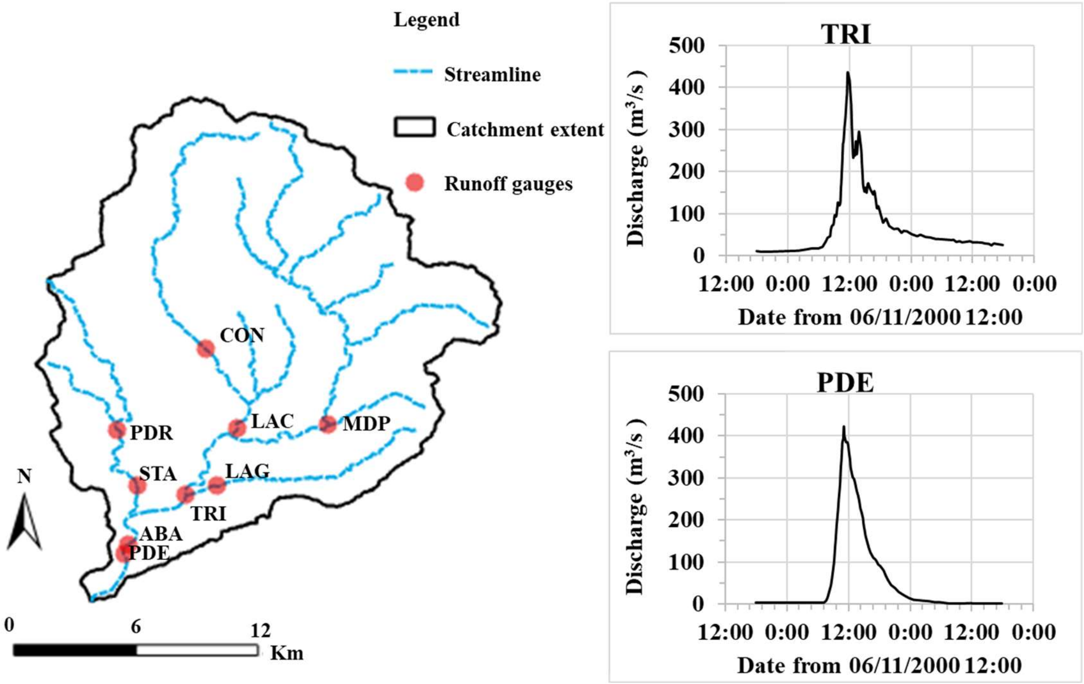

Figure 33 Discharges of flood event of November 6th, 2000, recorded at 2 gauges (PDE and TRI).

Another serious flood was recorded on December 20th, 2019. Compared to the November 2000 event, information is available as a spreadsheet with detailed information at 6-mn time intervals as opposed to being extracted from printed pdf documents like for the events in 2000. In fact, 9 national

(METEO-FRANCE) and 9 local (MNCA) rain gauges recorded the rainfall during the event. Previous studies showed that national rain gauges can be used to fill missing data in local stations and improve rainfall mapping. Runoff records were available at 10 gauges for water depths and 6 gauges for discharges (Figure 34). Runoff gauges are managed by MNCA. At the outlet, two new stations COTY and PAS provide water depths upstream and downstream of ABA gauge, respectively. The complex hydraulic environment on the last 3 km required additional runoff gauges. The covered part of the river also has measurement's locations (entrance, middle and end) not shown in the figure below. In recent years, data collection have increase to cover more sensitive areas in the Paillons catchment and its lower valley.

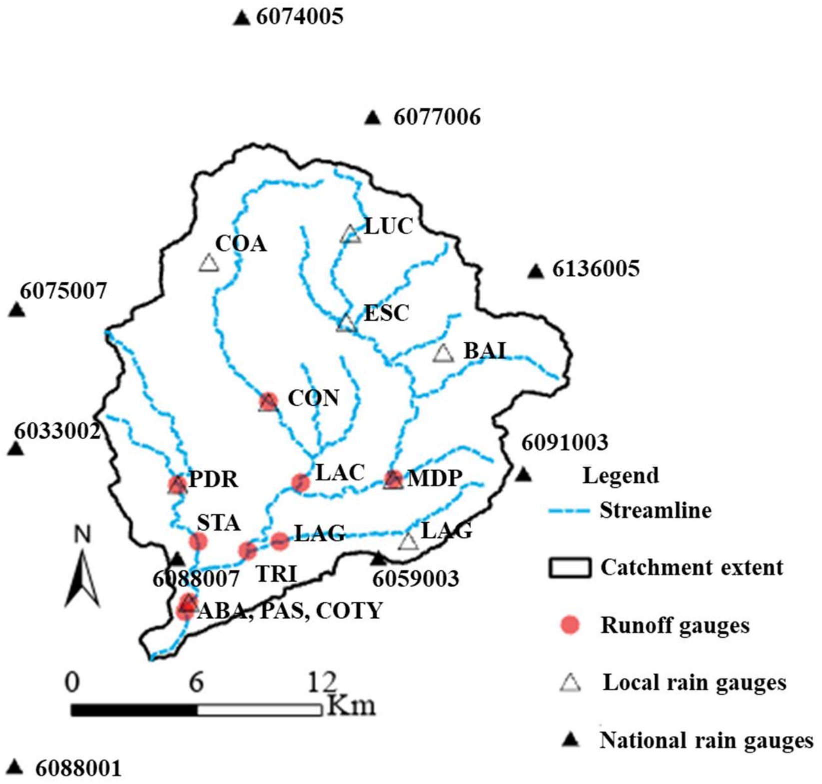

Figure 34 Available measured rainfall and runoff at 6-mn time intervals during flood event of December 20th, 2019. National gauges are managed by METEO-FRANCE, while local gauges are managed by MNCA.

The flood of December 20th, 2019, was mainly caused by extreme rainfall of a return period estimated less than 10 years. Compared to the previous event, this event also occurred in specific meteorological conditions. The October month received four important rainfall episodes: first event average cumulated rain 43 mm (max of local stations recorded at LUC is 92 mm); second event 46 mm (max at MDP is 79 mm); the third event 33 mm (max at CON is 41 mm) and the fourth event 40 mm (max at PDR is 52 mm). The maximum 6-mn rainfall was 14 mm for October. The November month also experienced several episodes. The event of November 2nd - 3rd generated an average of 55 mm of cumulated rainfall with a peak of 85 mm at ABA and 82 mm at MDP. It was followed by an event on 14th to 16th of November with an average cumulated rain of 72 mm (max recorded at LUC was 115 mm and 93 mm at MDP). The third event of November occurred on the 18th -19th. About 30 mm of cumulated rain was recorded on average with a maximum of 61 mm at BAI. The fourth episode started on 20th and lasted on the 25th with an average 206 mm and peak rain of 273 mm at BAI and a minimum of 155 mm at CON. The last event in November occurred on the 27th and recorded 39 mm on average with a range between 18 and 55 mm at local gauges. The most intense 6-mn record occurred on the 15th at 32 mm. For the episode of 20th - 25th,rainfall intensities were less than 5 mm in 6-mn time intervals. After these two rainy months, the December month had the soil saturated and any major event lead to an intense catchment response. At all local stations, rainfall recorded within 6-mn time intervals were less than 3.5 mm. Two important events occurred in December. The episode on 1st – 2nd generated a cumulus of 66 mm with peaks of 99 and 88 mm showing up at COA and LUC. The next heavy rainfall happened on 20th -22nd with on average cumulated 140 mm of rain and minimum of 95 mm at BAI and maximum of 177 mm at LUC.

Rainfall interpolation assessments of the flood of December 2019 used the map of the distribution in the Paillons catchment (Figure 35). The majority of the catchment was exposed to 120-150 mm of rainfall. The upper North and middle East parts received the highest rainfall between 150 and 240 mm.

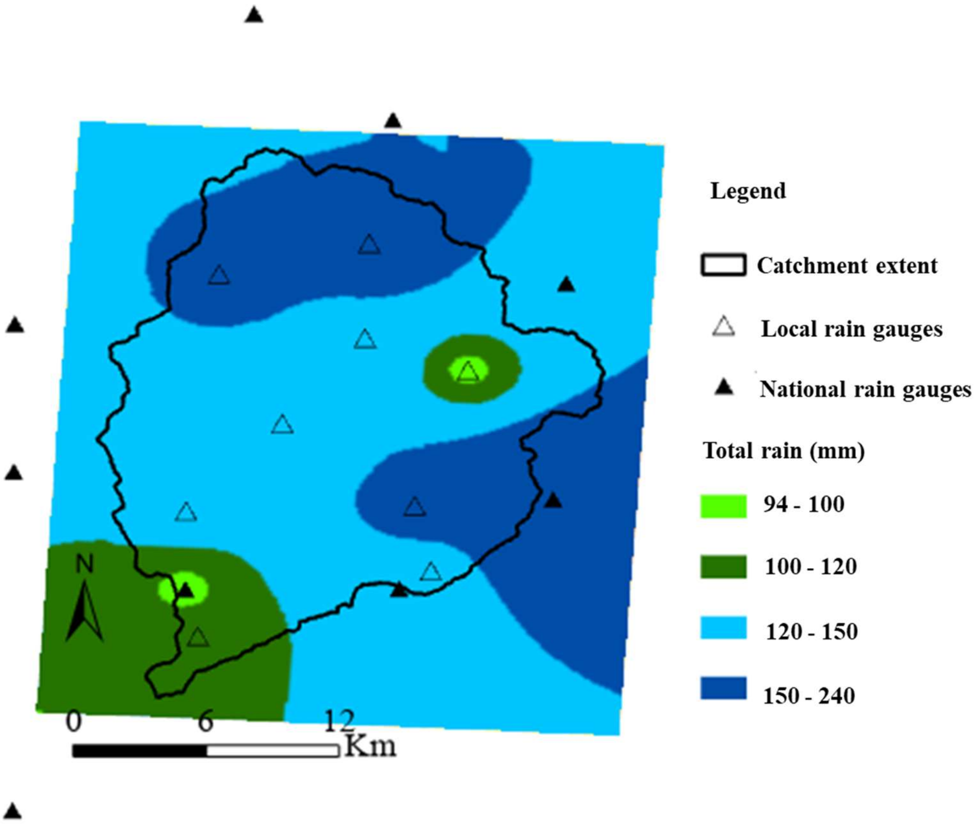

Figure 35 The total rainfall distribution map of the flood event of December 20th, 2019, over the Paillons catchment.

In Figure 36 & Figure 37 records of water depths and discharges for the gauging stations are displayed. The data was smoothed by averaging between t-6 min and t+6 min and repeating the process three times to remove noise which is often caused by free surface flow waves or seasonal vegetation near the runoff gauges. Ten gauges measured water depths variations less than + 2 m. The most downstream gauge shows variations less than that of November 6th,2000, +1.3 m against +2m. However, the outlet gauge location is not the same as in 2000. While water depths were recorded at 10 gauges, discharge is only available at 6 gauges. The maximum discharge is 184 m^3/s at ABA gauge. This is less than half of the flood event in November 2000 estimated at 420 m^3/s. PAS gauge in 2019 is the nearest to the PDE gauge in 2000. The difference in water depths is about 0.6 m. However, water depths are sensitive to the material transport and management in the riverbed. These factors are not included in the calculations of river discharges using rating curves. Therefore, uncertainties exist in observed flood magnitudes.

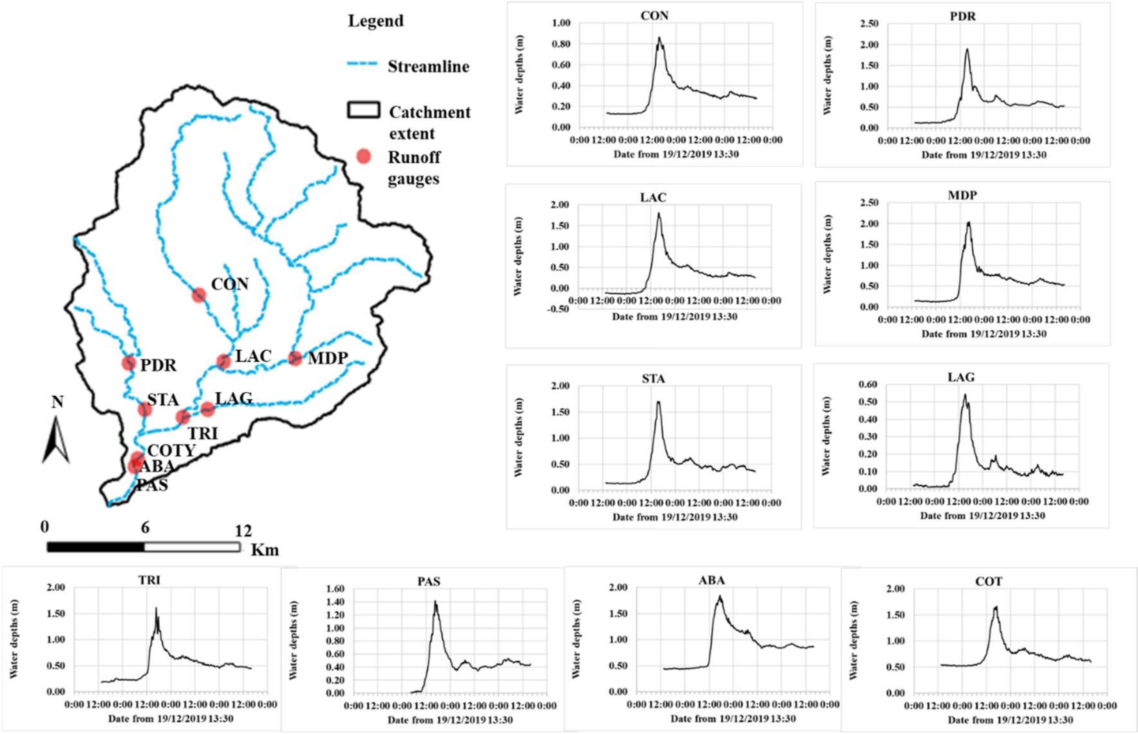

Figure 36 Water depths of flood event of December 20th, 2019, recorded at 10 gauges.

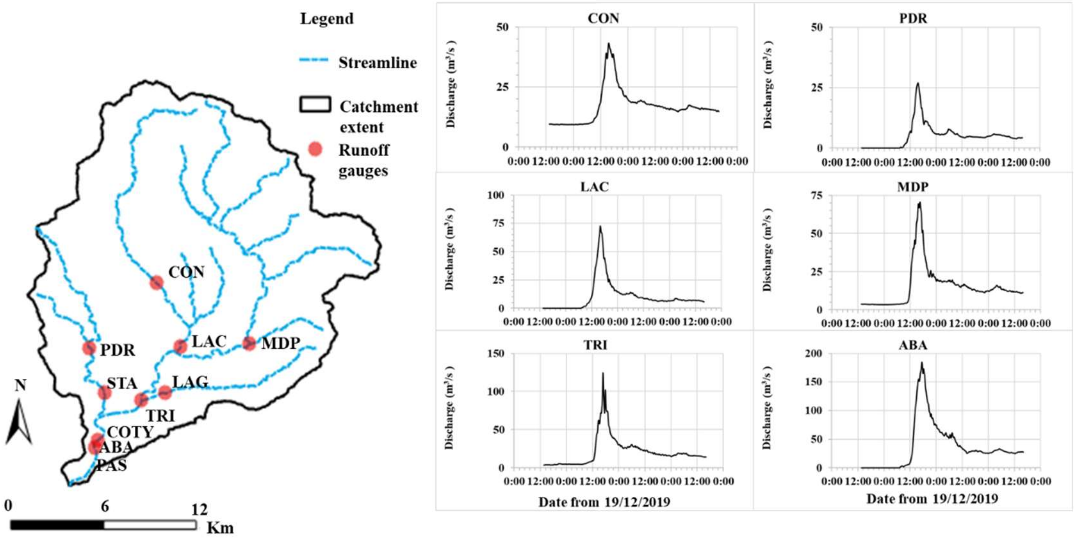

Figure 37 Discharges of flood event of December 20th, 2019, recorded at 6 gauges.

Figure 38 shows the rainfall-runoff process in the Paillons for the flood event of November 20th,2019. Generally, the rising time to the peak is shorter than the recession time in the Paillons catchment. The peak rainfall occurred at 13:42 pm while the peak discharge was observed at 16:36 pm local time. There are 3 rainfall peaks within 24 h. The two rainfall peaks after the maximum peak discharge resulted in slow recession for this event. The November 2000 flood event did not have additional rainfall peaks after its peak discharge. This led to faster recession of the flood.

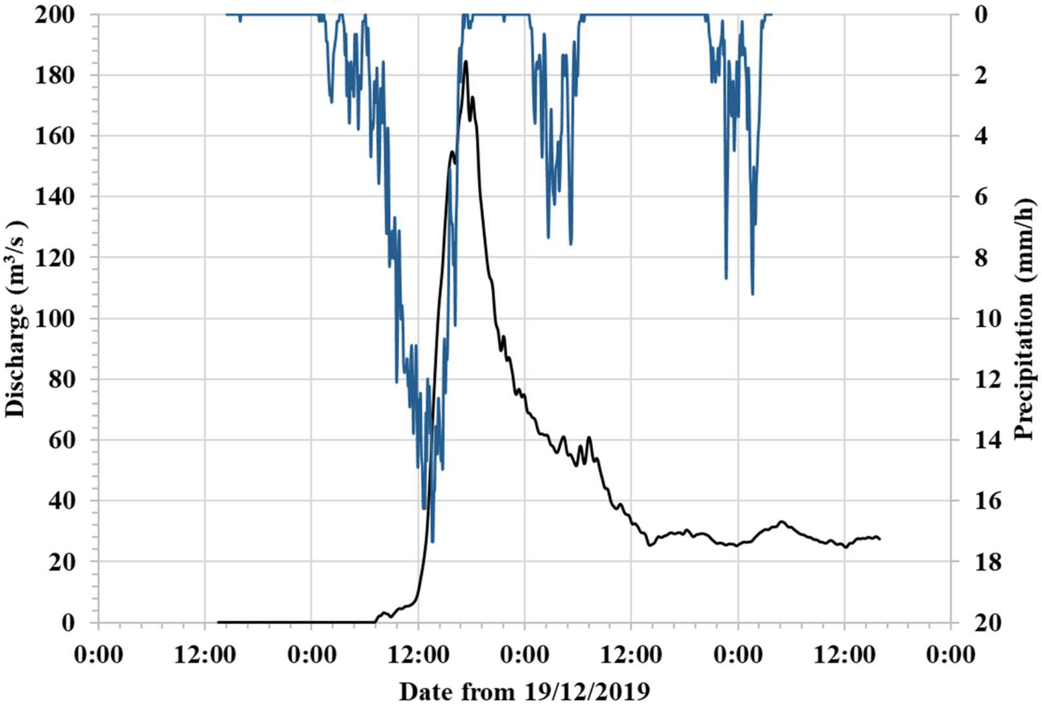

Figure 38 Rainfall-runoff process in the Paillons for the flood of 20/12/2019 recorded at ABA station (started at 19/12/2019 13:30).

These historical flooding events of the Paillons catchment highlight the vulnerability of the city of Nice and the surrounding area to heavy rainfall and flash floods, particularly in urban areas where the impervious surfaces are important. Gaps and errors in data pose a serious challenge in assessing through runoff measurements which year was the driest year in the period 2011-2020. In addition the Paillons is known to dry out at downstream in summer. Field surveys of low flow periods are sparse but show that every year, the river loses all its water in non-rainy periods (Tennevin et al., 2017). In the following sections, the characteristics of the Paillons catchment will provide better understanding of its response to rainfall events.

2.4.4. Geographical context

The Paillons catchment is located at the east side of the Var catchment in the French Riviera. It crosses the urban centre of Nice, the fifth largest city of France with a population of 340, 000 inhabitants. Due to the growth of local population and the increase of tourists, the urban area has been extending, claiming more land, and modifying the topography.

Figure 39 shows the geography of the Paillons catchment, its lower valley and associated groundwater study area with 9 cross-sections. The elevation varies from 0 m at sea level to a summit at 1495 m. The topography forms a steep streamline of 1.14% with “V” shape cross-sections characteristics of mountainous catchments. The downstream part is artificialized and covered on the last 2 km up to the sea. As delimited by grey lines in the figure, the area of 236 km^2 can be divided into 5 sub-catchments namely Banquière, Contes, Escarène, Laghet and Nice. The sub-catchment of Nice is the area directly contributing to the river discharge. The remaining downstream area is contributing to a larger Lower Paillons Valley (drawn in green and extends to part of the Sea) which is connected to the urban drainage system and includes the urban catchment of Nice centre. The urban catchment is included in the hydrological modeling, but its outlet is located downstream of the ABA station where discharge is assessed. The catchment and its lower valley are englobed in a groundwater study area which accounts for all the subsurface processes directly linked to the lower valley.

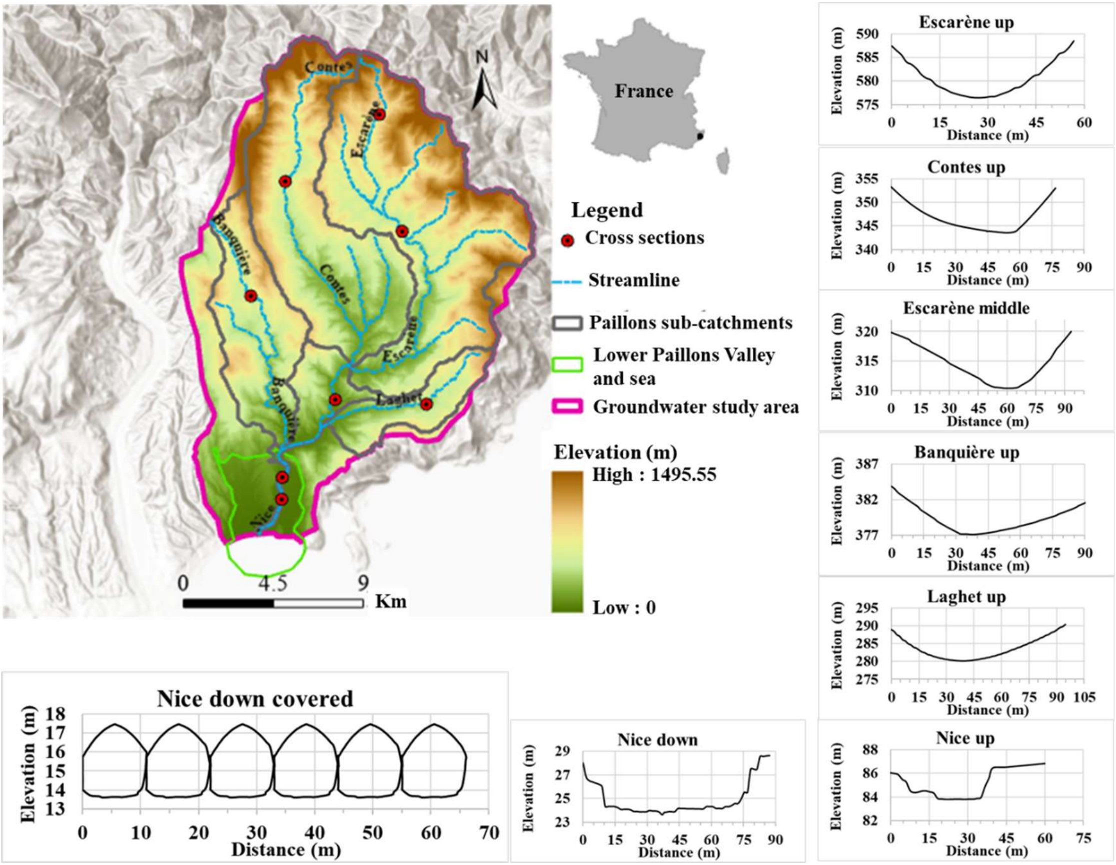

Figure 39 Geography of the Paillons catchment, Lower Valley, and associated groundwater study area with 9 cross-sections.

The las reach, the river Paillon of Nice long of 11 km starts at the merging point of its two main tributaries, Paillon of Escarène (24.8 km) and Paillon of Contes (22.6 km). There are two additional tributaries, the Paillon of Laghet (11.4 km) and Paillon of Levens or Banquière (18 km). Table 8 provides a summary of sub-catchment information in the Paillons catchment. Escarène is the longest tributary and the largest sub-catchment in the Paillons. The average slope is 23.2°. Most of the catchment has slopes higher than 10° and above 30° at the most upstream part (Figure 40). This results in fast flow with shorter concentration time (few h) in the Paillons. While the upstream parts have steep slopes, the downstream part is flatter. The flat and large floodplain in the downstream is a driver of its dense urbanization. In fact, the Paillon of Nice is the most artificialized (50% of area) of the sub-catchments. However, fast runoff exposes the lower valley to flood disasters.

Table 8 Summary of sub-catchment information in the Paillons catchment.

Sub-catchments	**Contes**	**Escarène**	**Laghet**	**Banquière**	**Nice** (without area connected to urban drainage)
Area (km^2)	71	94	16	36	17
Artificial area (%)	15	10	30	20	50
Elevation Range (m)	106-1495	106-1426	68-1147	41-1373	0 - 794
Maximum Slope (°)	83.94	83.66	85.25	84.33	84.12
Average Slope (°)	23.72	25.17	21.04	23.22	17.99
Slope Standard Deviation (-)	19.88	20.21	18.96	19.33	18.94

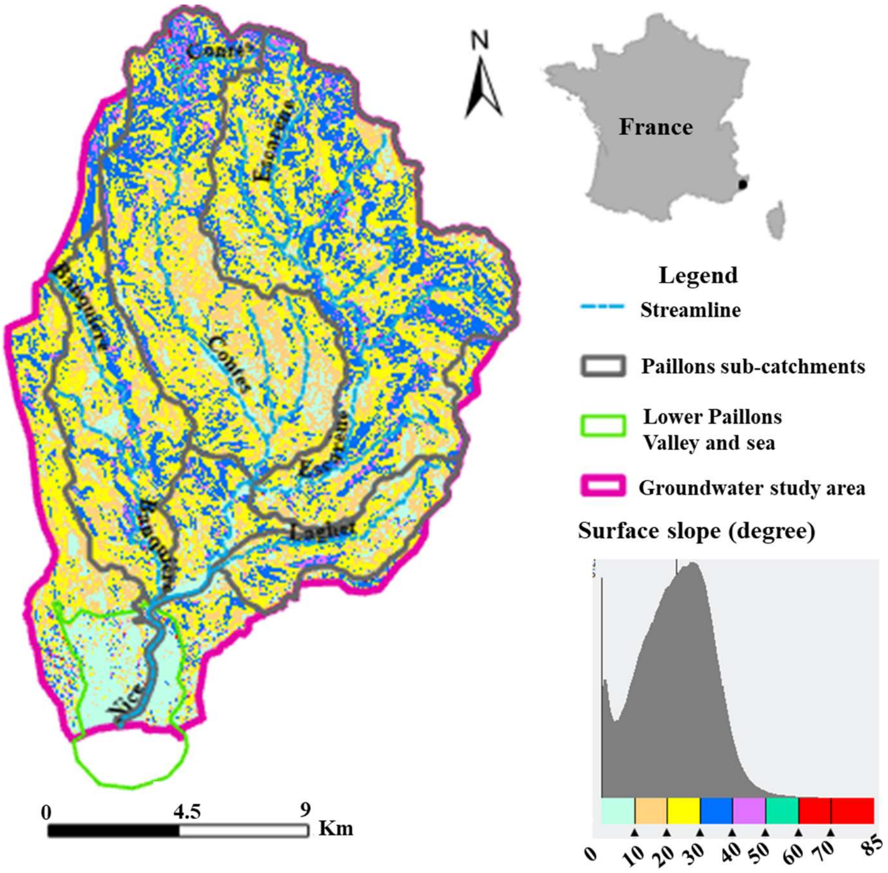

Figure 40 Slope distribution in the Paillons catchment, Lower Valley, and associated groundwater study area.

Available land-use information gives as many details as spaces for parking uses, beaches, sports facilities, or different types of vegetation. This information can be summarized into 6 main classes (Figure 41). Two categories dominate the land-use. Forests represent 68% of the total surface area, open spaces with scattered vegetation 27%, and agriculture for 4%. Artificial areas such as human settlements or urban areas represent less than 1% of the Paillons catchment. The remaining land-uses include grasslands and water bodies. Most of the artificial areas are concentrated along streamlines and coastal zone. It can be inferred that most of runoff in the Paillons catchment comes from forests and open spaces with few vegetation areas. In the Lower Paillons Valley, dense urbanization drives the surface flow processes and interactions with the river.

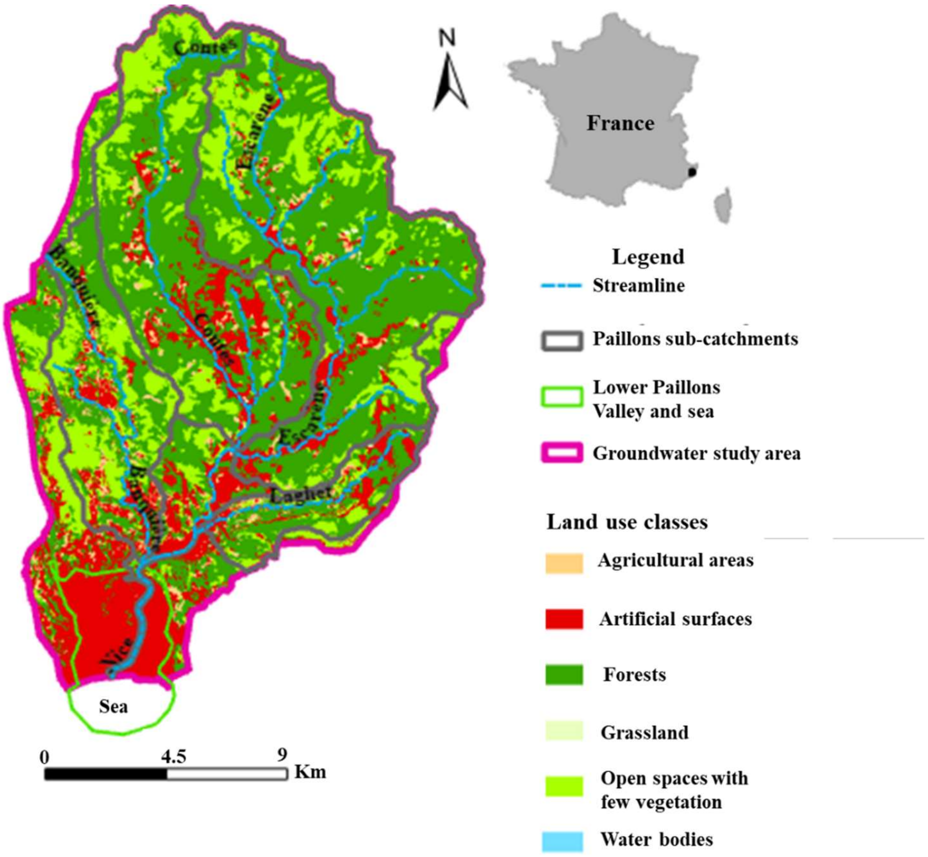

Figure 41 Land-use classes in the Paillons catchment, Lower Valley and associated groundwater study area.

Formerly used for agricultural purposes, the lands bordering the Lower Paillon River (LPR) which is the downstream part of the Paillon of Nice are now totally artificial. The river has been channelized and embankments have been built since the beginning of the XVIIth century, in order to gain space and safety (Figure 42). Between the middle of the XIXth century and the 2000s, different phases of covering the river were carried out. Today the bed is totally covered on 2.3 km to the outlet at sea and another section of 60 m wide is covered on 300 m length with a high school built on top of it (Archambaud & Berthet, 2021).

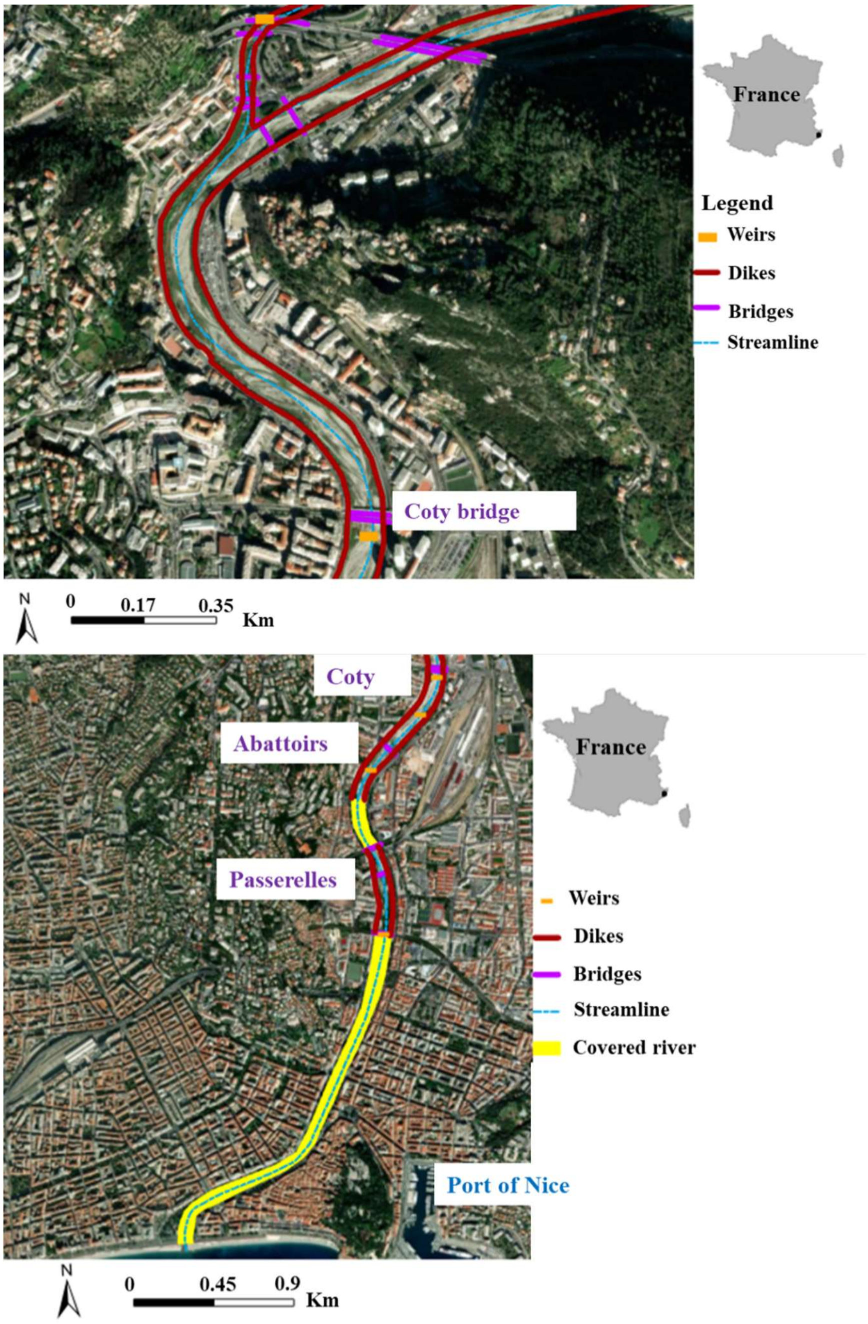

Figure 42 Embankments, covered river, bridges, and weirs in the Lower Paillons River.

The LPR is artificialized. Existing flood protection on the riverbanks and flood detention storages are made of concrete. Structures in the riverbed like weirs and materials traps control the flow and sediment transport. An estimated 1,100 m^3/s of water can flow under those channels (Le Gouz de Saint Seine, 1995). A corresponding estimated 147,000 m^3 of materials can be transported and partially accumulated inside the covered river (CR). To avoid overloading the system during extreme rainfall events and reduce flood risk, local authorities implement periodical removal of ton of materials (mixture of pebbles and clay). A two-year project, started in December 2017, planned to remove 100,000 m^3 of materials from the portion of the river going from Coty bridge to the Sea, including the CR. In 2018, about 15,000 m^3 of pebbles were retrieved from the riverbed (Frénois, 2018). After a dredging activity in October 2022, the riverbed level at Abattoirs (ABA) bridge was decrease by 0.55 m on average (Table 9). Every year, MNCA and “Syndicat Mixte pour les Inondations, l'Aménagement et la Gestion de l'Eau Maralpin” (SMIAGE) implement riverbed cleaning (grass cutting and removal of woods blocks (Mairie de Nice, 2022). Another type of activity that affects river geometry is construction works like building or maintaining bridges and flood protection walls. These activities can last several months and affect river flow measurements and can cause accidental flooding. Such events occurred between 2003 and 2016, when the bridge Passerelles (PAS) and the extension of the Tunnel André-Liautaud (TAL) were built (Figure 43). Therefore, careful considerations are required when investigating river discharge and water depths during flood events.

Table 9 Impact of dredging activity on riverbed level (m) at ABA bridge in summer 2022 (Game et al., 2023b).

	Bridge openings	1	2	3	4	5	Average
Before dredging	Upstream	23.32	23.76	23.05	23.15	23.88	23.43
	Downstream	23.43	23.44	23.37	23.73	23.71	23.54
After dredging	Upstream	22.71	23.53	23.07	22.64	23.77	23.14
	Downstream	22.68	23.02	23.06	22.80	23.37	22.99
Difference	Upstream	0.61	0.23	-0.02	0.51	0.11	0.29
	Downstream	0.75	0.43	0.31	0.93	0.34	0.55

The existing flooding monitoring system is used to manage the TAL located in the riverbed. The 9 rainfall and 10 runoff gauges across the associated river basin; and 4 cameras (2 at ABA bridge, 2 at Pont Anatole France) provided the needed information for real-time flood monitoring. Limitations in quantifying the flood events and the need to reduce false alerts require a new hydraulic model that can in real-time give water depths and discharges estimates with updated geometry of the river.

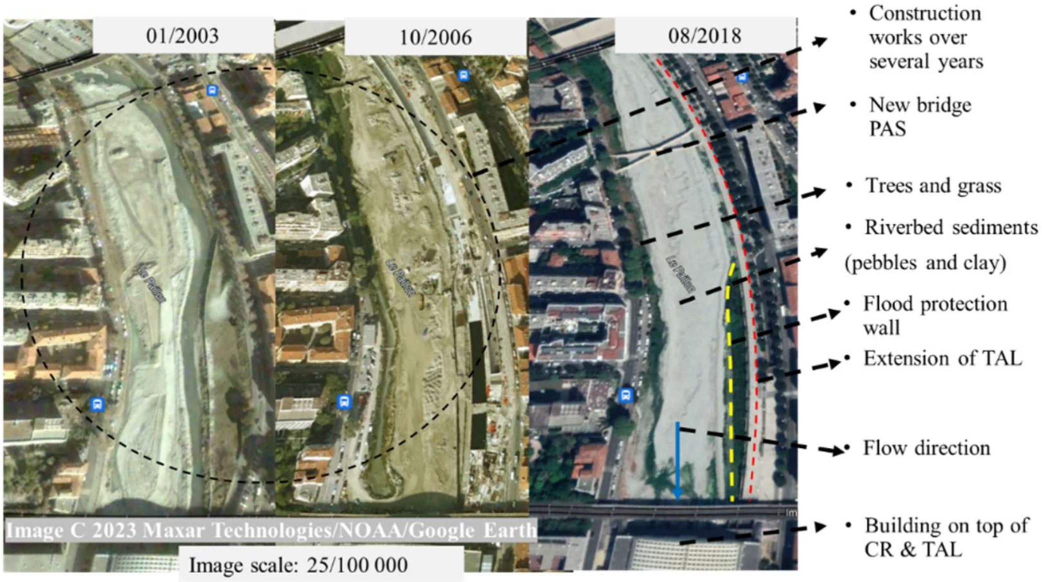

Figure 43 Impacts of construction works on land-use in of LPR bed in Nice urban centre 2003 to 2018 (Google Earth Images).

2.4.5. Geological context

The Paillons is characterized by a heterogenous geological units, of several rock types including limestone, some dolomites, sandstones, and marls. These rocks have been affected by tectonic movements, resulting in steep relief, deep valleys, and high crests. The basin is also affected by karst features such as dolines and caves, which are typical of limestone areas. The soil types in the basin vary widely depending on the underlying rock and the local climate. The soils on the valley floor are composed of alluvial deposits, which are composed of gravel, sand, silt and clay. The soils on the valley sides are made of residual soils, which are formed from the weathering of the underlying rock, namely "terra rossa" on the limestones and sandy soils on the sandstones. (Le Gouz de Saint Seine, 1995; Pline, 1991).

The river cut through the rock to create the valley, and in the past, that have also helped shaping the valley by eroding the rock and depositing sediment. The geological context of the Paillons catchment plays a significant role in the hydrology of the area, as geology controls the soil and rock characteristics and the infiltration rates which affect runoff and recharge of the groundwater. The karst features and underground drainage also influence the movement and storage of water in the area. Understanding the geological context is essential for the sustainable management of water resources in the basin.

Available geological maps and cross-sections (Figure 44, Figure 45, Figure 46, Figure 47, Figure 48 & Figure 49) describe the geometry of the subsurface (Le Gouz de Saint Seine, 1995; Pline, 1991; Tennevin et al., 2017). 54% of the area is formed by the Cretaceous rocks which provide the rivers with gravel and pebbles. The Jurassic limestone makes up 23% of the surface rocks. Only 4.6% of the area constitutes the alluvial zone. The quaternary alluviums are connected to the Pliocene conglomerate, the Jurassic limestone, and marls. Eocene and Oligocene share 8.8% and 9.7% of the territory, respectively. The main impermeable formations include clayey marls from the Upper Triassic, Cenomanian marls (Middle Cretaceous) and Priabonian marls (Upper Eocene). Three main aquifers such as karstic (Jurassic and Lutetian (Middle Eocene)), fissured (Upper Cretaceous and Oligocene), porous (Alluvium and scree slopes) provide water resources for several municipalities. Karstic formation behaves like "all or nothing" response (high initial retention capacity of the reservoir, which when full, no longer retains anything (Le Gouz de Saint Seine, 1995).

Alluvial deposits fill the lower valleys of the hydrographic network following profiles more or less symmetrical depending on the sectors. The layer can be vertically divided into three sub-layers. The information available makes it possible to specify that their maximum depth increases very significantly from upstream to downstream, with bottom elevation varying from + 75 m to – 15 m, and the following approximate thicknesses: about 15 m at the Grave de Peille, from 20 to 25 m in Sainte-Thècle, around 20 to 30 m in the Cantaron and Drap sector, between 35 and 40 m to the right of the village of La Trinité, from 45 to 50 m downstream of the municipality of Trinité (districts of Rostit and Oli), around 55 to 60 m at the entrance to Nice, in the area of the former gas plant, and about 70 to 80 m to the heart of Nice (Pline, 1991; Tennevin et al., 2017). A distributed map, produced by the consulting firm GUIGUES Environnement (Figure 49), of the bathymetry of the downstream part of the alluvial layer shows the variation of depth to bottom between 0 and 90 m. The western part is shallower than the eastern part.

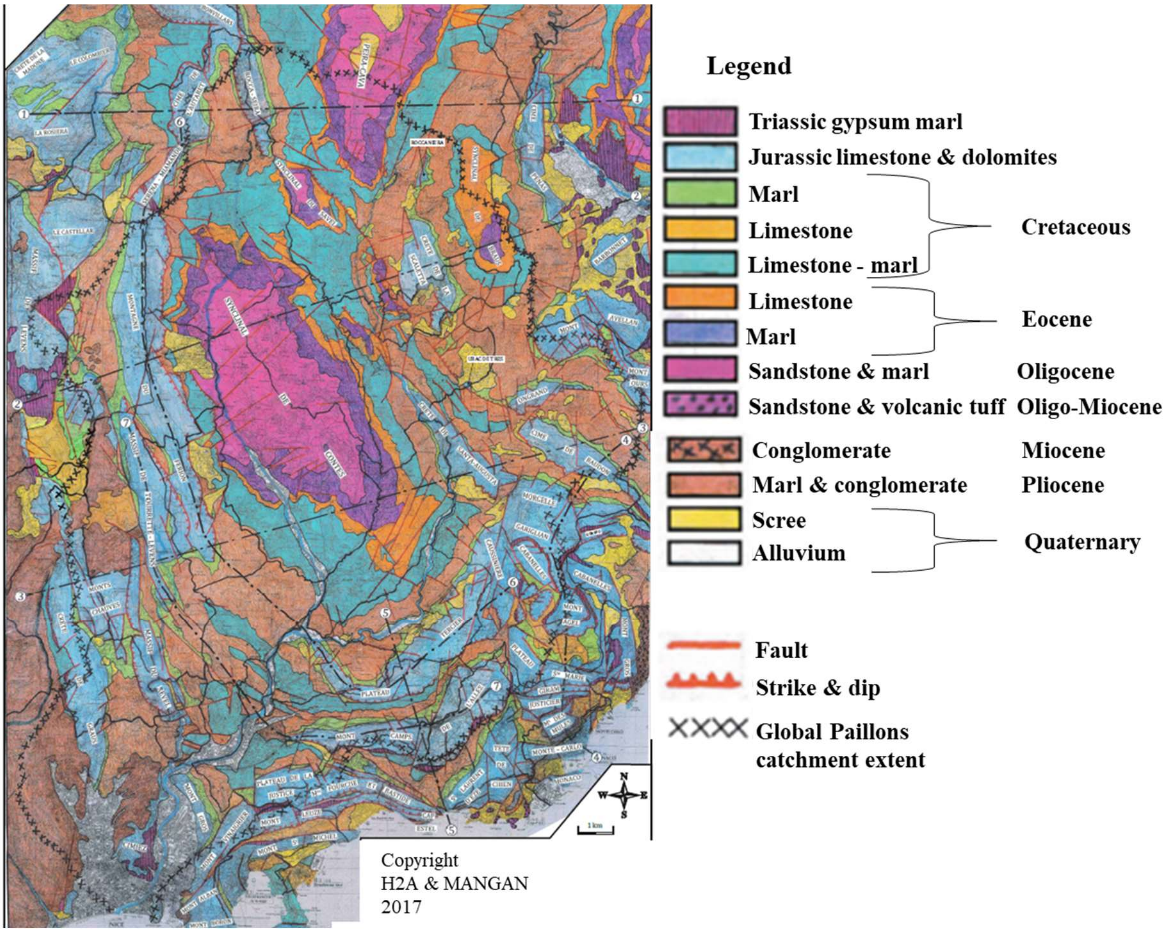

Copyright
H2A & MANGAN
2017

Figure 44 Geological map of the Paillons catchment (Tennevin et al., 2017).

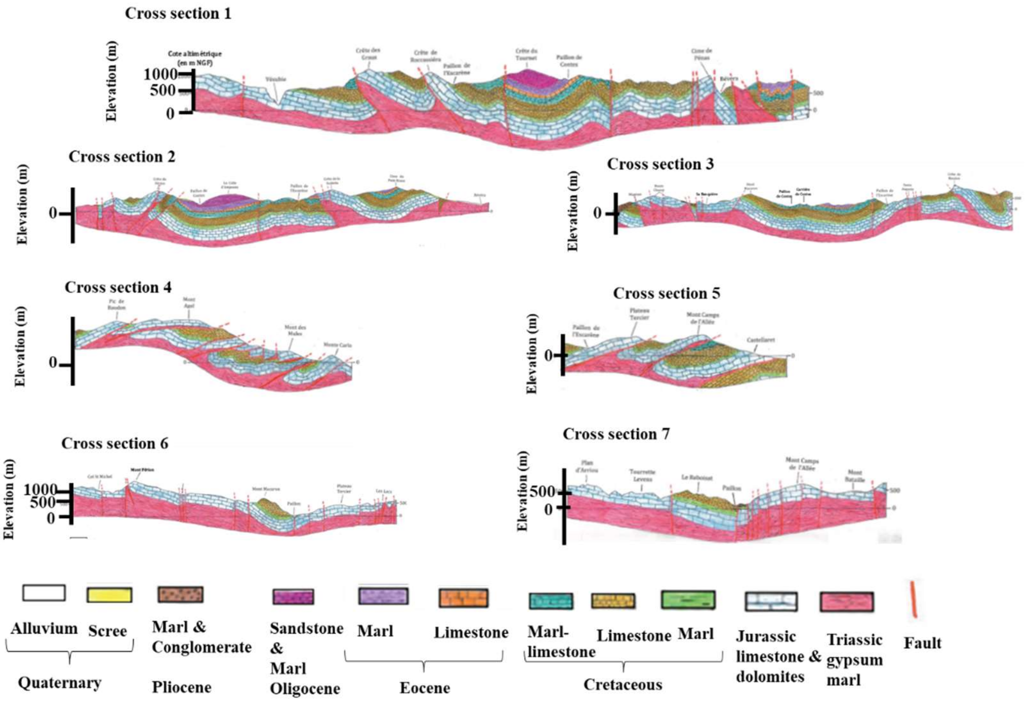

Figure 45 Profiles indicated in Figure 44 (Tennevin et al., 2017).

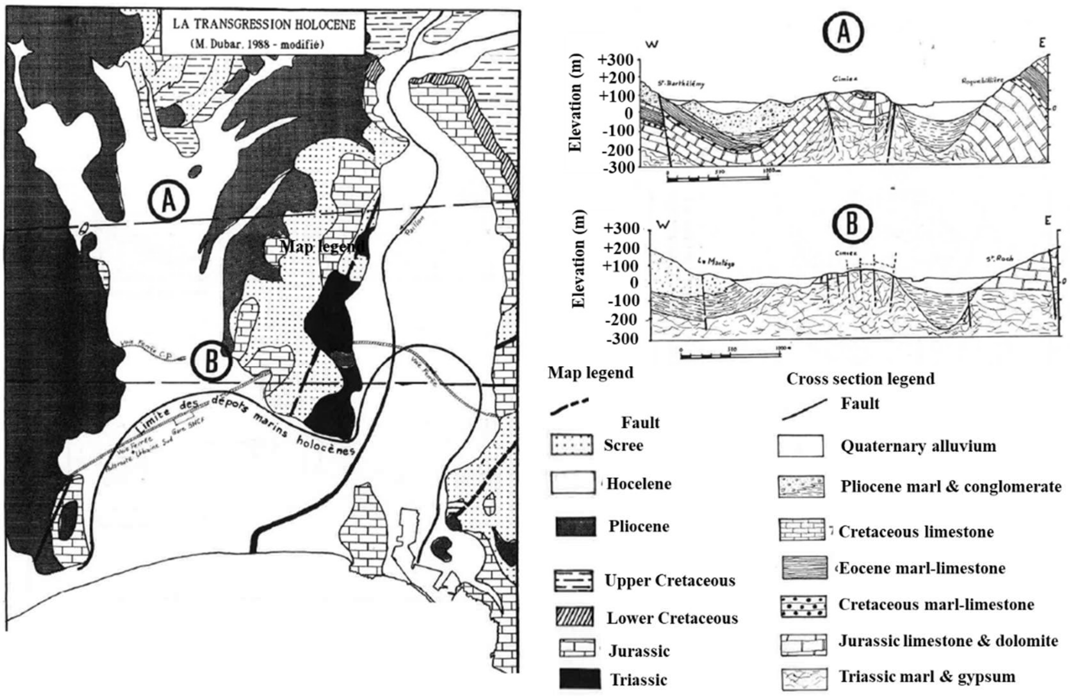

Figure 46 Geological map of the lower Paillons valley with profiles A and B (Pline, 1991).

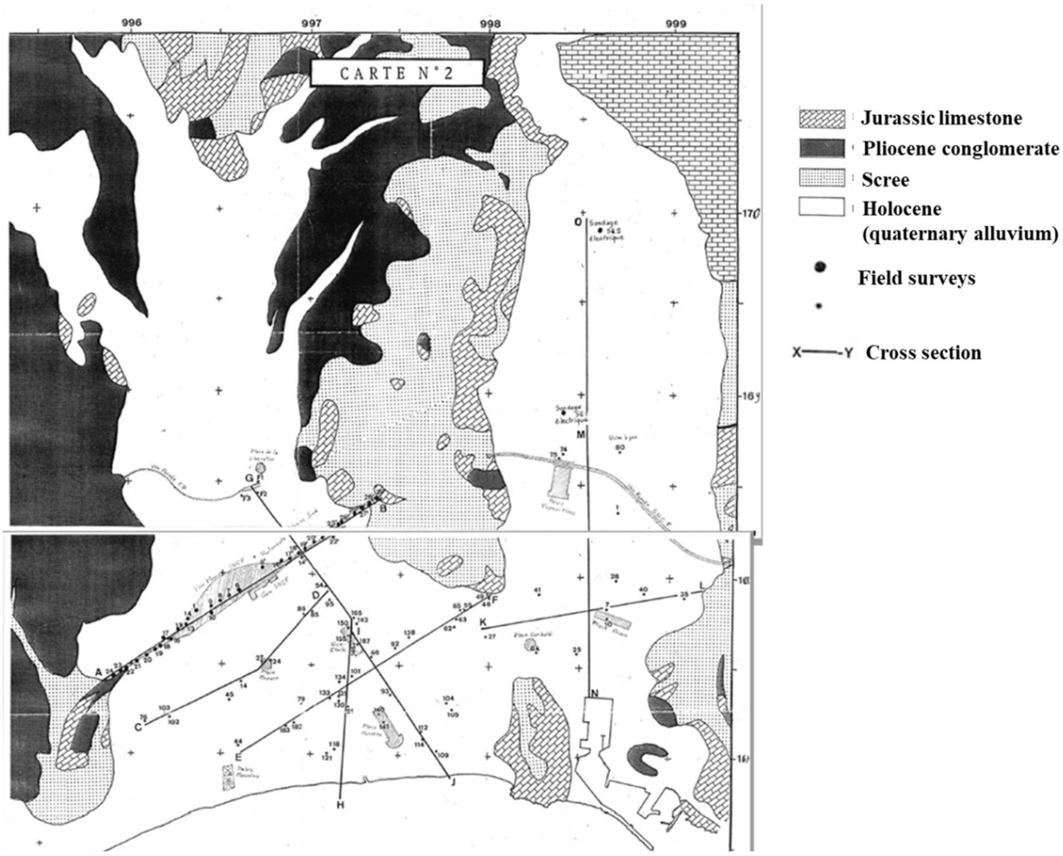

Figure 47 Geological map of the lower Paillons valley with more detailed profiles lines (Pline, 1991).

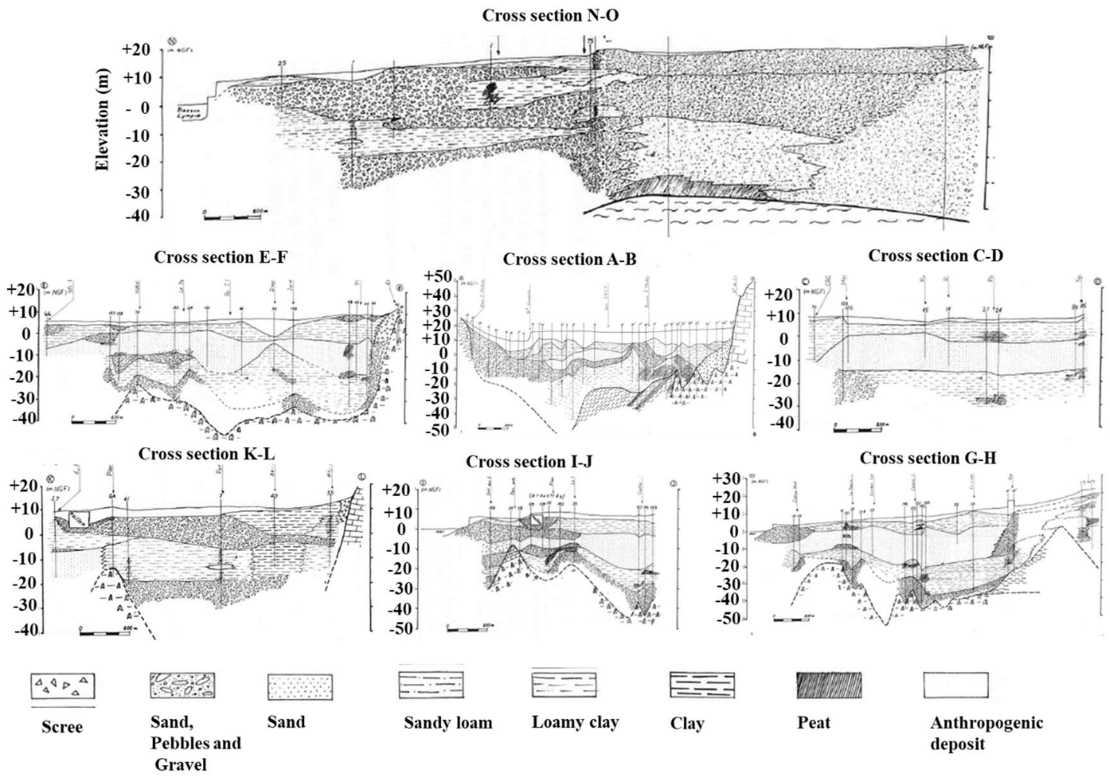

Figure 48 Profiles indicated in Figure 47 (Pline, 1991).

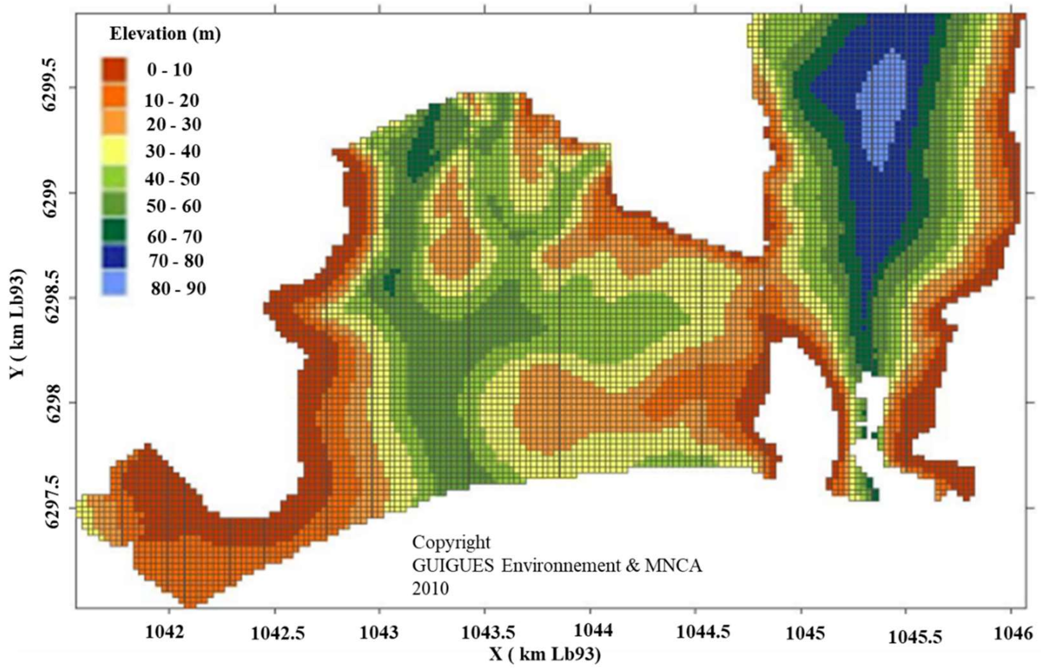

Figure 49 Bathymetry of the lower part of the alluvial zone of the lower Paillons valley (GUIGUES Environnement & MNCA, Tram Nice project 2010).

2.4.6. Hydrogeological context

The hydrogeological conditions in the Paillons catchment can be divided into three categories: the alluvial aquifers, the karstic aquifers, and fissured aquifers (Appendix **7**) (Le Gouz de Saint Seine, 1995; Pline, 1991; Tennevin et al., 2017). The alluvial aquifer is bordered to the west by a Pliocene conglomerate aquifer belonging to a different catchment. The groundwater resources are used for drinking, irrigation and industrial activities. All water sources and consumption types considered, the annual pumping volume is around 9.2 Mm^3. The surface water uptake represents only 21% of this volume. Groundwater constitutes the most important fraction consumed. The alluvial, karstic and fissured aquifers of the Paillons catchment provide respectively 16%, 10% and 27% of the total volume. The remaining 26% originates from the Vésubie Canal, an important water infrastructure using water resources from a neighboring catchment. Some uncertainties exist in these estimates due to the lack of information at some pumping stations or extraction points (Tennevin et al., 2017).

The porous aquifers are mainly represented by the alluvial fillings of low valleys and by slope scree in the Quaternary layer. The deepest depth under the ground of the alluvial layer is around 90 m. The groundwater levels vary from 1 to 5 m below ground. The unconsolidated deposits which constitute these fillings are very heterogeneous and present highly variable permeabilities (Appendix **5**). Only a superficial unconfined aquifer exists in the upstream part and up to the entrance to Nice. Beyond and according to the progressive growth of their thickness, the geometry of the sediments conditions the coexistence in the downstream part of several aquifers superimposed more or less anastomosed: a superficial unconfined aquifer, which circulates in the sandy gravels above more or less abundant silty matrix; one or more intermediate semi-captive aquifers, resulting from the intercalation horizons and clayey lenses within the gravelly-sandy reservoir, and frequently limited in extension and reduced exchange with the unconfined aquifer; a deep aquifer in the lower sandy gravels, captive under the clayey-loamy developments that offer great vertical extension and a lateral continuity (Tennevin et al., 2017). The captive alluvial aquifer has a groundwater table which is artesian with groundwater levels in pumping wells close to the ground surface (Pline, 1991a). The superficial alluvial aquifer is fed by infiltrations on its own impluvium, as well as by any runoff from the banks and by inputs from the bordering aquifers constituting the bedrock (Jurassic and Turonian limestones). The supply of semi-captive or captive deep aquifers, on the other hand, only benefits from alluvial inputs from upstream and supercharging from its aquifer bedrock. In the upstream and centre of the alluvium, the hydraulic conductivities are high. The observed values in Nice-Riquier are at $1.25x10^{-3}$ m/s at place Arson, $5x10^{-4}$ m/s at place Barberis, 1.3 to $8x10^{-3}$ m/s at avenues des Diables Bleus and 2 to $20x10^{-3}$ m/s at Theater Museum of Modern Art and Acropolis. In Nice centre and coastal area, the conductivity in silt lenses is in the range of 10^{-6} -10^{-7} m/s. The permeability in the gravel is $2x10^{-5}$ m/s and in coastal deposits the observed value is between 10^{-3} and 10^{-4} m/s (Pline, 1991a).

The karstic aquifers, represented by the Jurassic limestone layers (400 m of height on average) and, to a lesser extent, by the limestone horizon of the Eocene. On average, the first 100 m of the depth of the limestone layer is exposed to karst formation. The karst conduits network is more or less important depending on the area. They benefit from a high rate of infiltration and an underground network abundantly provided with conduits widened by the dissolution on the frame of the fissures of the massif. The drainage of these reservoirs has a good organization and a reduced number of large outlets. This aquifer constitute a well-developed impluvium and contain the most important aquifer resources in the region. Springs are frequently located on the outskirts of massifs, in contact with Upper Triassic or Cretaceous layers. However, the structural and paleogeographic conditions sometimes modified the control of underground flows: diversion of circulation by transverse accidents, remote or concealed drainage by placing separate reservoirs in deep communication outcrop and emptying of certain reservoirs at sea through submerged karstic networks. The drainage of these units offers a variable and sometimes very complex panorama (Tennevin et al., 2017). Apart from the springs of Sainte Thècle, Santa Augusta, La Tour, Ingram and Larvoto, with an average total flow of approximately 200 to 250 L/s, significant emergences in the sector of the arc of Nice are absent. Three marine and submarine emergences (Appendix **6**), the Pissarelles group in Èze, the Cabbé group in Cap Martin, and the Mortola group in Italy near the border, have an average cumulative annual flow evaluated at around 500 or 550 L/s (Audra et al., 2006). The hydraulic conductivity in the Jurassic limestone reported in the literature vary between $1x10^{-5}$ to $1x10^{-4}$ m/s, but the cave system in the karst have higher hydraulic conductivities.

Moreover, the fissured aquifers, are made up of limestone and marly-limestone from the Upper Cretaceous, as well as by the Oligocene sandstones. Underground flows are carried out in the network of fissures of the massif, which is characterized by a great spatial heterogeneity of its conditions of infiltration, circulation and of water storage. These reservoirs, often partitioned into small units by tectonics and facies variations, feed scattered outlets, frequently staged and of low flow (Tennevin et al., 2017). Their flow rate is usually low (0.1 to a few L/s), but can change significantly over time and sometimes be supplemented by temporary outlets.

The withdrawal of groundwater for the purpose of drinking water supply is managed by both the Veolia company and the local municipalities, namely Drap, Trinité, Cantaron, and Nice. This process involves meticulous planning and comprehensive documentation of pumping volumes. The creation of boreholes for this purpose is also overseen by industrial entities within the Paillons catchment and its downstream valley. Notably, the regional water agency (Agence de l'eau RMC) maintains a record of the pumping volume as well. Conversely, when it comes to agricultural water consumption, the pumping volume lacks comprehensive documentation, posing a significant challenge to effective groundwater management. The geographical distribution of boreholes, where groundwater extraction is predominantly carried out within the Paillons catchment, is depicted in the Figure 50.

Figure 50 Location of water pumping 15 stations representing the three types of aquifers in the valleys of the Paillons catchment.

Currently, for the karstic reservoir, there are the following outlets with allowed extractions: the two Sagna boreholes of 6x10^3 m^3/d, the Vernes of 2.64x10^3 m^3/d, the two boreholes of Cantaron with allowed 500 m^3/d, the spring of Sainte-Thècle with uptake of 200 m^3/d and the border springs on the eastern slope of the Férion mountain of 400 m^3/d. At the Sagna borehole, the evolution of the extraction is well known and reported in Tennevin et al.(2017). However, the temporal evolution of groundwater extraction is not clearly known in the Alluvium. Some historical pumping stations were closed. Table 10 shows the summary of major pumping stations of the alluvium and karst aquifers. Most of the known pumping stations in the alluvial aquifer are for industrial use and located in the Lower Paillons Valley. Pumping for drinking water is mostly upstream in alluvial zone or at deep depth in the karst. Some extraction for industrial activities are not known.

Table 10 Summary of major pumping stations of the Alluvium and Karst aquifers in the Paillons catchment.

Borehole	Depth from surface (m)	Ground elevation (m)	Annual extraction (m^3)	Aquifers	Usage
Forage des Vernes	250	105	70726	Jurassic Limestone (Karst)	Drinking
Forages de Cantaron	200	115	73080		
Forage de la Sagna	150	107	1040100		
Forage du Pilon	150	178	?	Miocene - Cretaceous	
Forage de Plan de Rimont	20	104	331700	Quaternary Alluvium	
Forage de la Rua	20	210	166044		
Forage Fonti	20	230	73880		
Forages Usine Vicat de Peille 1	15	200	112350		Industrial
Forage de l'usine Vicat de Peille 2	13	200	112350		
Puits de l'usine Lafarge de Contes	20	180	101600		
Puits SNTA Ligne Azur	7.25	80	2200		
Forage de Carrefour Nice TNL	22.15	12.25	?		
Forages du Palais des Arts	25	5	493800		
Forages du Port Nicéa	25	15	?		
Forage Palais des Expositions	40	17	?		
Forage d'Acropolis (Palais des congrès)	18	10.68	100000		

Historical piezometric monitoring from 1954 to 1974 of groundwater levels in the alluvium of the Lower Paillons valley are provided at 4 locations namely Ecole Barla (ground level 8.36 m), Bureau d'Hygiene (ground level 7.12 m), Rue Déroulède (ground level 6.56 m) and Rue Colonna d'Istria (ground level 6.74 m) (Figure 51). The downstream ground water levels variation from the mean state were less than 1 m at these four location, but monitoring was limited to few measurements each year.

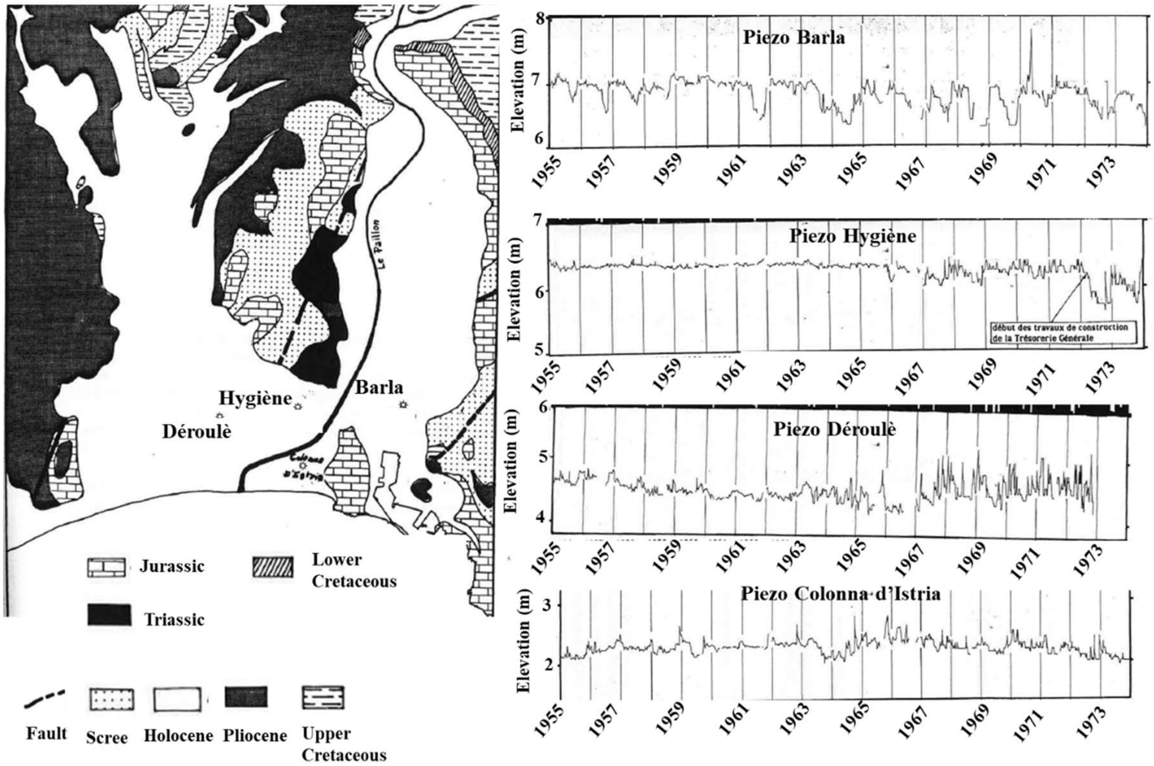

Figure 51 Piezometric monitoring of groundwater levels in the Alluvium from 1854-1974 (Pline, 1991).

Piezometric monitoring every semester of twenty piezometers by the DGA (Development and living environment, Environment, Sea, and Coastal Department) suggested a magnitude of variations of groundwater levels in the alluvium between 0.6 m and 4.85 m. But there are a lot of uncertainties and errors in the records and the data were not used by ESSIA group for the study related to the construction of the tramway tunnel of Nice city. Two sets of measurements in October and November 2010 confirms the dynamics and distribution near the coastal area, with the area near the port having a groundwater level around 4 m and the area on the west side reaching 3.65 m levels. The area between Hygiène and Barla show values around 6.6 m. Unfortunately, no recent time series are available to better understand the temporal evolution of the groundwater level in the unconfined and confined alluvial aquifers. The only contour map created from observations analysis was produced in 1991 by Pline C. (Figure 52). It depicts the dynamics of the free unconfined aquifer.

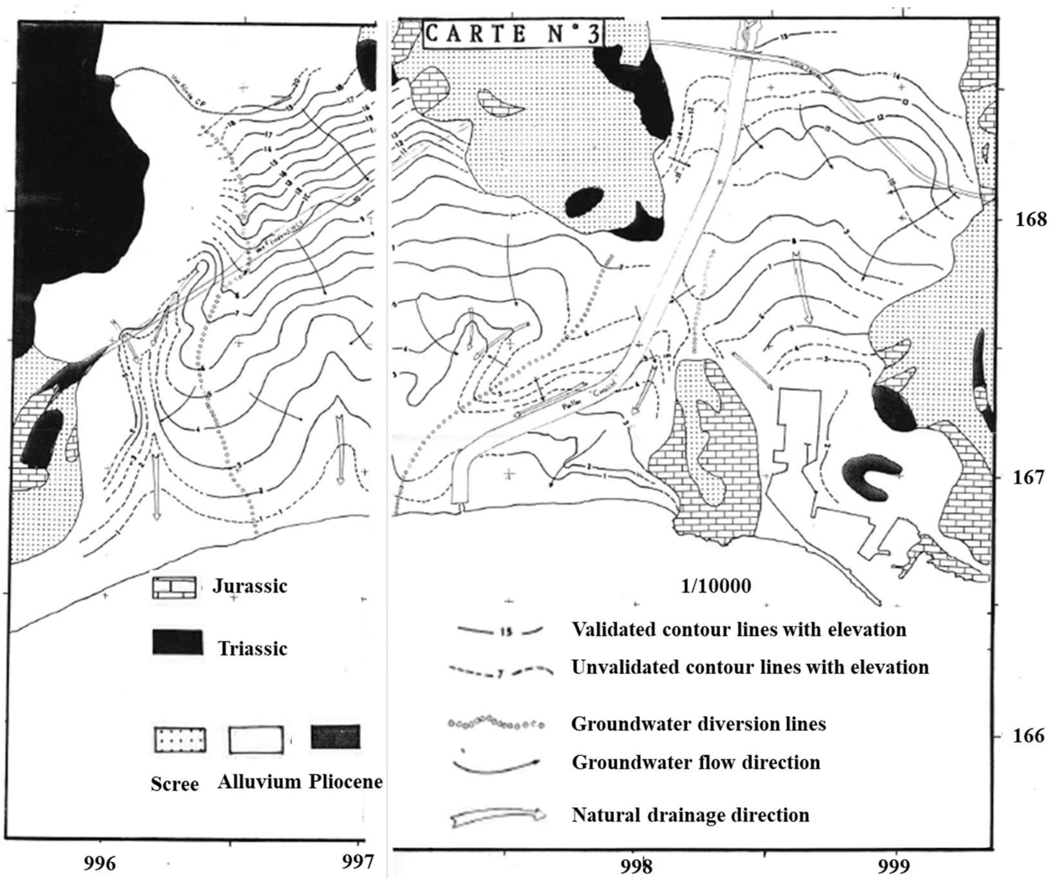

Figure 52 Groundwater contour map of the downstream part of the Alluvium in the Lower Paillons Valley (Pline, 1991).

2.4.7. Meteorological context

In this study, there are two types of meteorological information. The first group is managed by the French national meteorological service Météo-France and covers the outskirts and the downstream part of the Paillons catchment. Since 1921, 28 national stations and since 1987 12 local have operated in and around the Paillons catchment. Now, only 9 national and 9 local stations still exist with records at 6-mn, hourly and daily time intervals (Table 11). Within the limits of the catchment, station elevation covers 28 to 663 m. Around the catchment, station elevation varies from 2 to 1443 m.

Elevation variation (18 to 663 m) of local meteorological stations covers 68% of the direct contributing area of the catchment. Using national stations in addition fills the coverage gap and the gap in monitoring records which is frequent at local stations due to less resources dedicated to maintenance and validation of the stations. Elevation variation of national and local gauges (2 to 1443 m) now covers 99.98 %. But only one national station is within the boundaries of the Paillons watershed (Figure 53). All those stations could be used to create rainfall distribution maps over the area of study.

Table 11 Rainfall gauging stations distributed in the Paillons catchment (Source: Météo-France and MNCA).

Station	ID	Basin	Source	6-mn records	Hourly records	Daily records	Elevation
CARROS	6033002	Banquière	Météo-France (national)	Yes	Yes	Yes	78 m
EZE	6059003	Laghet					704 m
LANTOSQUE SAPC	6074005	Contes					550 m
LEVENS	6075007	Banquière					691 m
PEIRA CAVA	6077006	Escarène					1443 m
NICE	6088001	Nice					2 m
NICE-RIMIEZ	6088007	Nice					238 m
PEILLE	6091003	Escarène					1106 m
SOSPEL	6136005	Escarène					843 m
Plan de Revel (PDR)	B1	Banquière	SAC Paillons (local)	Yes	No	No	228 m
Contes (CON)	B3	Contes					181 m
Coaraze (COA)	B4	Contes					660 m
Lucéram (LUC)	B5	Escarène					600 m
Baissa (BAI)	B6	Escarène					663 m
Moulin de Peillon (MDP)	B7	Escarène					164 m
Laghet (LAG)	B10	Laghet					335 m
Abattoirs (ABA)	B15	Nice					28 m
Escarène (ESC)	B11	Escarène					330 m

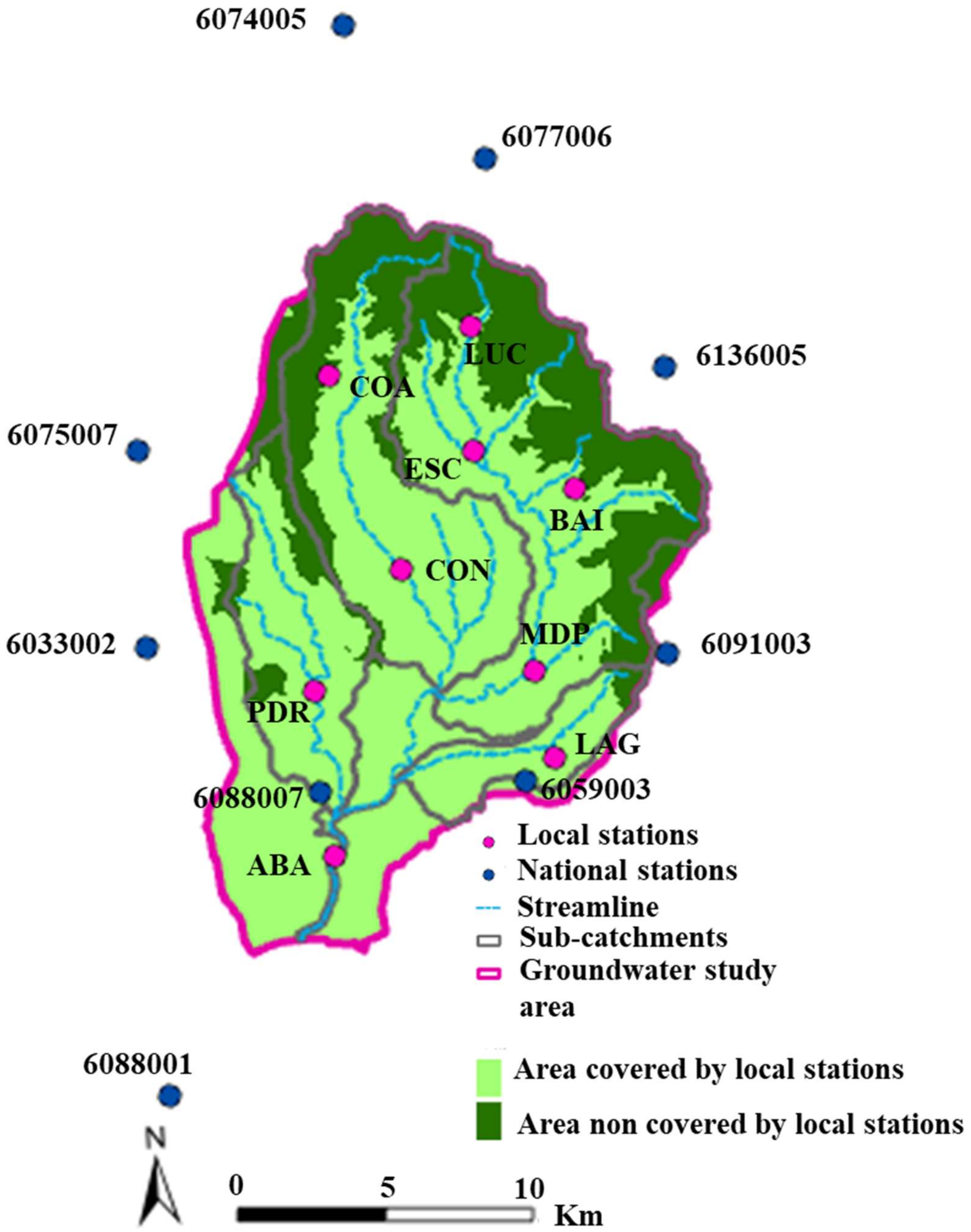

Figure 53 Rainfall gauging stations and their control area distributed in the Paillons catchment.

The meteorological attributes of the Paillons catchment align closely with the Mediterranean climate, characterized by wet winters and dry summers. Annual precipitation in the Paillons catchment can reach up to approximately 647 mm/year, with an average monthly value of 73 mm. However, the distribution of rainfall over time within the Paillons catchment reveals a notable degree of heterogeneity (Figure 54). During the drier months from July to September, the total amount of rainfall constitutes less than 14% of the annual average. Conversely, within the rainy season, a single month, such as November, can account for over 24% of the entire annual rainfall in the Paillons catchment. The contrast between the driest and wettest months can surpass 85%.

Further analysis of the average monthly rainfall within the Paillons catchment (indicated by the red line in the figure) reveals two prominent periods of increased rainfall, namely the spring rainy season (spanning from February to May) and the winter rainy season (occurring between October and January). Notably, the winter rainy season experiences significantly higher total rainfall and intensity compared to the spring rainy season. This heightened winter precipitation is a primary contributor to the occurrence of flash flood disasters in the downstream areas of the catchment.

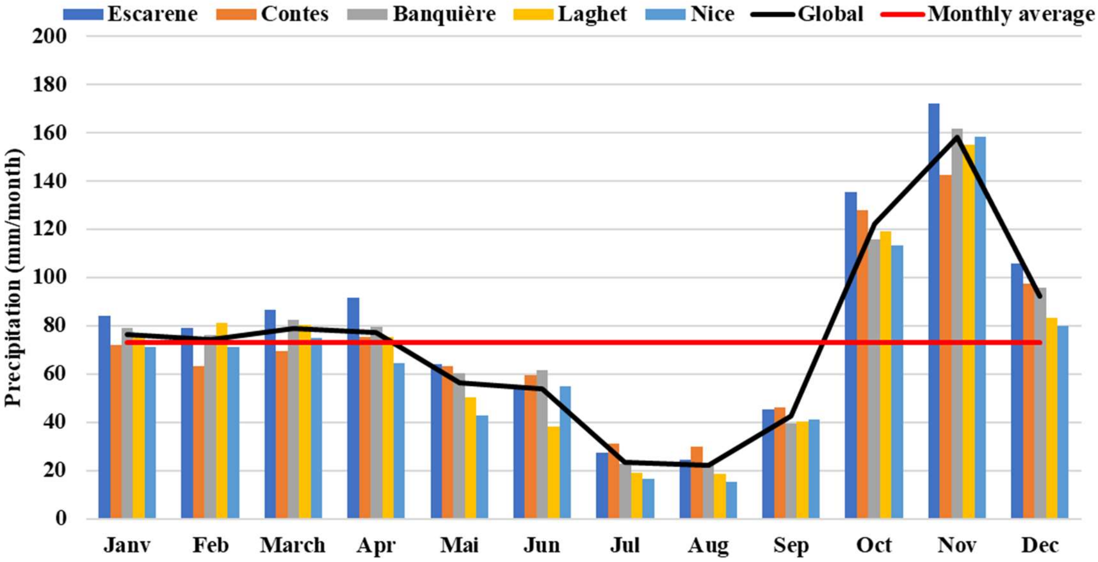

Figure 54 Monthly precipitation of the sub-catchments in the Paillons catchment (2010-2020).

Among the data collected over a span of 77 years (Figure 55), only a mere 11 days experienced substantial precipitation exceeding 100 mm, with a mere 2 days surpassing the threshold of 150 mm within a 24h period. In the majority of instances, daily rainfall remains below 50 mm, and statistical analysis of daily rainfall reveals that 97.2% of rainy days exhibit precipitation levels below this mark. Furthermore, precipitation exceeding 20 mm occurs with a frequency of only 15.6%. This indicates that occurrences of intense rainfall events like storms or heavy downpours have a low probability within the lower Paillons river valley. However, it is important to note that when such heavy daily rainfall does occur, it has the potential to trigger severe urban flooding. Analyzing the temporal distribution of extreme daily rainfall does not reveal a discernible trend. In other words, there is no clear evidence indicating a higher frequency of extremely intense precipitation events (Du et al., 2018b).

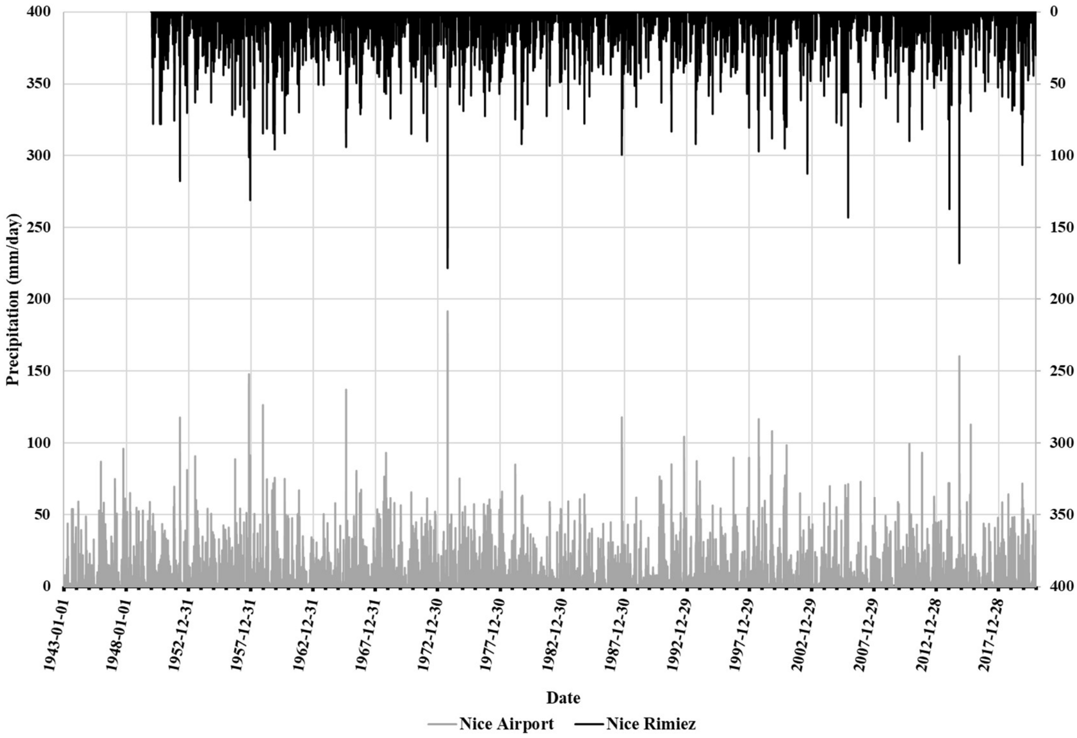

Figure 55 Daily precipitation recorded in Nice airport and Nice Rimiez (1943 -2020).

As Du et al.(2018) stated, the annual amount of rainfall serves as a defining factor for categorizing longer-term rainy and dry periods, as depicted in Figure 56. For Nice Airport and Nice Rimiez, the average yearly precipitation stands at 781 mm and 799 mm respectively. This demarcation illustrates the boundary between years characterized by ample rainfall and those marked by arid conditions. Notable dry spells within the time series encompass the periods 1942-1950, 1962-1970, 1980-1990, and 2001-2007, as well as 2015-2017 and 2020-2021. These are interspersed with alternating rainy periods, establishing a discernible rainy-dry cycle. While occasional anomalies like a rainy year amidst a dry period or vice versa are plausible, they are easily identifiable and generally do not disrupt the overall cycle. Within this pattern, it is evident that two significant droughts occurred in 1967 and 2015 in the valley. Interestingly, both instances coincided with dry years within dry periods. In addition, a trend emerges from the annual precipitation data, indicating a greater likelihood of consecutive dry years in more recent decades. At the two stations, the lowest recorded annual precipitation value is 317.7 mm for Nice Airport and 303.9 mm for Nice Rimiez in 2007, which followed a prolonged drought since 2001. This skewed distribution of water over time contributes to a heightened frequency of extreme meteorological events.

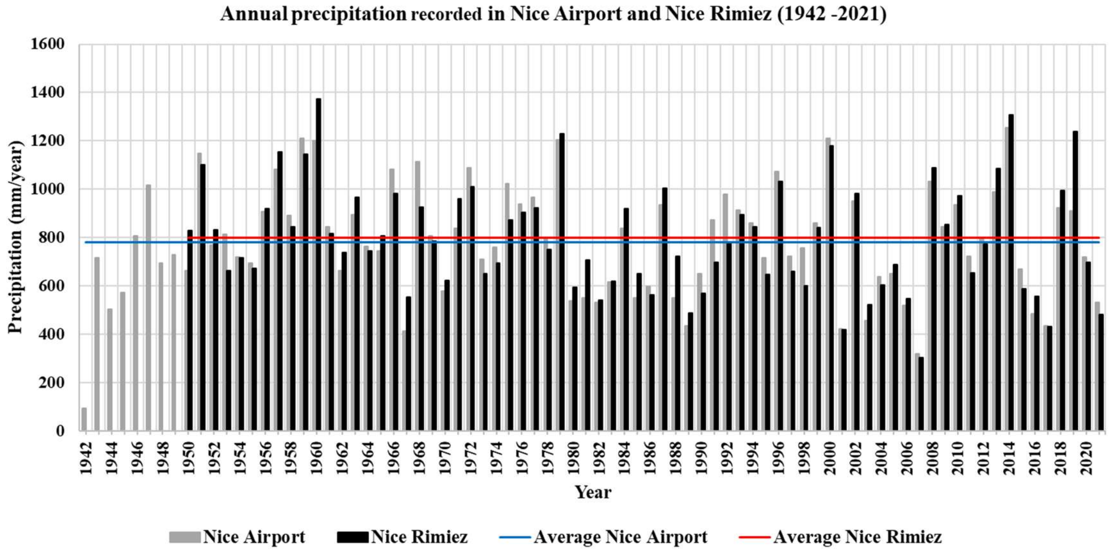

Figure 56 Annual precipitation recorded in Nice Airport and Nice Rimiez (1942-2021).

The evapotranspiration process, including both actual evapotranspiration (AET) and potential evapotranspiration (PET), along with temperature, is averaged across the entire catchment using 31 grid points derived from Météo-France SAFRAN data spanning from 1958 to 2023 (Figure 57). The SAFRAN dataset provides daily meteorological insights including rainfall, air temperature, and evapotranspiration through maps with a resolution of 8000m × 8000m. As expected in a Mediterranean climate, the average temperature values, ranging from 5 to 20°C, are highest in summer months and lowest in winter. The PET attains its highest value during July, owing to its strong correlation with temperature and sunlight duration. In contrast, the AET reaches its peak in June. Interestingly, the AET does not dip to its lowest point during summer, as might be anticipated due to precipitation constraints and soil water storage limitations. Upstream forested area with high retention of water may be contributing to maintaining the average AET values in summer. In aggregate, the annual PET can surge to 991 mm, while the annual AET maintains an average of 527 mm across the Paillons catchment.

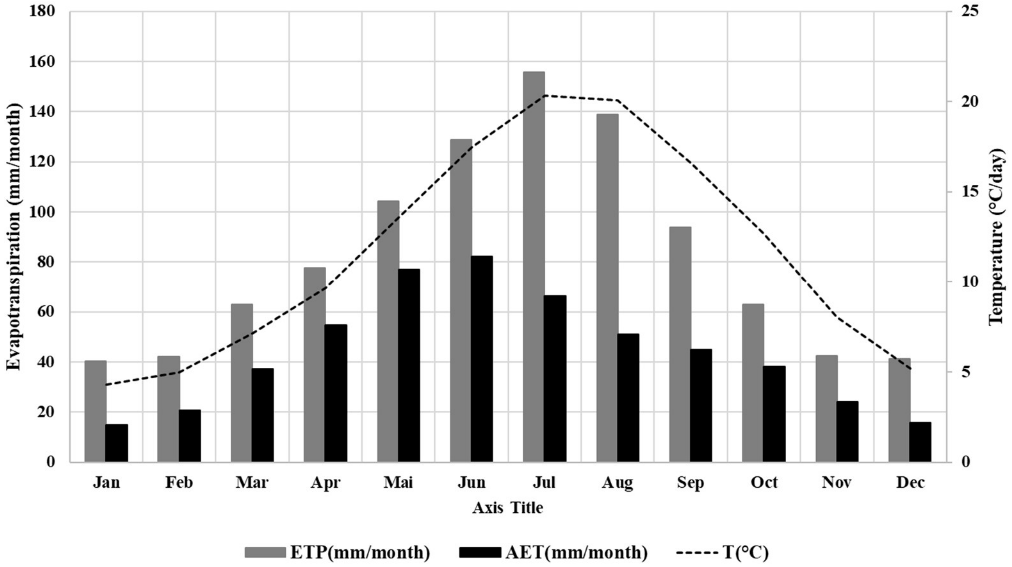

Figure 57 Average monthly evapotranspiration and daily temperature in the Paillons catchment using 31 grid points (Source: Météo-France SAFRAN database 1958-2023).

The national and local stations presented in Figure 53 also record temperature data. The longest series available are for the national stations. The local stations have gaps in records. To analyze the trends in observed temperature at daily levels the average all national 9 stations over the Paillons catchment are considered (Figure 58). Between a maximum of 30°C and a minimum of -3°C, the temperatures in the Paillons vary around an average (red line in the figure) of 13°C with a linear trendline (blue line in the figure) which is slightly increasing since 1993.

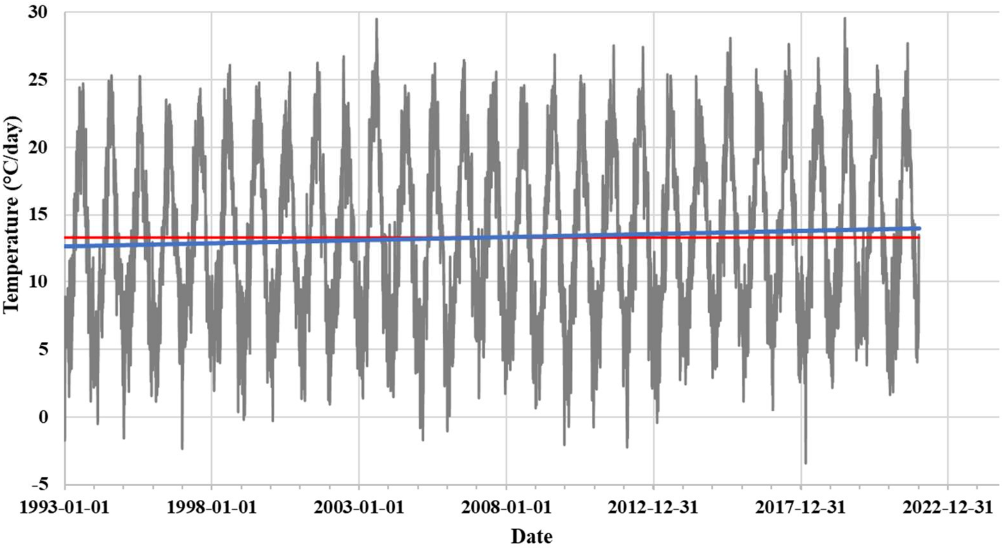

Figure 58 Average observed daily temperature of 9 national stations in the Paillons catchment (1993-2021).

2.4.8. Hydrological context

Runoff time series were collected for the period 2010-2020 at 10 stations in the open part of the river and at 3 locations in the covered part (Figure 37). 5 stations out of 13 are located in the Lower Paillon River due to the sensitivity of the area to flooding. Cameras records are also available in the area of the covered river and road tunnel. Raw data has gaps and errors that need to be addressed. Errors in records are caused by monitoring system failure and problems with transmission of information to the central database. In addition, rating curves used to estimate discharge were updated several times over the period of records. Data analysis should therefore fix errors and gaps and harmonize runoff time series. Additional field data measured during drought periods can be compared to the automatically recorded water depths and discharges to help improve the quality of runoff time series. To understand the characteristics of runoff in the Paillons, filtered records and review of literature are used.

The data for runoff records is derived from water depths measured and discharge estimated using distinct rating curves. When studying the reaction of a river under varying flow circumstances, the initial query is about the consistency of the records over time. At the ABA station, the most downstream stations with longest time series, two different types of rating curves were employed to calculate runoff based on the measured water depths (Figure 59). Interestingly, for identical water depths measured, the discharge varies between different time periods.

Available records from 2010 to 2021 can be separated in two periods, 2010-2016 and 2017-2021. The maximum difference in discharge for the same water depth is 100 m^3/s for estimated discharges less than 400 m^3/s. The raw datasets include systematic errors that should be corrected. From 0 to 1 m water depths the curves are very similar. The values diverge when water depths increase from 1 m upward. In addition, all values above 2.5 m or 300 m^3/s of discharge are incorrect because they rise and drop within 6 mi, unrealistically. Plotting with wrong values allows to have an idea of the rating curve validity range. Possible reasons for decreasing discharge for a given water depth are changes in river geometry or use of new methods. In the period 2010-2021, only up to 55 cm of sediment deposits or removal have been observed, with no change in the width of the bridge under which measurements are implemented. This is not sufficient to explain such changes in rating curves. The likely explanation lies in the technic used and the fact that after some years of experience, discharge was overestimated at that location. Direct field measurements to validate automated records are sparse and only available for discharges during drought or low flow periods. This is an opportunity to harmonize the data before comparing to model results.

From runoff data provider (MNCA), uncertainties exist in the water depth measurements. At ABA gauge, errors in measured water depth fluctuate up to 12, 20 or 40 cm depending on the location. Runoff data often vary from high values during flood to low values during drought or no rain, but in the raw data available, water depths in summer with no rain are higher than water depth with rain at several dates. This is a challenge in calibrating or validating modeling results for continuous and long periods. It is also delicate to use the raw data directly to assess the flow characteristics and river response to flood events. For hydraulic modeling, it is possible to select few events for calibration and validation. The strategy is to select several events after making the data consistent over the period of availability. A statistical approach can therefore be used to generate synthetic hydrographs for creating flood maps for different return periods.

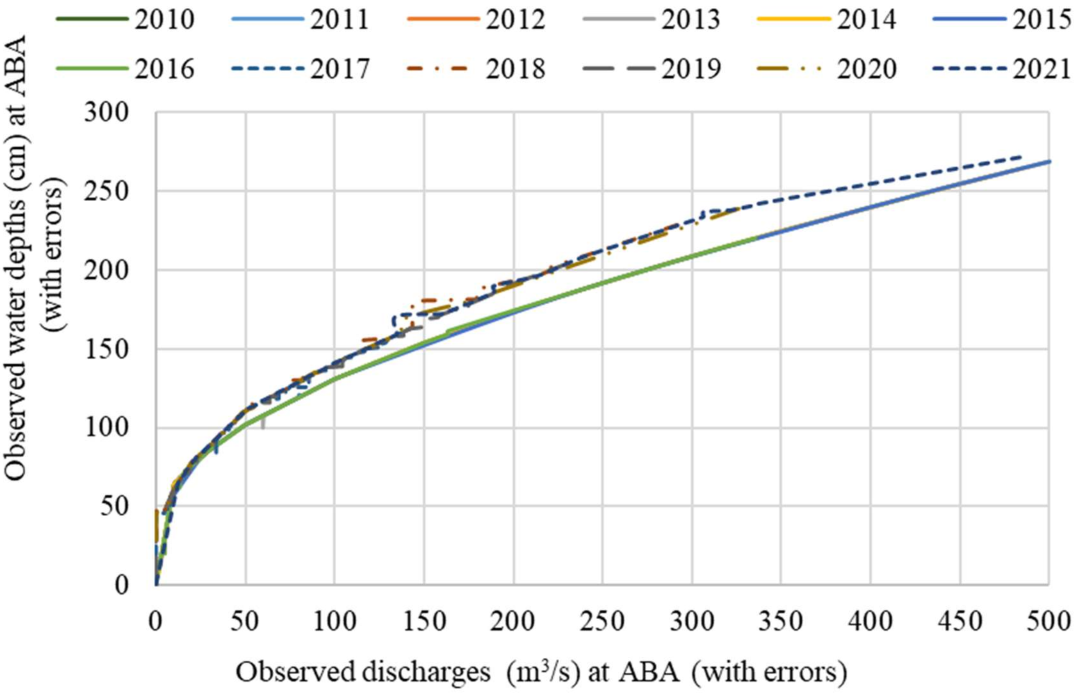

Figure 59 Plot of observed water depths and discharges 2010-2021 (Game et al., 2023b).

Besides ABA station, PAS and Coty are two other gauging station available in the LPR with water depths records only. In the covered river, the entrance, the middle, and the junction with the sea are also gauged, but water depths are only available in 2017 and 2018. Table 12 shows some statistics of the raw datasets. ABA is the station with the most available data (90%). PAS and COTY has less than 28 and 33% data available between 2010 and 2021. Min and Max of the raw data represent erroneous records, and not representative of the period of data. Factors like hardware issues, sediment transport and removal, waves on the free water surface and land-use can explain gaps and errors in automatic data measurements. Lower Paillon is a torrential river. Flow processes can generate waves of up to 1 m on the water surface during extreme events. In dry periods, artificial ponds at ABA, Coty or PAS bridges happen regularly due to erosion or anthropic activities. Ponded water increases measured water depths by the automatic system which does not reflect the flow conditions. In addition, erosion of the riverbed can decrease the bottom elevation and lead to wrong measurements of water depths. In consequence, unrealistic discharges are computed using rating curves.

Table 12 Statistics of raw data (water depths and discharges) available between 01/01/2010 and 30/04/2021 at ABA bridge (Game et al., 2023b).

Station _ Parameter	Min	Max	Mean	Std	Missing (%)
ABA, depth(m)	0.00	5.07	0.66	0.43	11
ABA, Q(m^3/s)	0	500	27	60	10
PAS, depth(m)	-1.00	4.75	0.80	1.63	73
PAS, Q(m^3/s)	0	22	5	8	72
Coty, depth(m)	0.00	4.00	0.25	0.45	67
Coty, Q(m^3/s)	0	0	0	0	100

Since water depths and discharges automatic measurements are affected by river management practices, this study explored the available field measurements during dry periods to have a better understanding of baseflow in the LPR. Figure 60 describes baseflow variations from 0 to 4.5 m^3/s. On average, it is about 1 m^3/s, but highly variable over time. In fact, the river is exposed to complete drying in non-rainy periods at any season (summer, winter, spring or fall). Floods occur so fast that field validation of discharge during flood events have not been implemented. Release of water from some human activities such as water treatment plant contribute to the baseflow in few l/s to some m^3/s in rainy periods. Water uptake in upstream tributaries for irrigation, drinking and industrial purposes have an unevaluated impact on baseflow, especially during dry season. Existing weirs and sediment traps can also retain flow that will benefit infiltration and evapotranspiration in the riverbed.

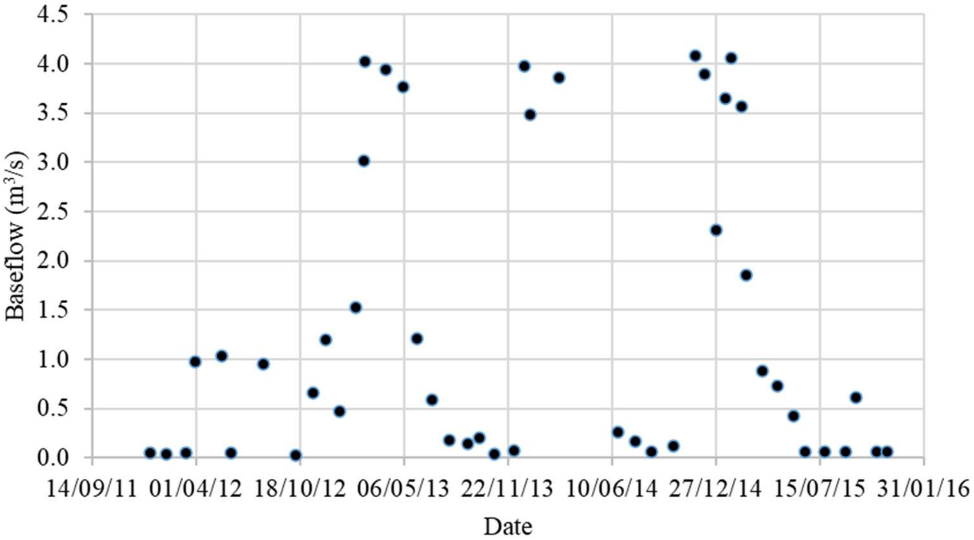

Figure 60 Baseflow measured at ABA (data extracted from Tennevin et al., 2017).

Combining automatic runoff records, baseflow measurements and rating curves, this approach improved the quality of time series of water depths and discharge estimates needed for model calibration and validation. Discharge is recomputed with the most recent rating curve. First, water depths and discharges values that do not fit the ratings curves are excluded from the datasets. Second, the unrealistic rises between three timesteps are replaced by the average of lowest values. Then, discharge is recomputed using the most recent rating curve. Additional moving average smoothing is performed to remove noise in the data. For non-rainy periods, the discharge is decreased to reflect the observed baseflow without recomputing equivalent baseflow water depths. The minimum discharge for driest months likes in July is assumed to be 0.02 m^3/s, except periods with flood events. This threshold reflects an almost dry river. The raw data have an undeniable quality, regarding the shape of the hydrographs and the timing of the pics. The calibration and validation of the hydraulic and hydrological models can rely on selected hydrographs that match the above quality criteria.

Figure 61 shows the observed 6-mn discharge and water depths at ABA station for 2011-2020. The data was corrected and smoothed. At least 9 events were above 100 m^3/s during this period. But there are events for which no records were available. The maximum observed water depth was in 2014 at 1.97 m for a peak discharge of 213 m^3/s. Only hourly and daily averages can be calculated, monthly and annual averages from this dataset will not be realistic.

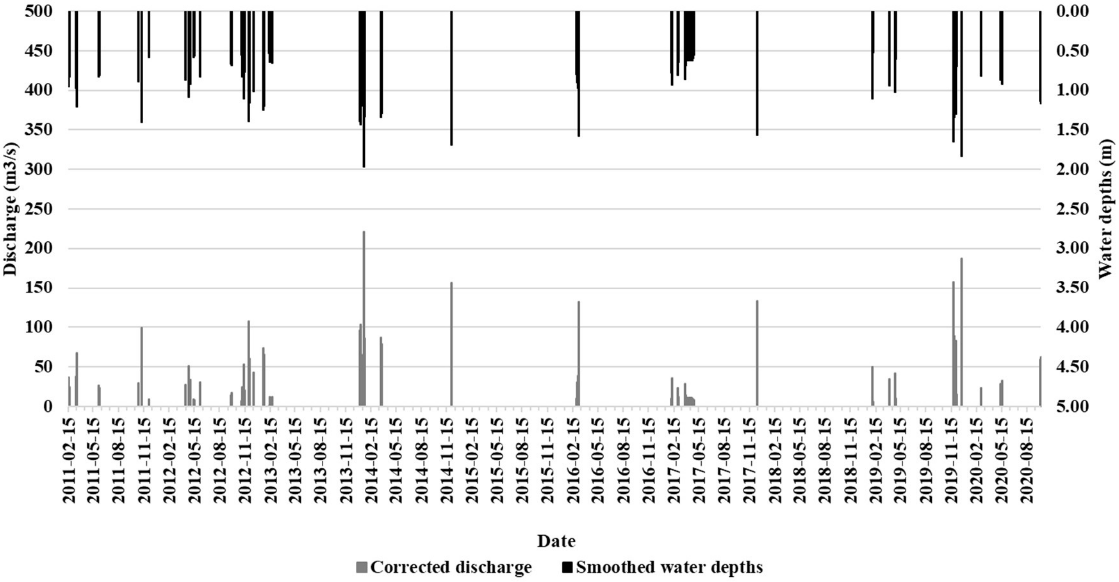

Figure 61 Observed 6-mn discharge and water depths at ABA station (2011-2020).

To analyze the characteristics of runoff hydrographs, this study uses the dimensionless hydrograph approach on selected 12 observed hydrographs including 6 annual maxima at ABA station. Figure 62 shows the annual maximum discharges for the periods 2000 and 2011-2019 but may not reflect the reality of that period due to missing records for major flood events and uncertainties in discharge estimates. After making corrections and smoothing on raw data, the maximum discharge for the period 2011-2019 is 213 m^3/s for the event in January 2014, followed by 184 m^3/s for the event in December 2019. In addition, the dimensionless hydrograph of the November 6th, 2000, flood event at a nearby station was included due to its proximity and estimated intensity of 400 m^3/s.

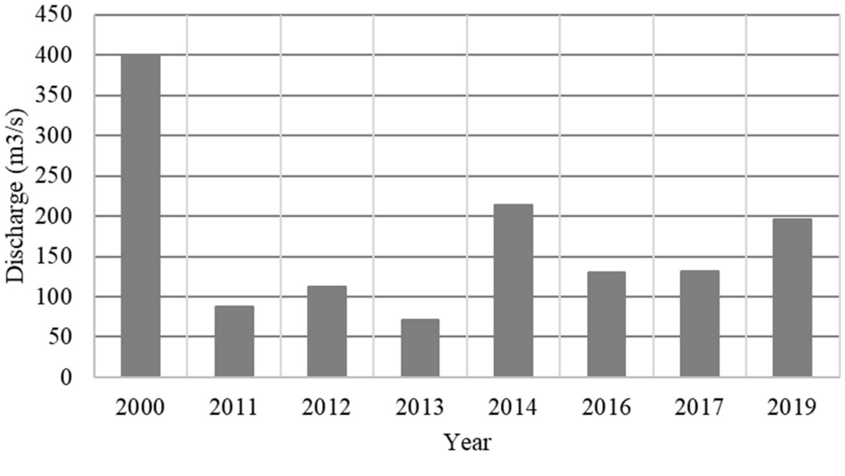

Figure 62 Annual instantaneous maxima observed at ABA station (Game et al., 2023b).

Le Gouz de Saint Seine (1995) estimated the 10-year and 100-year instantaneous flood to be 260 m^3/s and 825 m^3/s, respectively. In the 1999 flood prevention plan of MNCA, 260 m^3/s and 750 m^3/s were used for both return periods. A new study (Tennevin et al., 2017) suggested 373 m^3/s and 794 m3/s. For the 100-year flood there is a good agreement between different approaches. But the 10-year flood estimates differ by more than 40%.

Dimensionless hydrographs in Figure 63 show that the average response shape is triangular. But there is a strong variability between events. This approach was implemented successfully in Zavattero (2019). Intense events tend to be thinner and small and medium events are flat in shape. In fact, extreme events happen very fast in the LPR. Rising and recession times decrease with increasing intensity of flood events. Observed data is for medium to small events less 213 m^3/s, except for the event of November 2000 estimated at 400 m^3/s. Therefore, the average hydrograph (red curve) may not reflect the shape of extreme events. An estimate of the 100-year hydrograph (Tennevin et al., 2017) show that within 24 h an event of 794 m^3/s can occur. Between 0.46 and 0.65 dimensionless discharge, the red and green curves are very similar. Outside that range the two curves greatly diverge. The minimum of observed at each time step (light blue curve) has the same duration as that of the green curve but has a smaller volume. The associated catchment area is about 236 km^2. Heavy rain is often responsible for extreme flood events within a few h to a couple of days. Since the minimum observed (curve) represents a fast response event, it is assumed to be the synthetic hydrograph for calculation of return period hydrographs needed as boundary conditions in the 1D-2D hydraulic model of the lower Paillon valley.

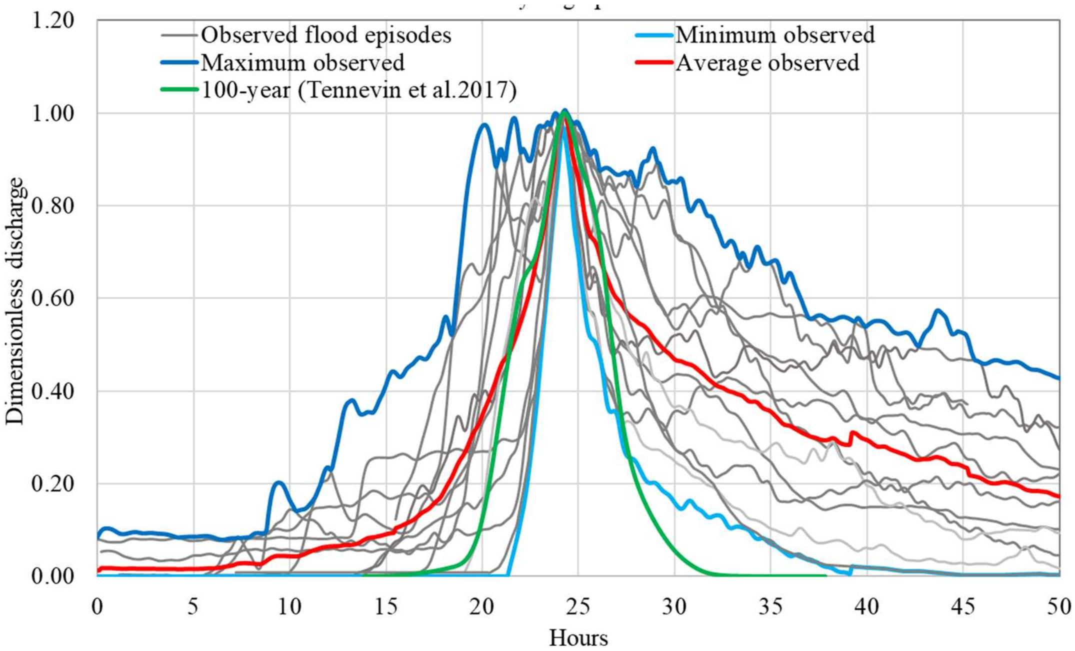

Figure 63 Unitless hydrographs for 12 events at ABA station (Game et al., 2023b).

Applying the Gumbel method to observed annual maximum discharges like in Figure 64, this analysis can estimate the peak discharge for 6 return periods. The best fit is a polynomial equation of order 2. Computed values are reported in Table 13. Results for 2-yr, 5-yr, 10-yr, 100-yr, 200-yr and 1000-yr return periods are computed. Estimated peaks for 100-yr and 10-yr are like those found in Tennevin et al. (2017).

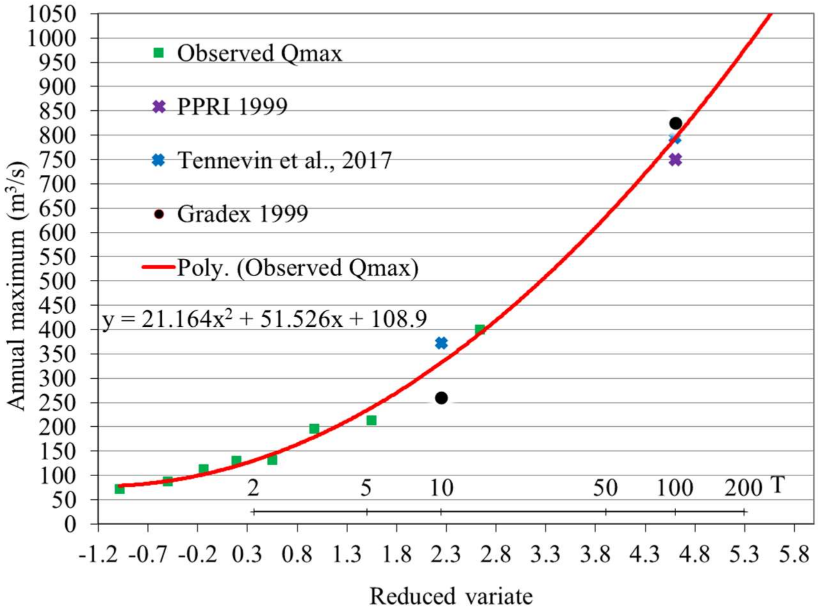

Figure 64 Plots of Gumbel distribution of observed annual max. discharges.

Table 13 Comparison of peak flood discharge for different return periods (x = no data) (Game et al., 2023b).

Return period in years	Gumbel variable	Estimated peak discharge (m^3/s)	PPRI 1999	Gradex 1999 (m^3/s)	Tennevin et al.,2017 (m^3/s)
2	0.3665	131	x	x	x
5	1.4999	234	x	x	x
10	2.2504	332	260	260	373
100	4.6001	794	750	825	794
200	5.2958	975	x	x	x
1000	6.9073	1475	x	x	x

With the peak discharges and the minimum observed dimensionless hydrograph, this method generates the boundary conditions for the hydraulic models for the study of exceptional events in the Paillons catchment. Figure 65 presents the resulting hydrographs for 2-year, 5-year, 10-year, 100-year, 200-year and 1000-year return periods.

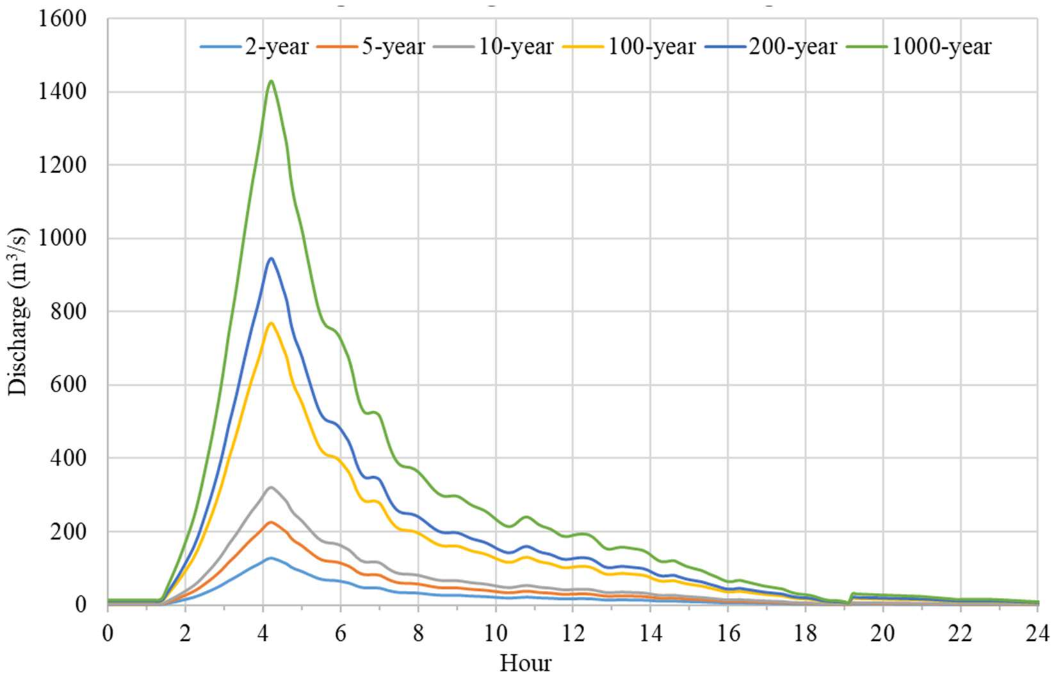

Figure 65 Estimated 6-mn timestep peak discharges for 6 return periods.

2.4.8. River exchanges with aquifers

The Lower Paillon River is actively managed. From one year to the other, local authorities clean the riverbed and banks to prepare for flood periods. The cleaning consist of the removal of vegetation and materials like pebbles and gravel. Therefore sediment distribution is affected by river management activities. There is no specific study on river-aquifer exchanges in the LPR. The water table is supposed to be generally below ground, but there are reports of groundwater leakage into the covered part of the river which is paved. Piezometric data in the riverbed is not available. A field visit of the riverbed in September 2021 collected images of the different faces of the riverbed between two cleaning periods (Figure 66). After the cleaning, the riverbed is generally dominated by sediments composed of gravel of different sizes and fine sediments.

Fine sediments

Fine sediments and gravel

Sediments and gravel

Small gravel

Enrockments, ponded water, vegetation , fine sediments and gravel

vegetation , fine sediments and big gravel

Stream, vegetation , fine sediments and big gravel

Vegetation , fine sediments and big gravel

Figure 66 Different faces of the riverbed in September 2021 between two cleaning periods.

Conclusion

This review and data analysis confirm the necessity to investigate how to model complex runoff processes and groundwater recharge for real-time DSS in the context of water hazards and resources management in the Paillons catchment, with a particular emphasis on strategies for long-term simulations. In fact the Paillons catchment is characterized by heterogeneous geology and highly variable meteorology. The downstream valley is heavily urbanized and needs to protect people and assets against flood hazards while providing water resources for drinking and economic activities.

Gaps and errors in monitoring data pose a serious challenge in understanding the characteristics of the hydrological cycle and the magnitude of extreme events. For the period 2011-2020, not even a single year has complete and reliable time series of runoff information in the Paillons.

Interestingly, innovative modeling approaches like image-based and deterministic methods can provide the solutions to fill the gap in data and improve knowledge of hydrological processes and extreme events in this catchment. Thus, the next chapters will focus on setting up, testing, and applying the different modeling tools previously mentioned to model the runoff, surface flow and groundwater flow in the Paillons catchment. The calibrated models are expected to be integrated in the AquaVar DSS as the AquaPaillons system.

Chapter III. Development of MIKE SHE, MIKEPlus (1D-2D), Feflow and Fudaa-LSPIV models in the Paillons catchment and its lower valley, Nice, France

Introduction

Coastal regions host densely populated urban centers where rapid economic development is intricately linked with swift urbanization (Zavattero, 2019). Rivers, often interwoven into these urban landscapes, offer both resources and potential hazards. The increasing competition between economic activities and the spatial demands of rivers necessitates efficient management grounded in dependable tools. The Paillons River, situated in the southern part of French Riviera, serves as an urban river intertwined with diverse land-uses including industries, agricultural fields, and urban zones. Unquestionably, this location falls within the purview of stressed coastal areas, grappling with the delicate equilibrium between economic advancement and the susceptibility to risks such as flooding, water contamination, and water scarcity.

Upon a comprehensive evaluation of the meteorological, geological, and hydrological attributes within the Paillons catchment, it becomes evident that the environmental system in this region is significantly influenced by multifaceted hydrological processes that interact at various times of the year. In alignment with the prerequisites of the AquaVar modeling system, the chosen modeling framework should be capable of simulating runoff, surface water flow, and groundwater flow processes within a time frame shorter than the Paillons' rapid concentration time. This temporal aspect is crucial to afford decision makers ample time for formulating and executing strategies or actions in response to extreme events.

In the expansion of the AquaVar Decision Support System (DSS) to encompass the Paillons, the sequence in which various modeling tools are constructed may not be rigid, yet the groundwater module demands river water depth data for an extended period, which is not readily available in the existing records. Consequently, initiating the modeling approach might entail the use of image-based techniques for the assessment of river discharge, along with the application of surface hydraulic modeling to depict river flow and flood occurrences. The employment of an image-based methodology for analyzing video records stems from the necessity to optimize collected runoff data and offer an alternative means for validating modeling outcomes, given the uncertainty surrounding the prompt resolution of data gaps in measurement records. Subsequently, the development of the hydrological model and the groundwater model can proceed in parallel, given that the latter is essentially an intricate refinement of the saturated zone component within the hydrological model. Such numerical models are frequently adopted as decision support tools to empower decision makers in evaluating the ramifications of climate variability.

This chapter commences with an overview of data requirements and a discourse on the distinct functions within the modeling tools. The subsequent segment outlines the establishment of Fudaa-LSPIV for image-based assessments. Following a cohesive modeling approach, the hydraulic model of the LPR (Local Paillons River) is constructed using MIKEPlus. As explained in the first chapter, MIKEPlus was used instead of MIKE21FM to take advantage of the additional 1D river network and sewer modules available in MIKEPlus. The next section delves into the exploration of data interpolation techniques, aimed at selecting the most suitable method for the Paillons context. The procedural steps for configuring Feflow to embody the detailed groundwater module are outlined. Given that hydrological and groundwater models necessitate spatially distributed information, which may be available only at limited locations, the assembly of the hydrological model through the use of Mike SHE is deliberated in the fourth section.

3.1. Overview of collected data

The available data within this project, along with their corresponding resources, are itemized in Table 14. The GIS department of MNCA has provided support for this endeavor. Topographical details for the Paillons area are accessible at resolutions of 0.25m×0.25m, 1m×1m, and 5m×5m. The purpose of the Digital Terrain Model (DTM) is to depict land-use excluding structures and vegetation, making it suitable for surface flow simulations. Notably, the 0.25m × 0.25m resolution data, collected in 2018 and encompassing MNCA territory, is particularly valuable for hydraulic modeling of the LPR. In contrast, the 5m × 5m resolution data from 2009 and the 1m × 1m data from 2013 cover the entire Paillons catchment, serving well for catchment-scale topographic representation.

Land-use and vegetation information, obtained in raster data format with a resolution of 100m × 100m, were sourced from the European Agriculture Center. This dataset offers comprehensive coverage of land-use across European countries, originating from 2006 and encompassing three tiers of land-use categories. From the third tier of classification onward, vegetation details can also be extracted. In 2017, MNCA performed an update, introducing a fourth classification level that furnishes more intricate land-use information.

Soil surveys within the Paillons catchment are relatively sparse, primarily concentrated in the lower valley due to urbanization's prevalence. The soil information integrated into the hydrological modeling assessment primarily derives from the European Soil Center. During April of 2016, the European Soil Center unveiled its latest soil distribution map, which encompassed a substantial portion of European countries. This dataset was generated using satellite imagery at a resolution of 500m × 500m, providing insight into the proportions of sand, clay, and silt within the soil composition (Ma, 2018). In the Paillons, the soil is made up on average of 31% of sand, 28% of clay and 41% of silt according to the classification from the European soil center. However, such description from remote sensing was not validated on the field, and do not describe the real complexity of soils depth and textures. This study assumes that it can depict in a raw way soil behavior regarding infiltration and surface runoff processes.

As reported before, the meteorological datasets used in this study was provided by Météo-France and MNCA. Moreover, one distributed database, so called SAFRAN data, produced by Météo-France was also available. The SAFRAN data include rainfall, snow, air temperature and evapotranspiration at 8000m × 8000m resolution. MNCA also supplied the video records of some flood events, the infrastructure and configuration details for the covered river. Data regarding sea level and the bathymetry of the near-shore were sourced from the database of France's Naval Hydrographic and Oceanographic Service (SHOM). Geological layers and groundwater levels were obtained through the extraction of information from technical reports and thesis studies provided by MNCA.

Table 14 Summary of data collected for modeling purposes.

Data	Source	Characteristics
DTM	MNCA	Resolution:0.25 m x 0.25 m & 1m x1 m
Land-use	European Agriculture Center & MNCA	Recorded at 2006 (100m x 100m resolution) Updated to level 4 in 2017 for MNCA territory
Soil maps (sand, clay and slit percentage)	European Soil Data Center	Recorded in 2009 (500m × 500m resolution)
Vegetation	European Agriculture Center	Recorded at 2006 (100m x 100m resolution)
Buildings/Roads	MNCA	All types
Geometry of the covered river and tunnels	MNCA	Plans and cross-sections
Riverbed profiles at gauging stations	MNCA	8 stations (2022)
Video records	MNCA	Stored every 30-mn during the flood for 3 flood events
Runoff records (discharges / water depths)	MNCA	13 stations (6-mn) Period: 2011 - 2021
Rainfall records	MNCA & Météo-France	9 national stations (daily, hourly, 6-mn) 9 local stations(6-mn)
Air temperature	MNCA & Météo-France	9 national stations (daily) 9 local stations (6-mn)
Reference Evapotranspiration	Météo-France	Daily SAFRAN data (8000m × 8000m distribution map)
Snow cover	Météo-France	Daily SAFRAN data (8000m × 8000m distribution map)
Sea levels	SHOM	1 station (10-mn) 2010-2021
Bathymetry of near shore		Resolution:1m x 1m
Geological layers	MNCA	Extracted from pdf reports
Groundwater information	Pline 1991 MNCA BRGM	Historical records (1954-1974) at 4 points Two days in 2010 in three areas Initial records of existing or closed pumping wells, piezometers, springs, etc.

3.1. Functions within the modeling tools

3.1.1. Functions in Fudaa-LSPIV

Figure 67 illustrates the function choices within Fudaa-LSPIV, which are determined based on the accessible video footage. The "Images" component serves as the platform for loading and annotating video records. To derive discharge information from these images, the video undergoes a mapping process using the "Orthorectification module," followed by the application of algorithms within the "Analyse LSPIV" module to calculate surface velocities. This involves establishing the interrogation area and search region. Subsequently, the "Post-traitement" module employs algorithms to eliminate implausible velocities and determine average velocities. Within the "Débit" module, users can define the cross-sectional profile and subsequently compute the discharge.

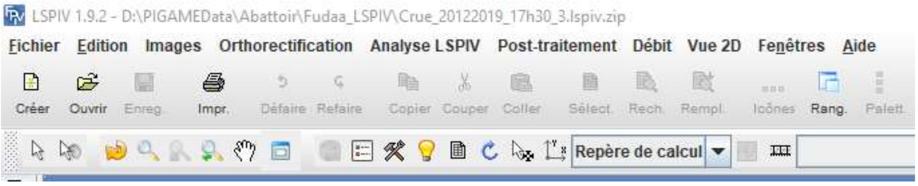

Figure 67 Functions selection of Fudaa-LSPIV at ABA station.

3.1.2. Functions in MIKEPlus

To simulate surface hydraulics and flooding within the LPR area, two key features, namely "River network" and "2D overland," are chosen from a selection of 4 available modules within the collection system network (Figure 68). These features necessitate accurate river geometry and floodplain topography data. The approach adopted in this study involves coupling a 1D river network model with a 2D floodplain model. This coupling strategy enhances the representation of the covered river's geometry while simultaneously reducing the computational time required in a full 2D riverbed model. Given that the river cross-section in the LPR region is less than 100 m, achieving a precise representation of the river profile and associated structures would demand a finely detailed grid resolution. For surface flow modeling, the hydrodynamic module is employed.

Expanding the river network to encompass the entire catchment area offers the advantage of integration with the available MIKE SHE product for hydrological simulations. Land-use information is incorporated through the assignment of Manning-Strickler coefficients within each of the features. Additionally nearshore bathymetry data contribute to an accurate depiction of coastal elevations within the domain.

Within the "River network" module, specifications for rivers, cross-sections, and bed roughness are established. In the "2D overland" module, configurations for the floodplain, infrastructures, and surface roughness are defined. All boundary conditions are comprehensively described within the "Boundary conditions" module. Finally, the "Simulation specifications" section encompasses the definition of hydrodynamic parameters, the simulation period, and time steps.

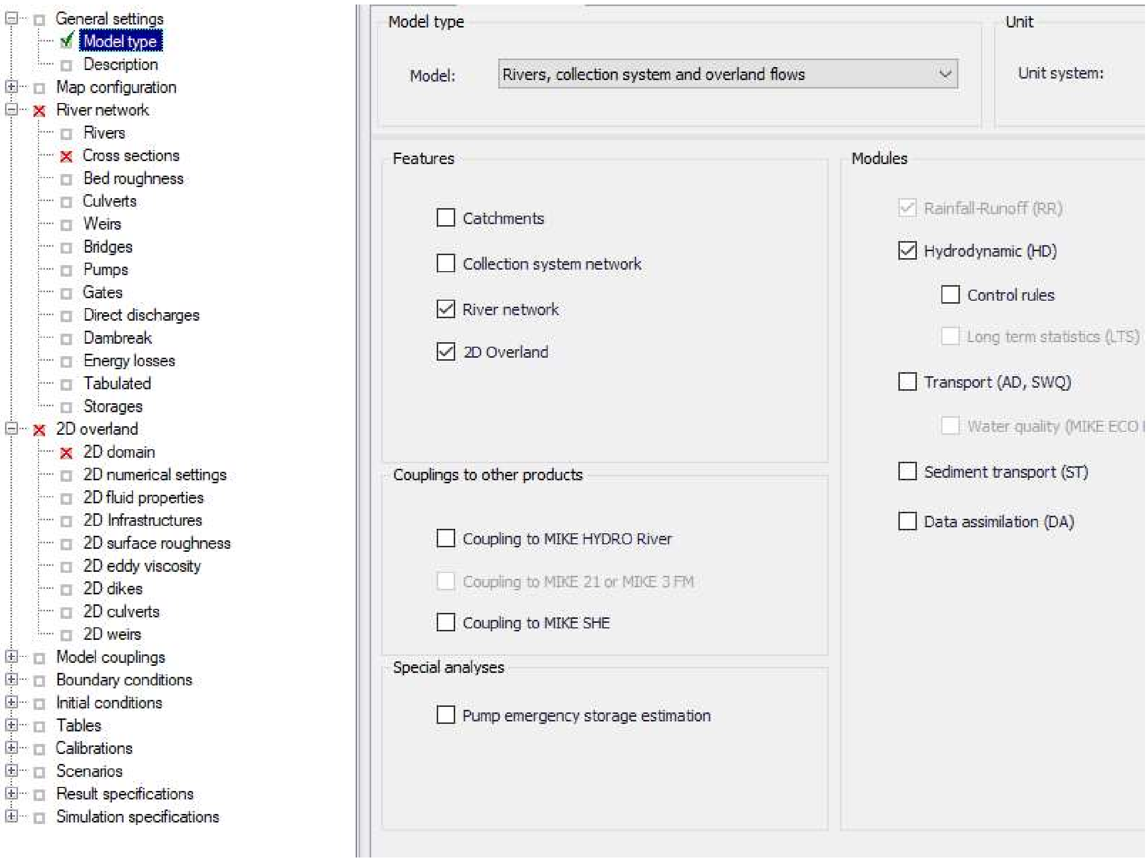

Model: Rivers, collection system and overland flows

☐ Catchments
☐ Collection system network
☑ River network
☑ 2D Overland

☑ Rainfall-Runoff (RR)
☑ Hydrodynamic (HD)
☐ Control rules
☐ Long term statistics (LTS)
☐ Transport (AD, SWQ)
☐ Water quality (MIKE ECO
☐ Sediment transport (ST)
☐ Data assimilation (DA)

☐ Coupling to MIKE HYDRO River
☐ Coupling to MIKE 21 or MIKE 3 FM
☐ Coupling to MIKE SHE

☐ Pump emergency storage estimation

Figure 68 Functions selection of MIKEPlus in the LPR.

3.1.3. Functions in MIKE SHE

The function selection in MIKE SHE model is presented in Figure 69. To simulate multi-hydrological processes in the Paillons catchment, the Water Movement (WM) module was activated. With DTM available at high resolution in this study, the “Finite Different” method in “Overland Flow (OL)” module was used to have more precise simulation of surface water flow. But, the flow movement in MIKE SHE is computed by the 2D St.-Venant equations with diffusive wave approximation, thus, the channel flow module “Rivers and Lakes (OC)” is executed by coupling with a MIKE 11 model (Ma, 2018).

The soil data collection in this project has large uncertainty mainly because the soil type generated with the material percentages were available. Therefore, an assumption was made on the soil parameters such as the connection between soil moisture and the hydraulic conductivity. Further, in the “Saturated Flow (SZ)”, the depth of the soil needed by the MIKE SHE model to describe the lower boundary simulation was assumed. To reduce the data requirements and uncertainty in inputs, the “2 Layer UZ” function was implemented in the “Unsaturated Flow (UZ)” module.

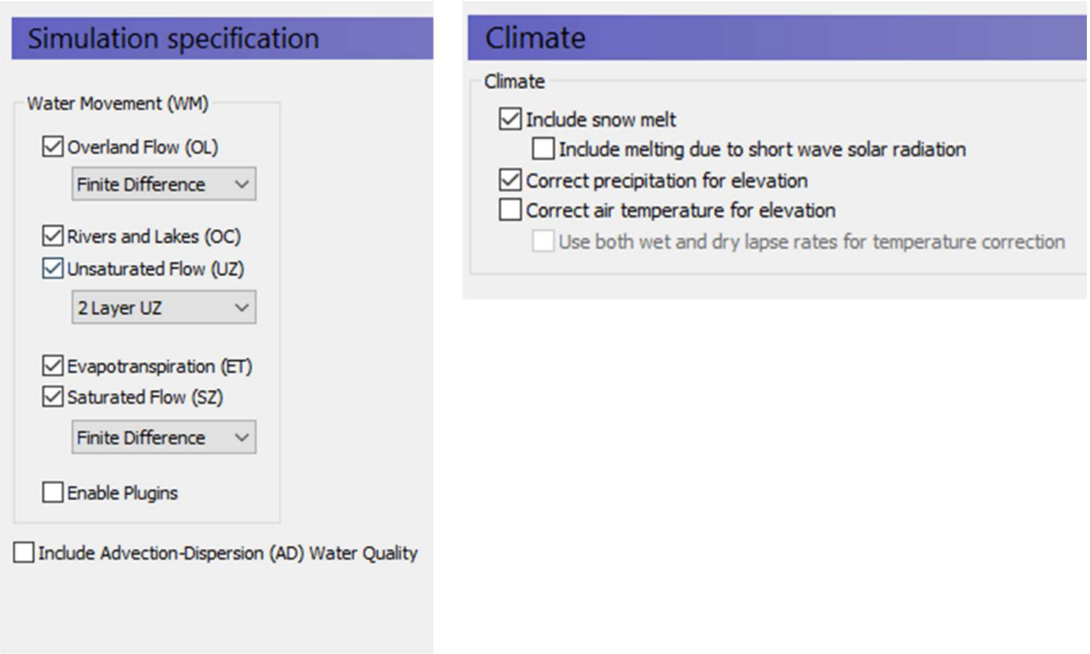

☑ Overland Flow (OL)
Finite Difference
☑ Rivers and Lakes (OC)
☑ Unsaturated Flow (UZ)
2 Layer UZ
☑ Evapotranspiration (ET)
☑ Saturated Flow (SZ)
Finite Difference
☐ Enable Plugins
☐ Include Advection-Dispersion (AD) Water Quality

☑ Include snow melt
☐ Include melting due to short wave solar radiation
☑ Correct precipitation for elevation
☐ Correct air temperature for elevation
☐ Use both wet and dry lapse rates for temperature correction

Figure 69 Functions selection of MIKE SHE in the Paillons catchment.

Within the climatic context, the simulation of snowmelt in MIKE SHE was selected to capture the potential effects of changes in snow cover. Nonetheless, it is noteworthy that snow cover occurrences in the Paillons region are not frequent and limited to the highest crest. Furthermore, although the SAFRAN database could provide distributed air temperature data for the entire Paillons catchment, its limited resolution (8000m × 8000m) rendered it unsuitable for representing temperature fluctuations in the area. Consequently, an alternative approach was taken. Instead of relying on a fully distributed air temperature map, the "Station based" functionality within MIKE SHE was selected. This function facilitates the representation of air temperature using data from various gauge stations (Figure 70). Notably, local stations are identified by single or double-digit numbers, while national stations are denoted by seven-digit numbers. Given that gaps exist in the data from local stations, adjacent national stations are used to supplement the missing information. Furthermore, the option to 'Correct air temperature for elevation' was employed. This feature serves to characterize temperature variations resulting from changes in elevation, with a global average rate of -0.649°C/100 m.

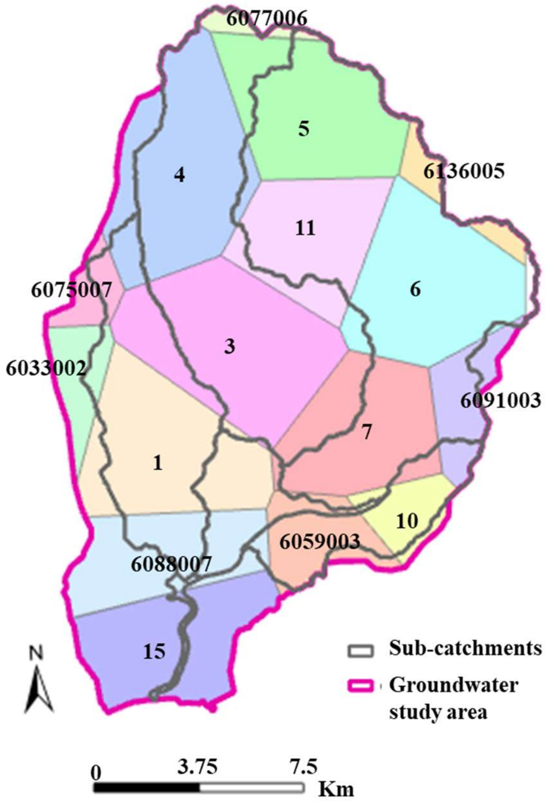

Figure 70 Station-based air temperature distribution in the Paillons.

3.1.4. Functions in Feflow

For simulating the groundwater processes within the unconfined aquifer of the Paillons catchment, the chosen approach involves employing a multi-layered 3D model (Figure 71). This 3D model, which can better represent the complexities of the saturated zone of MIKE SHE, encompasses all geological layers. Within the configuration parameters, the "unconfined aquifers" module is selected, allowing for an unrestricted head at the upper boundary of the domain. The "3D layer configuration" serves as the space to define the specific geological layers. Each layer's attributes, including geometry, process variables, boundary conditions, and material properties, can be established within the "Data" module. To establish connectivity between river runoff and groundwater, the "Fluid-transfer BC" function is used, while the assignment of outer or inner boundaries, such as sea levels or lakes, is accomplished using the "Hydraulic head BC" function. Given the limited availability of material property measurements in the Paillons area, assumptions are made, based on existing literature.

Recharge data estimated within MIKE SHE can be integrated into the "In/outflow on top/bottom" module. Notably, studies within the AquaVar project highlight the sensitivity of parameters like in-transfer and out-transfer rates, as well as drain-fillable porosity (or specific yield), within unconfined aquifers. Feflow stores all input data and simulation outcomes within a dedicated database, facilitating real-time visualization in both 2D and 3D modes during the simulation process. Additional sources or sinks can be introduced through the "Well BC" function for groundwater extraction and the "Fluid-flux BC" function for springs or inflow. Feflow is compatible with several formats including DFS2, ESRI shapefiles and ASCII Triplets files for spatial data, while time series data can be assigned using the "Time series" module. To assess and validate simulation results against measurements, "Observation points" are used.

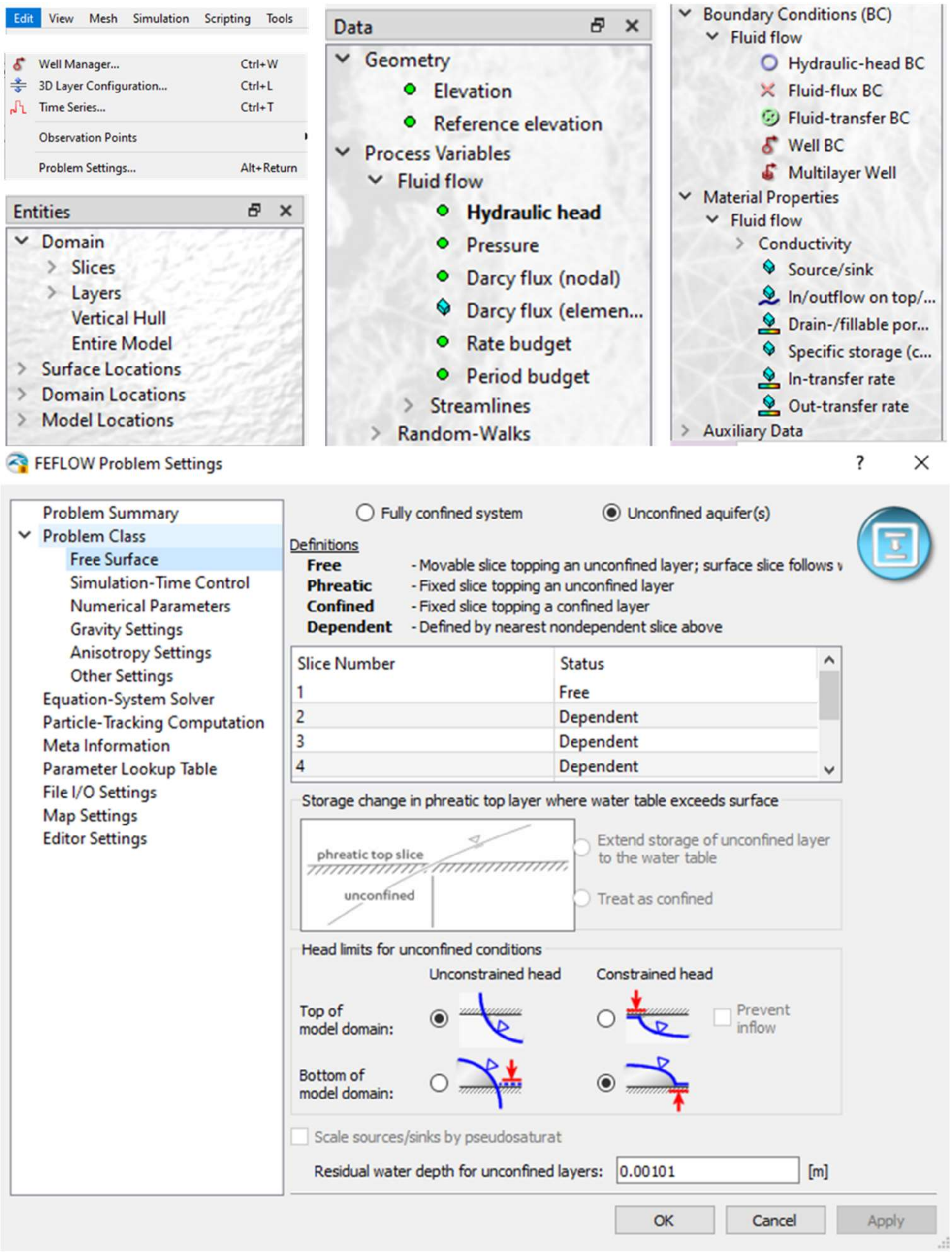

○ Fully confined system ● Unconfined aquifer(s)

Definitions

Free - Movable slice topping an unconfined layer; surface slice follows v
Phreatic - Fixed slice topping an unconfined layer
Confined - Fixed slice topping a confined layer
Dependent - Defined by nearest nondependent slice above

Slice Number	Status
1	Free
2	Dependent
3	Dependent
4	Dependent

Storage change in phreatic top layer where water table exceeds surface

○ Extend storage of unconfined layer to the water table

○ Treat as confined

Head limits for unconfined conditions

	Unconstrained head	Constrained head	
Top of model domain:	●	○	☐ Prevent inflow
Bottom of model domain:	○	●	

☐ Scale sources/sinks by pseudosaturat

Residual water depth for unconfined layers: 0.00101 [m]

Figure 71 Functions selection of Feflow in the Paillons catchment.

3.2. The Fudaa-LSPIV set up for the ABA station

The ABA gauge is at a bridge of the same name (Abattoirs) where the cross-section is about 73 m wide (Figure 72). Measurements include water depths and estimated discharge from rating curves. The rating curve was first estimated in 2009 then updated in 2017. The gauge is constructed with 3 measurement PARATRONIC US_{10} probes (left bank, centre, right bank) including 1 main, 1 backup and 1 inactive, 1 camera gauge scale, 1 camera on spillway, 1 scale on each bridge pier, 1 reverse scale on spillway, 1 water level bulb, and 1 water level reached probe. The validity range is 0 to 10 m with a precision of 0.2%. It averages water depths every 6 mn. Three thresholds have been defined for flood warning: 94 cm for vigilance, 112 cm for pre-alert and 136 cm for alert. Due to gaps in data, a reliable annual average discharge is unknown. However, estimates of floods for the 2 years and 100 years return periods are 130 m^3/s and 794 m^3/s, respectively.

Video records of 4 flood events in 2019 and 1 flood event in 2020 was provided by MNCA. For the 2020 event, gauging measurements are not available. This study aims to evaluate the peak discharges from the videos. The November 20th, 2019, is the reference event. Observed peak water depths and discharges estimated from rating curves of the other events are presented in Table 15. This study did not estimate discharge using rating curve. The discharge information was provided by the monitoring system and is a product of applying rating curves on water depths within the monitoring system. While waiting for the rating curve to be updated and new discharge information produced, the available data is implemented in decision making. Therefore it is considered as "observed" and correct data. The peak water depths vary from 0.51 m to 1.84 m. The associated discharges from rating curves are between 10 and 182 m^3/s.

Table 15 Conditions at ABA station for 4 flood events.

Date	Peak water depth H(m)	Rating curve discharge (m^3/s)
20/12/2019 17:30	1.84	181.41
23/11/2019 19:00	1.60	138.62
20/12/2019 12:00	0.51	10.00
21/12/2019 08:00	1.12	53.58
02/10/2020 17:30	1.31	83.98

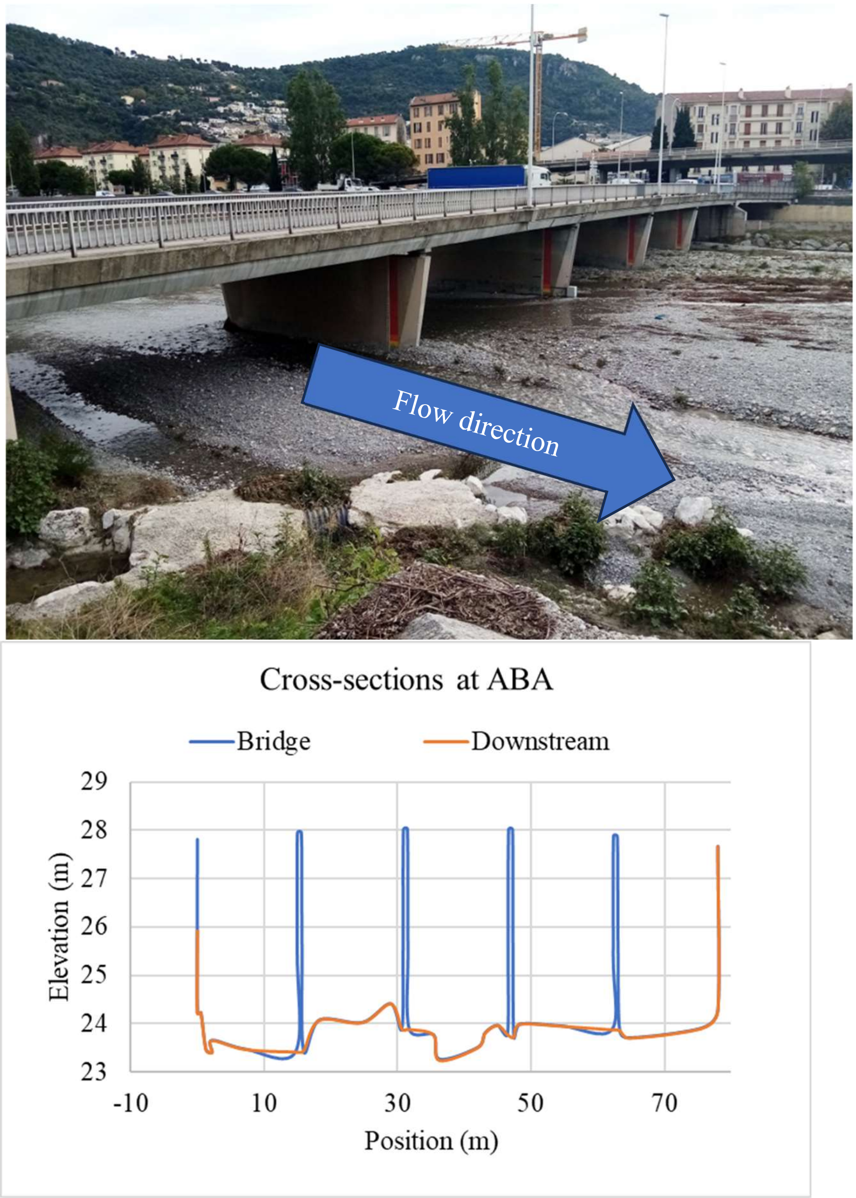

Figure 72 Image of ABA bridge with 5 openings (up) and corresponding cross-section plot from left bank to right bank in blue color (down). The orange plot is a cross-section 10 m downstream of the bridge.

The first step in processing images with Fudaa-LSPIV (Hauet et al., 2013; Jodeau et al., 2022) consists of importing images from video records (Figure 73). Two parameters describe each video: the number of frames per second (e.g., 25) and the timestep interval (e.g., 0.04 s). The video is converted into several frames. For example, the video record of the event of October 2nd, 2020, was converted into 204 frames.

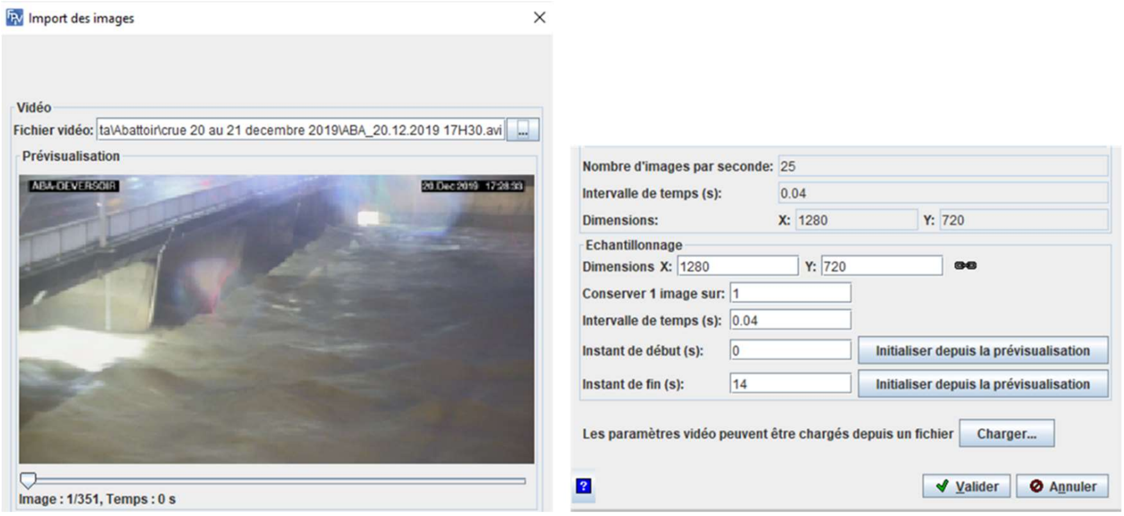

Fichier vidéo: ta\Abattoir\crue 20 au 21 decembre 2019\ABA_20.12.2019 17H30.avi

Image : 1/351, Temps : 0 s

Nombre d'images par seconde: 25

Intervalle de temps (s): 0.04

Dimensions: X: 1280 Y: 720

Dimensions X: 1280 Y: 720

Conserver 1 image sur: 1

Intervalle de temps (s): 0.04

Instant de début (s): 0

Instant de fin (s): 14

Les paramètres vidéo peuvent être chargés depuis un fichier

Figure 73 Setting up video images in Fudaa-LSPIV.

The second step is to define the flow area and to stabilize the video. This can be done by setting at least four reference points defining the extent of the flow. In fact, in some extreme weather conditions, high winds can affect the stability of the camera. Using the determinant of the Hessian matrix, the algorithm samples points of interest. Frames are coupled based on the identification of each point based on its size, orientation, and gradient of the neighborhood. Then a direct linear transformation method is applied to correct each frame. Each frame is orthorectified before computing flow velocities.

The third step involves cross-correlation analysis of all the frames to determine visible tracers on the free surface. An optimized algorithm is used to calculate the correlation between two points of the same interrogation area in two frames. The length of the displacements is then divided by the time interval to obtain the flow velocities.

The last step computes the discharges using surface flow velocities and the known cross-section. The cross-section should be defined from left to right bank. The default coefficient linking surface velocities to depth-averaged velocity is 0.85. The discharge is calculated using the method of the median section.

3.3. The MIKEPlus model for the LPR

In the complex hydraulic environment of the lower Paillons River, this study develops a model tailored to real-time DSS. The model covers an area of 20.9. km², including 6.5 km² for the sea extension (Figure 74). In upstream part, it considers the confluence between the Banquière River and the Nice River (red dot in the figure). The width of the model is around 3.3 km. The river length is 4.9 km from the upstream part to the mouth of Nice River, including 2.2 km covered.

Figure 74 Domain for the 1D-2D free surface and pipe flow model developed with MIKEPlus.

The process of generating a flexible mesh using DHI software tools involves several sequential stages. To create topographical data for the MIKEPlus overland module, the Mesh Generator toolbox is employed. For river network geometry within the MIKEPlus environment, streamline importation and cross-section drawing directly facilitate this task. In cases where the river network extends to the catchment level, tools like the MIKEHydro toolbox can be used.

The initial step entails defining the domain boundaries and segmenting the area into various polygons to establish distinct mesh resolutions. Simultaneously, boundary conditions are identified. Once the domain limits are established, the region undergoes triangulation to produce a mesh devoid of small angles, which permits rapid variation in triangle density over short distances. The Delaunay triangulation method is employed initially, followed by mesh refinement involving the addition of vertices until all constraints pertaining to minimum angles and maximum triangle area are met.

The toolboxes also provides the option to generate a quadrangular mesh through two techniques: a straightforward algebraic approach employing a boxing technique, or an algebraic grid generator using transfinite interpolation (Zavattero, 2019). In the context of this study, a triangular mesh is employed to construct the topography for the 2D floodplain and sea areas. Notably, a triangular mesh comprising elements with minimal interior angles necessitates longer computation times compared to a mesh featuring equilateral triangles. Additionally, the presence of large aspect ratios arising from small interior angles in triangles can introduce substantial interpolation errors. Consequently, during the mesh generation process, corrective measures are taken to ensure high mesh quality. This enhancement approach focuses on reducing elements with minimal interior angles and eliminating unnecessary elements to achieve an improved mesh structure.

Subsequently, the mesh undergoes a smoothing process aimed at maximizing the angles and element area. This procedure involves pinpointing the smallest angle along with its corresponding element area, prompting the relocation of nodes to achieve improved triangle convergence. Following this stage, users have the option to manually analyze and adjust the mesh as needed. Ultimately, the mesh is interpolated with the initial DEM through the use of natural neighbor interpolation.

In the model, the grid size is influenced by two primary factors: the significance of the area under study and computational time requirements. For complex regions, where detailed model inputs like topography and river water levels are crucial, a smaller grid size is adopted to ensure precise calculations and yield high-resolution outcomes. Conversely, in less critical areas, a larger grid size can be employed to reduce the overall cell count, thereby optimizing simulation time to a certain degree. Within this context, three distinct types of mesh are generated for the 1D-2D numerical model. (Figure 76):

The riverbed is an important area where a detailed output is also required. It is divided into 2 open rivers (OR) and 2 covered rivers (CR) interconnected to storages and the Tunnel André-Liautaud (TAL). Lateral links are implemented to couple the 1D cross-sections to the 2D cell elements. The model is designed in a way that it can be directly coupled, in the future, with the urban drainage model in the MIKEPlus. Of the 83 outlets of the Nice urban drainage network, the main pipes drain water directly to the sea (Figure 75). However, at least 20 outlets are connected to the Paillons River. These 20 outlets can be separated into two groups. The first group is connected to the OR and the second group to the CR. The connection to the OR, upstream of the ABA station is already considered in the calculation of runoff discharge as surface runoff in the hydrological model. The connection to the OR, downstream of ABA station, is not included in the calculation of river discharge at the concerned reaches, but the controlling area is small enough to be neglected during flood events. However, during low flow events at the Paillons catchment extent and extreme event in the urban area, this contribution could be significant. The connection to the CR occurs near the sea and is not included in the calculation of discharge or water levels at the end of the CR. When the river is flooded, the risk of overflow of the drainage system increases in case of extreme rainfall in the urban area. In fact; the Nice Sanitation Master Plan of 2003 highlighted the phenomenon of concomitant saturation of urban drainage networks with a strong flood of the Paillon during exceptional rainy events (Abily et al., 2015; Safege, 2013, 2015). This implies that river flood acts like an obstacle to flow at the outlets of the drainage network connected to the river. Therefore, the contribution of urban drainage to river discharge during flood events can be neglected in the OR. Studies of pluvial flood in Nice used the river water levels during dry and flood periods as boundary conditions at the outlets in connection with the river. The extreme flood discharge at these outlets are not well known. For example, on March 16th, 2011, while the recorded peak river discharge at ABA station was 90 m^3/s, a nearby gauging station (named Verany (Safege, 2012)) in the sewer (stormwater drainage) system recorded less than 1 m^3/s of peak discharge. At this point, this study does not consider the discharge from stormwater drainage outlets in the calculation of river discharge at ABA station. Future studies can delve into the interactions between river flood and stormwater drainage flood in real-time processes. The main concern could be the absolute amount of flood depth in the floodplain where river overflow water will be absorbed by manholes into the urban drainage; or where urban drainage will add more water to the floodplain if it is saturated.

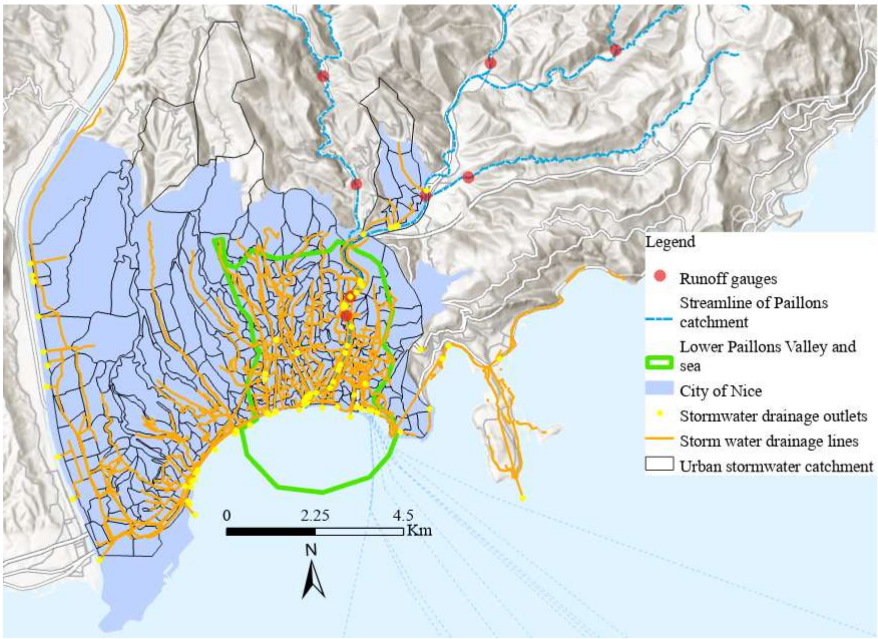

Figure 75 Map of the city of Nice showing the urban stormwater drainage sub-catchments, lines and outlets. The river valley, streamline and runoff gauges are also presented (Data source: MNCA, Safege).

The floodplain, which is urbanized, is depicted with triangular cells and a grid size of 25 m. The selection of 2D floodplain grid resolution is based on computation time. The objective was to be able to run on a classical desktop computer an event of two days duration within 12 h. It is assumed that with a fast-running hydrological model that can compute the same duration event in less than 1 h, the tool can be used in now- and forecasting. For case studies, it is possible to increase the 2D mesh resolution for detailed assessments of fluvial flooding in the urban area.

The sea area is represented by rough grids of 100 m. Actually, the model has been extended to offshore to avoid instability problems, but the sea area do not require many details (Zavattero, 2019).

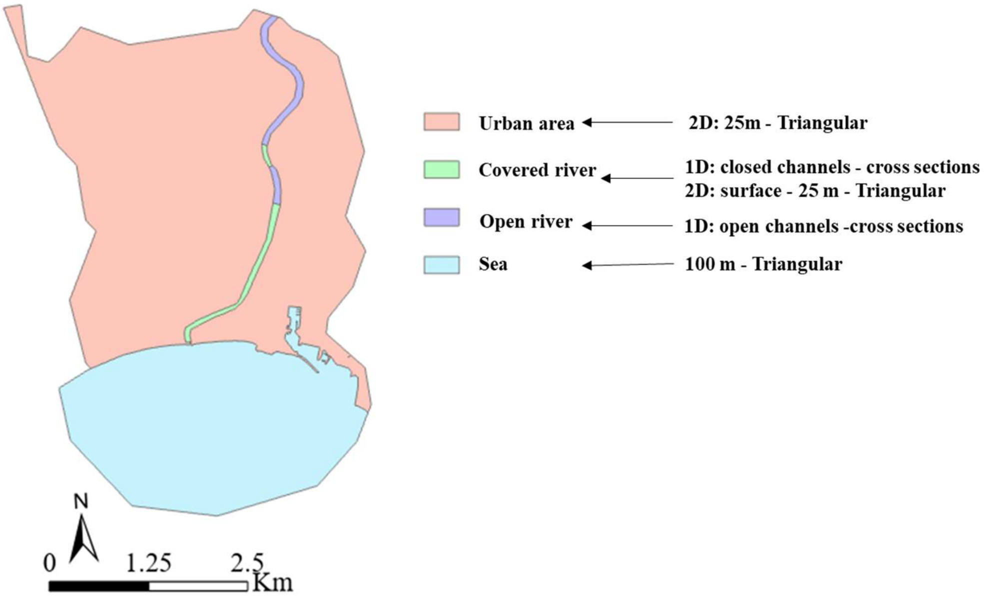

Figure 76 Description of mesh designed for MIKEPlus in the LPR.

The mesh of the numerical model is hereby generated (Figure 77). A total number of 120,378 nodes and 170,815 cells are generated without including building areas and high elevations. In the MIKE Mesh generator, the building shapefile was used to create polygons representing high elevation areas. Then those areas were deactivated before generating the mesh. Mostly, streets and places are represented in the floodplain. The 0.25mx0.25m DEM combined with the 1mx1m near shore bathymetry were used. Offshore, isobaths were used to interpolate elevation of the sea floor (Zavattero, 2019).

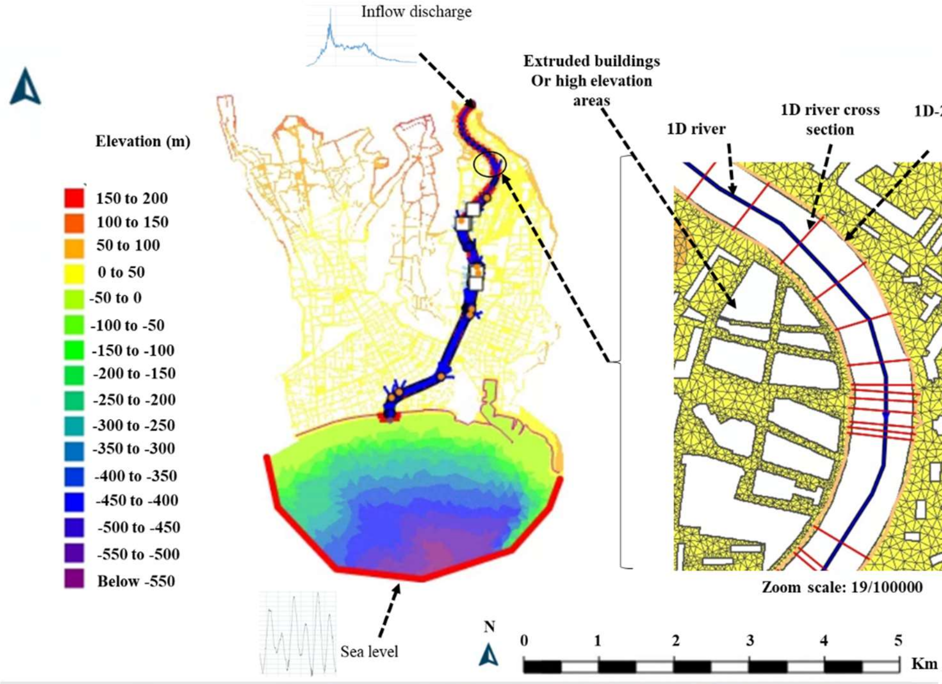

Figure 77 MIKEPlus mesh generated for the lower Paillons valley.

Three types of boundaries were used to build the model: the “land boundary” with zero flux, the “discharge boundary” condition applied upstream inflow to 1D river and the “level boundary” imposed for seal level. Extruded buildings and high elevations are also set up with “land boundaries”. The discharge recorded at the ABA station and the sea level recorded by SHOM are applied at discharge and level boundaries, respectively. The minimum discharge at the beginning of each event is selected to simulate the initial conditions.

Based on the land-use presented previously for the lower Paillons valley, the urban areas are assigned a Manning-Strickler coefficient of 70, the grass takes 15, the forests get 10 and water bodies are represented with 20. The open river is set up with a Manning-Strickler of 20 and the covered river 60. Manning-Strickler coefficients represent the inverse of the roughness coefficient for each land-use type.

The numerical parameters and configurations are established as outlined below: the mesh, the Courant-Friedrichs-Lewy (CFL) number, the thresholds for flooding and drying depths, the time integration settings, spatial integration approach, and time step (Table 16). All of these parameters and settings exert an influence on the numerical precision of the Shallow Water Equations (SWEs). Consequently, when these values are chosen accurately and appropriately, the physically-grounded model is poised to generate outcomes closely aligned with observed data.

The chosen CFL number is set at 0.8. Time steps used for solving the SWEs range between 0.01 and 1 s. Within the 2D models employed for computing water depth, specific thresholds are implemented to streamline simulation time by activating or deactivating cells involved in the computation process. This is particularly relevant when employing DHI software tools, where the use of flooding and drying depths serves as a strategy to save calculation time (Zavattero, 2019). These parameters’ function govern the selection of cells considered for resolving the SWEs.

Table 16 Summary of Manning-Strickler coefficients and numerical parameters.

Parameters	Values
S ($m^{1/3}/s$)	OR = 20 CR = 60 Floodplain forests = 10 Floodplain Grass 1 and vegetation = 15 Floodplain urban areas = 70 Water = 20
Max dx (m)	OR = 10 CR = 1000
Numerical settings values (m)	Wetting depth (WD) = 0.005m Drying depth (DD) = 0.05m CFL number = 0.8 Time integration = Lower order Space integration = Higher order Time step: variable between 0.01 to 1 s

3.4. The Feflow model for the Paillons catchment

Within this investigation, the hydrogeological catchment is adopted as the boundary for the numerical model. This hydrogeological catchment is defined by the limits of the impermeable layer or geological faults as explained by Du et al.(2018). It encompasses a larger area than the hydrological catchment of the Paillons, facilitating the incorporation of groundwater reservoirs and their interactions with both the alluvium and the river system. Notably, unconfined groundwater within this hydrogeological catchment possesses the potential for interchange with surface water bodies.

In the context of a hydrogeological assessment, even when infiltration occurs within an adjoining hydrological catchment, as long as permeable layers remain within the same hydrogeological catchment, the water invariably contributes to the same aquifer and can potentially interact with the river within the targeted hydrological catchment. The groundwater modeling effort for the Paillons region includes not only the alluvial aquifer, but also other aquifers that exhibit substantial water exchange interactions with it. Additionally, the absence of groundwater level data for upstream boundary conditions necessitates the use of an area englobing the entire hydrological catchment. This broader domain is adopted to investigate the dynamics of groundwater within the alluvium. Therefore, the model domain is constrained by the groundwater study area delineated in preceding sections (Figure 78).

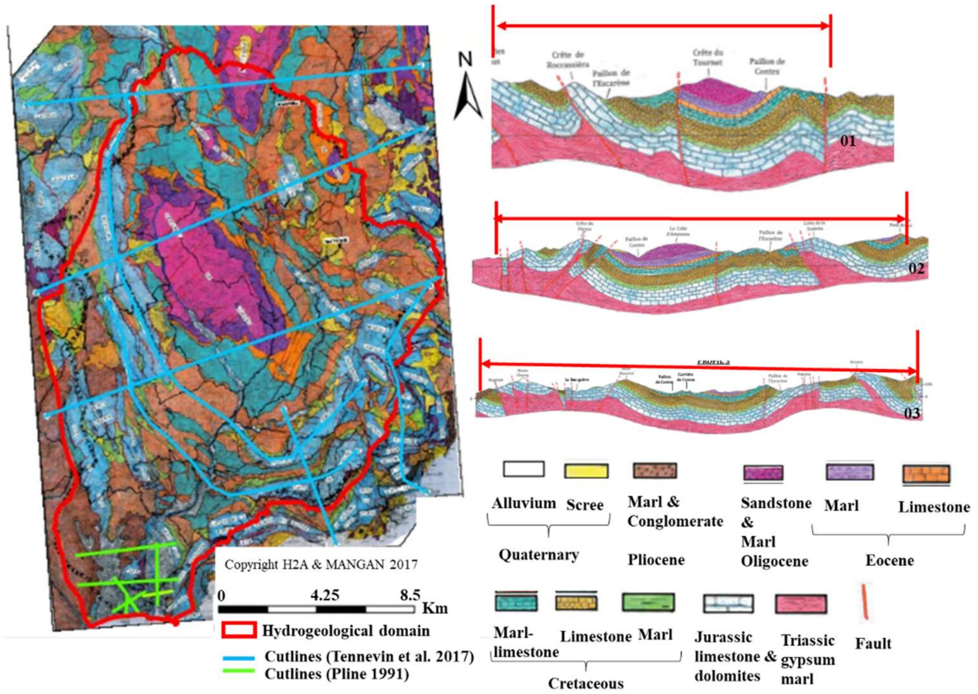

Figure 78 Model domain and limits on cross-sections of Feflow model of the Paillons hydrogeological catchment.

The geographical extent of the model domain is defined by the hydrological catchment in the upstream direction, and by karst-related faults and the limits of the conglomerate formation in the downstream direction. Consequently, no boundary conditions are assigned to the northern, eastern, and western boundaries of the model. Along the southern boundary, it has been verified that the alluvial aquifer is linked to the sea. Thus, the sea level serves as the downstream boundary condition for the unconfined aquifer. Encompassing an area of 283 km², the model exhibits depth variations spanning from 200 m to 2500 m. In the central and downstream sections of the domain, the alluvial aquifer directly interfaces with fractured limestone bedrock. However, modeling groundwater flow within fractured limestone presents challenges due to the violation of Darcy's equation resulting from high flow velocities in karst environments (Du et al., 2018b). Notwithstanding, limestone must be represented as a porous medium within the model, given that the Feflow software lacks dedicated functionalities for simulating groundwater flow in karst conditions.

Vertically, the model necessitates the inclusion of several strata: recent alluvium (including 3 lenses), alluvial terraces, conglomerate, marls as the bedrock layers spanning from Miocene to Cretaceous, Jurassic limestone and the Triassic. For simplicity and due to a dearth of groundwater information, the layers from Miocene to Cretaceous, predominantly composed of limestone and marls, are amalgamated into a single layer within the numerical model. However, the Jurassic limestone and dolomite layer has a karst system which is supposed to take the first 100 m of the total depth of this layer. This system is included on top of the deep part of the Jurassic limestone.

With 3 types of grid size (riverbed, floodplain and mountainous areas) the mesh of the numerical model is generated (Figure 79). In the numerical model, a 25m grid size is employed to accomplish a correct computation in the riverbed. The floodplain is described by a grid size of 50 m which is larger than that of the riverbed. The reason is that the hydraulic gradient is generally milder and commonly no boundary conditions are allocated on the floodplain with an exception for the boreholes (Du et al., 2018b). Coarse grids of 150 m are used on the rest of the model domain, where the major land-use is forest. Nevertheless the grid size cannot be too coarse because the complex geology should be represented correctly. By using Feflow software, 9 layers (10 slices) are generated by a total number of 224,298 nodes and 393,360 2D cells. Through analysis of the mesh of the model, the interior angles vary between 60° to 90°. One can observe few elements with an interior angle of more than 90°, which means that the passage between the three grid sizes is smooth enough.

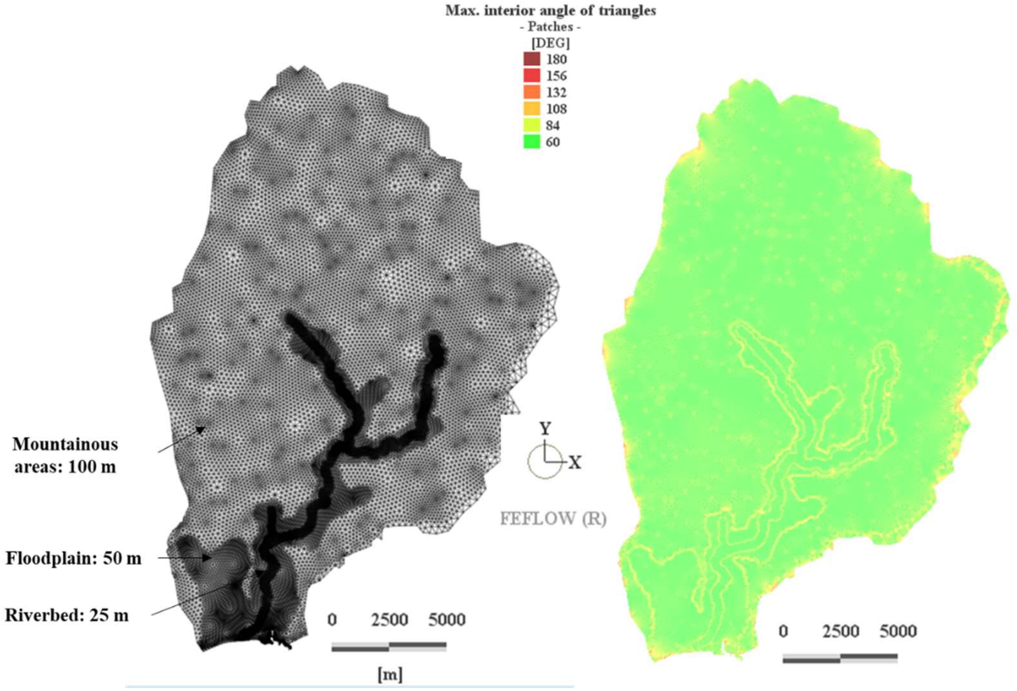

Figure 79 Grid sizes and maximum interior angles of triangles of the Feflow mesh.

The representation of geological layers in the numerical model is implemented by using the 7 cross-sections from Tennevin et al (2017) for the main geological layers at catchment extent. The alluvial zone is represented in details thanks to the cross-sections and knowledge provided by Pline (1991). Moreover, GUIGUES Environnement and MNCA in their study related the impact of the Tramway of Nice in 2010, produced a detailed bottom elevation of the downstream part of the alluvial zone. This information was used to improve the representation of the spatial distribution of elevation in the alluvium.

Discontinuities in geological layers are represented by thin layers as suggested in Du et al. (2018). The upper slice is constructed with the DEM data of 0.25m and 1m resolutions provided by MNCA. The other slices are digitized by using ArcGIS geographical software. Figure 80 & Figure 81 show a comparison between the original map and the digitalized cross-sections. In general, the geological layers are simplified representation of complex cross-sections. Then all cross-sections are interpolated with Feflow software by using IDW (inverse distance weighted) method or in MIKE SHE with the bilinear interpolation to generate the 3D geological layers (Figure 82). The downstream part of the Alluvium, at the entrance of Nice up to the Sea, which is heterogenous, was set up with three sub-layers. The depth of these sub-layers was assumed to be 8 m for the top slice, 20 m for the middle slice and the bottom slice. In theory, using a small number of cross-sections derived from three maps may not provide input data that possesses the requisite precision for a numerical model. Additionally, these cross-sections have been digitized from two manually crafted maps characterized by a lower resolution. To generate the map, several assumptions and individual interpretations have been incorporated due to the constraints of limited geological drilling tests. As a result, the information employed to establish the geological layers within this model also introduces an element of uncertainty.

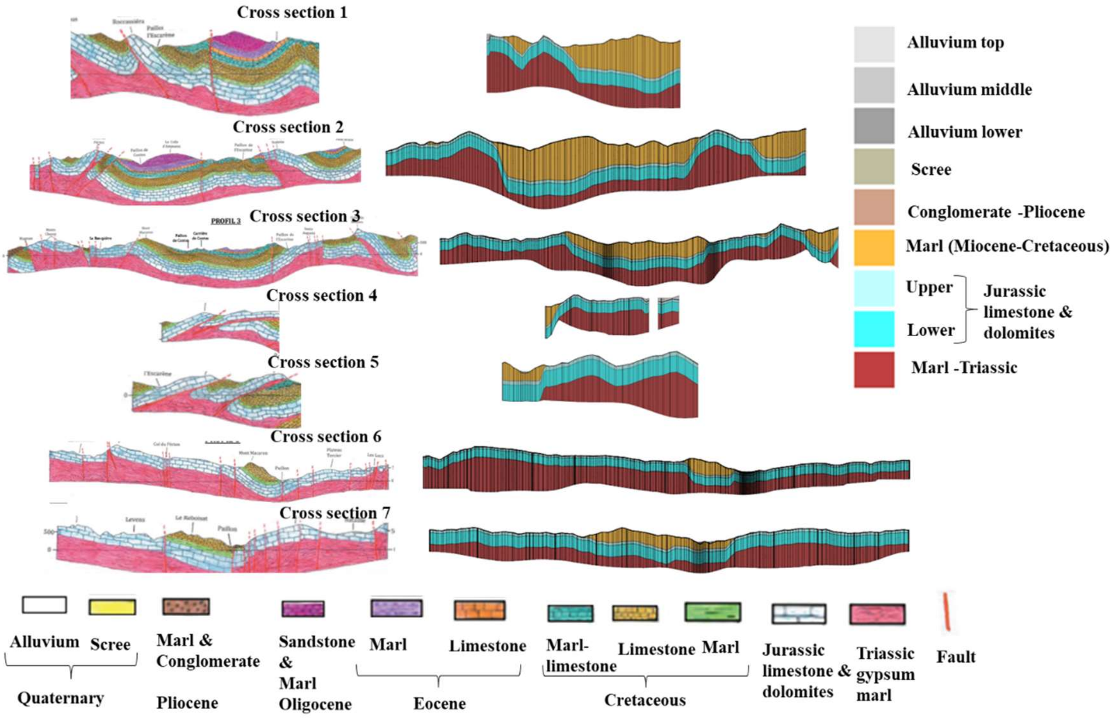

Figure 80 Catchment scale original cross-sections (left) and digitalized cross-sections (right) used in the Feflow model of the Paillons. The legend on the right is for the digitalized and the one at the bottom is for the original cross-sections.

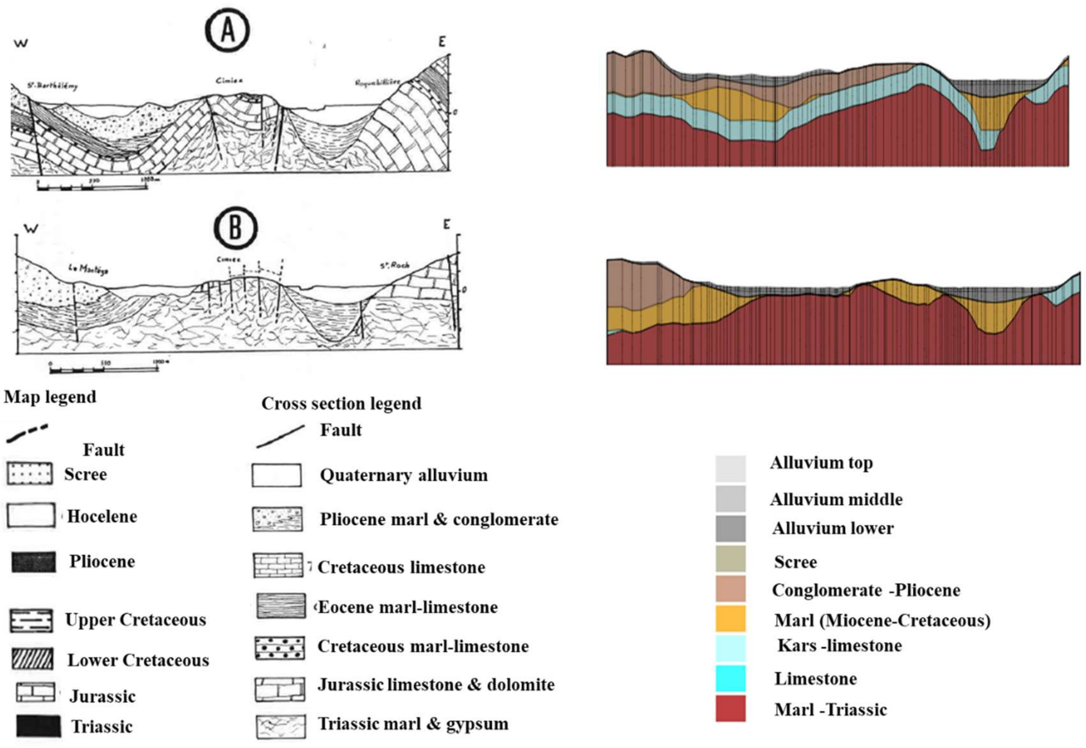

Figure 81 Alluvial extent cross-sections (left) and digitalized cross-sections (right) with their associated legends on the bottom.

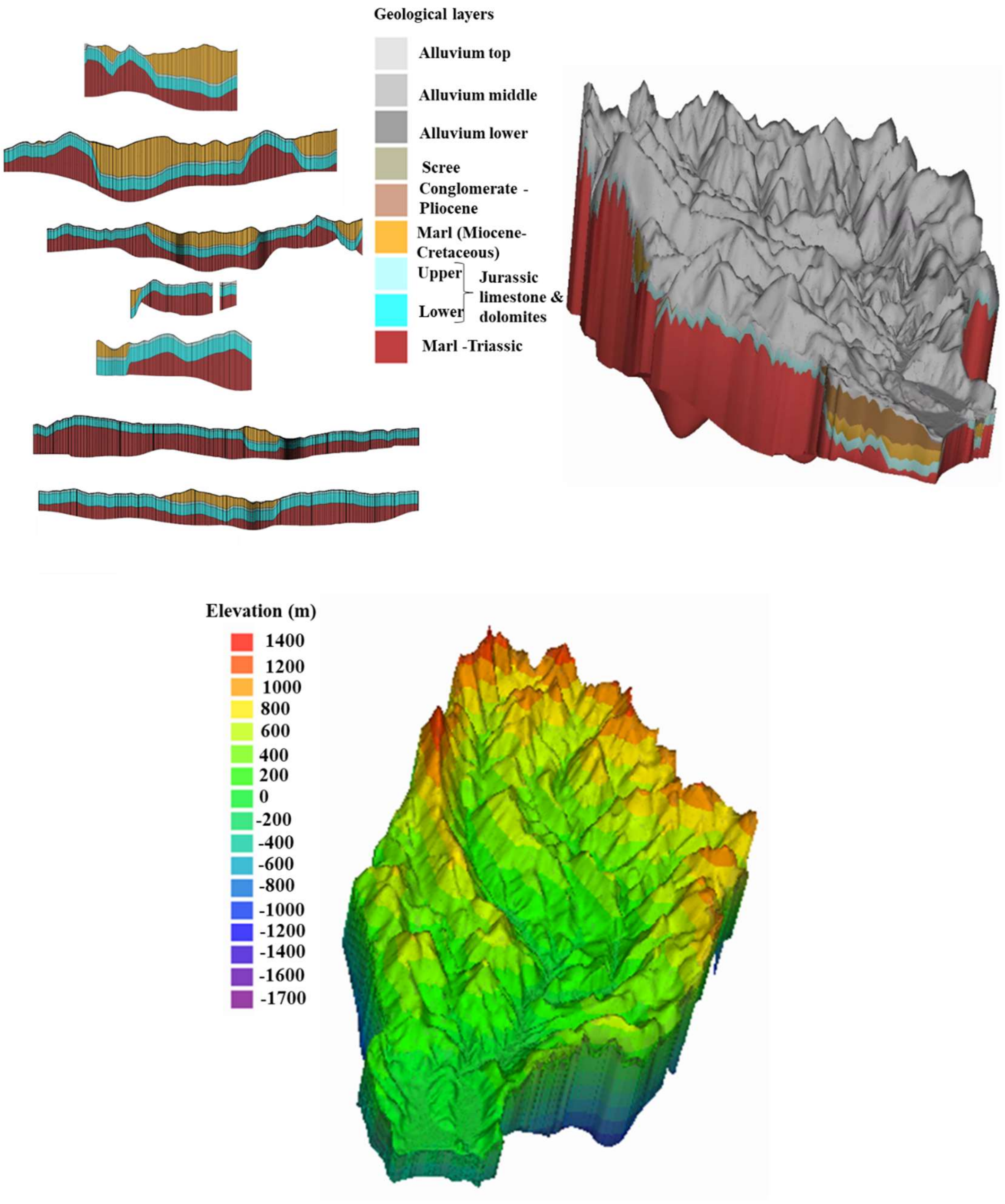

Figure 82 Interpolation of the cross-sections for the 3D model.

4 main hydraulic parameters are required for each geological layer in Feflow: specific storage, specific yield, and hydraulic conductivity. For the top layer, in-transfer and out-transfer rates are also needed where there are connections with rivers. Understanding that for the main structure of the alluvium in the Paillons is similar to that of the Var consisting of sand and gravel, the reasonable range of the value of Sy used to set up the numerical model is between 0.04 and 0.3 (Du et al., 2018b). Concerning the alluvial terraces, because of the similarity of their geophysical characteristics with the alluvium, the value of Sy and its spatial distribution are presumed to be the same as the alluvium. For the bedrock, the Sy of layers is set to be 0.1. A uniform value of 10^{-4} m^{-1} is used in the entire domain for the value of Ss of the bedrock layers, due to its negligible impact compared to Sy (Du, 2016).

In the alluvium, the hydraulic conductivity, K, varies from 0.04 m/s to 10^{-5} m/s. For the bedrock layers, the conglomerate is set at 2.6 x 10^{-6} m/s, the Jurassic limestone at 10^{-5} m/s, the karst at 0.01 m/s, the marls (Pliocene, Miocene to Cretaceous and Triassic) at 10^{-9} m/s. To reproduce the anisotropy of the alluvium, the vertical conductivity is a tenth of the horizontal conductivity. K and Sy of the top Alluvium can be calibrated. The exchanges between the river and the aquifer are given a transfer boundary condition (in-transfer and out-transfer rates, 10^{-6}-10^{-3} /s) of the numerical model where the river hydraulic model in MIKE SHE or in MIKEPlus will exchange water with the Feflow model. The groundwater extraction is represented by a "well boundary condition" in the model. It is a discharge assigned on a node of the upper slice of the model. While the primary emphasis of the numerical model lies in simulating groundwater flow within an unconfined aquifer, incorporating the pumped volume from the confined aquifer becomes essential to maintain mass conservation within the model(Du et al., 2018b).

3.5. The MIKE SHE model for the Paillons catchment

3.5.1. Selection of rainfall interpolation methods

The precision of deterministic distributed hydrological simulation hinges significantly on the caliber of input data, with a particular emphasis on factors such as precipitation, which is frequently regarded as the pivotal element in the hydrological processes (Ma, 2018). In DHI MIKE zero toolbox there are two available rainfall interpolation methods based on deterministic approach: Theissen and Inverse distance weighting (IDW). However, these interpolation techniques are simple and do not consider geo-factors which may influence the accuracy of the results. Geostatistical techniques include Kriging and Geographically Weight Regression. In the AquaVar project, the IDW was selected as the best interpolation method after a quantitative assessment of 6 interpolation approaches. In the Paillons, Le Gouz de Saint Seine (1995) used Spline for daily interpolation and Kriging for 6-mn interpolation basing their selection on literature review.

In this particular context, this study has recognized the additional benefits brought by the IDW, Spline, and Kriging methods, along with their applicability within the Paillons catchment.

Inverse Distance Weight (IDW) interpolation method

The IDW interpolation technique, introduced by the US National Weather Service in 1972, involves estimating values within cells by calculating a weighted average of sample points in nearby neighborhoods (Goovaerts, 2000). The accuracy of this interpolation method is notably influenced by the density of gauge points. When neighboring gauge points are distributed unevenly, the quality of the interpolation outcomes tends to diminish.

Various formulas have been formulated to determine the weight values in the IDW interpolation process. For the purpose of comparing interpolation methods, this study employed the most straightforward version proposed by Shepard (1968). The Shepard method proposes that the weight function wi can be defined using the following equation:

$$\boldsymbol{w_i} = \frac{\mathbf{h}_i^{-p}}{\sum_{j=0}^{n} \mathbf{h}_i^{-p}} \qquad \text{Eq. 28}$$

where p is the power parameter (typically p=2) and h_i is the distance from the dispersion points to the interpolation point:

$$\boldsymbol{h_i} = \sqrt{(\boldsymbol{x} - \boldsymbol{x_i})^2 (\boldsymbol{y} - \boldsymbol{y_i})^2} \qquad \text{Eq. 29}$$

where (x, y) are the coordinates of the interpolation point and (x_i, y_i) are the coordinates of the dispersion point respectively. The weight function changes from a value of unity at the dispersion point to a value close to zero as the distance to the dispersion point grow.

The weight functions are normalized as a sum of the weights of the unit. Hence, the interpolated value of the electric field $P(x,y)$ is:

$$\boldsymbol{P}_{(x,y)} = \sum_{j=0}^{n} \boldsymbol{w_j} \boldsymbol{P}_{(x_j,y_j)} \qquad \text{Eq. 30}$$

Spline interpolation method

The Spline interpolation technique involves estimating values through a mathematical function that minimizes the curvature of the surface, ultimately yielding a smooth surface that precisely intersects the input gauge points (Ma, 2018). The algorithm used for the Spline interpolation tool within ArcGIS software is defined as follows:

$$\boldsymbol{P}_{(x,y)} = \boldsymbol{T}_{(x,y)} + \sum_{j=0}^{n} \lambda_j \boldsymbol{R}(\boldsymbol{r_j}) \qquad \text{Eq. 31}$$

Where n is the number of points; λ *is the coefficients obtained by solving a system of linear equations;* r_j *is the distance from the point (x,y) to the* j^{th} *point* $T(x,y)$ *and R(r)is described differently, depending on the preferred options.*

Kriging interpolation method

The Kriging interpolation approach is widely recognized as one of the most effective interpolation solutions. It encompasses a range of least-squares linear regression algorithms that are employed to estimate random fields based on observed data (Le Gouz de Saint Seine, 1995). The equations used in the Kriging method bear similarities to the IDW method, however the weight coefficient wi in Kriging is determined not solely by the distance between the observation points and the prediction locations. It also considers the overall spatial distribution of the measured points (Ma, 2018).

To incorporate spatial distribution into the weight estimation, it is essential to quantify spatial autocorrelation. In this assessment, the Spherical and Linear Kriging interpolation processes were implemented using the available function within ArcGIS software.

To assess the efficacy of each interpolation technique, the cross-validation approach was employed. This method involves temporarily removing one observation point at a time from the dataset and then using various tested interpolation methods to re-estimate the values of the removed point based on the remaining data, as outlined by Mair & Fares (2011). The evaluation of correlation between individual stations and the accuracy of each interpolation method was conducted using metrics such as the total amount, the correlation coefficient (R), root mean squared error (RMSE), and Nash-Sutcliffe coefficient (NSE). The formulas for these metrics, along with their corresponding performance levels (Table 17), are presented below:

- $$\boldsymbol{R} = \frac{\sum_{t=1}^{T}(obs_0^t - \overline{obs_0})\ \sum_{t=1}^{T}(sim_m^t - \overline{sim_m})}{\sqrt{\sum_{t=1}^{T}(obs_0^t - \overline{obs_0})^2\ \sum_{t=1}^{T}(sim_m^t - \overline{sim_m})^2}} \qquad \textit{Eq.32}$$
- $$\boldsymbol{NSE} = 1 - \frac{\sum_{t=1}^{T}(obs_0^t - sim_m^t)^2}{\sum_{t=1}^{T}(obs_0^t - \overline{obs_0})^2} \qquad \text{Eq. 33}$$
- $$\boldsymbol{RMSE} = \sqrt{\frac{1}{n}\sum_{t=1}^{T}(obs_0^t - sim_m^t)^2} \qquad \text{Eq. 34}$$

where, obs_0^t *is observed value,* sim_m^t *the simulated value,*$\overline{obs_0}$ *the average of observed values,* $\overline{obs_0}$ *the average of simulated values,n number of values and t the time.*

Table 17 Performance indicators for model evaluation (Ma, 2018)

Indicator	Excellent	Good	Fair	Poor
R	>0.95	0.85-0.95	0.75-0.85	<0.75
NSE	>0.85	0.65-0.85	0.5-0.65	<0.5

In Paillons catchment, there are steep slopes which yield short response time during rainfall episodes. To represent the real-time hydrological condition in the catchment and to have the ability to predict future conditions, the model can be set up with daily or sub-daily time interval.

To identify the most appropriate rainfall interpolation function, this study used the approach implemented by Ma (2018). First the relationship between different rainfall stations is analyzed. Then different rainfall interpolation methods are applied in daily rainfall. After assessing the performance of the interpolation methods, the best method was used in hourly and 6-mn time intervals, in addition to find the suitable resolution.

The evaluation covered the period 2010-2021. Besides the currently operating rainfall stations (9 national and 9 local stations), any other available station (closed or newly open) was added to the rainfall mapping for real-time objectives. The correlation between stations decreases from daily data to 6-mn data (Appendix **1**, Appendix **2**, Appendix **3** and Appendix **4**). The idea is to have the maximum information on rainfall from different stations or sources to optimize the representation of the spatial distribution of rainfall. In the case of this assessment, the evaluation was done by removing each time one of the 9 local stations and the no. 6088007 station from the list, performing interpolation and then calculating the statistics at the location of the excluded station. The processes is repeated each time with another station while putting back the previous station into the list. Table 18 summarizes the statistical coefficients of the rainfall interpolation methods.

Regarding the exceedance of the total amount of rainfall cumulated during the period of evaluation, on average, IDW showed 1% exceedance while Spline gave 2%and Kriging (L and S) reached 3%. Positive exceedance means overestimation and negative values refer to underestimation. Across stations, there is a variability in smallest exceedance between the selected interpolation methods. Spline has the highest and lowest absolute exceedance of 28% at CON station and 1% at ABA station. To reduce the risk of overestimation of rainfall, it is preferable to select IDW even though there are only slight differences between interpolation methods.

About the correlation between different stations, the average R was 0.90 for IDW and Kriging, and 0.84 for Spline. As for IDW, there is a variability of performance across stations. The national station no. 6088007 showed the highest coefficients. In this case too, Spline has the lowest value of 0.74 across stations and interpolation methods. Using the criteria in Table 17, on average, Spline showed a "fair" performance while IDW and kriging showed a "good" performance. It can be noted that only the national station no. 6088007 showed "excellent" performance for IDW and Kriging. For R coefficient, IDW and Kriging have similar qualities.

The RMSE showed 4.20, 5.48, 4.12 and 4.13, respectively for IDW, Spline, Kriging L and Kriging S. There is a slight advantage to the Kriging methods. Spline still performed the worst. All values ranged from 2.04 to 7 with higher values found in Spline.

Finally, the NSE coefficients on average were similar for IDW and Kriging, respectively 0.81 and 0.82. The spline showed a value of 0.67. Interestingly, all these values are in "good" performance. Thus, any of these interpolation methods are acceptable for daily rainfall mapping in the Paillons. In details, Spline performed again the worst. IDW and Kriging showed competing performances depending on the station. Therefore, IDW or Kriging can be selected due to their lead in NSE.

Table 18 Summary of statistics of rainfall interpolation methods.

Exceedance of total amount (%) =100*(total simulated-total observed)/total observed										
Stations	**ABA**	**PDR**	**LAG**	**MDP**	**CON**	**BAI**	**ESC**	**COA**	**LUC**	**6088007**	**Average**
IDW	5	-9	4	-12	19	-2	14	-5	-7	6	1
Spline	1	-13	7	-11	28	8	17	-12	-12	7	2
Kriging L	7	-8	7	-11	16	1	14	-4	-2	6	3
Kriging S	7	-8	7	-11	16	1	14	-4	-3	6	3
R											
Stations	ABA	PDR	LAG	MDP	CON	BAI	ESC	COA	LUC	6088007	Average
IDW	0.84	0.78	0.90	0.83	0.94	0.91	0.92	0.94	0.93	0.97	0.90
Spline	0.83	0.74	0.89	0.78	0.79	0.8	0.91	0.81	0.87	0.94	0.84
Kriging L	0.84	0.81	0.90	0.84	0.94	0.9	0.93	0.93	0.93	0.97	0.90
Kriging S	0.84	0.81	0.90	0.84	0.94	0.9	0.92	0.94	0.93	0.97	0.90
RMSE											
Stations	ABA	PDR	LAG	MDP	CON	BAI	ESC	COA	LUC	6088007	Average
IDW	4.84	6.28	4.06	6.09	3.10	4.34	3.86	3.46	3.88	2.13	4.20
Spline	5.05	6.82	4.23	7	6.31	6.81	4.26	6.24	5.21	2.90	5.48
Kriging L	4.8	5.89	4	5.89	2.96	4.51	3.56	3.62	3.90	2.08	4.12
Kriging S	4.78	5.92	3.96	5.89	2.95	4.51	3.74	3.59	3.89	2.04	4.13
NSE											
Stations	ABA	PDR	LAG	MDP	CON	BAI	ESC	COA	LUC	6088007	Average
IDW	0.68	0.78	0.81	0.69	0.85	0.83	0.79	0.88	0.87	0.94	0.81
Spline	0.65	0.74	0.79	0.6	0.39	0.57	0.74	0.61	0.76	0.88	0.67
Kriging L	0.69	0.81	0.81	0.71	0.87	0.81	0.82	0.87	0.87	0.94	0.82
Kriging S	0.69	0.81	0.82	0.71	0.87	0.81	0.8	0.87	0.87	0.94	0.82

The results of the assessment of rainfall interpolation methods showed variable but acceptable performances across stations for the selected interpolation methods. IDW and Kriging showed similar performances. IDW seems to take the lead in smallest exceedance fraction. Therefore, this study preferred using IDW for rainfall mapping in the Paillons catchment. This is not a surprise because a similar conclusion was drawn in the AquaVar project on rainfall interpolation in the Var catchment. It is also expected that IDW will show decreased performance at hourly and 6-mn intervals. Therefore, it is recommended to use all available rainfall stations and sources for rainfall mapping because a dense network will improve the quality of rainfall distribution.

Moreover, the resolution of the rainfall map, whenever possible, should simply corresponds to the resolution of the hydrological grid resolution due to the fact that in MIKE SHE when the maps are not matching cell by cell, a built-in bilinear interpolation method is applied to the input data to assign values to each grid cell.

3.5.2. Selection of simulation resolution

Depending on the catchment characteristics and modeling objectives, the suitable simulation resolution in different cases can change. It is important to identify this suitable model resolution first. In deterministic distributed modelling, the majority of the inputs are the data collected from various producers at different resolutions. Thus, the resolution selected in the model needs to refer to the study objectives and the roles of the different inputs (Ma, 2018).

In the Paillons, the topography is available at 0.25 m, 1 m and 5 m resolutions. The rainfall information can be interpolated at any resolution down to 0.25 m topographic information. The land-use and the soil information are downloaded at 100 m resolution. The reference evapotranspiration from SAFRAN database is available at 8000 m resolution. The two most important factors in hydrological modeling are rainfall and topographic information. The surface area of the Paillons is only 236 km^2. The soil information is also important to know how much of rainfall can infiltrate. The objective of runoff modeling in the Paillons is to accurately estimate water depth and discharge at any location within the river network within a reasonable amount of time. Preferably, the entire modeling system, including hydrology, surface hydraulic and groundwater flow should be processed for 72 h in less than a day. The surface hydraulic model requires a lot of time; therefore the hydrological model should be fast enough. In previous chapters, the riverbed width varying up to 80 m were discussed. Since the modeling system include a 1D hydrological model to better represent river geometry, the resolution of the distributed hydrological model is constrained by the length of the drainage network it can represent, assuming that the more drainage lines, the better runoff will be calculated.

Table 19 presents an assessment of different resolutions of the DTM in the Paillons catchment. The length of the total drainage lines (TDL) fluctuates between 436 and 468 km. A maximum of 32 km difference in TDL is observed across different resolutions. From 300 m resolution to 1 m resolution, the maximum slope increases from 57.19° to 85.97 °. The smallest average slope is found with the 300 m resolution. Only the 300 m resolution show a significant decrease in parameters. It is challenging to argue on that basis that either resolutions can or cannot represent flow processes in the Paillons. However, higher resolutions like 1 m to 25 m will require high computing time as it was observed in the surface hydraulic models used in the Var or in the Paillons. It is preferable to use a resolution between 25 m and 100 m for hydrological modeling in the Paillons.

Regarding the river network definition, the main river branches and tributaries are assumed to be sufficient in capturing runoff in the Paillons. In MIKEPlus 1D as in Mike11 for the first versions of the model, the river network was defined with cross-sections spacing of 50 m upstream and 20 m downstream. It contains 25 branches and 2894 cross-sections (Figure 83). At the downstream, the configuration used in the surface hydraulic model is represented with open and closed channels.

Table 19 Assessments of DTMs with 9 resolutions in the Paillons.

Data resolution	TDL (km)	MAX_S (°)	MIN_S (°)	AVG_S (°)	STD (°)
1 m x 1 m original	455.68	85.97	0	23.25	10.52
3 m x 3 m	451.93	80.88	0	23.2	10.47
5 m x 5 m original	467.98	85.25	0	23.43	19.88
10 m x 10 m	446.22	72.32	0	22.99	10.32
25 m x 25 m	464.01	78.9	0	23.3	10.64
75 m x 75 m	459.78	73.33	0	22.51	10.15
150 m x 150 m	450.88	66.85	0	21.3	9.63
300 m x 300 m	436.76	57.19	0.04	19.21	8.84

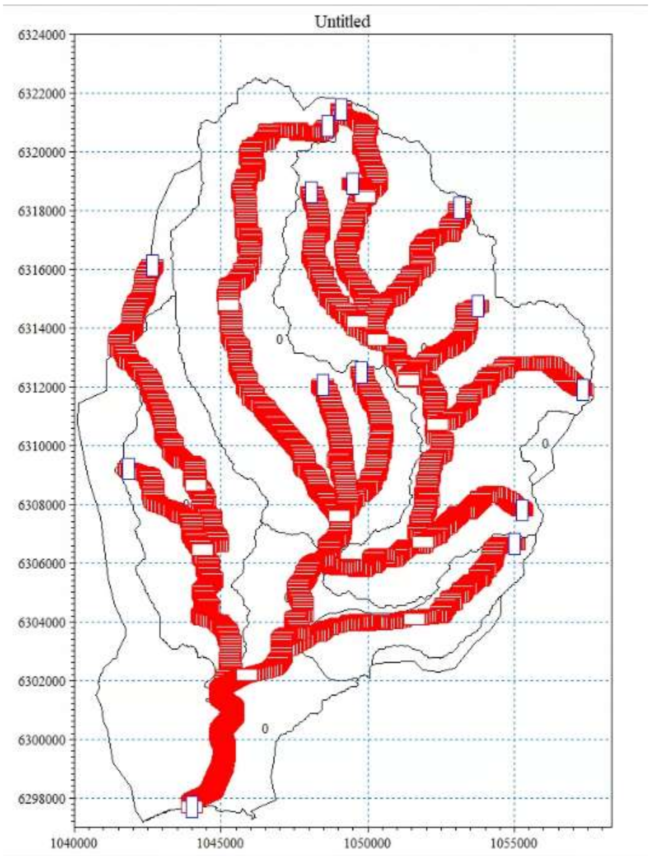

Figure 83 River network applied in the MIKEPlus 1D model coupled with MIKE SHE in Paillons catchment.

3.5.3. Set up the model domain and topography

The domain in MIKE SHE has the same extent as the Feflow model. The initial topography is resampled from combined 0.25 m and 1 m elevation data. After processing to fill sinks in the topography using ArcGIS tools, the topography was added into the model (Figure 84). Due to obstacles to flow in the DTM, especially in flood plains and mountainous areas or the covered part of the river, initial simulations serve to fill for the remaining sinks and a final DTM at 100 m resolution is saved for runoff calculations.

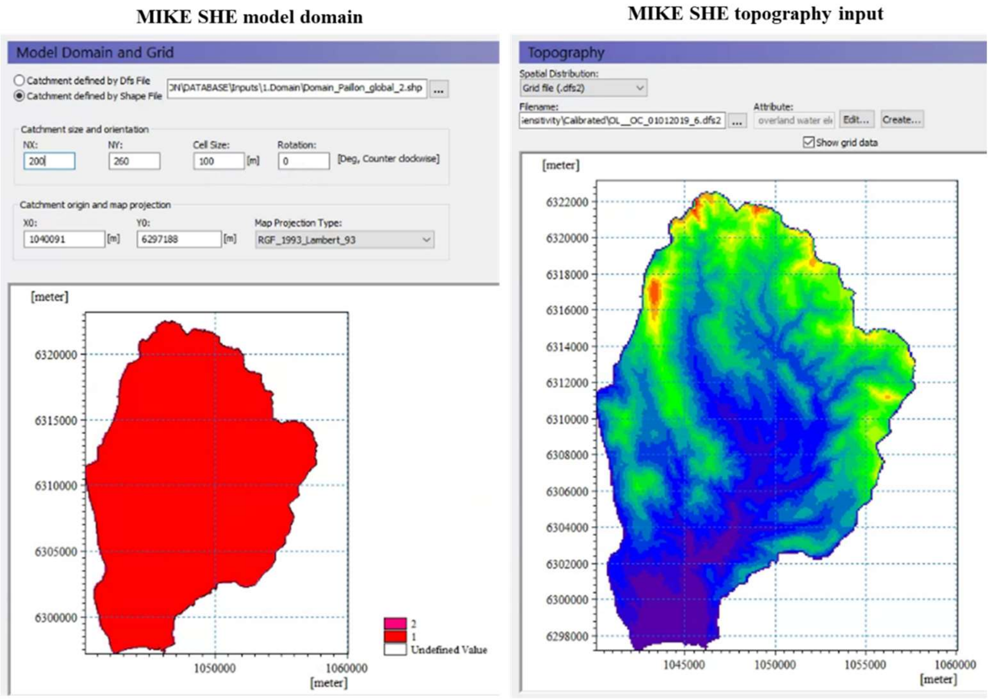

MIKE SHE model domain

Model Domain and Grid

○ Catchment defined by Dfs File
● Catchment defined by Shape File: ЭN\DATABASE\Inputs\1.Domain\Domain_Paillon_global_2.shp

Catchment size and orientation
NX: 200
NY: 260
Cell Size: 100 [m]
Rotation: 0 [Deg, Counter clockwise]

Catchment origin and map projection
X0: 1040091 [m]
Y0: 6297188 [m]
Map Projection Type: RGF_1993_Lambert_93

MIKE SHE topography input

Topography

Spatial Distribution: Grid file (.dfs2)
Filename: iensitivity\Calibrated\OL__OC_01012019_6.dfs2
Attribute: overland water el
☑ Show grid data

Figure 84 Model domain and topography input in MIKE SHE in the Paillons catchment.

3.5.4. Set up of the climate

Within the climate function of the MIKE SHE simulation, the model calculation can incorporate a comprehensive range of data, including precipitation, air temperature, evapotranspiration, and snow cover information. The rainfall distribution was set up at 100 m resolution using IDW interpolation of data from 18 gauging stations (Figure 85).

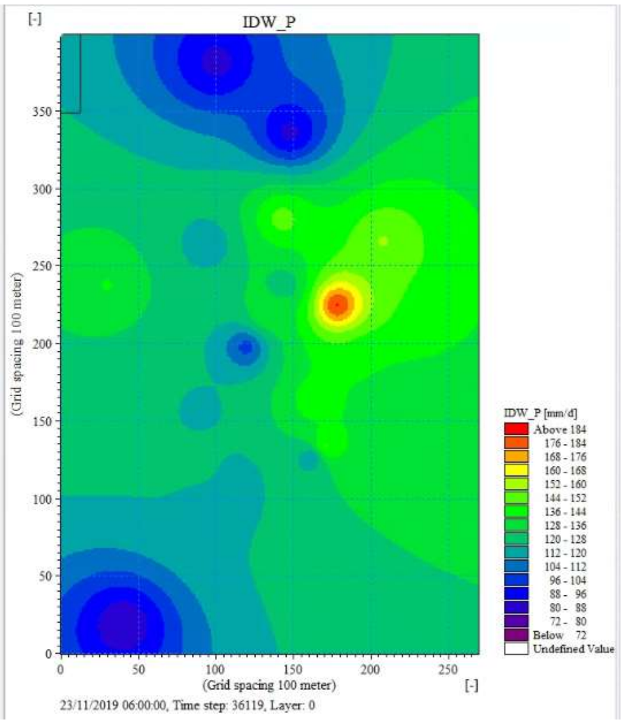

Figure 85 Set up of rainfall distribution in the Paillons.

Both the air temperature data derived from 18 gauging stations and the evapotranspiration data obtained from SAFRAN and collected by Météo-France and MNCA were integrated into the MIKE SHE model for analysis (Figure 86).

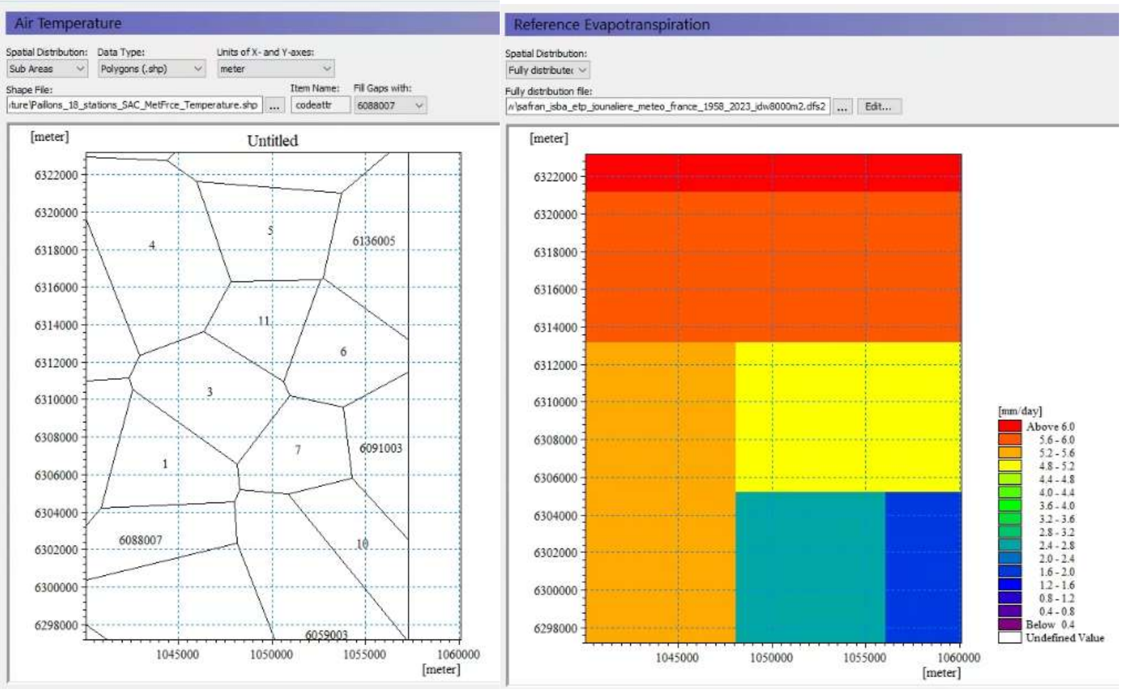
Air Temperature

Spatial Distribution: Sub Areas
Data Type: Polygons (.shp)
Units of X- and Y-axes: meter
Shape File: \ture\Pallons_18_stations_SAC_MetFrce_Temperature.shp
Item Name: codeattr
Fill Gaps with: 6088007

Reference Evapotranspiration

Spatial Distribution: Fully distributed
Fully distribution file: \safran_isba_etp_jounaliere_meteo_france_1958_2023_idw8000m2.dfs2

Figure 86 Set of station-based air temperature and evapotranspiration in the Paillons.

The model simulation included the snow melting process. However, direct snowfall is only available as liquid precipitation. Therefore, this section is focused on the initial snow cover at the beginning of the simulation and the freezing/melting process. As a result, the initial snow cover was established using data obtained from SAFRAN (Figure 87). Additionally, since the snow melting process within the

Paillons catchment can be influenced by both temperature fluctuations and the duration of sunshine, the model incorporated an elevation correction for air temperature and introduced a distributed melting coefficient. It should be noted there is no snow cap in the Paillons. Only exceptional events can generate important snowfall in the area. Similarly to the Var, it is assumed that potential melting will depend on the difference surface slope direction. Hence, the values of melting coefficients were assigned for 3 classes: flat, southward and northward.

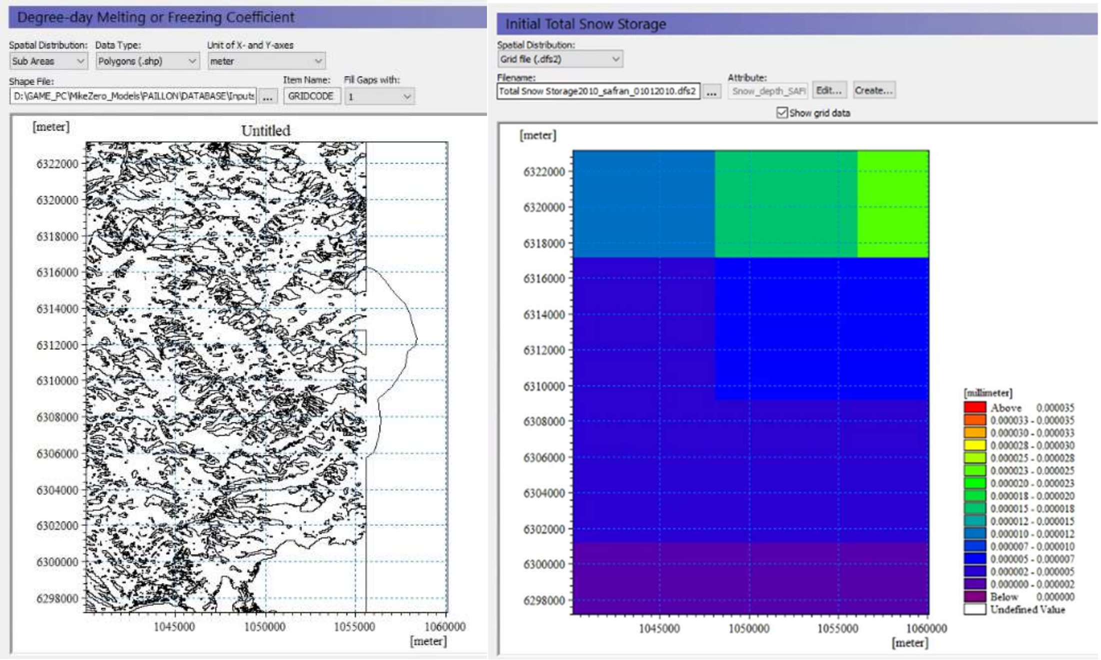

Degree-day Melting or Freezing Coefficient

Spatial Distribution: Sub Areas
Data Type: Polygons (.shp)
Unit of X- and Y-axes: meter
Shape File: D:\GAME_PC\MikeZero_Models\PAILLON\DATABASE\Inputs
Item Name: GRIDCODE
Fill Gaps with: 1

Initial Total Snow Storage

Spatial Distribution: Grid file (.dfs2)
Filename: Total Snow Storage2010_safran_01012010.dfs2
Attribute: Snow_depth_SAFI
☑ Show grid data

Figure 87 Degree day melting coefficient map (left) and initial snow cover (right) in the Paillons.

3.5.5. Set up the land-use and vegetation

The calculation of interception and soil water evaporation was influenced by the vegetation parameters, specifically Leaf Area Index (LAI) and Root Depth (RD). Using the 100m land-use map and vegetation data from DHI 2012, which is extrapolated to 2021, the MIKE SHE simulation for the Paillons catchment encompassed eight vegetation classes like in the Var catchment. These classes included three types of grass, grain crops, broad-leaved forest, coniferous forest, mixed forest, and bare soil (Figure 88).

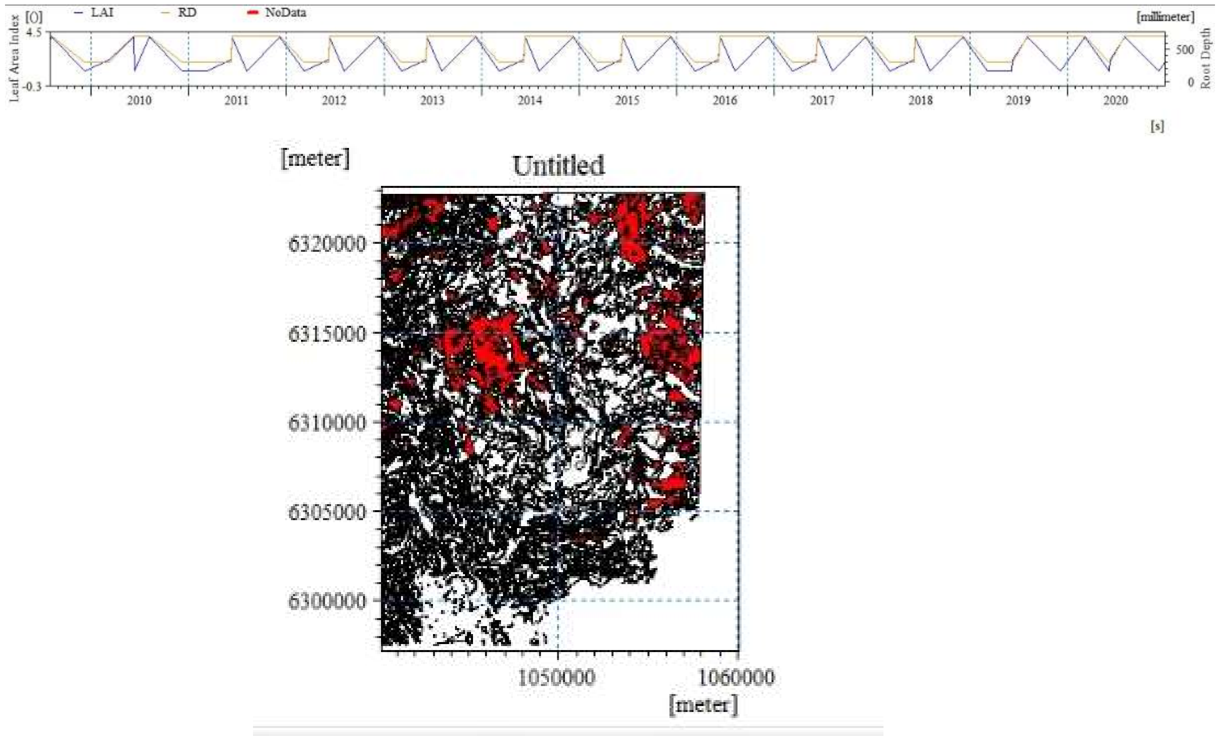

Figure 88 Vegetation parameters (Leaf area index (LAI), root depth (RD)) defined for different vegetation types in MIKE SHE model of the Paillons.

3.5.6. Set up the river network

As previously discussed, the river network within the MIKE SHE model was integrated through coupling with the MIKE 11 model and later update to MIKEPlus ID. A total of 24 branches were chosen. These branches were defined using cross-sectional data extracted from a 0.25m and 1m resolutions to accurately portray stream flow in the MIKE SHE simulation for the Paillons catchment (Figure 89). In addition, in order to execute the model, the boundary conditions for each branch were determined based on the minimum recorded discharge at the outlet of each sub-catchment, which is close to zero.

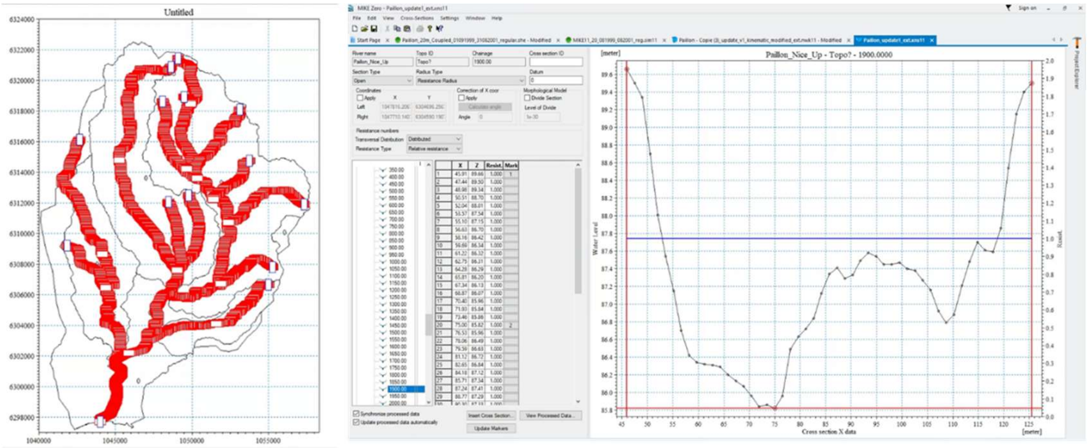

Figure 89 River network and cross-sections in MIKE11.

Within the MIKE SHE model, cells adjacent to the branches can be designated with a flood code. This code distinguished computation cells capable of facilitating water transfer in both directions between the river and the ground. In line with this, the floodplain area where overbank spilling can occur for each branch was established based on the branch locations across the catchment, with a buffer of 50 m (Figure 90).

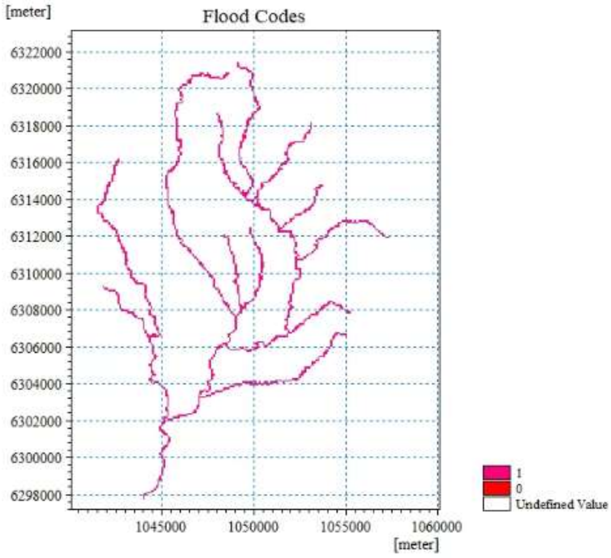

Figure 90 Floodplain defined in MIKE SHE model.

3.5.7. Set up the overland flow

Within the overland flow simulation, a critical input parameter was the Manning-Strickler coefficient. This coefficient characterizes the surface roughness in the calculations and is determined by the land-use data within the project. Based on the distinct land-uses, the initial Manning-Strickler coefficients in the MIKE SHE model were provided in Table 20. The distribution maps illustrating these coefficients were presented in Figure 91.

Table 20 Manning-Strickler coefficients based on different land-use types (Ma, 2018).

Land-use type	**Manning-Strickler coefficient($m^{1/3}/s$)**
Artificial surfaces	25
Agricultural areas	20
Grassland	10
Forests	4
Open spaces with little or no vegetation	5
Water bodies	15

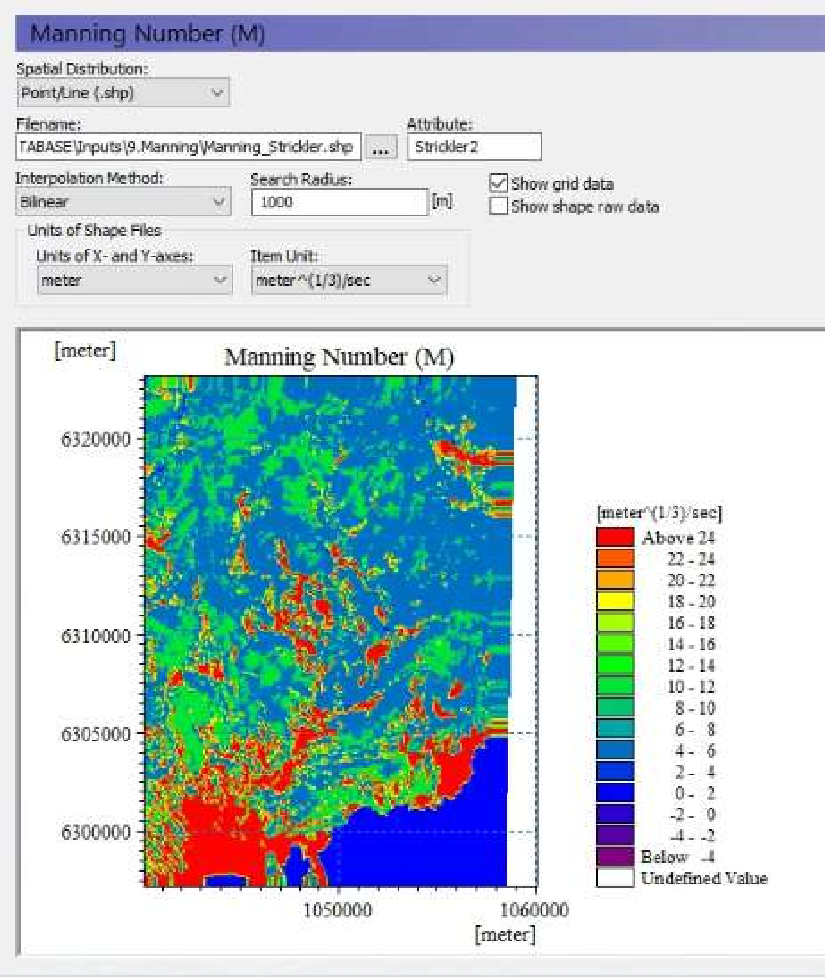
Manning Number (M)

Spatial Distribution: Point/Line (.shp)

Filename: TABASE\Inputs\9.Manning\Manning_Strickler.shp

Attribute: Strickler2

Interpolation Method: Bilinear

Search Radius: 1000 [m]

☑ Show grid data

☐ Show shape raw data

Units of Shape Files

Units of X- and Y-axes: meter

Item Unit: meter^(1/3)/sec

Figure 91 Set up of the distribution of the Manning-Strickler coefficients in MIKE SHE of the Paillons.

3.5.8. Set up the unsaturated flow

When conducting simulations of unsaturated flow, it is essential to specify the soil types within the model. Using the proportions of soil materials obtained from the European Soil Center and the "Soil Texture Triangle," the MIKE SHE model for the Paillons catchment incorporated 4 distinct soil types in the same way as in the Var (Figure 92).

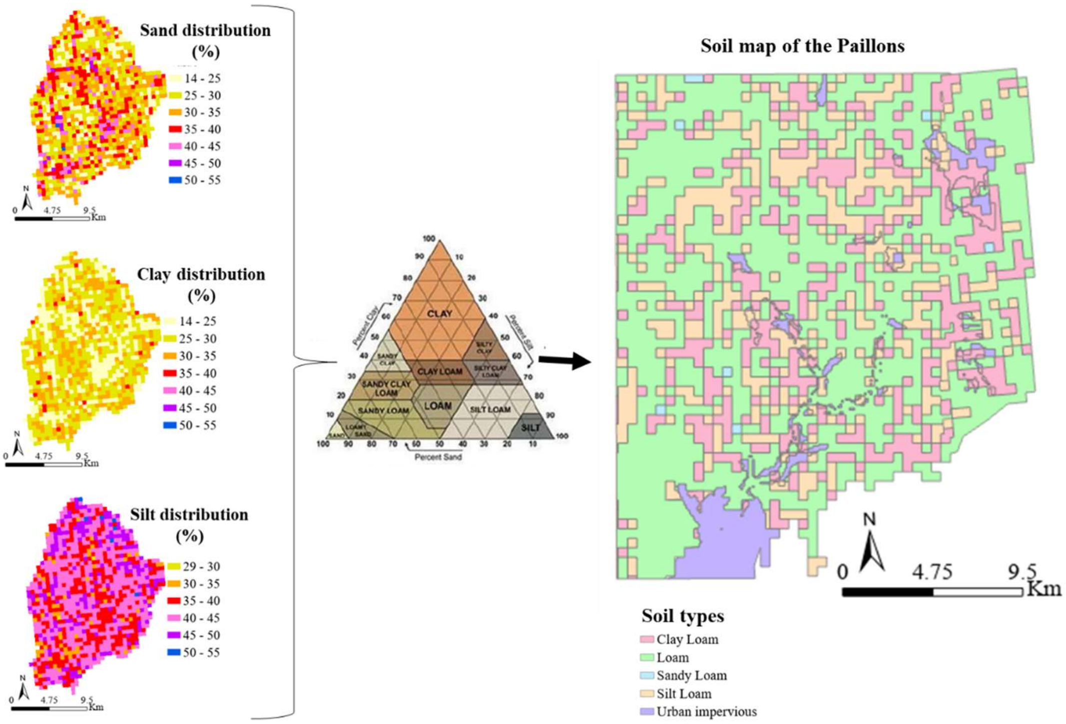

Figure 92 Soil distribution map in the Paillons.

Furthermore, owing to data constraints, the unsaturated zone simulation employed the "2-layers" function within MIKE SHE. The initial data used in the model is presented in Table 21.

Table 21 Soil parameters defined initially in MIKE SHE (Ma, 2018) model of the Paillons.

Parameters	Clay Loam	Loam	Sandy Loam	Silt Loam
Water content at saturation (-)	0.56	0.48	0.38	0.51
Water content at field capacity (-)	0.36	0.28	0.18	0.31
Water content at wilting point (-)	0.22	0.14	0.08	0.11
Saturated hydraulic conductivity (m/s)	2.50E-06	6.00E-06	1.00E-03	2.50E-05

3.5.9. Set up the saturated flow

During the saturated flow simulation, the aquifer's attributes are primarily characterized by parameters such as soil depth, horizontal hydraulic conductivity, and vertical conductivity (Ma, 2018). Given the scarcity of field measurements for hydraulic conductivity across the entire Paillons catchment, two constant and uniform values were initially designated for horizontal and vertical conductivities. These values were determined based on the ratio of horizontal hydraulic conductivity to vertical hydraulic conductivity, which fell within the range of 0.1 to 0.5. Additionally, the soil depth was initialized according to a recent national classification of soil in the region valued between 0.3 and 1 m (Le Bas, 2022). Areas with slopes higher than 40 ° are assigned 0 m soil depth, those with slopes between 10° and 40 ° get -1 m and those with slopes lower than 10° take -2 m. The figure shows the resulting saturated zone depth (Figure 93).

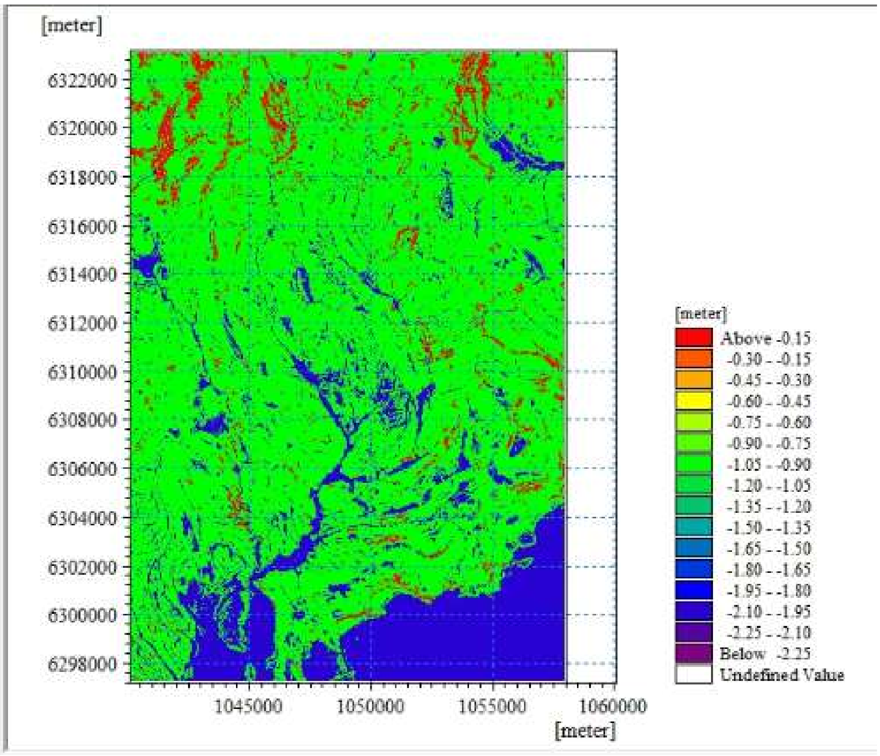

Figure 93 First layer of the saturated zone in the Paillons catchment.

Conclusion

This chapter presented the setup of the different models and their data requirements. Several assumptions were made to generate the required inputs. IDW was selected as a “good” interpolation method for rainfall mapping in the Paillons catchment. MIKE SHE can provide boundary conditions to Feflow and MIKEPlus.

Data such as geological layers were extracted from paper reports, therefore additional uncertainties affect the input data. MIKE SHE is the most demanding of inputs among the selected tools. Numerical parameters were extracted from literature because there are insufficient field measurements in the Paillons.

The lack of consistent monitoring runoff data is a serious challenge in model validation of long-term simulations. While the ground water flow dynamics can be modeled, there is no time series for calibration and validation in the unconfined aquifer. This study recommends setting up at least one piezometer in the Alluvium to have a minimum reference over time. Other groundwater resources are sufficient for the needs of the area, but in the context of extreme events, it is prudent to not neglect any resource.

Chapter IV. Results and uncertainty analysis of image-based discharge estimation and surface hydraulics modeling

Introduction

As in many places around the world, flash floods can be devastating for Nice Côte d'Azur metropolis (MNCA) (Chochon et al., 2022; Gourbesville & Ghulami, 2022; Lanini et al., 2022; Payrastre et al., 2022; Pons et al., 2022; Wacheux, 2022). To mitigate these issues and other water related problems, discharge and water depths measurements are required. However, the existing monitoring system failed to provide that information in times where it is most needed, due to gauging stations being destroyed by flooding or to technical issues.

This paper focuses in the first part on assessing discharge estimation based on image analysis and discussing the role of video records in the LPR modeling system. To achieve this assessment, 5 flood events are used. In details, the results section presents and discusses the findings. Then, the following section explores the role of this approach in the modeling system of the Paillons river.

The second part explores the use of 1D-2D coupling in river hydraulics and flood mapping in a complex hydraulic environment. This model will be an important component of the DSS tool for the Paillons. It must be flexible, fast computing set-up and able to be integrated with the other components of the DSS. The sensitivity of the model to surface roughness and maximum distance between cross-sections is analyzed. In addition, the performance of the model is evaluated using five statistical parameters. The results are compared and discussed for the selected events and measurement's locations. Finally, an application of the model to flood mapping is presented.

4.1. Image-based discharge estimation at ABA station

4.1.1. Sensitivity analysis

To assess the influence of parameters used to estimate discharge from video records on modeling results, a sensitivity analysis is applied. The event of December 20th, 2019, was used for this purpose. The cross-section velocity coefficient of 0.85 was initially selected. As previously explained, this coefficient links average surface velocity to depth average velocity needed for the calculation of the discharge. The effect of changes of this coefficient between 0.75 and 1 is presented.

The first challenge with images resides in identifying reference points for georeferencing the frames (Figure 94). In this case, the stage water depth is known. 4 reference points were placed on the video based on their approximate location on google map. In the best-case scenario, these reference points could be set up in advance for all the video records. In addition, the water level gauge under the bridge is not readable in the image. The cross-section of the transect is deducted from the known cross-section at that location. This may introduce some uncertainties.

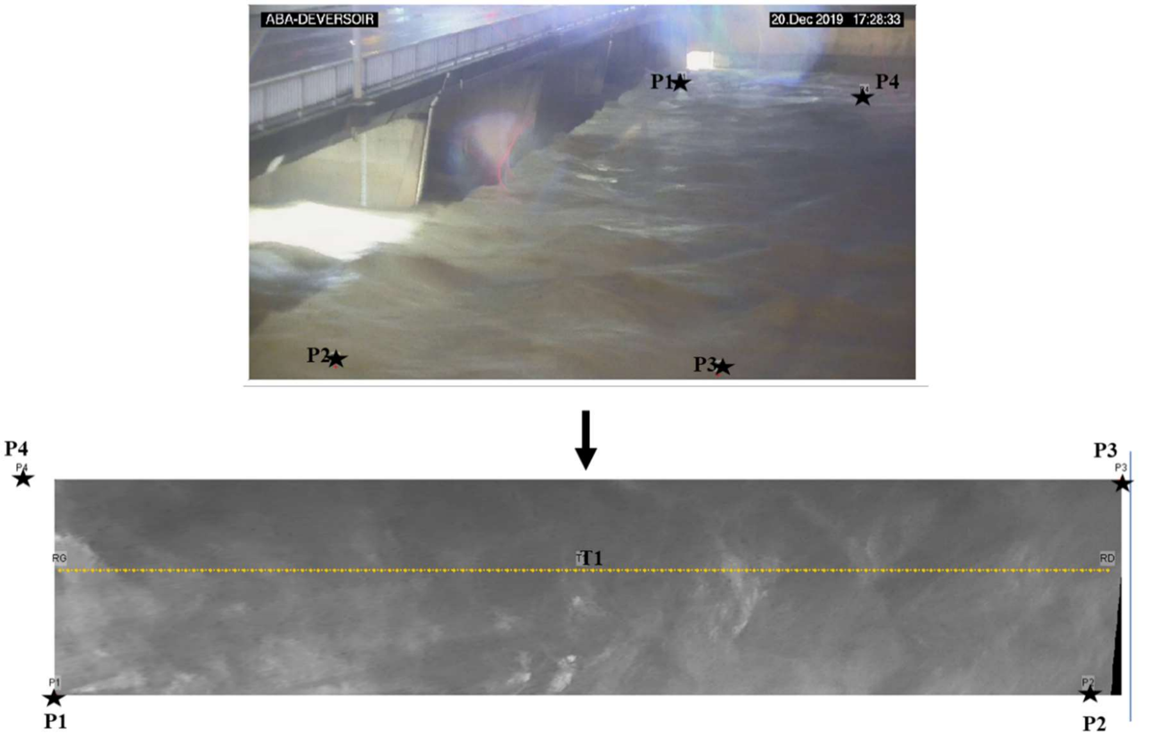

Figure 94 Reference points (P1 to P4) and image georeferencing in Fudaa-LSPIV. The yellow line is a transect used to compute discharge.

The second challenge deals with filtering estimate velocities to remove unrealistic values. It requires knowledge of the characteristics of the floods and associated stage discharge and velocities. Unfortunately, at ABA station, no velocity measurements are available. In high quality images where visible tracers or turbulence figures are clearly identifiable, there may be few unrealistic values. In that case, filters can span -inf. to +inf. In most cases, filters need to be more rigid. In fact, at ABA, this study set velocities filters between 0 and 5m/s. However, for low intensity flow events, this range should be lowered. Moreover, in some videos, lights from passing cars can interfere with the recorded flow field. This interference has not been assessed.

Figure 95 shows the effect of changing the velocity coefficient on the peak discharge. An increase in the velocity coefficient increases the discharge. The average rate of change is 22 m^3/s per unit change in coefficient value. With a coefficient of 0.85, the difference between discharge from rating curves and that of Large Scale Particle Image Velocimetry (LSPIV) method is about 0.2%.

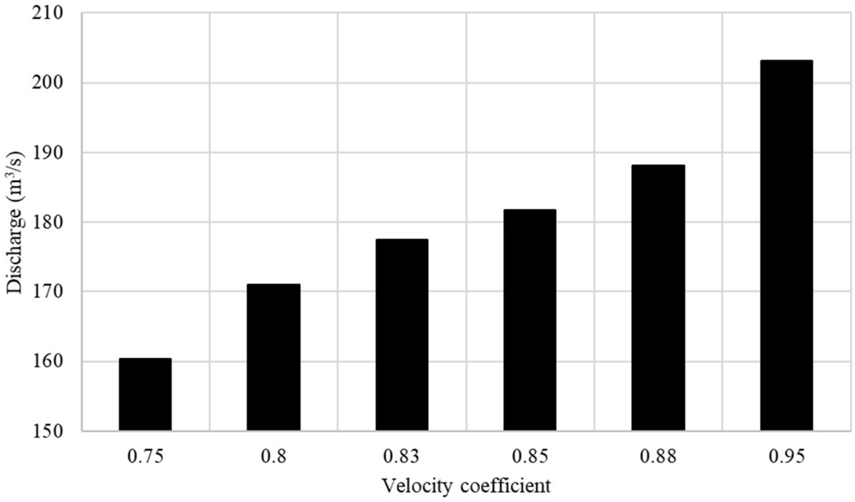

Figure 95 Sensitivity of peak discharge to velocity coefficient.

4.1.2. Results and discussions

5 videos were processes to evaluate discharge at ABA station. In this case the water depths were extracted from measurements. Table 2 shows the average surface velocities and computed discharges from LSPIV. The highest difference of 37% appears for the smallest event of 0.51 m stage water depth. This low performance can be attributed to uncertainties in discharge estimates from rating curves at low water depths. The computed average velocities are reasonable. A maximum of 2.04 m/s is obtained for the most intense event.

The most sensitive step in this approach is getting the average velocities. The minimum correlation selected to filter surface velocities was set at 0.4 and the range of reasonable flow velocities was set between 0 m/s to 5 m/s.

Table 2 Estimated peak discharges and average surface velocities at ABA for 5 events.

			Peak discharge		
Event	**Stage H (m)**	**Average surface velocity (m/s)**	**Observed (m^3/s)**	**Estimated from LSPIV (m^3/s)**	**Diff (%)**
20/12/2019 17:30	1.84	2.04	181.41	181.71	0.2
23/11/2019 19:00	1.60	2.06	137.62	159.3	14
20/12/2019 12:00	0.51	0.29	10.00	7.26	37
21/12/2019 08:00	1.12	0.94	53.58	51.2	4.6
02/10/2020 17:30	1.31	1.26	83.98	79.95	5

The results demonstrate that estimation of flow directly from video records is an efficient way to complete the flow estimation in the LPR, when gauging information is missing. This is useful when there are missing records due to damages of gauging stations during floods events. In fact, it is common in the LPR that flash floods disrupt the good functioning of the monitoring system. Sometimes, water depths are available but not discharges. Other times, erratic water depths are recorded. During flood events, perturbations near the piers of the bridge can have a negative effect on the quality of the measured stage depth used for computing the discharge with the rating curve. In addition, rating curves are often updated over time. This poses serious problems in understanding flood events for long periods. In the absence of post-processing of the raw records, it is challenging to use measurements for decision-making. Image-based analysis of floods will provide the necessary information for validation of measurements in real-time. Image-based runoff estimation at night was evaluated with only 3 peak discharges. The results are acceptable but additional events are required to draw robust conclusions. Possible interferences with traffic and vehicles lights were not assessed.

The recording frequency for each flood event was set at 30-mn intervals. However, only specific videos were subjected to evaluation. To establish a comprehensive discharge time series for entire events, a greater number of records is essential. Attaining valuable video footage for nocturnal flood events, especially when surface flow lacks distinctiveness, could prove challenging. As a result, in the context of LSPIV, supplementary modeling techniques such as deterministic modeling will retain their importance. For efficient use of video records, their integration into the LSPIV modeling system stands as the most effective strategy. Within this study, video assessment was conducted on an individual basis through manual methods.

To facilitate the real-time incorporation of image-based river flow estimation, the LSPIV method's Python source code could be employed to automatically parse the videos and quantify flow characteristics. In general, a sequence of three primary processing stages is essential. This involves initial video pre-processing, followed by the determination of flow velocity using LSPIV, and ultimately culminating in the computation of discharge by amalgamating insights from the preceding phases. The present study involved the calibration of the velocity coefficient. Nevertheless, future investigations should delve deeper into alternative methodologies, such as hydraulic modeling, to ascertain their potential in refining velocity coefficients. This prospect gains significance given the emergence of advanced techniques for acquiring high-resolution bathymetric and topographic data (Eltner et al., 2020).

Aside from conducting further validation tests in the field, the exploration of uncertainties and sensitivity through numerical simulations holds pragmatic value. The site-specific nature of the velocity coefficient underscores that merely measuring surface velocities and gauging their uncertainty does not suffice to ensure the precision of LSPIV discharge measurements. While a more exhaustive study on the accuracy of LSPIV flood discharge measurements remains imperative, the efficacy of this technique as a crucial hydrological instrument for both monitored and unmonitored stream segments is affirmed. Particularly, the LSPIV approach proves invaluable in furnishing velocity and discharge data during rapid floods, situations where conventional methodologies falter or encounter substantial deployment challenges (Le Coz et al., 2010).

4.1.3. Role of video records in LPR modeling system

In previous sections hydrological, hydrogeological and hydraulic models were set up for the Paillons catchment and the LPR. The main purpose for building those models is to extend the AquaVar DSS system to the Paillons for real-time management of flood and water resources in Nice. The complexity of the hydraulic system of the LPR required to construct models adapted to its specific needs. The challenges with data quality motivated the integration of video monitoring into the Paillons modeling system. To achieve this goal a framework presented in Figure 96 summarizes the different components of the system and their connections to each other.

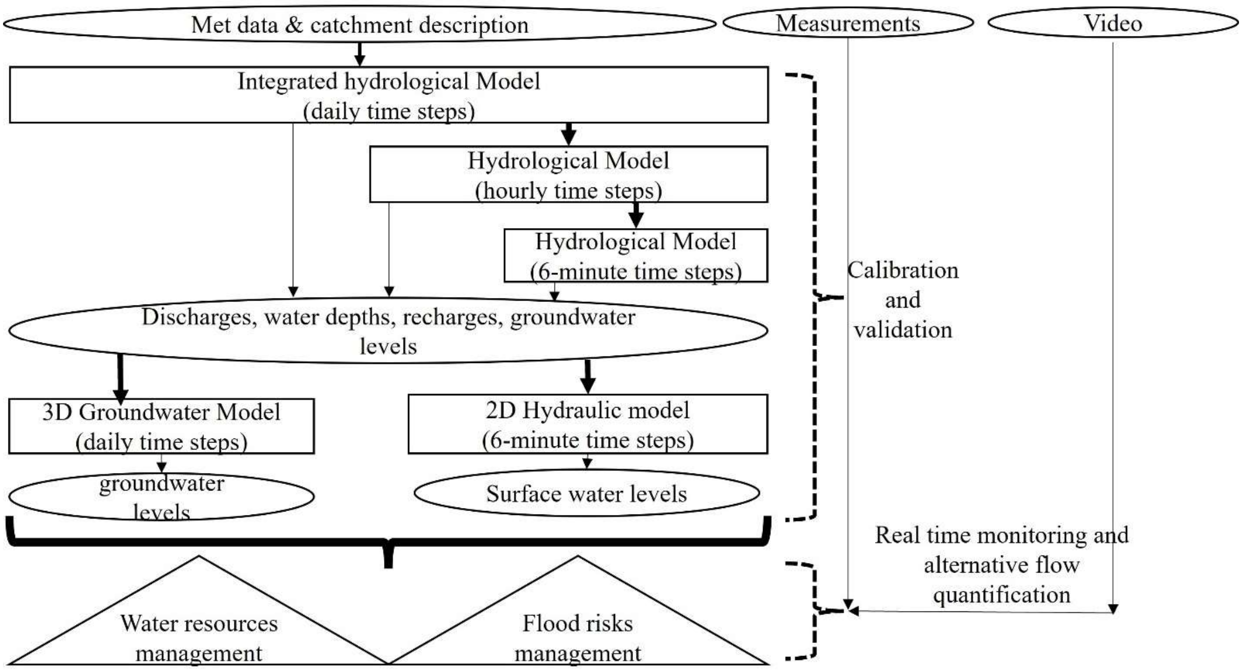

Figure 96 Framework of the modeling system of the Paillons catchment and lower valley.

Within this framework, deterministic modeling assumes a pivotal role in generating information about runoff and groundwater flow dynamics. The underlying presumption is the availability and expansion of meteorological data, which tends to be less susceptible to the adverse impacts of river floods on gauging stations. Empirical evidence demonstrates that deterministic models can effectively replicate flow processes. Nonetheless, uncertainties stemming from meteorological data and catchment characteristics cannot be disregarded. Hence, video records can contribute to validate both gauging measurements and model outcomes. Video analysis is widely used for calibration of gauging stations. It can also be used to reconstruct past event if image records are available. Additionally, it serves at sources of information for assessments of riverbed sediment dynamics.

The construction of a hydrological model on daily time intervals hinges upon meteorological data and catchment descriptions. Leveraging existing weather data, daily simulations have the capacity to include multiple decades, thus offering a comprehensive overview of runoff and groundwater flow dynamics in the Paillons region. The results from these daily simulations furnish boundary conditions for sub-daily simulations, which in turn support water resources management strategies. Given the paucity and incompleteness of groundwater information in the Paillons area, a groundwater model is employed to simulate the behavior of the unconfined aquifer.

Flash floods, characterized by their rapid onset over a span of few hours to several days, necessitate representation at finer intervals such as hourly or 6-mn segments. This explains the rationale behind developing 3 versions of hydrological models, both calibrated to yield intricate runoff insights and boundary conditions for flood mapping exercises.

In this modeling system, measurements serve not only for calibrating and validating model outputs but also for real-time flood risk management. Video records assume a comparable role, filling gaps in water depth and discharge quantification, and further acting as a validation tool for measurements and deterministic model predictions. Through this integrated modeling strategy, all essential components are in place to provide dependable insights into the Paillons region's overall water cycle, while optimizing the management of the growing repository of collected data stored in the database.

4.2. The surface hydraulic modeling with MIKEPlus 1D-2D coupling

4.2.1. Sensitivity analysis of hydraulic model parameters

To evaluate the impact of hydraulic parameters on modeling outcomes, a sensitivity analysis has been executed. The default values for Wetting Depth (WD) and Drying Depth (DD) of the floodplain have been established. Parameters such as the Manning-Strickler coefficient, maximum dx, and leakage coefficient exert influence on the modeling results. The maximum dx (Max dx) denotes the distance at which interpolated cross-sections are introduced into the 1D river network. The ranges encompassing these parameters are summarized in Table 22. For this evaluation, the flood events occurring on 05/02/2017 and 11/12/2017, depicted in Figure 97, were selected. The findings presented in Figure 98 & Figure 99, and Table 23 demonstrate that the Manning-Strickler coefficient wields the most substantial impact on simulated water depths, corroborating Zavattero (2019) findings. Conversely, the influence of Maximum dx is marginal. Indeed, the existing number of defined cross-sections proves sufficient for reproducing flow dynamics within the 1D river system. Nonetheless, due to the absence of data concerning major events in the covered river, the behavior of the covered river under higher discharges remains somewhat uncertain.

In Figure 97, two flood events achieved peak discharges of 140 m³/s and 38 m³/s, respectively. The event on 11/12/2017 endured for 40 h, while the event on 05/02/2017 was a smaller flood with data available only over a span of 7 h. Notably, the more intense flood exhibited a smaller baseflow. These particular events were chosen due to the availability of water depth data in the OR and CR for the sensitivity analysis. Regrettably, records for more intense CR events were unavailable. The parameter range, as detailed in Table 5, spans from 20 $m^{1/3}/s$ to 60 $m^{1/3}/s$ for the Manning-Strickler coefficient, and from 10 to 100 m for Max dx. Within this coupled 1D-2D hydraulic model, the 2D floodplain is established with fixed parameters, with WD set at 0.2 m and DD at 0.5 m.

Table 22 Summary of parameters for sensitivity analysis.

Parameters	Value range	Constant parameters
Manning-Strickler coefficient, S (**$m^{1/3}/s$**)	OR 20 to 60 CR 20 to 60	Floodplain WD = 0.2 m Floodplain DD = 0. 5 m OR Max dx = 50 CR Max dx = 1000
Maximum dx, Maxdx(m)	10 to 100	WD = 0.2 m and DD = 0.5 m S_{OR} = 20 and S_{CR}=20

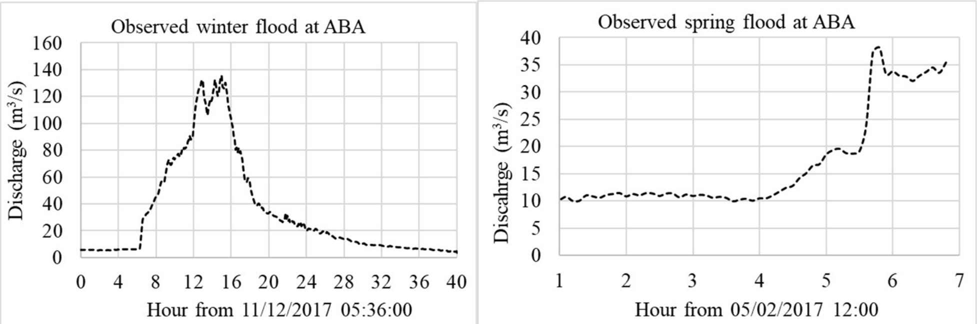

Figure 97 Selected observed flood events at ABA station for sensitivity analysis.

In Figure 98, six graphs depict alterations in water depths resulting from variations in parameters "S" and "Max dx" at 3 distinct stations: ABA, Coty, and PAS, focusing on the event of 11/12/2017. The respective peak water depths are 1.6 m for ABA, 1.1 m for Coty, and 1.15 m for PAS. The curves are generated subsequent to the application of data filtering to remove noise in data. The model remains configured with constant parameters, while the value of one of the designated parameters is modified for each instance, yielding the outcomes presented in the figures. As anticipated, an elevation in "S" leads to a reduction in water depths. The most notable water depth decrease, when "S" shifts from 20 to 60, amounts to 0.6 m. Conversely, minimal variation is observed with "Max dx" fluctuating between 10 and 100.

To delve deeper into flow characteristics, an examination is carried out within the CR, as depicted in Figure 99. Measurements acquired at the entry and midpoint of the CR are employed for this analysis. At the entry point, the peak water depth registers at 0.5 m, accompanied by a baseflow of 0.2 m. Analogous conditions are observed at the middle of the CR. Notably, altering "S" from 20 to 60 induces a decline in peak water depths by 0.4 m at the entry and 0.6 m at the midpoint. This divergence can be attributed to the geometric dissimilarities spanning the CR. For reasons of stability, "Max dx" within the CR remains established at 1000, and all cross-sections delineating the geometry are encompassed.

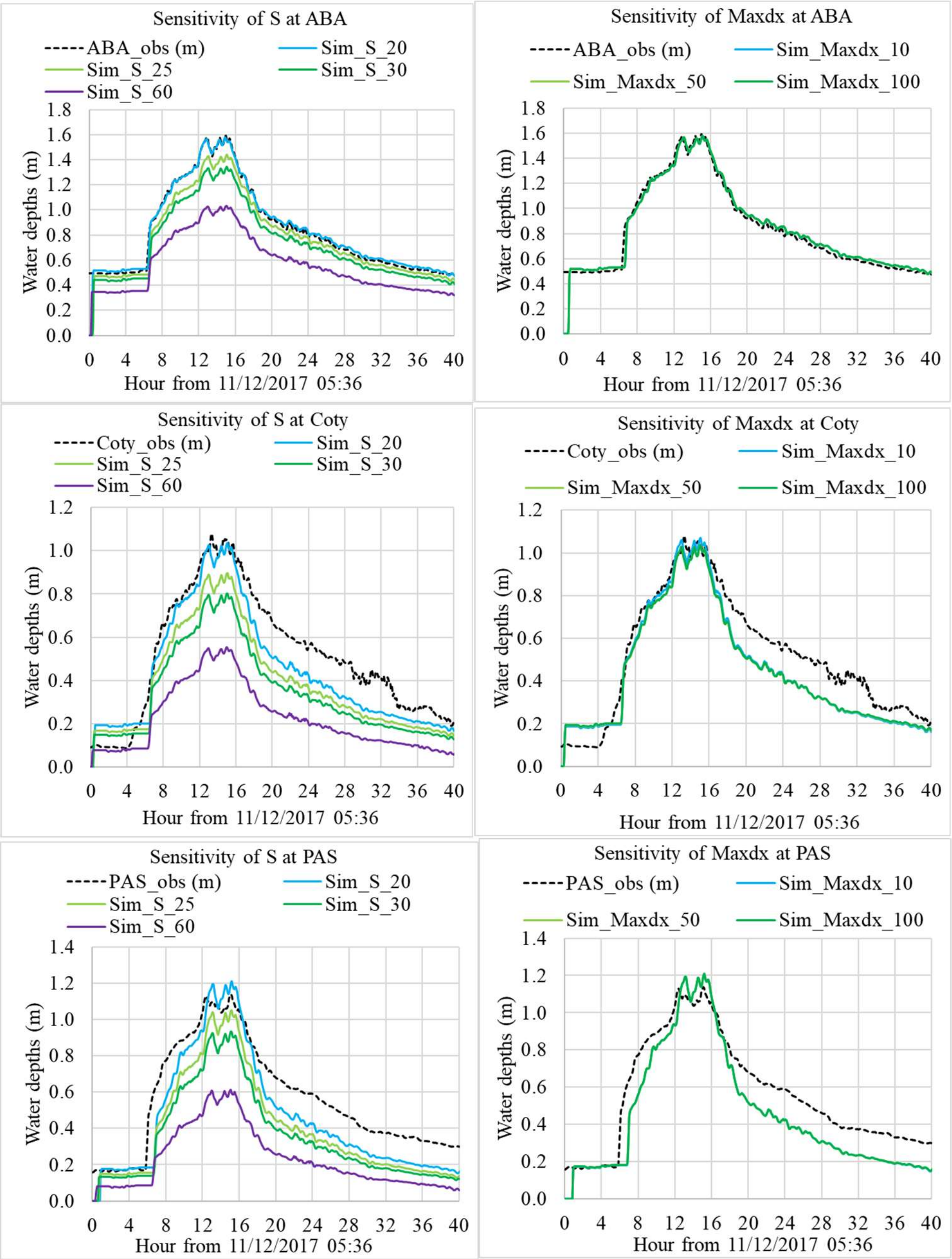

Figure 98 Sensitivity analysis of the model to Manning-Strickler coefficient S and Maximum dx (Maxdx) at ABA, Coty and PAS in the OR for the event starting from 11/12/2017 05:36:00.

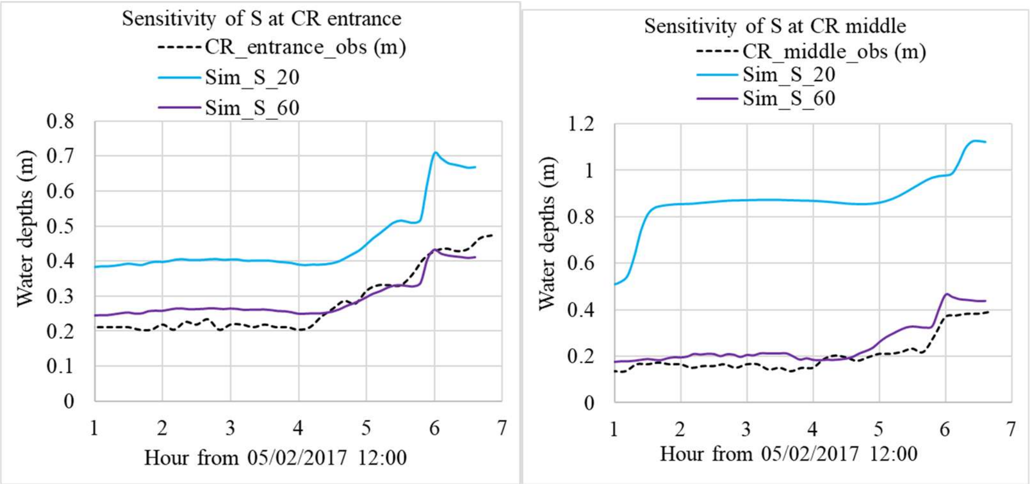

Figure 99 Sensitivity analysis of the model to Manning-Strickler coefficient S at CR entrance and CR middle for the event starting from 05/02/2017 12:0:00.

In Table 23, the average and maximum change in water depths at ABA, Coty, PAS, CR entrance and middle are summarized. The average change is between 0.14 m and 0.27 m. for S and less than 0.05 for Max dx. This implies that S has a strong impact on water depths. Calibrating the model based on S will be sufficient to get a good model.

Table 23 Summary of sensitivity analysis results.

Parameters	**Manning-Strickler coefficient, S**		**Maximum dx, Max dx**	
Range	20-60		10-100	
Variation of simulated water depths (m)	Average	Maximum	Average	Maximum
ABA station	0.27	0.55	0.00	0.05
Coty Station	0.21	0.49	0.01	0.03
PAS station	0.22	0.62	0.00	0.01
CR entrance	0.14	0.28		
CR middle	0.20	0.35		

Based on the outcomes of sensitivity analysis, range of Manning-Strickler coefficient was determined. Then the model was calibrated by making some adjustments to parameters and numerical settings. Table 24 summarizes the results of the calibration process. The optimized S values are 20 for OR 20 for floodplain and 60 for CR during flood periods. During drought periods, the floodplain has higher roughness. Therefore, vegetation is assigned 15 and urban areas get 70. The numerical settings were set as default values 0.005 m and 0.05 m for WD and DD, respectively.

Table 24 Summary of calibrated parameters and settings in the coupled 1D-2D hydraulic model built with MIKEPlus.

Parameters	Flood period	Drought period
S ($m^{1/3}/s$)	OR = 20 CR = 60 Floodplain = 20	OR = 20 CR = 60 Floodplain forests = 10 Floodplain Grass & vegetation = 15 Floodplain urban areas = 70 Water = 20
Max dx (m)	OR = 10 CR = 1000	
Numerical settings values (m)	WD = 0.005m DD = 0.05m	

4.2.2. Model evaluation criteria

To evaluate the model five performance statistics were applied during the calibration process and at the validation stage: Linear regression (R^2) captures the temporal analogy between two series; Nash-Sutcliffe efficiency criteria (NSE) estimates the relative magnitude of the residual variance compared to the measured data variance; Percent bias (PBIAS) determines the middling inclination of the simulated data to be smaller or larger than their observed equivalents; Root Mean Squared Error (RMSE) measures the differences between predictions and observations; and Kling-Gupta Efficiency criteria (KGE) evaluates the average accuracy of the simulated data. These statistics were used in several studies to assess hydraulic models (Ma et al., 2016; Zavattero, 2019; Zavattero et al., 2018).

- $\boldsymbol{R^2 = \frac{cov(obs,sim)}{\sigma_{obs}\sigma_{ysim}}}$ Eq. 35

where,

$cov(obs, sim) = \frac{\sum_{i=1}^{n}(obs_i - \overline{obs})(sim_i - \overline{obs})}{(n-1)}$ *(covariance), σ_{obs} (standard deviation of obs) and σ_{sim} (standard deviation of sim), range (0 to 1, with 1 being the highest analogy to observed data).*

- $\boldsymbol{PBIAS = \frac{\frac{1}{N}\sum_{i=1}^{N}(sim_i^* - obs_i^*)}{\overline{obs^*}} * 100}$ Eq. 36

where, sim_i^* *and* obs_i^* *(simulated and observed respectively),* $\overline{obs^*}$ *(average of the observed values).*

- $\boldsymbol{KGE = 1 - ED}$ Eq. 37

where, $ED = \sqrt{(r-1)^2 + (\alpha-1)^2 + (\beta-1)^2}, \beta = \frac{\mu_{sim}}{\mu_{obs}}, \alpha^2 = \frac{\sigma_{sim}^2}{\sigma_{obs}^2}$ *(the ration between simulated and observed variances),* $\beta_n = \frac{(\mu_{sim} - \mu_{obs})^2}{\sigma_{obs}^2}$ *(standard error of average simulated and average observed data), and* $r = \frac{1}{n}\sum\frac{(P_i^{obs} - \mu_{obs})(P_i^{sim} - \mu_{sim})}{\sigma_{sim}\sigma_{obs}}$ *(correlation coefficient), range (maximized).*

4.2.3. Evaluation of model performance and validation

Four distinct events were singled out for analysis, encompassing the two events already employed in the sensitivity analysis to validate the 1D-2D hydraulic model. These selected events consist of two winter flood occurrences, one spring flood incident, and a summer drought episode (Figure 100). Notably, measurements taken during periods of low flow might not accurately reflect actual river flow conditions due to inherent measurement uncertainties.

One of the chosen events, on 20/12/2019, yielded a discharge of 184 m³/s, ranking among the most intense events witnessed in the LPR over the last decade. Another event on 12/05/2020 was also included in the model validation process. This event recorded a peak discharge of 28 m³/s. It is important to acknowledge that certain events within the LPR can persist for durations exceeding 24 h.

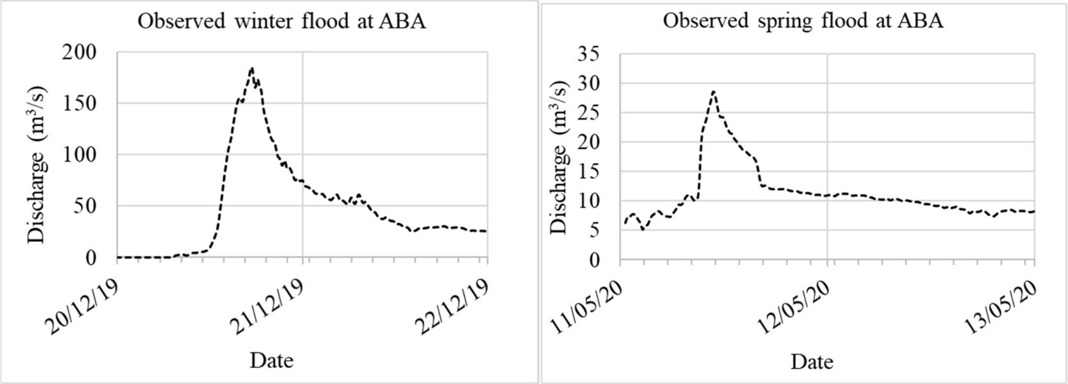

Figure 100 Selected events for model validation and performance analysis.

In Figure 101, the flood event on 11/12/2017 is used to juxtapose the results obtained from the model with the observed data. The graphical representations illustrate a commendable concordance between the model's predictions and the actual observations. This alignment is further substantiated by the strong correlation coefficient and the high NSE value. The smallest NSE value, measuring 0.76, is discerned at PAS. The KGE metric tracks the trends of NSE, with a higher value observed at ABA and a comparatively lower value recorded at PAS.

Comparing the simulated peak arrival times with the observed peak arrival times reveals a slight advancement in the model's predictions. Specifically, at ABA, the simulated peak arrives 6 mn earlier, at Coty it arrives 12 mn earlier, while at PAS it arrives 6 mn later. Analysis of water depths indicates that, at PAS and Coty, there's an approximately 0.2 m disparity between the model's outputs and the observations for water depths below 0.7 m. Conversely, the baseflow water depths exhibit an exact match between the model's estimations and the observed values at ABA and PAS. In the case of Coty, the variance in baseflow depth is less than 0.1 m.

The bias, encompassing a range between -1.25% and 18.81%, showcases the degree of deviation at the three monitoring stations. An overall underestimation of water depths becomes evident at Coty and PAS. Overall, the model effectively replicates the dynamics of this flood event at all three stations.

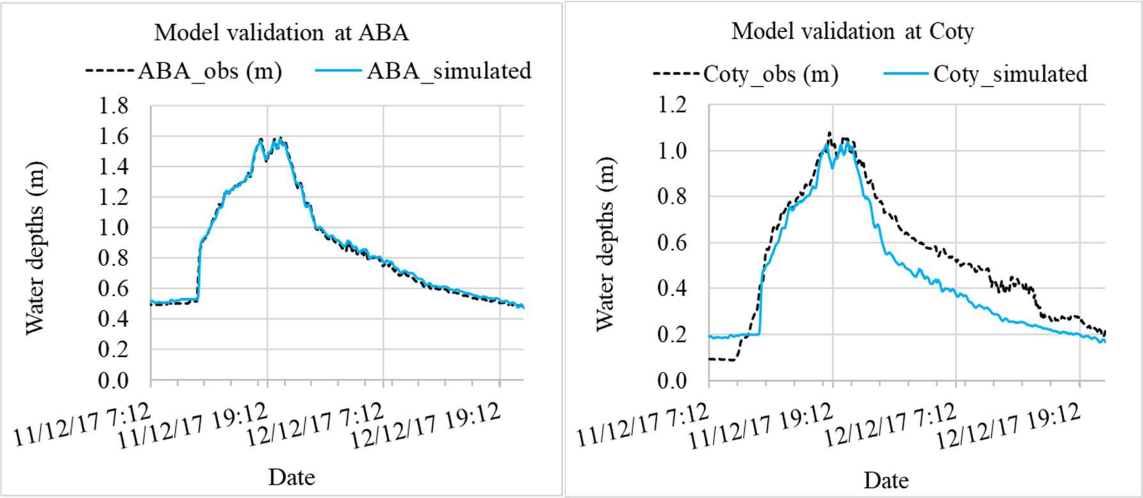

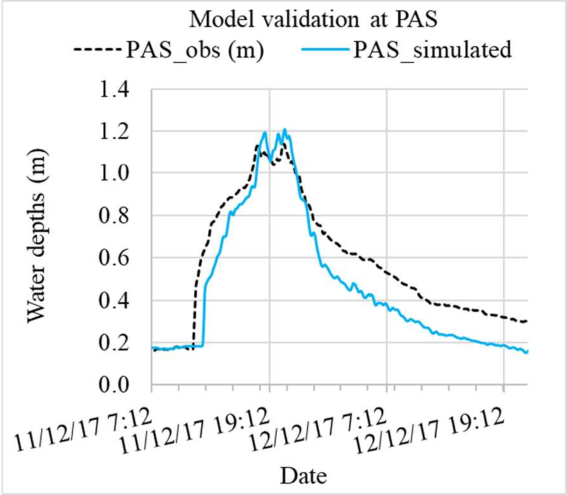

Statistics of model performance in winter 2017			
Events	11/12/2017		
Station	ABA	Coty	PAS
R^2	0.99	0.92	0.93
Time arriving of simulated peak after observed peak	-6 min	-12 min	6 min
NSE	0.99	0.84	0.76
PBIAS	-1.25%	14.82%	18.81%
RMSE	0.02	0.11	0.14
KGE	0.97	0.84	0.77

Figure 101 Results of simulation for model validation, event of 11/12/2017.

In Figure 102, the flood of 20/12/2019 is presented. The peak water depth and shape of hydrograph are perfectly matching the observed at ABA.

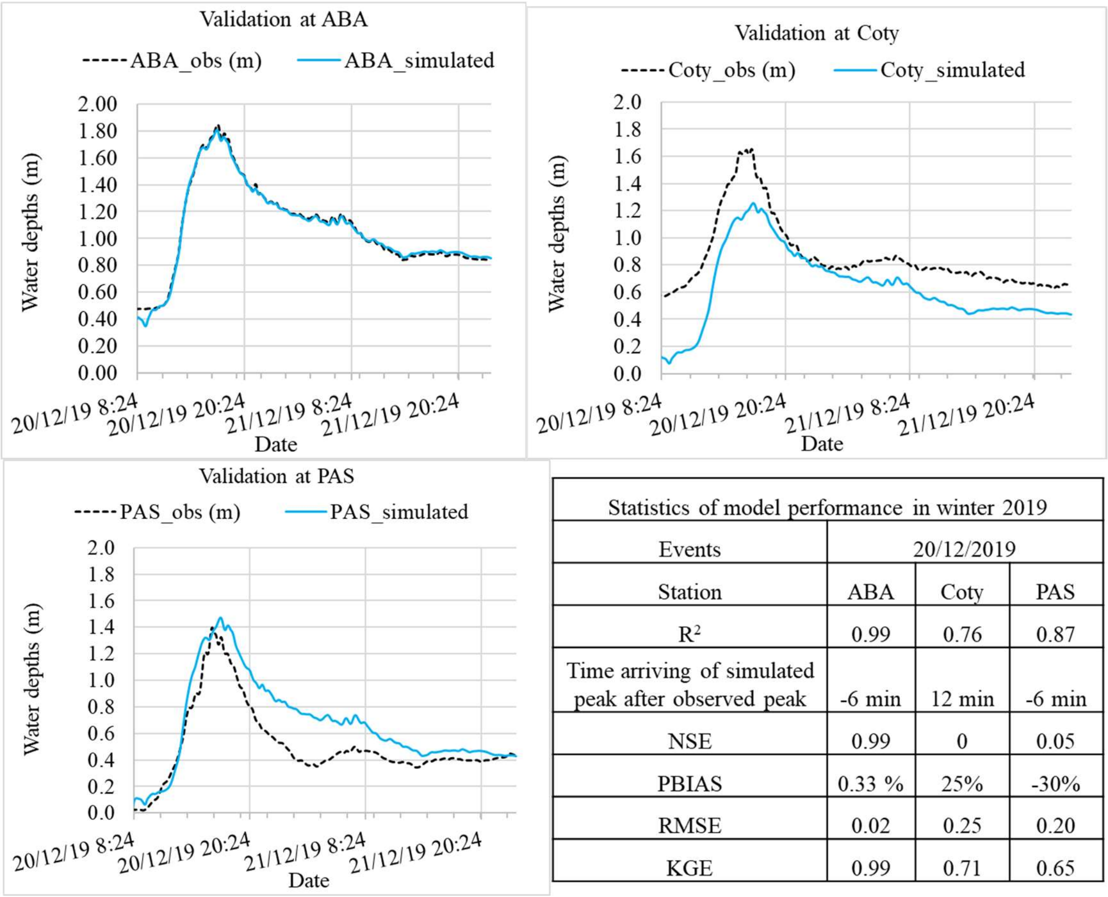

Statistics of model performance in winter 2019			
Events	20/12/2019		
Station	ABA	Coty	PAS
R^2	0.99	0.76	0.87
Time arriving of simulated peak after observed peak	-6 min	12 min	-6 min
NSE	0.99	0	0.05
PBIAS	0.33 %	25%	-30%
RMSE	0.02	0.25	0.20
KGE	0.99	0.71	0.65

Figure 102 Results of simulation for model validation, event of 20/12/2019.

At Coty and PAS, disparities between the model's outputs and observations are more pronounced. The simulated water depth at Coty exhibits a noticeable discrepancy of 0.4 m compared to the observed data. Conversely, at PAS, both the baseflow and peak flow are captured well by the model. However, discrepancies arise during the recession period, where the simulated water depths deviate from the observed values.

The predicted time of peak flow arrival also displays variations: it arrives 6 mn earlier at ABA, 12 mn later at Coty, and 6 mn earlier at PAS. In terms of statistical evaluation, the regression coefficient is least favorable at Coty. For ABA and PAS, the coefficient of determination (R^2) exceeds 0.87. Although the NSE is substantial at ABA (0.99) and relatively low at Coty and PAS, the KGE remains above 0.65 for all three stations. This implies that the model's performance is reasonably satisfactory.

The RMSE measures at 0.02 m for ABA, 0.25 m for Coty, and 0.2 m for PAS. Barring the instance at Coty, the model effectively replicates the flood dynamics with a high degree of accuracy.

Figure 103 illustrates the model's assessment using a minor flood event that occurred on 05/02/2017. Throughout this event, the recorded peak water depths were observed to be 0.9 m, 0.6 m, 0.5 m, and 0.4 m, correspondingly, at ABA, Coty, the entrance of the CR, and the middle of the CR, respectively. While the records are incomplete, they still prove sufficient for validating the model's performance within the CR. The disparities in baseflow between the model's predictions and the observed values remain under 0.2 m.

Performance metrics reveal favorable NSE and KGE values for all stations except the middle of the CR. However, the bias metric signifies a tendency toward underestimation, albeit the average difference is not substantial. In terms of the time of peak arrival, the disparities remain within a 6-mn window. Among the stations, the highest bias is detected at the middle of the CR, while the lowest bias is evident at ABA.

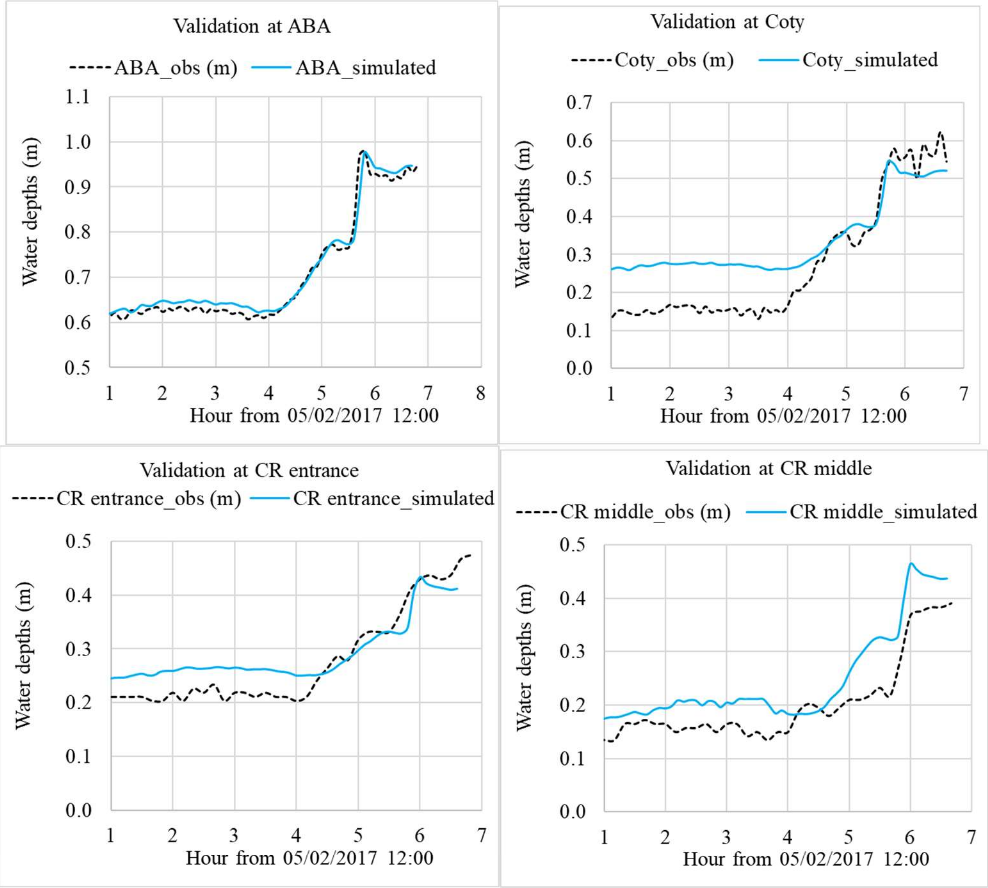

Statistics of model performance in winter 2017				
Events	05/02/2017			
Station	ABA	Coty	CR entrance	CR middle
R^2	0.97	0.96	0.93	0.90
Time arriving of simulated peak after observed peak	0 min	-6 min	+6 min	-6 min
NSE	0.97	0.67	0.81	0.37
PBIAS	-1.1%	-22%	-7.85%	-24.8%
RMSE	0.02	0.09	0.03	0.06
KGE	0.96	0.54	0.72	0.63

Figure 103 Results of simulation for model validation, event of 05/02/2017.

Figure 104 presents an evaluation of the model's performance during the spring of 2020. At ABA, the model exhibits outstanding accuracy. The peak water depth of 0.9 m corresponds precisely between the model's predictions and the observed data. Notably, the Nash-Sutcliffe Efficiency (NSE) attains a value of 0.95, and the Root Mean Square Error (RMSE) is a mere 0.02 m.

Conversely, the model's performance at Coty demonstrates a less favorable outcome, considering metrics like NSE, KGE, and PBIAS. However, the R^2 is remarkably high. Furthermore, the time of peak arrival is divergent by only 6 mn. Given the context of the previously discussed events, the model's performance exhibits inconsistency. Plausible explanations for this inconsistency can be attributed to uncertainties inherent in the recorded data and the river's geometry at that specific location.

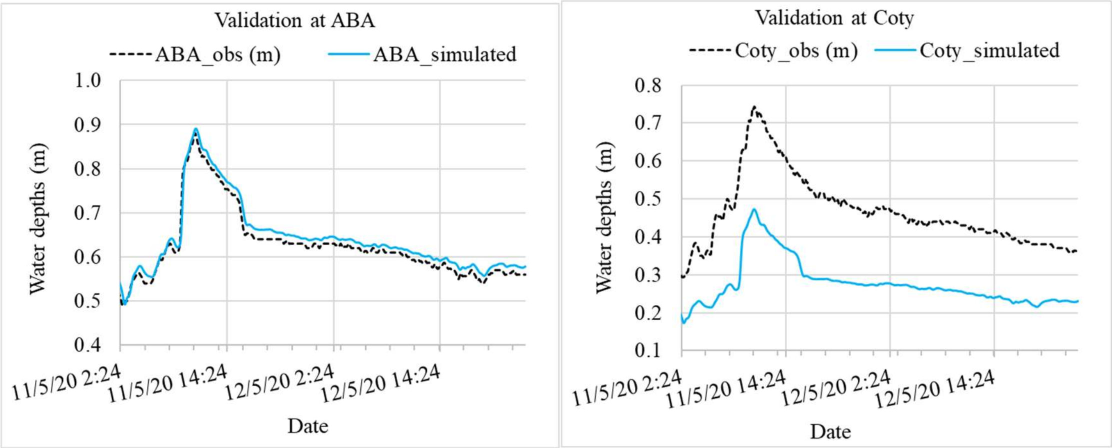

Statistics of model performance in spring 2020		
Events	11/05/2020	
Station	ABA	Coty
R^2	0.99	0.95
Time arriving of simulated peak after observed peak	0 min	-6 min
NSE	0.95	-3.2
PBIAS	-2.46%	40%
RMSE	0.02	0.19
KGE	0.97	0.45

Figure 104 Results of simulation for model validation, event of 11/05/2020.

Overall, the outcomes demonstrate varying performance across different monitoring stations. Linear regression analyses reveal satisfactory R^2 above 0.8 for all stations. At the ABA station, the NSE and KGE consistently exceed 0.9, while the RMSE remains close to 0.02. However, at PAS and Coty stations, NSE values are notably low, yet KGE varies between 0.4 and 0.8. At Coty, the model underestimates observations by over 30% during significant flood events. Discrepancies in peak timing range from 0 to 12 mn. Given the potential for errors in observed discharges due to rating curve use and uncertainties in water depths, the reliability of peak timing stands validated. Consequently, the model effectively captures flow dynamics within the LPR. Nonetheless, suboptimal performance at the Coty station might stem from geometry inaccuracies in cross-sections. Sediment transport and dredging activities could also introduce substantial errors in water depth measurements, impacting baseflow magnitude. The simulated baseflow water depths are consistently 10 to 20 cm lower than observations, except for the event on 05/02/2017 where it is higher. The possible reason is that the interpolated cross-section in the model at the bridge has a bottom level slightly lower than the reality. A survey of the bridge cross-section by taking into account deposited or eroded sediment will be useful. Another possible reason is errors in the monitoring system when the bed level changes but the monitoring system does not take this into consideration when reading the water depth. In fact, water depth in the monitoring system is computed as the difference between the detected free surface elevation and the bottom elevation.

In summary, both high and low flow events are accurately simulated by the 1D-2D MIKEPlus coupled model. The implemented tool operates efficiently on standard hardware, notably outperforming the fully 2D model by producing accurate results for a 48-hour intense event within 12 h. Furthermore, the 1D-2D model accommodates the varying geometry of the covered river and enables seamless connection of open and closed channels through the DHI MIKEPlus coupling systems. This tool facilitates real-time quantification of overflow within the tunnel TAL and other storage areas. Its flexibility permits rapid adjustments of cross-section geometry for incorporating river bathymetry evolution compared to a fully 2D model. However, the model does not perfectly capture bidirectional flows within the riverbed, especially in a torrential river like the LPR. The influence of 2D flows near riverbanks during overflow is also not thoroughly explored. Additionally, meandering during low flows and perturbations from piers under the measurement stations can affect water levels and discharge measurements.

Looking ahead, future development will involve integrating the urban drainage system into the model, facilitated by MIKEPlus, offering an integrated approach for managing flood situations in complex urban environments that encompass both river and pipe flow modeling. While the 2D floodplain implemented in this model features a coarse resolution suitable for assessing overall flow directions, speed, and water depths, urban settings may necessitate finer street-level details for improved flood representation. The model's stability and calculation speed render it reliable for managing real-time extreme events such as a 1000-year flood. Although the current model is confined to the confluence of major tributaries of the Paillons river, its adaptability allows for future integration of upstream floodplains. This extension will ensure comprehensive coverage of vulnerable areas on the eastern side of the territory of MNCA, providing real-time flood information for efficient management.

4.2.4. Application of calibrated model to mapping of flood events

A flood map is generated to visualize the effects of a hydrograph with a 1000-year return period. In Figure 105, the highest water depths across the floodplain are highlighted. It is important to acknowledge that this map does not consider the mitigation effects of urban drainage systems.

Most of the flooding is concentrated on the left bank of the river, with the flow directed towards the Port of Nice. Near the ABA bridge, the road on the left bank begins to flood when the river discharge reaches 480 m^3/s. At Coty bridge, left bank overflow occurs at 900 m^3/s. Upon entering the domain, overflow starts at 1190 m^3/s. The flood-prone road tunnel, TAL, becomes inundated at a river discharge of 480 m^3/s. At the PAS bridge, overflow into an existing flood retention storage is initiated at 250 m^3/s, followed by inundation of the left and right banks of the OR near PAS from 570 m^3/s onward. The expanded TAL structure significantly contributes to minimizing inundation within the urban area. For instance, during a peak discharge event with a 100-year return period (794 m^3/s), localized overflow occurs within the floodplain, but a substantial portion of excess water is directed to the sea via the TAL.

In an urban environment characterized by continuous evolution, including changing building configurations and riverbank elevations, replicating flood routes presents a challenge. While the model can simulate flows at the street level, refining the resolution of the floodplain grid could better depict flow dynamics. Moreover, the riverbed geometry experiences constant adjustments due to sediment transport and anthropogenic alterations, necessitating updates to the 1D riverbed and 2D floodplain model whenever new topographic data becomes available. Addressing errors in riverbank elevation is paramount before evaluating flood risks.

Sediment transport assumes significance within the river context, potentially leading to blockages of bridges and covered river sections during flood events. In the calibrated model, a Manning-Strickler coefficient of 60 is applied to the covered river, accounting for potential material deposits or clogging.

Figure 106 presents a scenario where the roughness of the covered river matches that of the OR due to such deposits or clogging. The uniform roughness value of 20 is then applied across the entire domain, including covered river stretches. The results unveil that this scenario leads to widespread river flooding in the study area. This underscores the importance of maintaining a clean covered river to fulfill its intended function. If two consecutive extreme events occur before the river is cleaned, the risk of overflow increases.

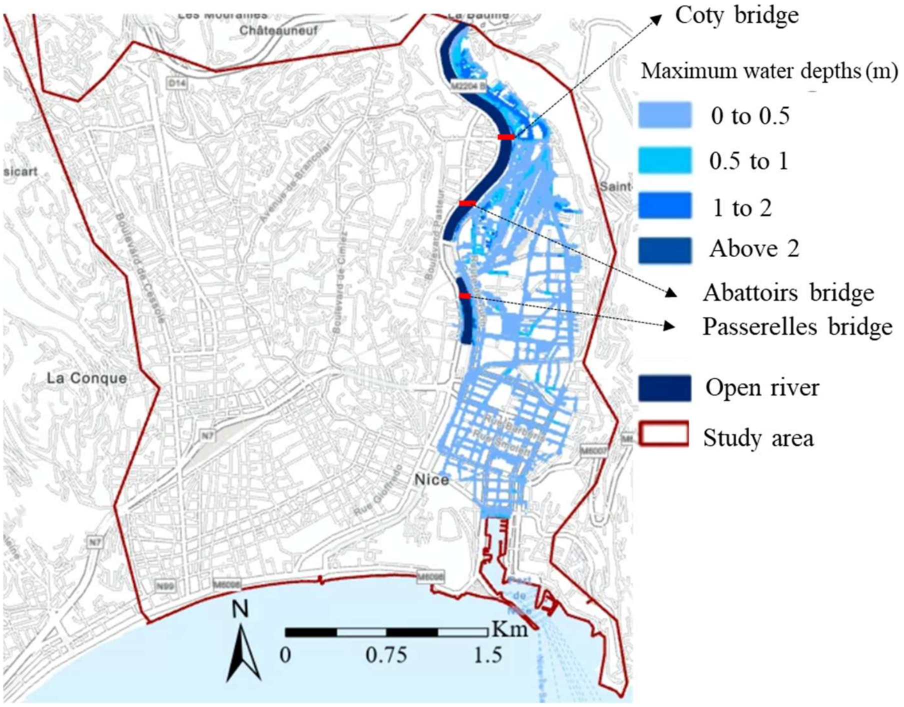

Figure 105 Maximum water depths for 1000-yr inflow hydrograph of peak discharge 1475 m^3/s, with roughness S_{OR}=20, S_{CR}=60 and S_{FP}=20 (Background image: ESRI, HERE, Garmin, Foursquare, geotechnologies, Inc, METI/NASA/USGS).

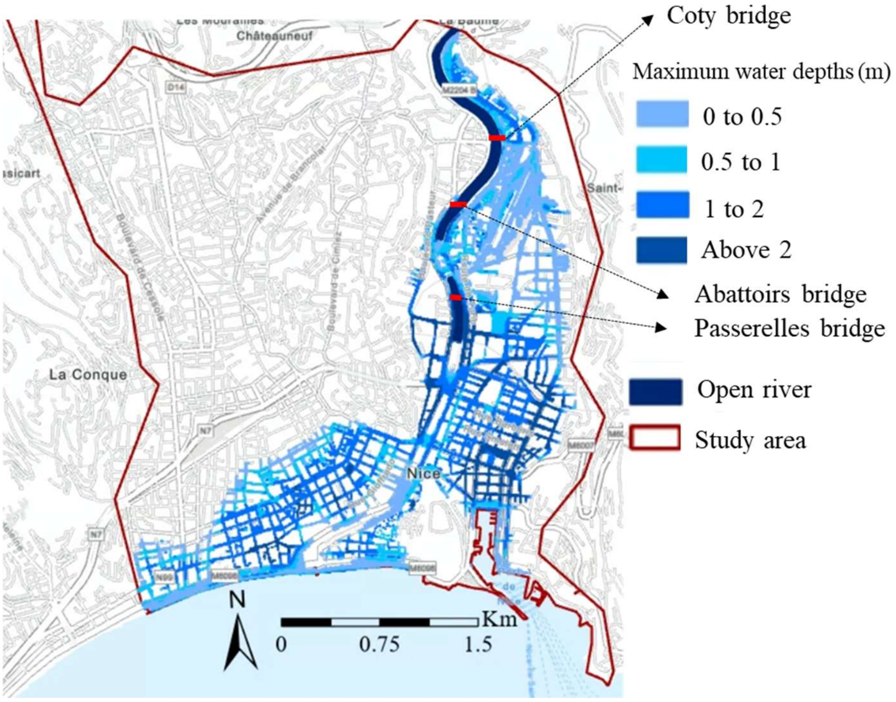

Figure 106 Potential extreme clogging effect: maximum water depths for 1000-yr inflow hydrograph of peak discharge 1475 m^3/s, with uniform roughness S_{OR}=20, S_{CR}=20 and S_{FP}=20 (Background image: ESRI, HERE, Garmin, Foursquare, geotechnologies, Inc, METI/NASA/USGS).

Conclusion

The initial segment of this study delved into the use of video records for the estimation of flow discharge within the Lower Paillons River (LPR). The findings underscore the viability of this approach in furnishing dependable estimates of stream discharge and water depths. Employing the LSPIV technique, the method necessitates video records containing discernible tracers such as plant debris, small floaters, bubbles, or turbulence patterns. However, the challenge lies in securing real-time access to video records during sudden floods. While video records can substantially contribute to validating measurements and model outcomes, it is important to acknowledge that measurements and models remain indispensable in the context of the Paillons River. The forthcoming stages of the Paillons decision support system will explore the integration of these algorithms.

In the subsequent phase, a surface hydraulic model for the LPR was developed and assessed, using the MIKEPlus river network and 2D overland modules. By adopting a 1D representation for open sections and the CR, computational efficiency was optimized without compromising result accuracy. The model adeptly simulates both free surface and pressurized flow conditions, even though the latter could have detrimental effects on infrastructure within Nice. The results underscore the model's capability to replicate flow dynamics and produce inundation maps. This modeling tool is valuable for assessing flow conditions within the CR, the tunnel TAL, and generating urban flood maps for Nice. Integration into a real-time flood warning system, to manage TAL and flood risks, is feasible.

An appraisal of management practices and data quality underscores the model's sensitivity to the quality of input information and validation data. Sediment transport and dredging activities emerge as pivotal factors influencing flow dynamics. Enhancing data quality could be achieved through periodic on-site verification of water depths and discharges. Given that discharge values are automatically derived from measured water depths, refining the precision of water depth measurements would enhance overall data quality. Nonetheless, ground-based runoff gauges might experience interruptions for various reasons, particularly during extreme discharges, necessitating the exploration of alternative discharge estimation techniques. The region is already equipped with cameras for river flood monitoring, opening the possibility of reliable discharge estimates through image-based methods using camera records.

While the hydraulic model is designed to address river flooding in urban areas, urban drainage aspects have yet to be incorporated. To comprehensively comprehend flood dynamics, refining the floodplain mesh to street level and coupling the model with an urban drainage model are warranted. Although the current version excludes buildings, it effectively reproduces river floods in primary streets and locations. The model's limitations encompass the selection of calibration and validation events, as well as the resolution of river geometry. The 1D representation does not accommodate bidirectional flows in the river, which can heighten overflow risks. Additionally, clogging and sediment transport are not accounted for. The scenario involving reduced roughness due to clogging or sediment deposition underscores the imperative of maintaining a clean CR. Furthermore, during dry periods, the river experiences desiccation due to evapotranspiration and infiltration, implying the significance of subsurface flow. However, this model does not encompass groundwater leakages. A groundwater model has been developed to evaluate river-aquifer interactions.

Further endeavors are essential to seamlessly integrate the model into a real-time Decision Support System (DSS). The model demonstrates an impressive capability of simulating two-day events within a mere 12-hour period, rendering it suitable for real-time nowcasting and forecasting. Given the data gaps and errors in monitoring runoff data, an integrated hydrological model has been constructed to furnish real-time boundary conditions. Notably, MIKE SHE's modular nature permits the incorporation of diverse modules to simulate both surface and subsurface flow conditions.

Chapter V. Results and uncertainty analysis of rainfall-runoff and groundwater flow modeling

Introduction

The simulation performance of the deterministic distributed hydrological and groundwater models is limited by uncertainties and defined resolution which impacts on how physical properties of the area of study can be captured. In the context of MIKE SHE and Feflow simulations in the Paillons catchment, the challenges posed by the absence of information regarding catchment characteristics (soil profiles, groundwater table evolution, etc.) were particularly noticeable. This required the application of several assumptions to bridge the gap between available data and model requirements. Following the steps in AquaVar (Du et al., 2018b; Ma, 2018) and the feedback on hydrological modeling in Paillons (Archambaud & Berthet, 2021; Le Gouz de Saint Seine, 1995), a calibration process was deemed necessary in the Paillons catchment to determine the optimal parameter values that could best represent catchment behavior with high accuracy.

Nonetheless, the calibration process for the MIKE SHE and Feflow simulation in the Paillons catchment was intricate due to the numerous parameters affecting various hydrological processes. With no available measurements time series of unconfined groundwater in recent period, Feflow simulation of the unconfined aquifer cannot be calibrated for long period simulations. In addition, too many parameters are involved in these simulations and a selection of keys parameters through sensitivity analysis is required to determine optimal parameters for this specific catchment. In the sensitivity analysis, changes in selected parameters oriented the calibration process. The purpose was to modify individual modeling parameters and observe how they affected the discharge patterns at the catchment outlet (ABA Bridge), aiming to quantify the degree of discharge dependence on parameter changes. This approach aids in achieving a more accurate and efficient calibration process for the model (Du et al., 2016; Ma, 2018; Salvan et al., 2018; Zavattero, 2019).

The modeling of MIKE SHE was extended over a significant period from the beginning of 2011 to the end of 2016, covering diverse hydrological events such as notable floods in November 2011 and November 2012, a winter flood in January 2014, and a drought event in July 2012. These events' discharge variations were designed as response indicators to evaluate the sensitivities of the tested parameters. Sensitivity of parameters in Feflow was also conducted in the same period.

Following the sensitivity analysis, the subsequent section of this chapter revolves around model calibration and validation. The model was calibrated using five years of simulation data from 2011 to 2015 and validated using data from 2016 to 2020. Nevertheless, while these statistical evaluations provide a broad perspective on simulation performance, a more detailed analysis was deemed necessary to determine the alignment between simulation outcomes and specific modeling goals. Consequently, after comprehensive assessment of all evaluation factors, the calibrated MIKE SHE simulation for the Paillons catchment exhibited satisfactory results, meeting the modeling objectives and contributing to extension of the AquaVar Environmental Decision Support System (EDSS) to the Paillons.

Moreover, the chapter explored uncertainty analysis, connecting the modeling results with field-collected data. This approach aimed to gain a nuanced understanding of the quality of observations and simulations in the Paillons. The chapter concluded by summarizing the assessment of simulation quality and reflecting on the experience of designing an optimized modeling strategy for establishing a deterministic distributed hydrological and groundwater models within the Paillons catchment, despite the challenges posed by significant missing field information.

5.1. Sensitivity analysis in MIKE SHE

Previous studies of the Var catchment showed that the most sensitive parameters in MIKE SHE simulation are Leakage coefficient, Saturated hydraulic conductivity, and Horizontal hydraulic conductivity (Ma, 2018). However, each catchment may respond differently to the modeling parameters due to its specificities. The Paillons catchment has steep slopes as in the Var. It is assumed that the baseline parameters for MIKE SHE simulations in Paillons can be set with the optimized parameters of the Var simulation. However, the major difference between the Var model and the Paillons model is that the Paillons catchment is 12 times smaller than the Var catchment.

Because of the substantial uncertainty stemming from data gaps within the Paillons catchment, the construction of the MIKE SHE model involved numerous assumptions and considerations under different circumstances. The sensitivity analysis of this model primarily concentrated on the computational parameters embedded in the various hydrological functions within the model. Among the parameters subjected to testing, some were categorized as "numerical," lacking a direct link to the physical attributes of the catchment. Others pertained to physical parameters intended to directly depict the physical processes within the study area (Ma, 2018).

Table 25 comprehensively enlists all parameters encompassing the sensitivity analysis. This collection includes 3 numerical parameters governing calculation time intervals, alongside 18 parameters characterizing the physical attributes within the catchment, spanning across climate, overland flow, stream flow (rivers and lakes) and flow through unsaturated and saturated zones.

Table 25 Summary of parameters used in the sensitivity analysis of MIKE SHE simulation in Paillons catchment (adapted from (Ma, 2018)).

Functions	Parameters	Units
Domain grid resolution	Grid resolution	m
Time Step Control	Max. precipitation depth per time step	mm
	Max. infiltration amount per time step	mm
	Input precipitation rate requiring its own time step	mm/hour
Climate	Degree-day coefficient	mm/°C/day
Rivers and Lakes	Bed resistance	$m^{(1/3)}/s$
	Leakage coefficient	/s
	Muskingum delay parameter at every 500 m of a river branch	mn
Overland Flow	Manning-Strickler coefficient of Forest	$m^{(1/3)}/s$
	Manning-Strickler coefficient of Open space	$m^{(1/3)}/s$
	Manning-Strickler coefficient of Artificial area	$m^{(1/3)}/s$
	Manning-Strickler coefficient of Agriculture area	$m^{(1/3)}/s$
Unsaturated Zone	Hydraulic Conductivity of Clay loam	m/s
	Hydraulic Conductivity of Loam	m/s
	Hydraulic Conductivity of Silt loam	m/s
	Hydraulic Conductivity of urban impervious	m/s
	Evapotranspiration (ET) Surface Depth	m
Saturated Zone	Horizontal hydraulic conductivity	m/s
	Layer depth	m
	Initial potential head	m
	Number of layers	-

These parameters assume a crucial role in the model simulation, serving as fundamental components within the computation equations. Their diverse impacts on the simulated discharge at the catchment outlet are anticipated due to their central role. Furthermore, their influence on catchment runoff is projected to extend beyond mere simulation magnitude, extending to the temporal patterns of peak discharges.

It should be noted that the baseline parameters of the saturated zone assumed the soil depth of 1m thickness on average to be representative of a shallow reservoir interacting with stream runoff. Its horizontal hydraulic conductivity is set at 1.00E-06 m/s close to the dominant saturated hydraulic conductivity in the unsaturated zone. Small horizontal hydraulic conductivities tends to slow the emptying of the saturated zone and its contribution to baseflow during extreme events. Small values also preserve a good convergence of model calculations which ensures accurate results.

5.1.1. The impact of changes in the grid resolution

The baseline grid resolution is 100 m. This grid is suitable for the objectives of the research project. However, future projects may require higher resolution. In order to make informed suggestions in cases where grid resolution will change, the influence of changing its values was assessed.

Modifying the resolution from 100 m to 40, 55 and 80 m grid resolution yield variations in peak discharges without changing the time of the peaks (Figure 107). For the event of May 2013, a spring flood, simulated discharge varied between 2.40 and 8.78 m^3/s, representing less than 9% change from the baseline value of 98.25 m^3/s. As expected, increasing the grid resolution tends to increase the simulated discharge. However, there is an exception with the 100 m grid. Its discharge is higher than the one of 55 and 80 m grid resolutions. This discrepancies may be caused by the difference in topographic data used. In fact, the 100 m grid was a result of a filling sinks preprocessing. Meanwhile, a 20 m resolution elevation data was used directly in the model. Then the model automatically resample this data to fit the grid resolution using bilinear interpolation. Similar variations are observed for the January 2014 winter flood event which has its baseline value at 209.84 m^3/s. In summer flood, the July 2012 event was in good agreement with the expectation that the discharge increases with increasing grid resolution.

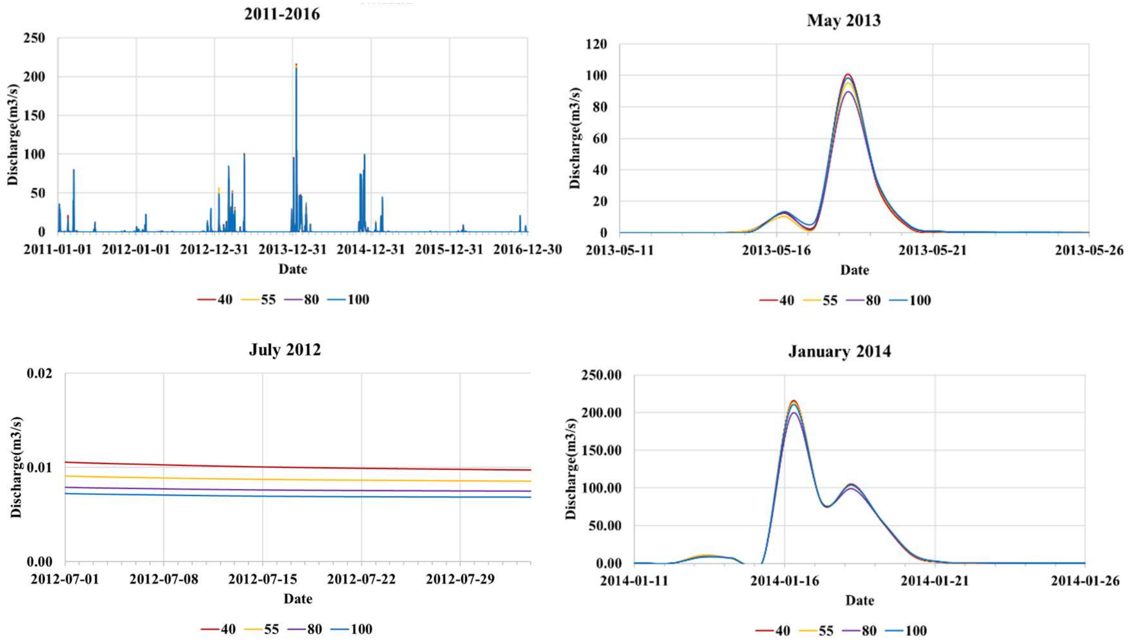

Figure 107 Sensitivity analysis of Grid resolution.

The notable change in peak discharge with changing grid resolution stay within the uncertainty range of discharge measurements of 20 %. Therefore, future projects with different grid resolution may only be concerned with changes in peak estimates without a need to recalibrate the entire model. However, careful consideration should be given to extreme event like the 100 year return flood event of 794 m^3/s because they are beyond the range of values simulated in the period of study.

In this project, further analysis will focus on using the selected 100 m grid resolution for model calibration, validation and applications.

5.1.2. The impact of parameters in "Time step control" module

The role of the "Time step control" module is to mitigate numerical instabilities by adjusting the time step for rainfall data resampling when the current computational time step is too long. It should be noted that each hydrological function in MIKE SHE operates with its own independent time step.

If the cumulative rainfall in the current time step surpasses the threshold specified by "Max precipitation depth per time step", the model's computational time step will be reduced by a predefined increment rate. In the Paillons model, this value is set at 0.05. Subsequently, the precipitation data will be resampled to line up with the new time step. This iterative process will continue up to the precipitation amount per time step reaches the predefined maximum value (DHI, 2023d; Ma, 2018). Therefore, assessing the impacts of parameters in this module is expected to have some influence on simulated results.

The first control parameter to be assessed is "Max precipitation depth per time step" ($P_{\text{Max depth}}$). Figure 108 shows that changes of $P_{\text{Max depth}}$ from 50 to 1 and 100 does not lead to notable variations in peak discharge for the three selected events. Less than 2.02 m^3/s of change in peak discharge occurred. Other floods in the period showed changes higher than 2.02 m^3/s. However, there was no change in timing of the peaks. Therefore it is reasonable to select 50 mm as the parameter value for $P_{\text{Max depth.}}$

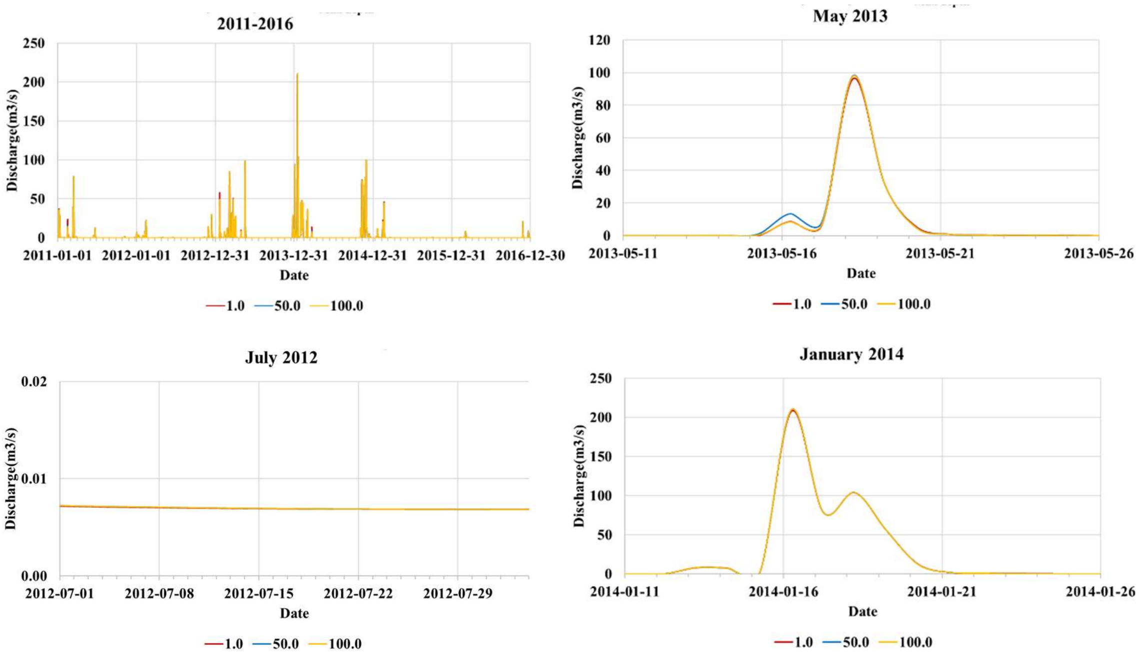

Figure 108 Sensitivity analysis of "Max precipitation depth per time step".

The "Max infiltration amount per time step" ($P_{\text{Max inf}}$) is the second control parameter to be evaluated. This parameter was also varied between 1 and 100. In this case, notable changes were observed for the spring flood, but not for the summer drought and winter flood. This parameter did not affect the timing of the peak. For the event in May 2013, Figure 109 shows a maximum change of 7.67 m^3/s corresponding to a parameter value of 100 mm. The 1 mm parameter yield a similar peak as the 50 mm. however, the computation is very long for the 1 mm. Therefore, acceptable value $P_{\text{Max depth}}$ can be selected close to 50 mm.

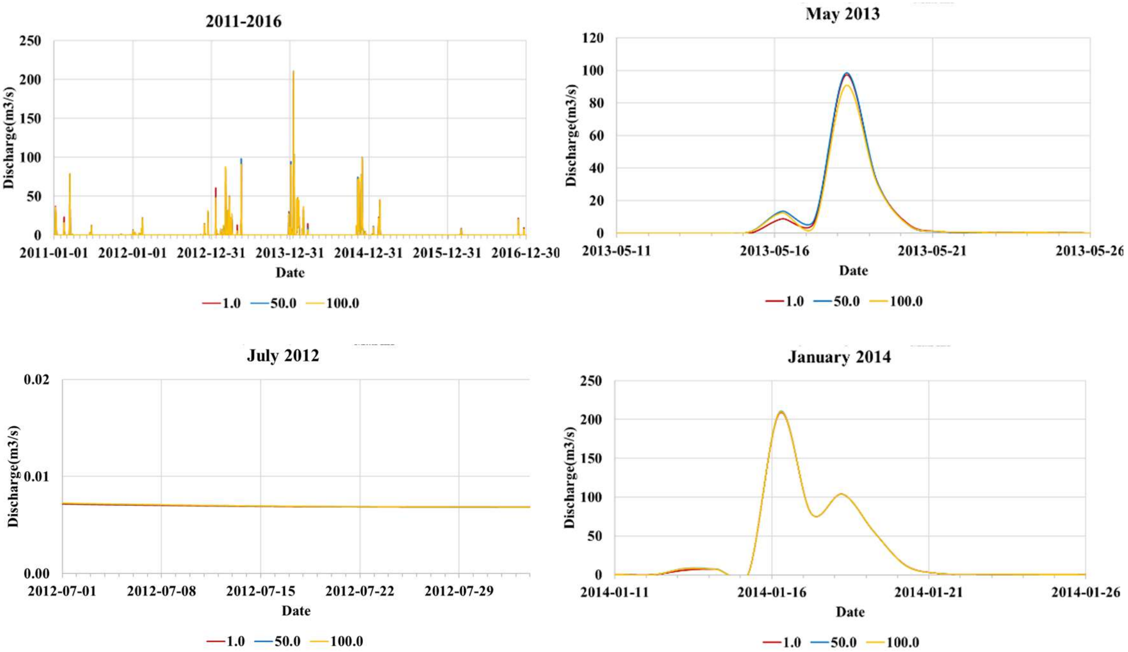

Figure 109 Sensitivity analysis "Max infiltration amount per time step".

Finally, the third control parameter namely "Input precipitation rate requiring its own time step" ($P_{\text{Input rate}}$) did not induce notable change in peak discharges during the period of evaluation. As presented in Figure 110, a small change of -0.15 m^3/s was noted at the peak of the spring flood for the parameter value 1 mm/hour. $P_{\text{Input rate}}$ is supposed to capture short term rainfall events by decreasing its value. In the Paillons, a value evolving around 5 mm/hour seems to be sufficient for that purpose.

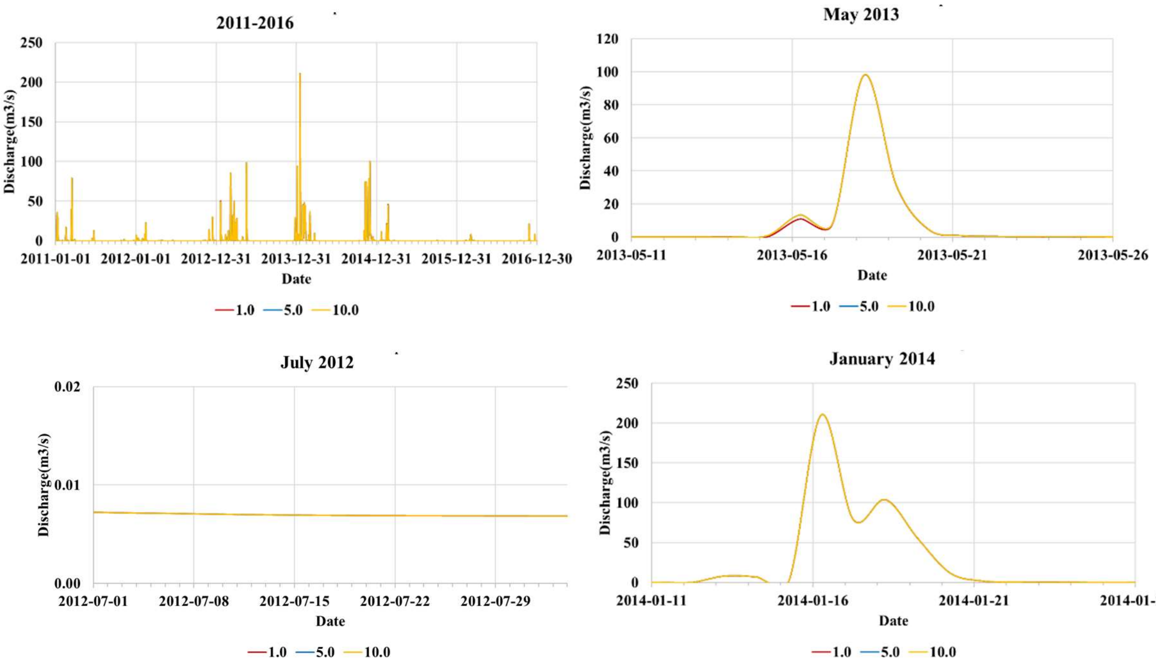

Figure 110 Sensitivity analysis of "Input precipitation rate requiring its own time step".

5.1.3. The impact of parameters in "Climate" module

In the "Climate" module, the "Degree day" coefficient was evaluated to identify the influence of the speed of snow melting and freezing in the study area. Higher values are expected to enhance the change of state depending on temperature values above or below 0°C. However, there is no significant permanent or seasonal snow cover in the Paillons. Therefore, as expected, Figure 111 highlights that there was no significant change in simulated discharges. Less than 0.01 m^3/s of change was observed when the parameter value varied from 4 to 2 and 8. In short, the baseline values was judged acceptable for the model of the Paillons.

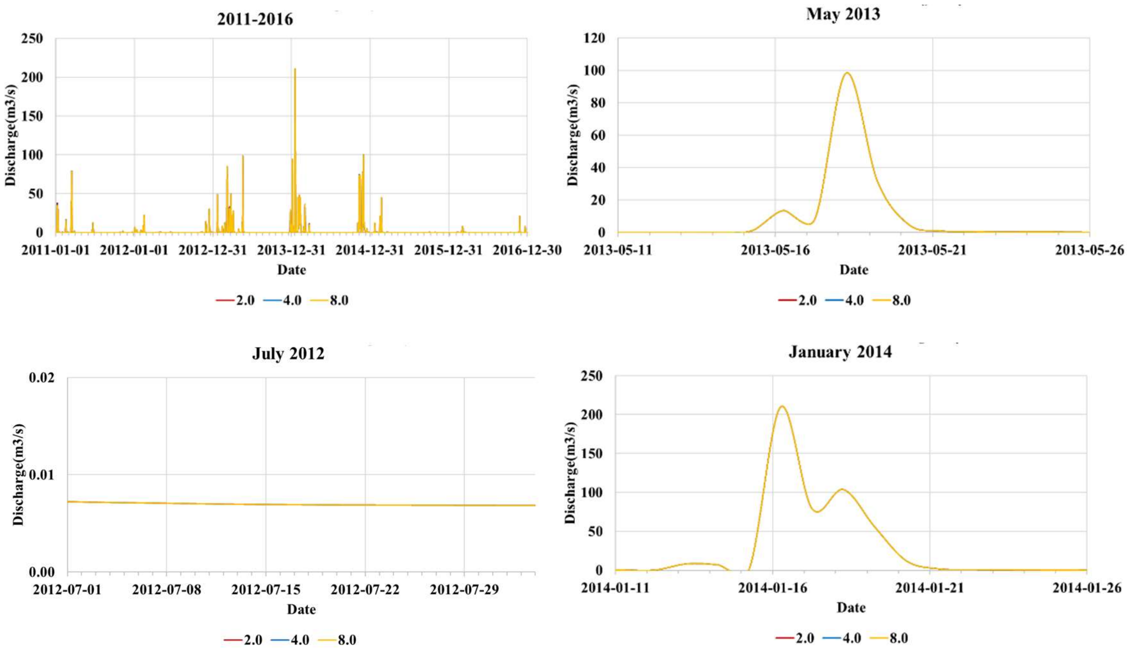

Figure 111 Sensitivity analysis of "Degree day coefficient".

5.1.4. The impact of parameters in “Rivers and Lakes” module

In the “Rivers and Lakes” module, 3 parameters were included in the sensitivity analysis: Manning-Strickler coefficient of the riverbed (S_{Bed}), Leakage coefficient (C_{Leak}) and Muskingum delay parameter at every 500 m of a river branch (k_{Delay}). The Manning-Strickler coefficient was expected to influence the peak discharge and its timing. The leakage coefficient was projected to affect the exchange between the river and the aquifer. And the delay parameter would modify the peak discharge and its timing. In fact, kinematic routing is used in the 1D river hydraulic model coupled with MIKE SHE. The baseline condition for the delay parameter was zero. Meaning that any water flowing to the river is instantaneously added to the estimates at every cross-section without considering the flow duration along the streamline. The choice of this method is to take advantage of its stability in any flood case. However, in the downstream part where hydraulic processes may become complex with hydraulic jumps and back water effects, this approach may not be suitable. On the other hand, using the full Shallow water equations may accurately represent flow processes but longer computation time and risk of instabilities cannot be avoided. Since the objective of this study is to build tools for real-time simulations, kinematic routing is preferred.

As presented in Figure 112 & Figure 113, changing the Manning-Strickler coefficient and leakage coefficient did not lead to significant changes in discharge (less than 0.01 m^3/s). The Manning-Strickler coefficient was varied between 10 and 50 m$^{(1/3)}$/s, while the leakage coefficient changes from 7.50E-05 /s to 1.00E-04 and 1.00E-06. The impact of riverbed Manning-Strickler coefficient was expected to be negligible due to steep slopes and small size of the catchment and consideration of routing method with no delay parameter. As seen in the surface hydraulic modeling, the roughness has a major effect when the Shallow water equations are considered independently to the slope and size of the study area. A possible explanation of the low sensitivity to leakage coefficient is the low thickness of 1 m selected for the saturated zone in the baseline set up. For deeper saturated zones, the leakage coefficient is expected to have more influence on river discharge.

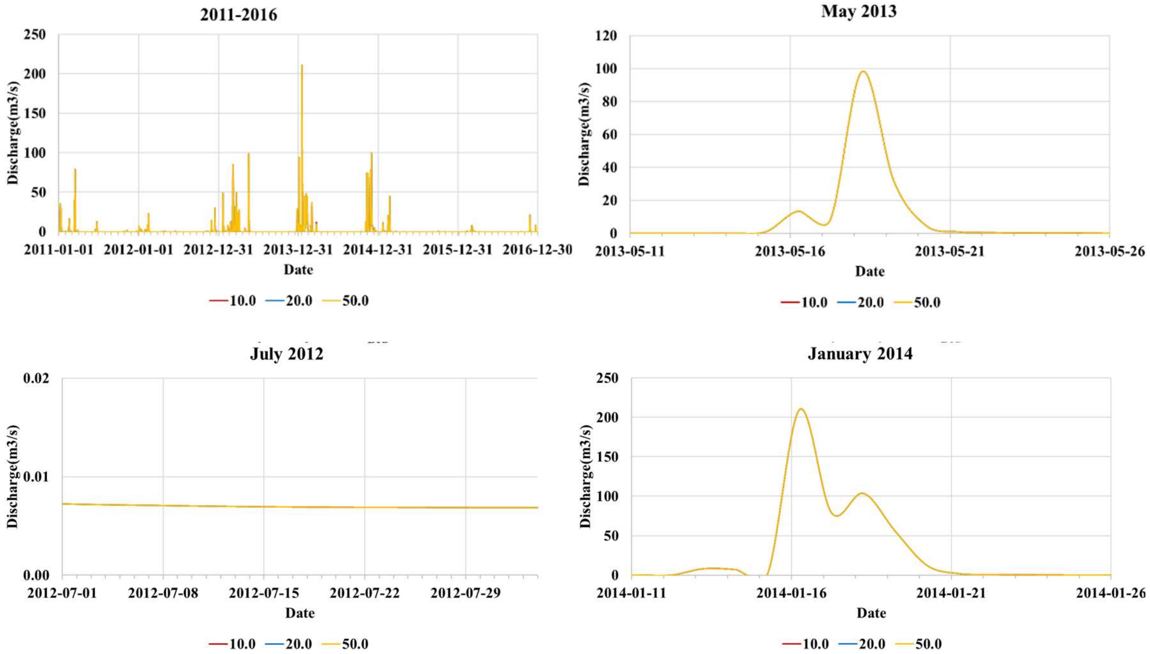

Figure 112 Sensitivity analysis of the model to Manning-Strickler coefficient of the riverbed.

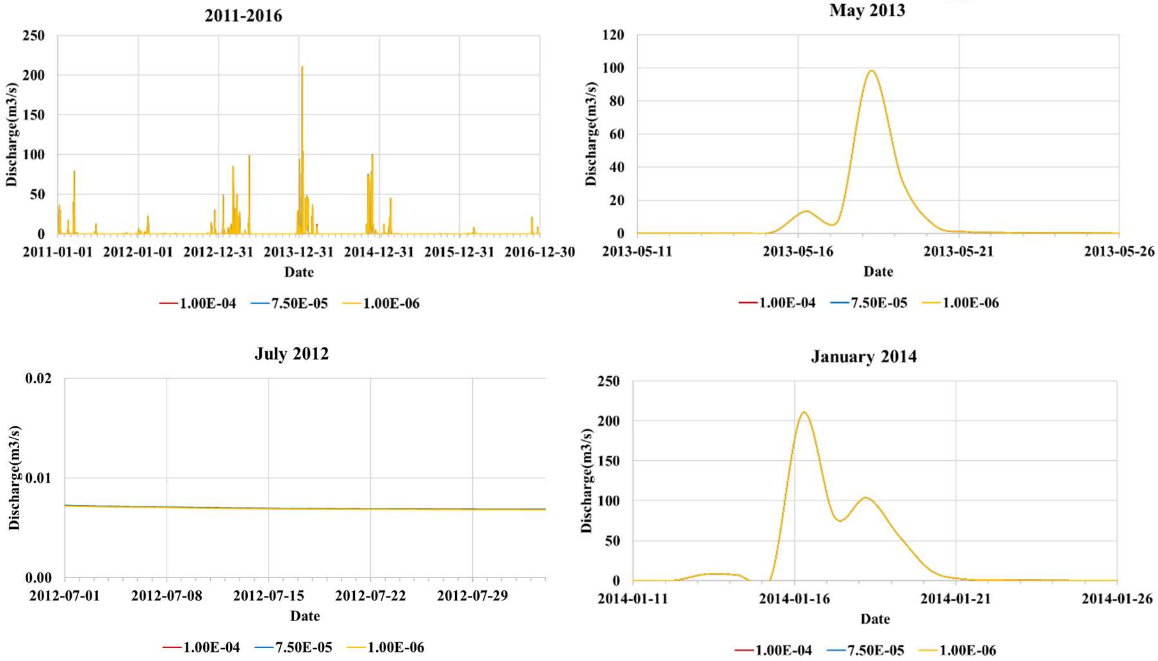

Figure 113 Sensitivity analysis of leakage coefficient.

Moreover, the assessment of the delay parameter yield significant changes in discharge estimates and timing of peak discharges (Figure 114). For the spring and winter floods, varying this parameter between 0 and 120 mn affected both the peak discharges and timing of peaks. However, no change was observed for the July 2012 low flow period. For the event of May 2013, increasing the delay parameter value shifted the timing of the peak to later dates. In fact, for a parameter value of 3 mn, the peak of 70.11 m^3/s was simulated on the same day as the baseline peak estimate. However, the peaks of 82.48 and 35.60 m^3/s appeared 1 day and 2 days later, respectively. These two peaks were obtained for the parameter values 30 and 120 mn. In terms of magnitude of discharge, increasing the delay parameter value tends to decrease the peak discharge and flatten the runoff hydrograph. It should be noted that flood events occurs within a few h to a couple of days. Therefore, flat hydrographs spanning several weeks are not representative of runoff within the Paillons catchment. Daily catchment response time should be less than 3 days.

The flood event of January 2014 displays the same trend as for the spring flood. However, the peak time for the 120 mn parameter value occurred 3 days later. In addition, the multi-peaks event almost disappeared. The peak discharges estimates were 180.85, 177.78, and 84.92 m^3/s, which diverged significantly from the baseline value of 209.84 m^3/s. It is expected that reasonable values of the delay parameter will range from 0 to 30 mn at every 500 m distance along the streamline. In addition to the delay parameter, a default shape factor of 0.2 required for the routing method was applied. Its sensitivity was not assessed in this study.

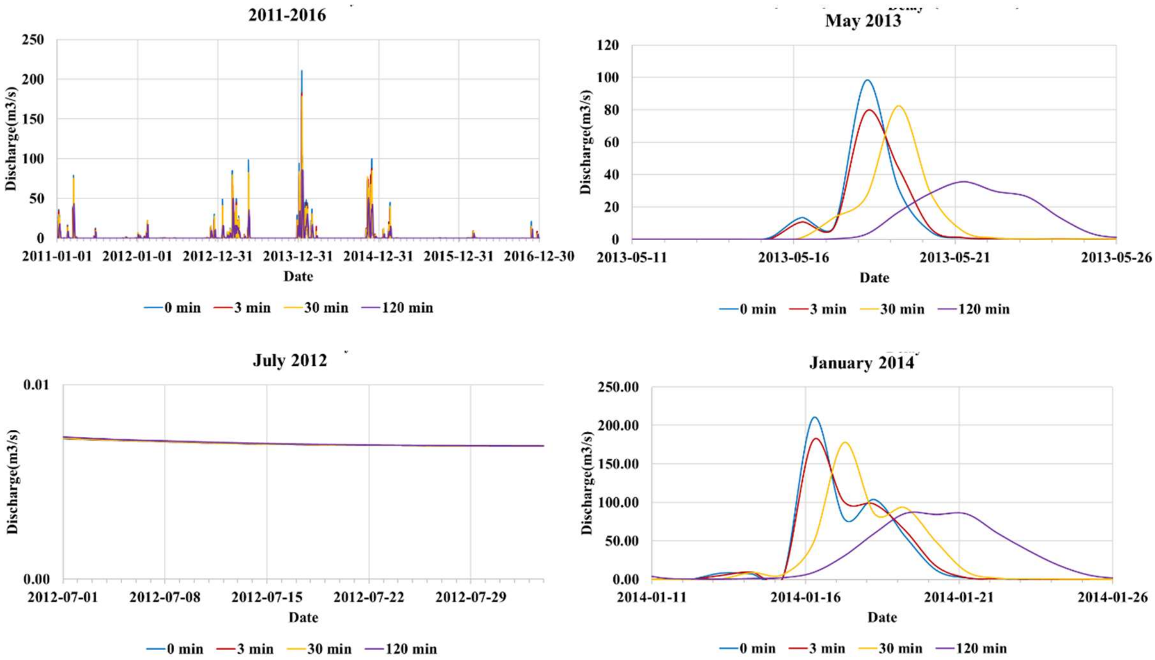

Figure 114 Sensitivity analysis of the model to Muskingum delay parameter at every 500 m along the streamline.

5.1.5. The impact of parameters in "overland flow" module

Same as the Manning-Strickler coefficient of the riverbed, the Manning-Strickler coefficients of the surface in the "overland flow" module was expected to affect the peak discharge and timing of the peaks. Four main classes of land-use were selected for this assessment: Forest areas, Open spaces with few vegetation, agricultural areas and artificial surfaces.

The analysis of the sensitivity of the model to the Manning-Strickler coefficients are presented in Figure 115, Figure 116, Figure 117 & Figure 118. Only the spring and winter flood were affected by changes of the value of this parameter. As expected, increasing Manning-Strickler coefficient resulted in an increase in peak discharges. However, no change in timing of the peaks were observed. The biggest change of 15.68 m^3/s was observed for the Forests parameter value of 1 $m^{(1/3)}/s$ during the winter flood event. The surface area occupied by Agricultural areas is small compared to Forest and Open spaces which are dominant. Therefore, it was expected that its influence would be the lowest. The artificial surfaces concentrated in the floodplains were also expected to have a significant influence on simulated discharge.

In short, reasonable Manning-Strickler coefficients between 2 and 60 $m^{(1/3)}/s$ to represent the characteristics of the land-use in the Paillons. Forests and Open spaces with few vegetations are expected to have lower values than agricultural and artificial surfaces.

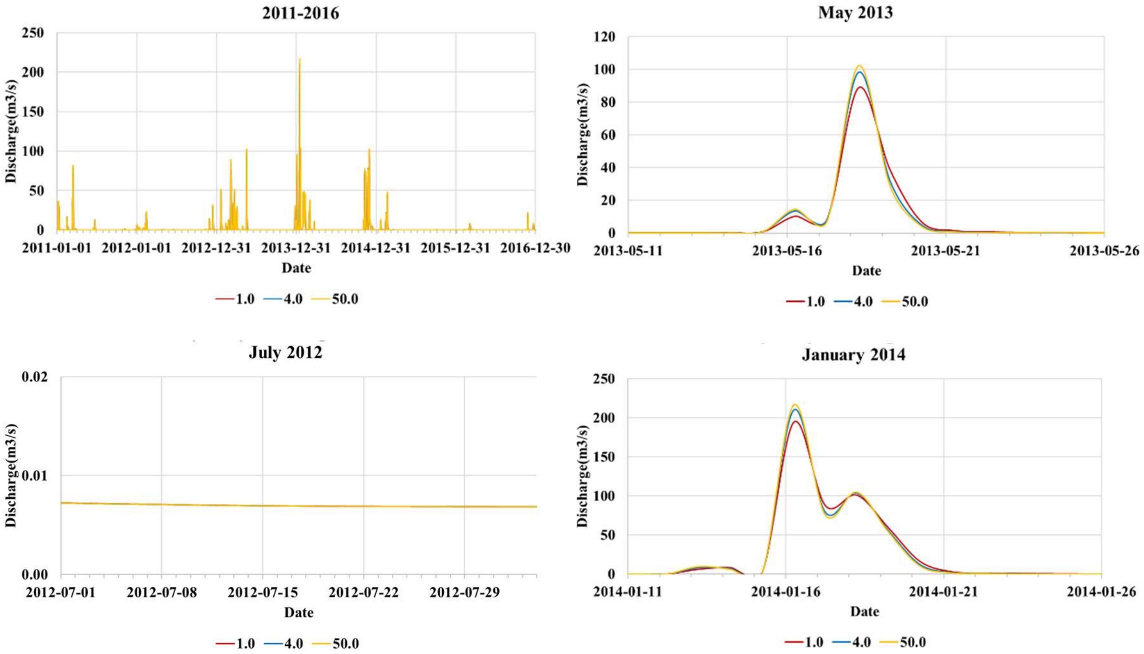

Figure 115 Sensitivity analysis of the model to Manning-Strickler coefficient of Forests.

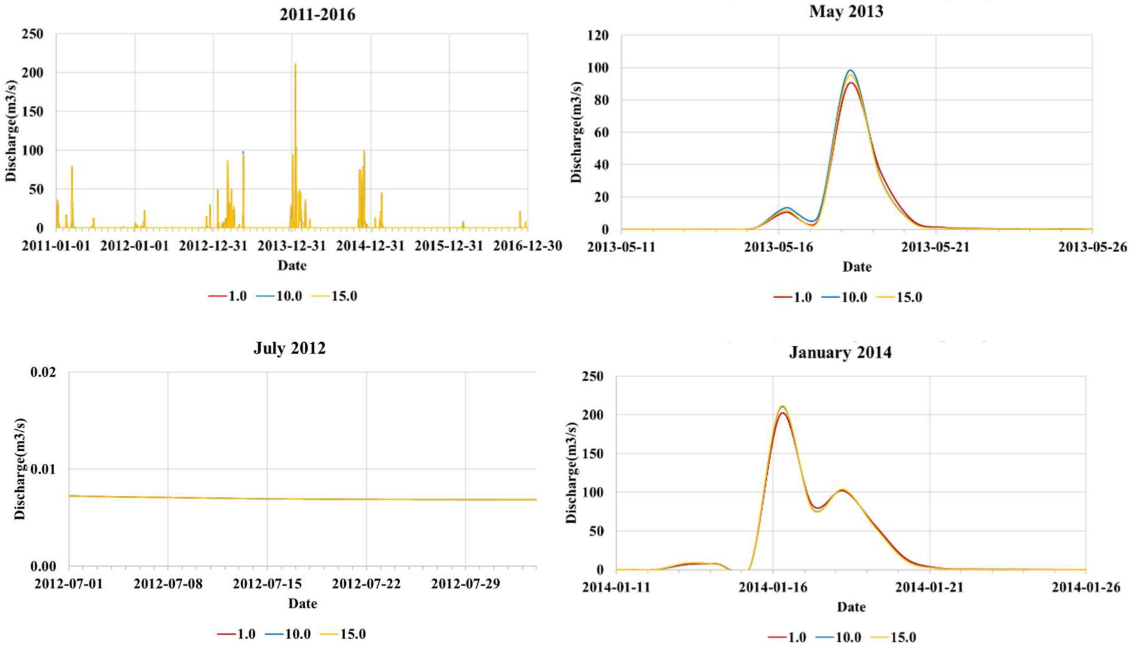

Figure 116 Sensitivity analysis of the model to Manning-Strickler coefficient of Open spaces.

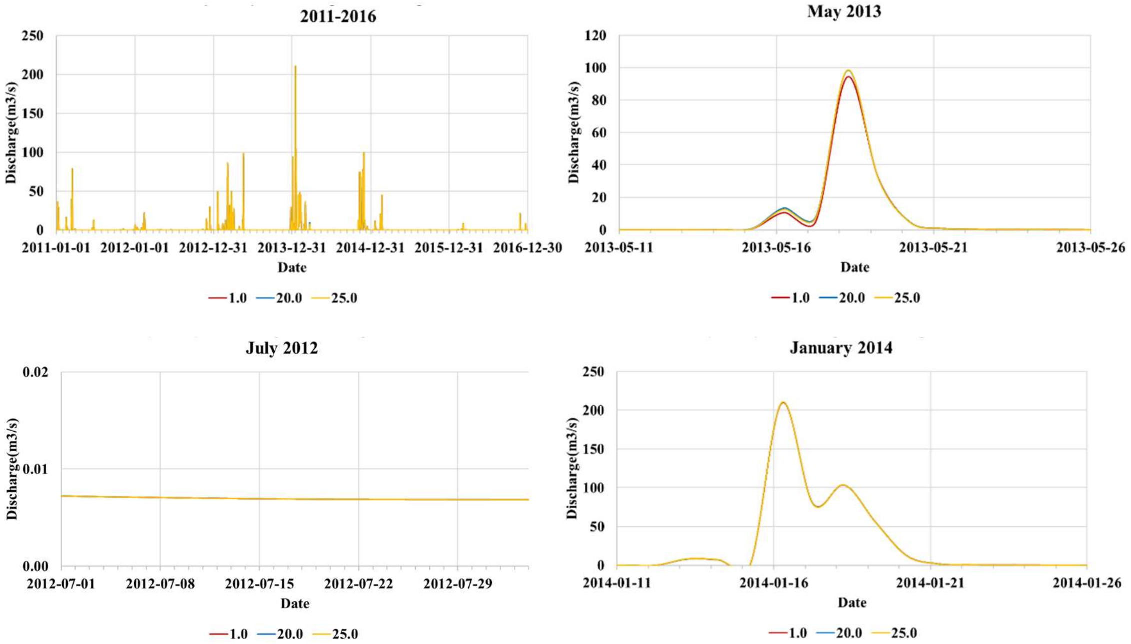

Figure 117 Sensitivity analysis of the model to Manning-Strickler coefficient of Agricultural areas.

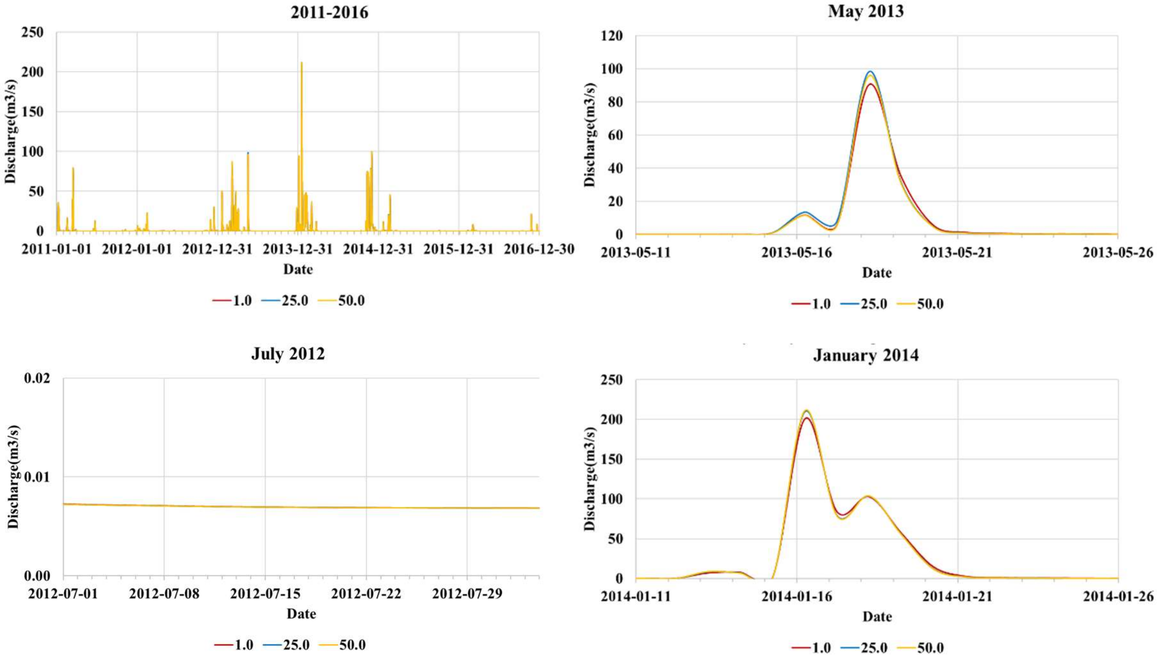

Figure 118 Sensitivity analysis of the model to Manning-Strickler coefficient of Artificial surfaces.

5.1.6. The impact of parameters in "unsaturated zone" module

The saturated hydraulic conductivity (K_{uz}) and ET surface depth (ET_{depth}) are the two parameters tested in this evaluation. The two-layer water balance method was selected in this module for its simplicity and low data requirements. While ET surface depth is assumed uniform, the saturated hydraulic conductivity was classified according to the 4 soil classes defined in the study area: Loam, Clay loam, Silt loam and urban impervious. A fifth soil class, Sandy loam, was not included because it covers only two grid cells. The urban impervious was introduced to the soil classification to evaluate the effect of urbanization on runoff processes. None of these parameters affected the timing of the peaks (Figure 119, Figure 120, Figure 121, Figure 122 & Figure 123). While negligible variations were observed in drought period, the influence of these parameters were significant in spring and winter periods.

The $K_{uz\ Loam}$ varied between 5.00E-04 and 1.00E-06 m/s from its baseline value of 4.00E-06 m/s. There were negligible changes observed during drought and winter periods. However, the spring flood displayed changes between 0.22 and 6.25 m^3/s. For this parameter, there was no increasing or decreasing trend expected. Within the parameter value interval, the variations remain quite modest.

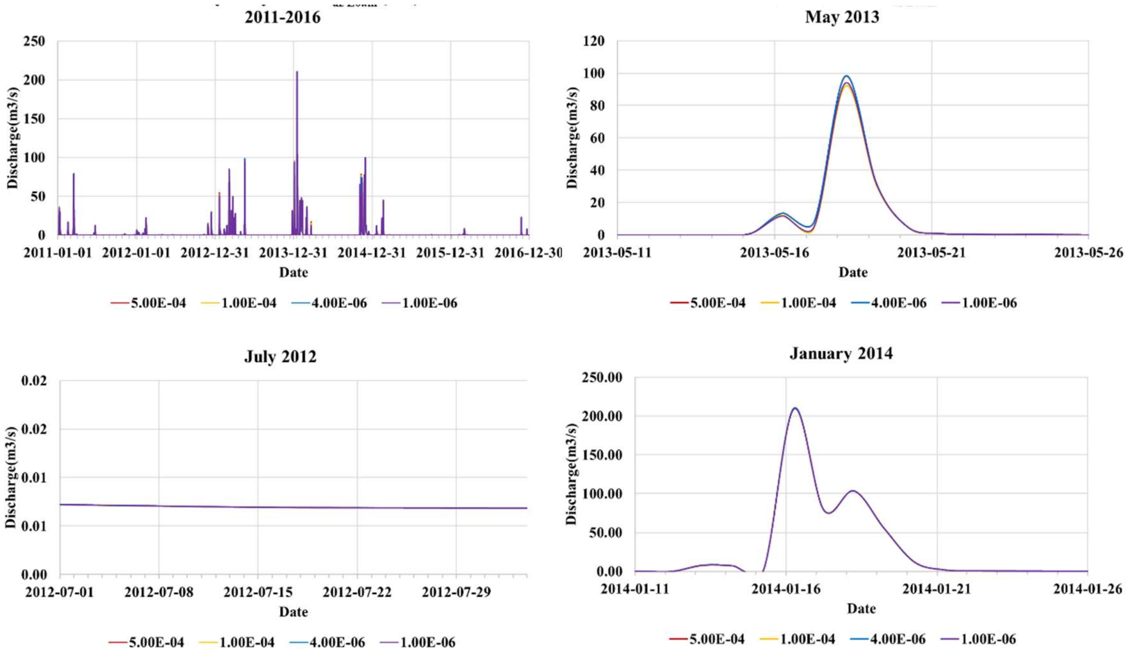

Figure 119 Sensitivity analysis of saturated hydraulic conductivity of Loam.

The second soil class, Clay Loam also played a notable influence on simulated discharge compared to the Loam soil. In fact, it affected the second peak of the winter flood and the peak of the spring flood. However, the changes were less than 5 m^3/s.

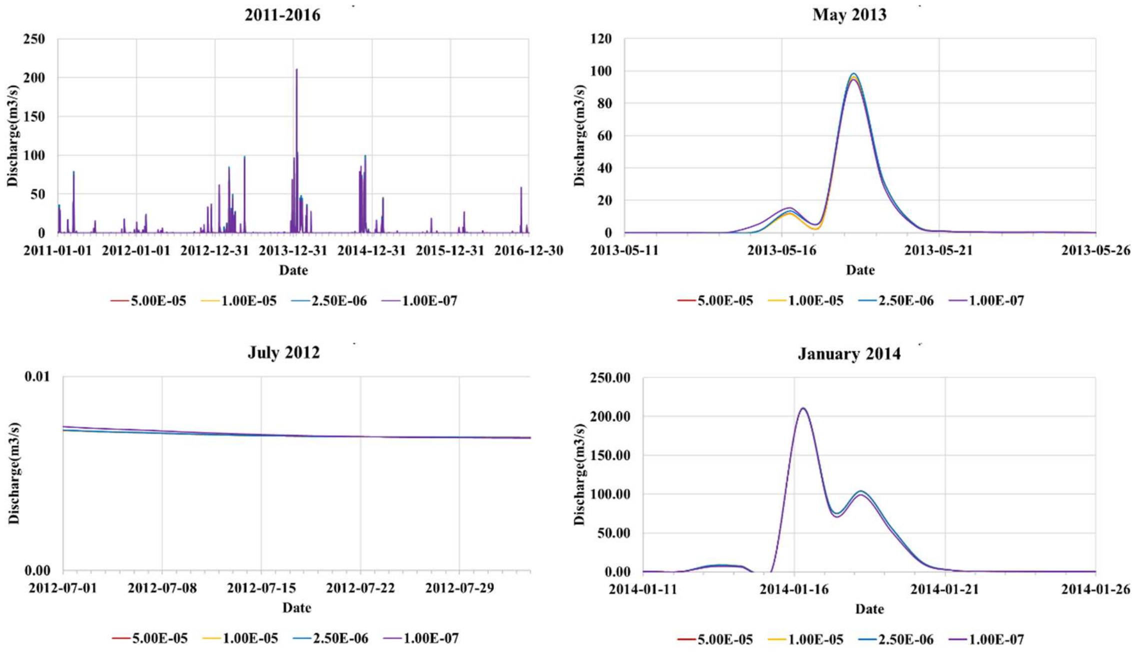

Figure 120 Sensitivity analysis of saturated hydraulic conductivity of Clay Loam.

The Silt loam soil class affected mostly the spring flood. Negligible changes were observed during summer and winter flow periods. The maximum change occurred with the parameter value 1.00E-06 m/s but all the changes were lower than 5.1 m^3/s.

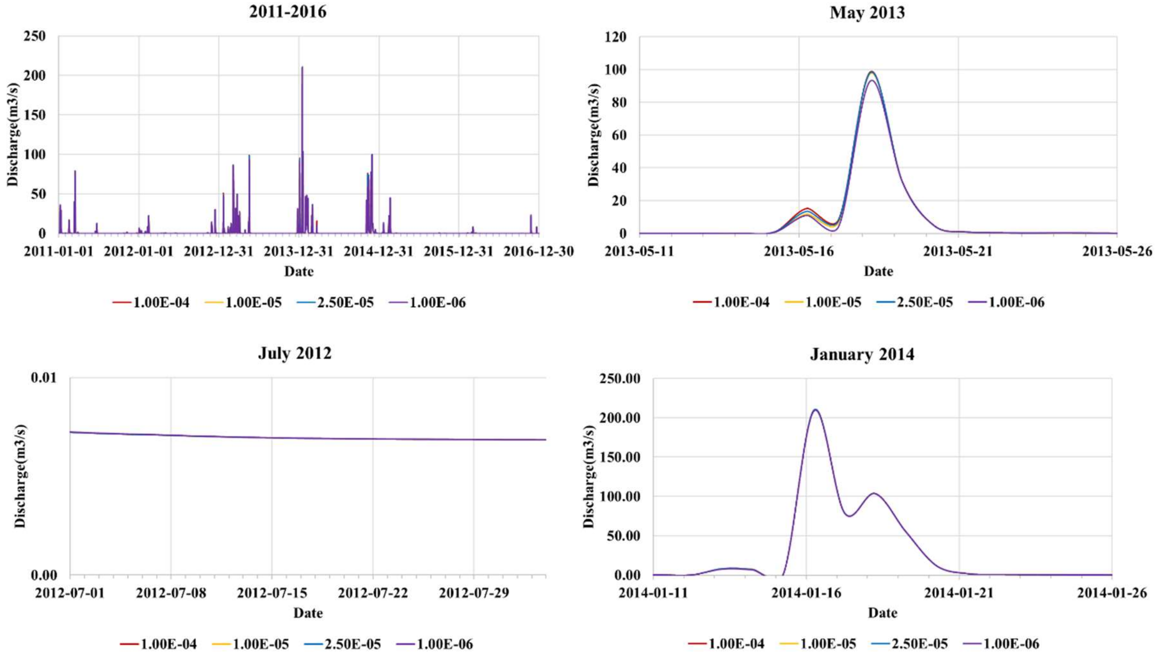

Figure 121 Sensitivity analysis of saturated hydraulic conductivity of Silt Loam.

For the area under a strong influence of urbanization, small changes were observed during the spring flood. The parameter value was changed between 1.00E-08 and 1.00E-05 m/s. The maximum change was obtained with 1.00E-08 m/s at 3.31 m^3/s. The secondary peak of the spring flood was also affected.

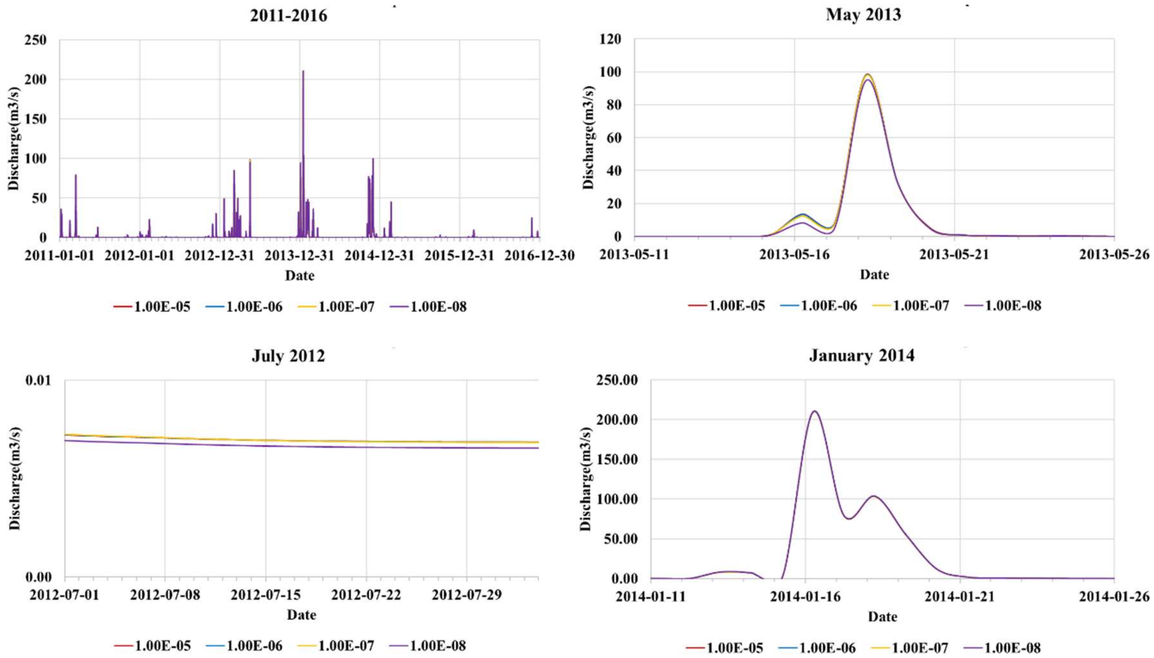

Figure 122 Sensitivity analysis of saturated hydraulic conductivity of Urban impervious.

In MIKE SHE simulations, ET surface depth is involved in the estimating soil evapotranspiration. Changes in this parameter showed visible changes of discharge in all periods. But during the drought period, the changes are negligible. Increasing ET decreased the discharge estimates, with a maximum change observed during the winter flood: -23.96 m^3/s for the ET surface depth of 1 m.

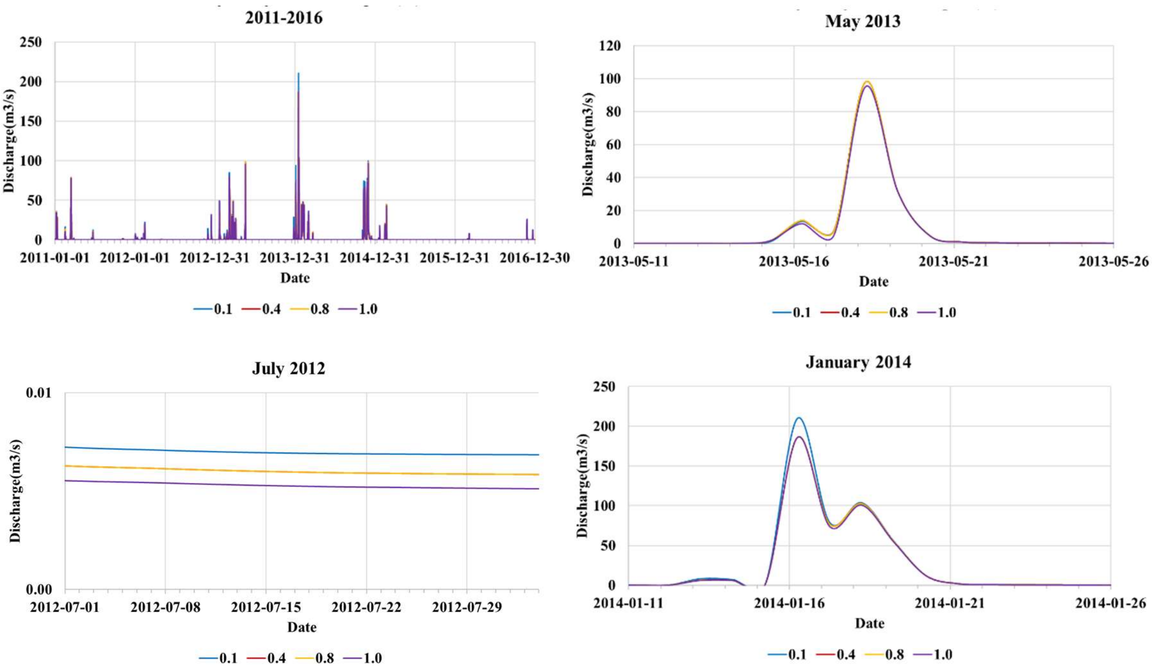

Figure 123 Sensitivity analysis of ET surface depth.

In summary, parameters in the saturated zone affect to a certain extent the magnitude of the runoff discharges without affecting the time of peak. Except for ET, no specific trend can be deducted. The selected ranges of the saturated hydraulic conductivity are much smaller than that used in the study on the Paillons conducted by Le Gouz de Saint Seine (1995) which were in order of 3 to 4E-03 m/s. That study assumed the values to integrate uncertainties in the modeling input data. Further calibration of this parameter is required to reproduce runoff in the Paillons.

5.1.7. The impact of parameters in "saturated zone" module

Reported as playing an important role in runoff calculations, the "saturated zone" was considered carefully. Previous studies of the Var catchment focused on assessing the impact of the horizontal hydraulic conductivity after assuming a shallow reservoir thickness (Ma, 2018). This is in good agreement with the selection of the 2-layer water balance method. And, it is motivated by the fact that the level of the free unconfined aquifer at catchment scale is not well known in the region. However, it is possible to use deep reservoirs for the saturated zone with the 2-layer water balance method if a proper calibration process is implemented (DHI, 2023d). In the Paillons, it was first assumed that the thickness of the saturated zone influencing runoff is close to the soil depth. However, the geological formations within the catchment show the existence of karstic and fissured rock reservoirs even if most of the surface area is dominated by marls formation beneath the soil layer. Those reservoirs tends to interact with surface runoff on several meters of thickness through high infiltration rates and numerous spring outlets. In fact, in the Paillons catchment there are dozens of springs from Jurassic, Turonian, Senonian, Eocene and Oligocene rocks (Appendix 7). Some of those springs are permanent and others are seasonal. In addition, groundwater levels recorded at a borehole, namely the Sagna borehole, located in Jurassic aquifer at the center of the Paillons catchment shows a strong correlation with seasonal variations of rainfall (Tennevin et al., 2017). In addition the base groundwater level at this borehole showed a decreasing trend at an average rate of 1.00E-08 m/s which is more pronounced in dry years.

In this study, in addition to the horizontal hydraulic conductivity (K_{sz}), the thickness of the saturated zone (named "Soil depth"), the initial potential head and the number of layers of the saturated zone were assessed to identify their influence on streamflow discharge. The horizontal hydraulic conductivity is assumed to be 10 times the value of the vertical hydraulic conductivity. Therefore, the values of these two parameters were varied in parallel. Assumed to be uniform in study, this value is actually distributed in reality. The expectation is that a uniform value can be used to represent part of the saturated zone that contribute effectively to runoff. Figure 124 presents the simulated hydrographs for each change in the parameter value. As expected, changes in K_{sz} has a significant impact on peak discharge and time of peak. During the simulation periods, other recorded flood events (e.g. November 2011 and November 2012) appeared in the simulation results, which were not visible with the baseline parameter value of 1.00E-06 m/s. The new peaks were particularly noticeable for a parameter value of 1.00E-02 m/s. In May 2013, the peak discharge decreased for changes in parameter value to 1.00E-02, 1.00E-04 and 1.00E-08 m/s. Only the simulation with 1.00E-02 m/s shifted the time of peak to 1 day later. For the summer drought, higher hydraulic conductivity generated fluctuations in the results. In addition, the winter flood event which has two peaks was transformed into a single peak and flat hydrograph. In terms of magnitude of peak discharge, the simulation with 1.00E-02 m/s displayed a change of 71.41 m^3/s in May 2013 and 83.89 m^3/s in winter 2014. The largest decrease in peak was observed with 1.00E-04 m/s. However, there is no specific decreasing or increasing trend with this parameter. Its influence is expected to follow a flipped bell curve where the parameter leading the highest decrease will be found within the selected range.

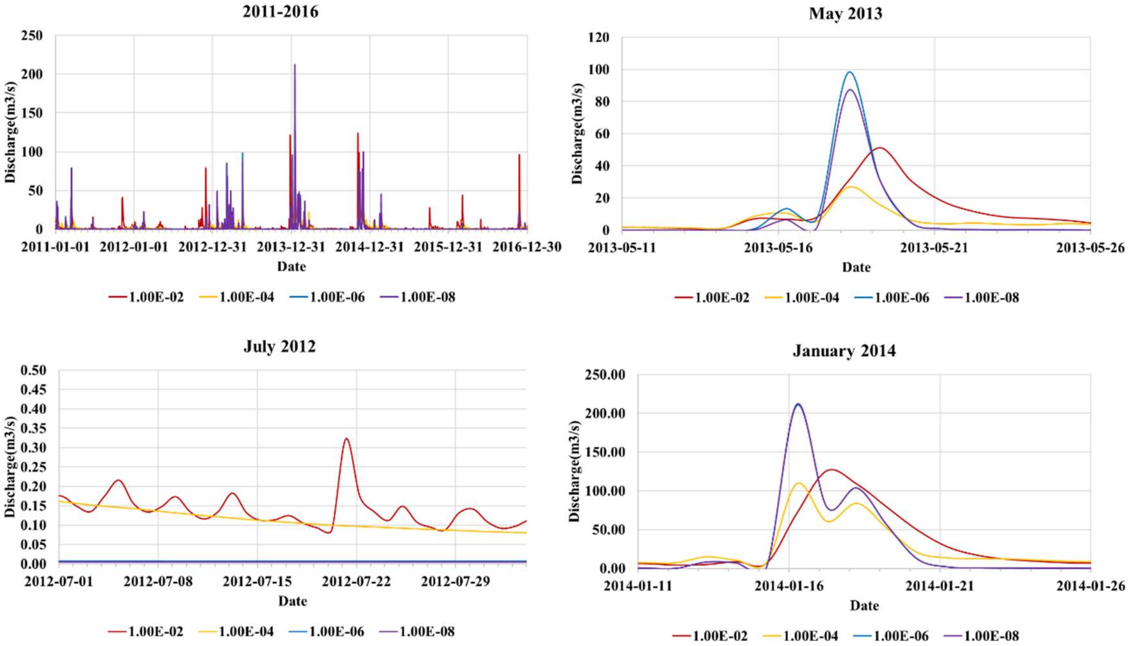

Figure 124 Sensitivity analysis of the model to horizontal hydraulic conductivity.

Moreover, the thickness of the saturated zone was expected to also have a strong influence on runoff. Even though the information on the geological layers span down to - 2000 m below sea level, only the first few meters of depth were tested. The baseline soil depth was presented in Figure 93. It is on average 1 m thick. In Figure 125, changes of the depth by multiplying the baseline by 0.4, 4, 16 and 64 resulted in significant variations in runoff hydrographs. These changes did not affect the timing of the peaks. However, increasing soil depth led to a decrease in discharge during the entire simulation period. In fact, since the reservoir is empty, it needs to fill up before generating runoff. For thickness of 1 m it seems like setting up the reservoir as empty does not have a major effect on runoff magnitude. For 16 and 64 times the reference depth, the discharge was decreased by more than 95 m^3/s and was near zero for most of the floods in the study period. For 0.5 and 4 times reference depth, the simulated discharge varied by less than 32 m^3/s.

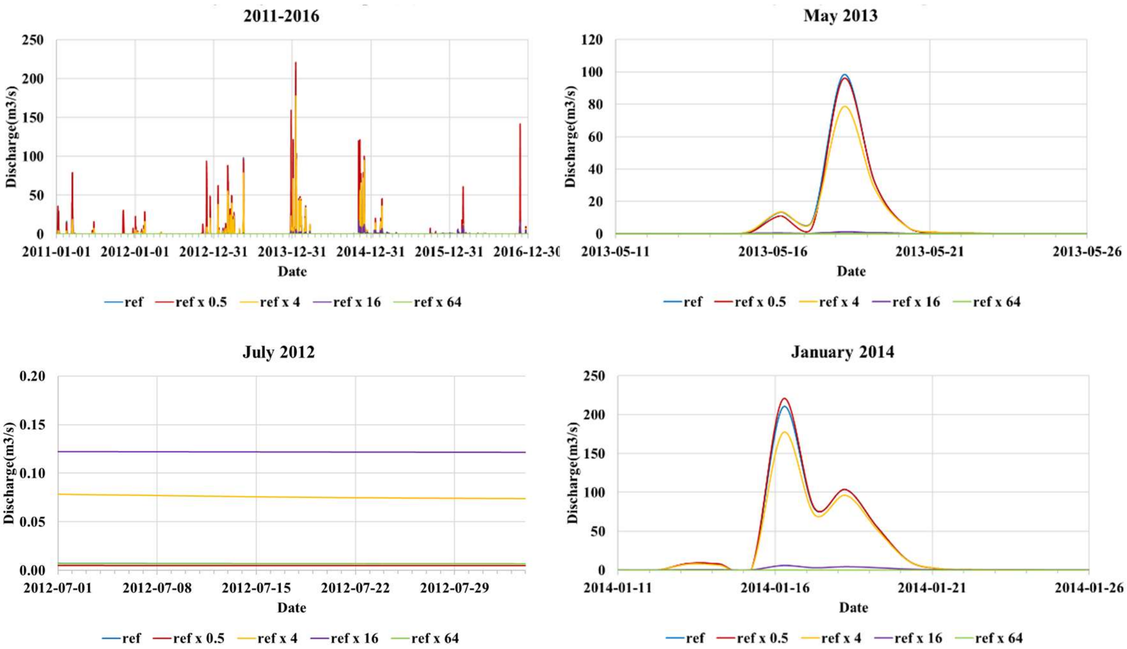

Figure 125 Sensitivity analysis of thickness of the saturated zone.

As opposed to the empty reservoir condition in previous testing, the following section considers two conditions where the reservoir is half full and completely full. It was expected that shallow and empty reservoir of 1 m thickness will not have an effect on runoff discharge. This was the case presented in Figure 126. In fact no change in discharge was observed. However, it is expected that with higher thickness the impact will be significant. Also with higher horizontal hydraulic conductivities the full reservoir may yield significant changes.

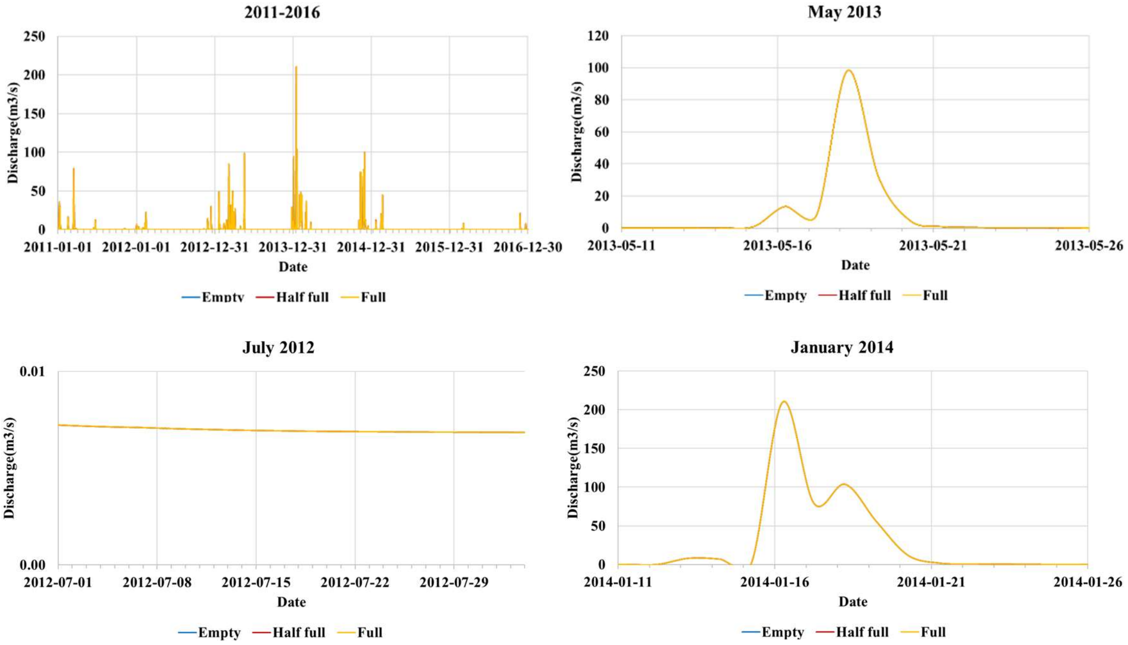

Figure 126 Sensitivity of the initial potential head from empty to full reservoir.

The last parameter to be assessed in the saturated zone is the number of layers defined. In fact, since the geology is composed of several geological layers, it is expected that runoff is influenced by reservoir beneath the soil layer. This condition is similar to having a single but deep reservoir. However, it allows to discretize hydraulic conductivities vertically based on the number of layers. To run simulations, each reservoir was assumed to be full. In the first case the upper layer has higher hydraulic conductivity than the lower layer (2 layers SZ top fast) with a ratio of 1.00E-06/1.00E-07. In the second case the situation was reversed (2 layers SZ bottom fast) with a ratio of 1.00E-06/1.00E-05.

Figure 127 highlights the impact of using two layers vs using a single layer. In the case where the lower layer has a hydraulic conductivity of 1.00E-07, a small change is observed in the spring peak discharge and summer low flow. The latter case showed a baseflow of 6 m^3/s and peak discharges near 20 m^3/s. A maximum decrease of 193.65 m^3/s was recorded for the winter flood. It was expected if the bottom layer is impermeable, no change will be observed. However, the degree of permeability of the layers underneath the soil layer is not well known in the Paillons. For example, the heterogenous marls layer may be completely impermeable (1.00E-09 m/s of hydraulic conductivity) or have some level of permeability (1.00E-05 m/s as the one used in the second case).

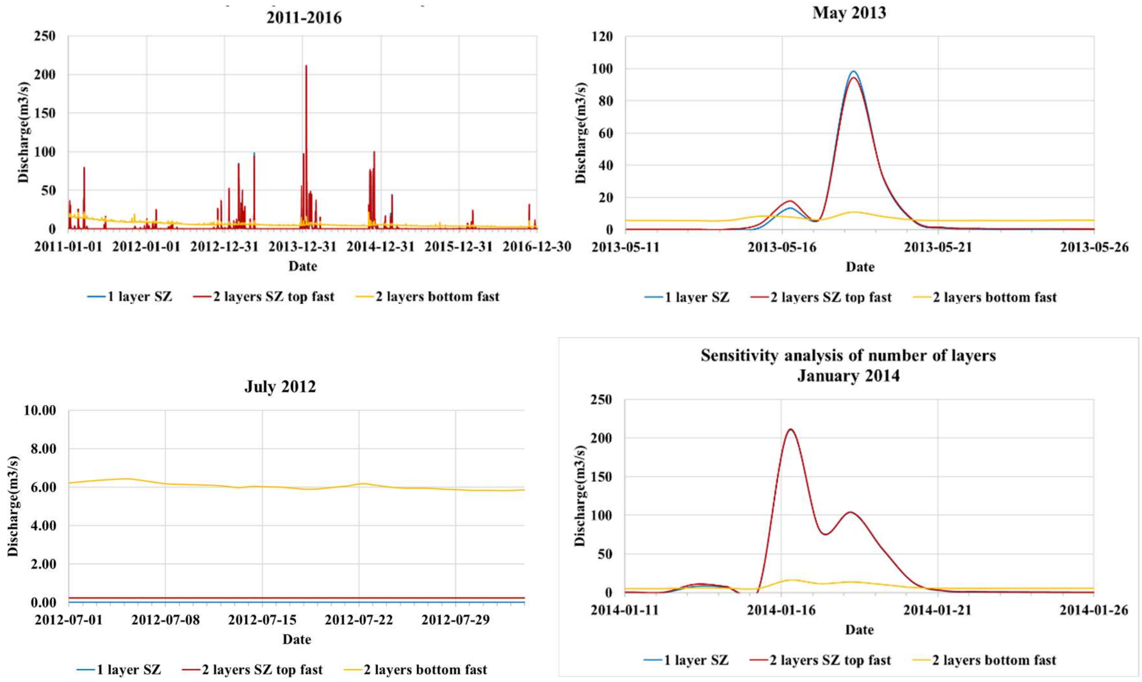

Figure 127 Sensitivity analysis of 2 layers used in the saturated zone.

In summary hydraulic conductivity, soil depth and the number of layers defined in the saturated zone have a major role in runoff simulations. The priority in the calibration will be given to varying the horizontal hydraulic conductivity, but if there are discrepancies in the simulated resulted further calibration should consider selecting higher thickness or combined layers for the saturated zone. Interestingly, in the Feflow model all the geological layers are presented. This is actually possible in MIKE SHE. However, the calibration process will require longer time for daily simulations and even greater time for hourly and 6-mn simulations.

5.1.8. Summary of sensitivity analysis

The summary of the parameter values and the resultant relationship between river flow and the alteration of tested parameters are displayed in Table 26, Table 27 and Table 28. As expected, the saturated zone plays a crucial influence on runoff calculations. It is followed by the Muskingum delay parameter and then by saturated hydraulic conductivities. The leakage coefficient was not expected to have a low impact on discharge. However, it is highly dependent on the available saturated zone storage.

Table 26 Summary of sensitivity analysis of MIKE SHE parameters

Functions	Parameters			Units	Δspring peak flow (m^3/s)	Δsummer low flow (m^3/s)	Δwinter peak flow (m^3/s)
Domain grid	Resolution	Grid resolution	100 (baseline)	m	-	-	-
			40		2.40	0.01	5.32
			55		-3.14	0.01	3.12
			80		-8.78	0.01	-10.86
Time Step Control	Max. precipitation depth per time step	$P_{Max\ depth}$	50 (baseline)	mm	-	-	-
			1		-1.83	0.00	-2.02
			100		-0.33	0.00	-0.19
	Max. infiltration amount per time step	$P_{Max\ infiltration}$	50 (baseline)	mm	-	-	-
			1		-1.22	0.00	-1.36
			100		-7.67	0.00	-0.57
	Input precipitation rate requiring its own time step	$P_{Input\ rate}$	5 (baseline)	mm/hour	-	-	-
			1		-0.15	0.00	0.00
			10		0.00	0.00	-0.07
Climate	Degree-day Coefficient	$C_{Degree\ day}$	4 (baseline)	mm/°C/day	-	-	-
			2		-0.01	0.00	-0.01
			8		0.01	0.00	-0.01
Rivers and Lakes	Bed resistance	S_{Bed}	20 (baseline)	m$^{(1/3)}$/s	-	-	-
			10		0.00	0.00	-0.02
			50		0.01	0.00	0.00
	Leakage coefficient	C_{Leak}	7.50E-05 (baseline)	/s	-	-	-
			1.00E-04		0.01	0.00	-0.01
			1.00E-06		0.00	0.00	0.00
	Muskingum delay parameter at every 500 m of a river branch	k_{Delay}	0 (baseline)	mn	-	-	-
			3		-19.15	0.00	-29.00
			30		-15.77	0.00	-32.05
			120		-62.65	0.00	-124.92

Table 27 Summary of sensitivity analysis of MIKE SHE parameters.

Functions	Parameters			Units	Δspring peak flow (m^3/s)	Δsummer low flow (m^3/s)	Δwinter peak flow (m^3/s)
Overland Flow	Manning-Strickler coefficient of Forest	S_{Forest}	4 (baseline)	$m^{(1/3)}/s$	-	-	-
			1		-9.54	0.00	-15.68
			50		3.97	0.00	6.42
	Manning-Strickler coefficient of Open spaces	$S_{Open\ spaces}$	10 (baseline)		-	-	-
			1		-7.86	0.00	-8.2
			15		-2.97	0.00	1.22
	Manning-Strickler coefficient of artificial areas	$S_{Artificial}$	25 (baseline)		-	-	-
			1		-7.81	0.00	-9.07
			50		-2.44	0.00	1.35
	Manning-Strickler coefficient of agricultural areas	$S_{Agricultural\ areas}$	20 (baseline)		-	-	-
			1		-4.02	0.00	-0.61
			25		0.20	0.00	0.09

Table 28 Summary of sensitivity analysis of MIKE SHE parameters.

Functions	Parameters			Units	Δspring peak flow (m^3/s)	Δsummer low flow (m^3/s)	Δwinter peak flow (m^3/s)
Unsaturated zone	Hydraulic conductivity of Silt loam	$K_{uz\ Silt\ loam}$	2.50E-05 (baseline)	m/s	-	-	-
			1.00E-04		0.41	0.00	0.00
			1.00E-05		-0.57	0.00	-0.43
			1.00E-06		-5.10	0.00	-1.08
	Hydraulic conductivity of Loam	$K_{uz\ Loam}$	4.00E-06 (baseline)		-	-	-
			5.00E-04		-0.22	0.00	-0.01
			1.00E-04		-6.25	0.00	-0.15
			1.00E-06		-4.42	0.00	-1.09
	Hydraulic conductivity of Clay loam	$K_{uz\ Clay\ loam}$	2.50E-06 (baseline)		-	-	-
			50E-05		-2.16	0.00	0.25
			1.00E-05		-2.11	0.00	-0.20
			1.00E-07		-3.76	0.00	-0.69
	Hydraulic conductivity of Urban impervious	$K_{uz\ urban\ impervious}$	1.00E-06 (baseline)		-	-	-
			1.00E-05		0.15	0.00	0.08
			1.00E-07		-0.4	0.00	-0.70
			1.00E-08		-3.31	0.00	-0.20
	ET surface depth	ET_{Depth}	0.1 (baseline)	m	-	-	-
			0.4		0.00	0.00	-24.00
			0.8		0.00	0.00	-24.00
			1.0		-2.93	0.00	-23.96
Saturated zone	Horizontal hydraulic conductivity	$K_{sz\ Horizontal}$	1.00E-06 (baseline)	m/s	-	-	-
			1.00E-02		-71.41	0.14	-83.89
			1.00E-04		-46.96	0.08	-100.68
			1.00E-08		-11.21	0.00	1.79
	Soil depth	Lowel level	distributed (baseline)	m	-	-	-
			-divided by 2		-2.31	0.00	10.248
			multiplied by 4		-19.66	0.07	-32.93
			multiplied by 16		-96.96	0.11	-206.71
			multiplied by 64		-98.12	0.00	-209.7
	Initial potential head	Initial head	Empty reservoir	m	-	-	-
			Half full		0.00	0.00	-0.03
			Full		-0.01	0.00	0.00
	Number of layers	N layers	1	-	-	-	-
			2: Kh 1E-06/1E-07		-3.98	0.23	1.06
			2: Kh 1E-06/1E-05		-87.36	6.17	-193.65

5.2. Calibration and Validation the hydrological model in MIKE SHE

The hydrological model was calibrated for daily, hourly and 6-mn simulations from 2011 to 2016 and validated from 2017 to 2019. The previously defined statistics of NSE, KGE, correlation r, RMSE, regression coefficient R^2, and Maximum absolute difference were used to evaluate model performance, in addition to trend lines fitting plots of observations versus simulations. The main criteria for calibration is to reproduce accurately all observed discharge hydrographs using these statistics and detail analysis of major floods during the evaluation period.

Due to large uncertainties in the definition of the saturated zone and its controlling effect on the catchment response, the calibration strategy involved two cases: a saturated zone defined by the soil depth of 1 m on average, which distribution is based on slopes; and deep saturated zone represented by a thickness above 1 m which was estimated during the calibration process. Both cases were expected to represent extreme catchment response due to the fact that for a saturated zone of 1 m most of the rainfall is forced to contribute to surface runoff while the opposite trend can be observed for the second case. For case 1, two sub cases were defined to explore model's behavior when model parameters such as saturated hydraulic conductivities and horizontal hydraulic conductivities converge toward the optimized parameter values defined in the AquaVar hydrological model and that defined in the hydrological study on the Paillons conducted by Le Gouz de Saint Seine (1995).

In addition the calibration strategy applied an optimization method based on the calibrated results from both cases. In fact, previous studies show that model performance may decrease from daily simulations to 6-mn simulations. Generally, daily rainfall gauges are strongly correlated while sub-daily gauges show a high degree of randomness. This affect the quality of rainfall mapping and as a consequence poor quality of simulations over a long period of time. Moreover, uncertainties in catchment description and observed runoff information exacerbate the issue. An obvious improvement method when several outputs of model simulations are available is the artificial neural Network approach (ANN). Instead of applying ANN on upstream observed records to obtain downstream information, model results can be used. The issue with stream gauge observations in the Paillons is the large gaps and uncertainties in measurements. Using modeling results which will always be available in real-time as long as rainfall information is inputted to the model ensures a robust way of maintaining and improving the knowledge of hydrological processes and extreme events in the Paillons.

ANN is relevant in situations where the feasibility of representing complex relationships among various facets of these processes through physical or conceptual modeling is extremely limited (Liong et al., 2000). The pattern mapping is the category applied in this study among other categories associated with ANN including pattern association, pattern classification, and pattern clustering. In this pattern, the particular type of ANN selected is the so-called multilayer perceptron or feedforward neural network. Several layers or neurons compose the structure of this network and are interconnected through weighted connections between the layers. Typically, there is an input layer that receives inputs from the environment, an output layer responsible for generating the network's response to its input, and one or more intermediate layers known as hidden layers. Each neuron computes a response from the weighted sum of its inputs and bias from connected neurons, using a predetermined activation function. The output of one neuron serves as the input for other neurons in the subsequent layer. According to Liong et al. (2000), while various activation functions exist, the sigmoid function is the most widely employed. Moreover, the training of a feedforward network involves employing the back-propagation method (Khan et al., 2023; Noori & Kalin, 2016). This training process entails adjusting the connection weights within the network to optimize the network's response to match the desired response. Though this task may be seen as an optimization challenge, back-propagation methods offer an efficient alternative by approximating a gradient descent approach. Specifically, at each configuration of connection weights, the network's error can be calculated by determining the difference between the desired and the actual responses determined by the network. The feedforward neural networks share affinities with statistical models, which adopt a data-driven approach. One of the primary strengths of ANNs lies in their capacity to recognize or accurately classify patterns that have not previously been presented to the network. The set up of the ANN model based on NeuroShell 2, a commercially available software, can be found in Appendix 8.

Noori & Kalin (2016) coupled Soil and Water Assessment Tool (SWAT) and ANN by using outputs from SWAT model as inputs into ANN model. First, they run SWAT to get baseflow and stormflow at day t. Next, ANN model uses baseflow and stormflow as inputs to predict streamflow on day t. The authors concluded that the coupling can improve river flow predictions at daily timesteps. Khan et al.

(2023) compared SWAT and ANN techniques for simulating streamflow based on historical records. The authors split their observed records into a training and testing phases. Then the network is trained by comparing modeled values to observed data with the objective of minimizing the network error. The inputs to ANN were precipitation and temperature. Their study found that if high flow values are absent in the training phase, ANN cannot capture extreme events in the testing phase.

In this thesis, the assumption is that the defined cases represents extreme conditions where all catchment characteristics are already represented. A combination of those cases will further improve the simulation of the shape of the hydrographs. In the calibration and validation phase ANN was applied only on observed times steps from 2011 to 2020. Periods with no observations were not computed. Future investigations could use this approach to reconstruct runoff time series from the start of rainfall records, and include periods with no measurements and for future forecasts.

5.2.1. Daily simulations

In this section, results of the daily calibrated discharges and validation analysis is presented. Daily simulations are required for water resource and extreme events assessments over long periods; the longest meteorological records are available in daily time steps since 1921. The step led to calibrate 3 versions of MIKE SHE model. The difference between Case 1a and Case 1b is that the saturated hydraulic conductivity of the soil types are in the order of 10^{-6} m/s in Case 1a and in the order of 10^{-3} m/s in Case 2b. In fact, Case 1a targets a behavior of the catchment similar to that of the MIKE SHE model of the Var catchment. However, a previous study in the Paillons suggested that saturated hydraulic conductivities of the shallow soil are in the order of 10^{-3} m/s (Le Gouz de Saint Seine, 1995). Therefore this study assumes to reach acceptable simulations results with both hypotheses. The situations in Case 1 were expected to yield high catchment response well-suited for the worst case scenarios that may be needed for extreme event management. The third hypothesis corresponding to Case 2 assumes that the catchment response is instead controlled by deep and low permeability saturated zone. Case 2 is expected to preserve proportionality between flood events over longer periods. If for example two events separated by several years, the earlier event is more intense than the latter event, the model should be able to capture that trend. The calibration process relied on manual changes of parameters and visual analysis of runoff hydrographs.

From 2011 to 2016, 10 flood events of magnitude between 10 and 120 m^3/s were selected. While the simulations was performed continuously for the entire period, performance statistics were calculated after selecting a set of events due to large gaps and errors in measurements data. Figure 128 shows the simulated hydrographs for Case 1a, case 1b and Case 2 along with the observed hydrographs. These three cases confirms that baseflow in the Paillons vary between few l/s to few m^3/s. In fact baseflow is near zero in drought periods as reported by field surveys in the area. Moreover, there are differences in peak discharges between the cases. Case 1a showed the highest peaks for most of the flood events because of its lower saturated hydraulic conductivity compared to Case 1b. Due to its deeper reservoir (average thickness of the saturated zone of 40 m), Case 2 showed underestimation of peak discharges and higher baseflows. For the flood peaks, it should be noted that the rainfall interpolation method may have a strong influence on some flood peaks where local stations had no record and only national (but out of the catchment boundaries) stations were used. The Paillons catchment functions like a valley surrounded by high elevations which is weakly affected by rainfall episodes recorded outside its limits such as the Alex storm.

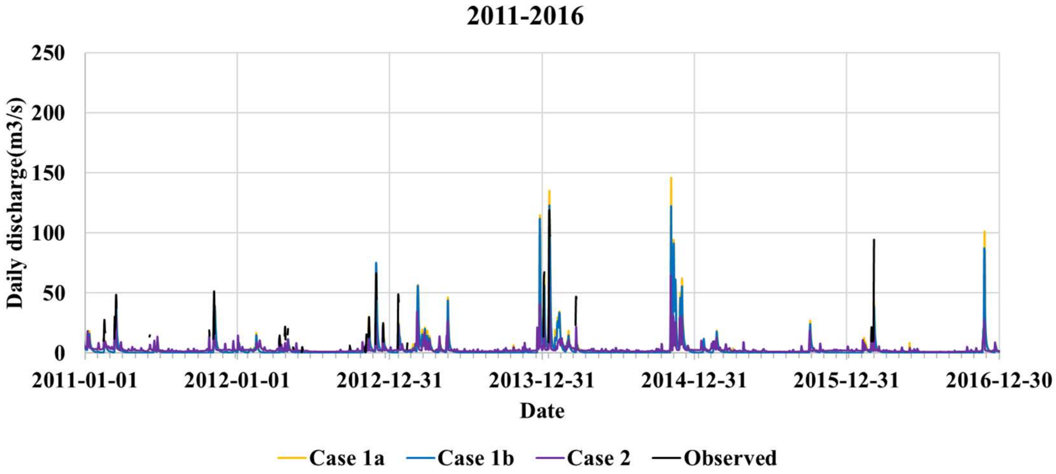

Figure 128 Daily calibration results with MIKE SHE at ABA station over the period 2011-2016.

The first goal of completing daily runoff information in the Paillons by filling the gaps in estimates is reached. The next step is to evaluate how well the models reproduced those hydrographs through statistical parameters. Additionally, the benefits of applying ANN to calibrated model outputs can be discussed. The number of days with selected records during the daily calibration phase was 71 out of the total number of days of record of 145. The regression analysis in Figure 129 showed similar values for Case 1a and case 1b (0.7707 and 0.7804 respectively). This implies that when the shallow reservoirs is set, changes in saturated hydraulic conductivity from 10^{-6} to 10^{-3} had little impact on $R^{2.}$.Case 2 performed worse with R^2 equaling 0.5835. To improve the model results ANN was applied to case 1b and case 2. In fact, R^2 of ANN at 0.9153 was significantly higher than that of the tested cases.

The improvement with ANN was obtained by using standard nets module in NeuroShell 2 with 1 hidden layer, 2 neurons, 0.1 as learning rate and momentum, and 0.3 as initial weights. The stop training criteria was set to 500 000 epochs on random pattern selection and momentum weights updates. The best training set was automatically saved.

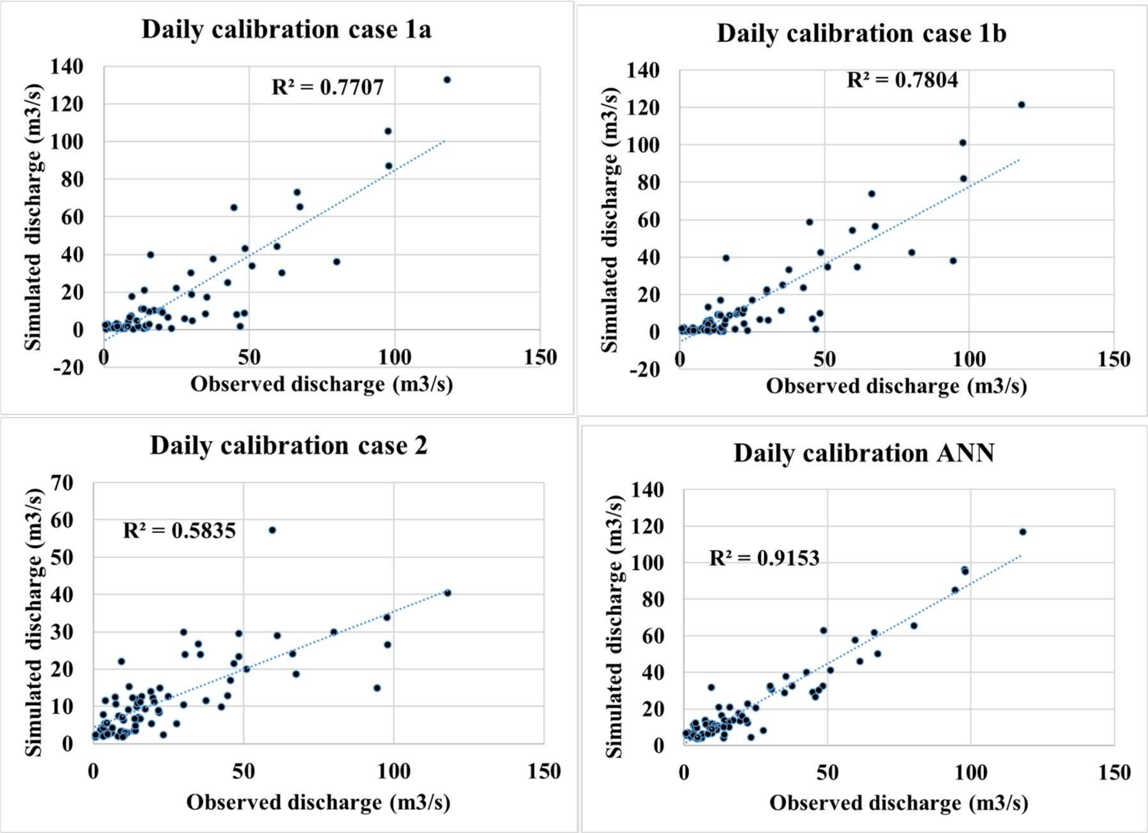

Figure 129 Regression analysis of the daily calibration results at ABA station.

Additional statistics were applied to further analyze the performance of the simulations (Table 29).

Table 29 Performance statistics of daily calibration in MIKE SHE at ABA station.

Daily simulations	**Calibration 2011-2016**			
Indicators	Case 1a	Case 1b	Case 2	ANN (case 1b,case 2)
NSE	0.64	0.67	0.26	0.90
KGE	0.64	0.62	0.21	0.87
R correlation	0.88	0.90	0.79	0.95
RMSE	15.04	14.37	21.55	8.00
R^2 regression	0.77	0.78	0.58	0.91
Maximum absolute difference	45.09	45.44	77.50	22.49

As a reminder, the performance criteria is set as NSE and KGE >0.5 and r > 0.75, for “Acceptable” results. Below these thresholds poor performance is considered. When NSE or KGE and R are above 0.65 and 0.85, respectively, the performance is “Good”. Above NSE or KGE = 0.85 and r = 0.95, the performance is “Excellent”. In the table above, R is more than 0.85 for all cases except case 2, for which its more than 0.75. The NSE and KGE show poor performance for case 2, “Acceptable” performance for Case 1a and 1b, and “Excellent” performance for ANN. Case 1b performs “Good” with its NSE 0.67. For RMSE, R^2 and Maximum absolute difference ANN shows the best performance and case 2 performed worst. As expected, all these statistics confirm the similarity between case 1a and Case 1b, where the catchment response is mostly controlled by the saturated zone description for values of saturated hydraulic conductivities ranging between 10^{-6} and 10^{-3} m/s. Compared to case 1a, case 1b takes the lead in performance. The low performance of case 2 is mostly due to its underestimation of stream discharge peak and volume. However, visual analysis of hydrographs shows that case 2 represents well the trend in peak discharges over the simulation period. Therefore, using Case 1b and case 2 as inputs to ANN, yielded “Good” or “Excellent” performance as expected. A close look in the hydrograph of the major flood event in the calibration period gives more insights into model performance (Figure 130). The peak discharge occurred on the 17th of January 2014. The rising of the hydrographs is perfectly reproduced by all cases. In addition, case 2 was good enough to simulate this flood. ANN provides a slight improvement compared to case 1b. Unfortunately, observed records beyond January 19th were not used because they were unrealistic and not supported by any rainfall event. In fact, large errors and uncertainties affected observed data during some flood events. According to previous reports, this flood is one of the few events that lasted several days, from the 15th to the 26th of January 2014, assuming the rest of the simulated hydrographs to be true. The shape of the hydrograph was supported by two consecutive rainfall episodes on the 15th and the 19th. Generally in the Paillons, hydrographs that span several days are caused by multiple and successive rainfall episodes around the peak time.

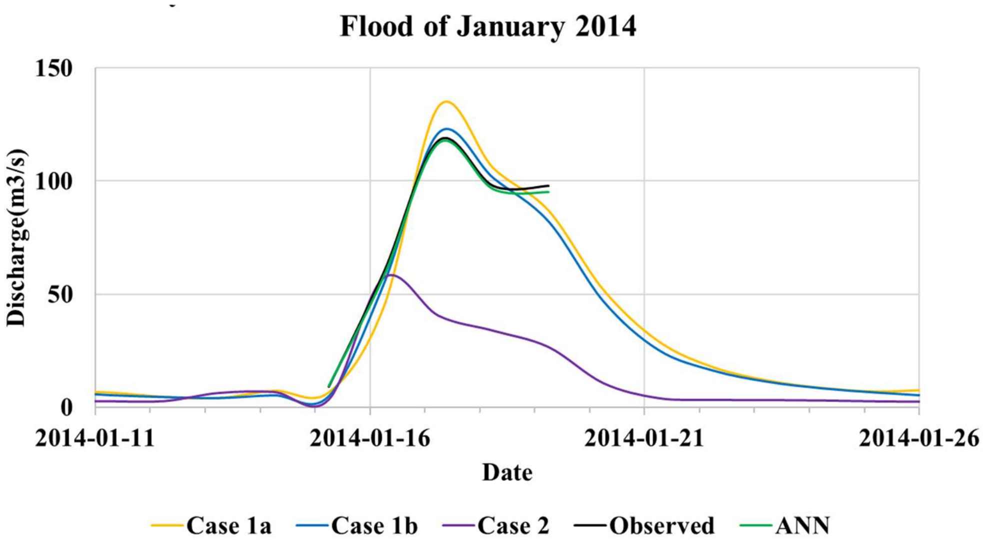

Figure 130 Evaluation of daily calibrated and observed hydrographs at ABA station for the flood of January 2014.

Following the calibration process, the model was validated in the period 2016-2020. The performance statistics of the validation process are presented in Table 30.

Table 30 Performance statistics of daily validation in MIKE SHE at ABA station.

Daily simulations	**Validation 2016-2020**			
Indicators	Case 1a	Case 1b	Case 2	ANN (case 1b,case 2)
NSE	-1.46	-3.16	0.29	0.83
KGE	0.01	-0.26	0.34	0.87
R correlation	0.56	0.06	0.78	0.92
RMSE	25.51	33.18	13.67	6.62
R^2 regression	0.31	0.34	0.60	0.84
Maximum absolute difference	119.31	140.79	79.58	27.74

R^2 is fairly above zero for Case 1a and case 1b. However, their NSE values are negative. The model in case 1 capture some variations of the real processes but not the mean. The case 2 exposed poor performance with NSE but its R^2 and R values were acceptable. Interestingly, ANN was able to improve simulations results by reaching NSE value of 0.83 and R^2 value of 0.84. This good performance of ANN is confirmed by the other statistics in the table. The analysis of the scatter plot in Figure 131 shows the improving trendline from the cases to ANN. This optimization approach is able to capture the runoff processes and produce reliable forecast for future extreme events.

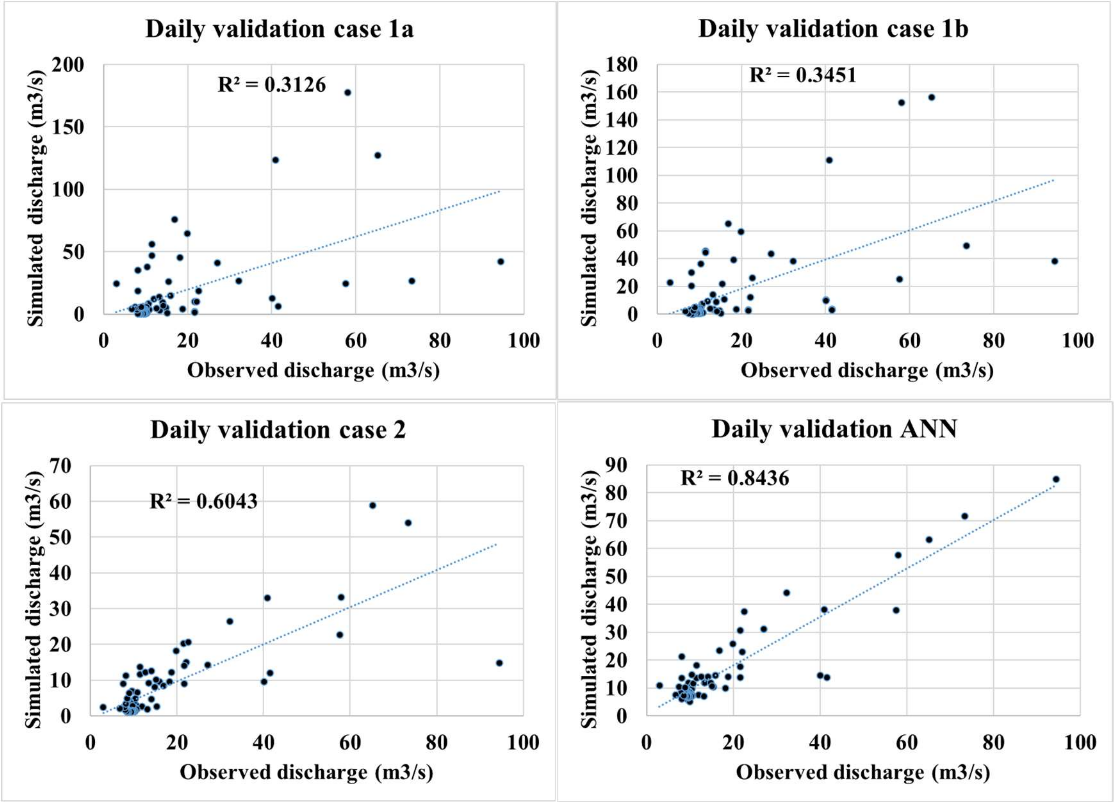

Figure 131 Regression analysis of the daily validation results at ABA station.

Plotting the simulated hydrograph with observation in Figure 132 & Figure 133 shows that overestimation of discharges in case 1a and 1b is source of poor performance. The case 2 and ANN in contrast are performing well. The consistency in good performance of ANN makes it a reliable tool for forecast based on deterministic modeling outputs. In periods where the deterministic models perform well, ANN preserves or improve the performance. In addition, wherever the deterministic models fail to reproduce the flood hydrograph, ANN greatly improve the results. The plots also validate the near zero base flow in the Paillons during dry periods.

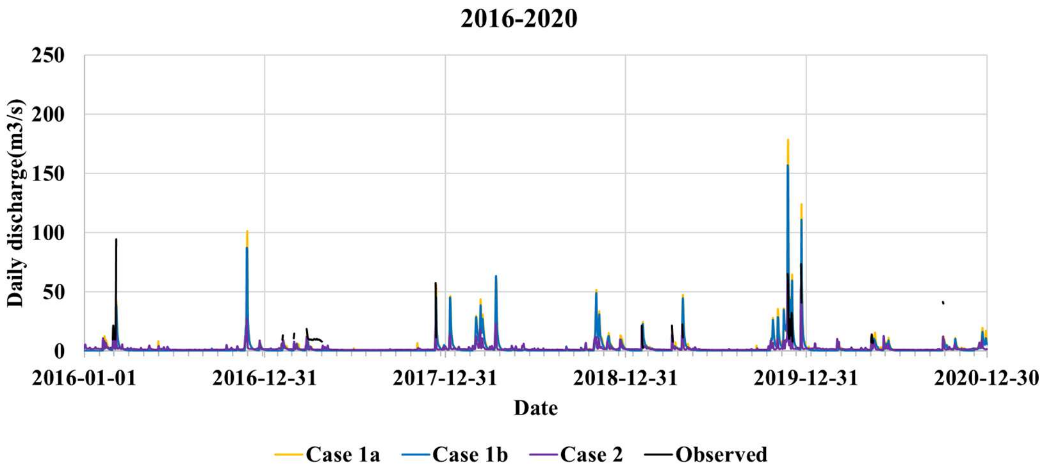

Figure 132 Daily validation results with MIKE SHE at ABA station over the period 2016-2020.

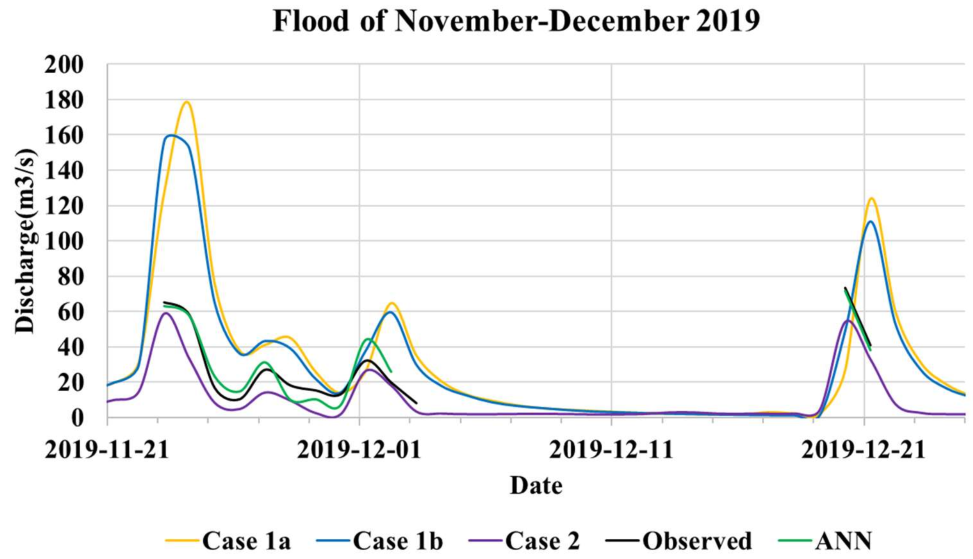

Figure 133 Evaluation of daily validated and observed hydrographs at ABA station for the flood of November-December 2019.

5.2.2. Hourly simulations

The performance statistics of hourly MIKE SHE calibration is presented in Table 31. It was expected that Case 1b and Case 2 perform poorly at hourly and 6-mn time scales due to the strong randomness in sub-daily rainfall information in addition to uncertainties in runoff records. However, the hourly Case 2 performed better than the daily Case 2 considering NSE and KGE. While NSE and KGE of Case 1b are "acceptable", the value for Case 2 is below the 0.5 threshold. Interestingly, their correlation coefficients were above 0.75, which is "acceptable". The hourly model is indeed able to capture variations better than the mean value. Applying ANN to these two cases resulted in improving NSE and KGE to above 0.65 threshold. The correlation coefficient R, the RMSE, the R^2 and the maximum absolute difference were also improved. In this calibration period, case 1b performed better than case 2. However the regression analysis plot (Figure 134) shows that case 2 fits observations better than case 1b at lower values and at higher values case 2 is oriented toward overestimation, which is more acceptable for extreme condition simulations. ANN in the plot shows a good fit with observations and confirms the improvement from the initial cases.

Table 31 Performance statistics of hourly calibration in MIKE SHE at ABA station.

Hourly simulations	**Calibration**		
Indicators	Case 1b	Case 2	ANN
NSE	0.57	0.43	0.82
KGE	0.63	0.40	0.78
R	0.82	0.77	0.91
RMSE	20.28	23.31	13.12
R^2	0.67	0.59	0.83
Maximum absolute difference	118.61	89.15	75.81

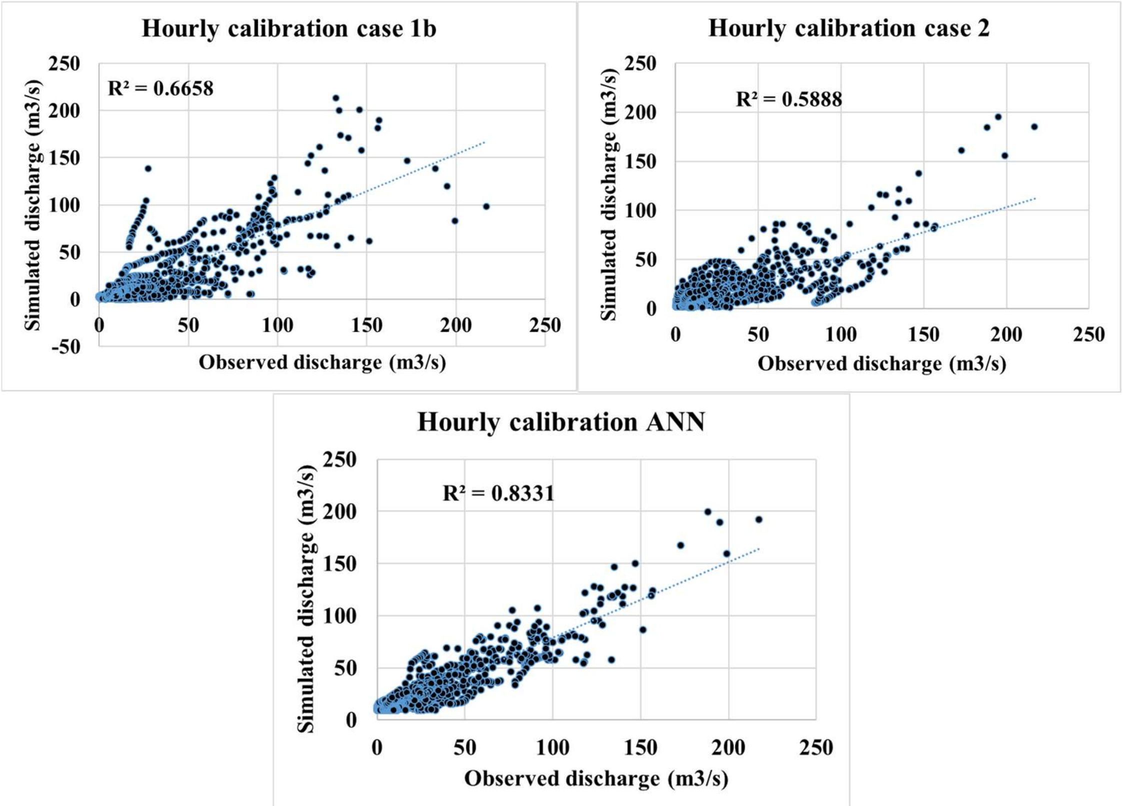

Figure 134 Regression analysis of the hourly calibration results at ABA station.

The hydrographs of simulated cases 1b and 2 from calibration were plotted with observations in Figure 135. Few observations are available, therefore these results serves as filling the gap in runoff time series at hourly time scales. Low baseflows and major peak discharges are well reproduced. This is clearly visible in the following figure focused on the flood of January 2014. Case 1b tends to generate higher values than case 2.

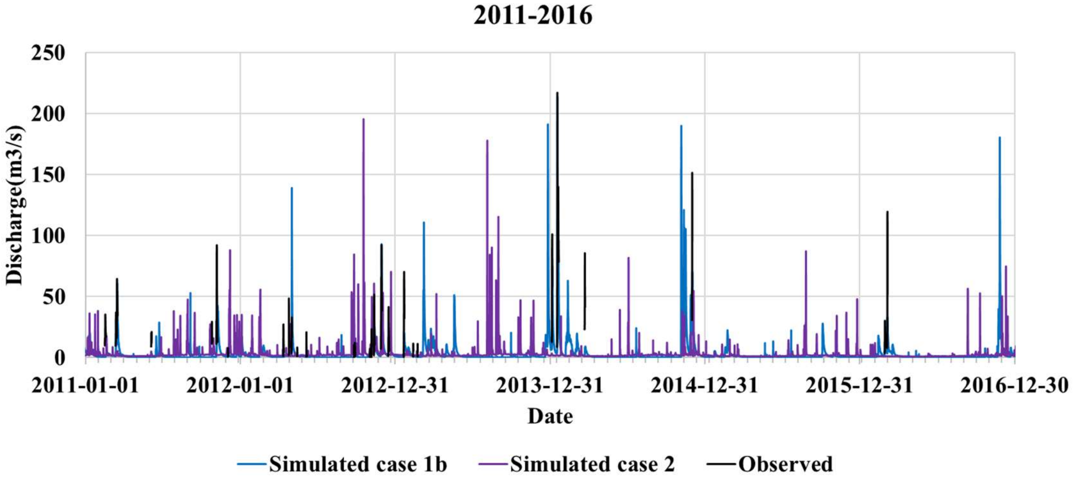

Figure 135 Hourly calibration results with MIKE SHE at ABA station over the period 2011-2016.

As shown in the Figure 136, Case 1b represents well the volume of the flood and Case 2 the peak discharge and time of peak. Both cases capture accurately the rising of the observed hydrograph. Optimizing the simulation results with ANN yielded a better representation of the flood hydrograph.

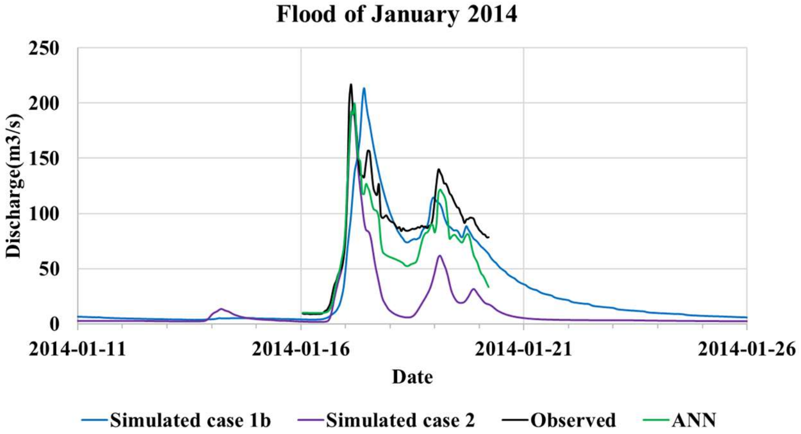

Figure 136 Evaluation of hourly calibrated and observed hydrographs at ABA station for the flood of January 2014.

With the calibrated parameters and continuing the simulations from the end of the calibration, the validation of hourly simulations was performed during the period 2016-2020. As presented in Table 32, Case 1b performed worst. Case 2 is better in hourly simulations than in daily simulations. Applying ANN was also beneficial for all statistics. However, the NSE and KGE values of hourly ANN are lower than that of daily ANN.

Table 32 Performance statistics of hourly validation in MIKE SHE at ABA station.

Hourly simulations	**Validation**		
Indicators	Case 1b	Case 2	ANN
NSE	-1.04	0.51	0.73
KGE	0.00	0.53	0.79
R	0.71	0.85	0.89
RMSE	26.20	12.80	9.54
Maximum absolute difference	208.60	85.55	69.55

The regression analysis of hourly simulations highlights the fact that Case 2 reproduce the variations better than Case 1b but slightly worse than ANN (Figure 137). In fact, R^2 value of Case 2 is very close to that of ANN.

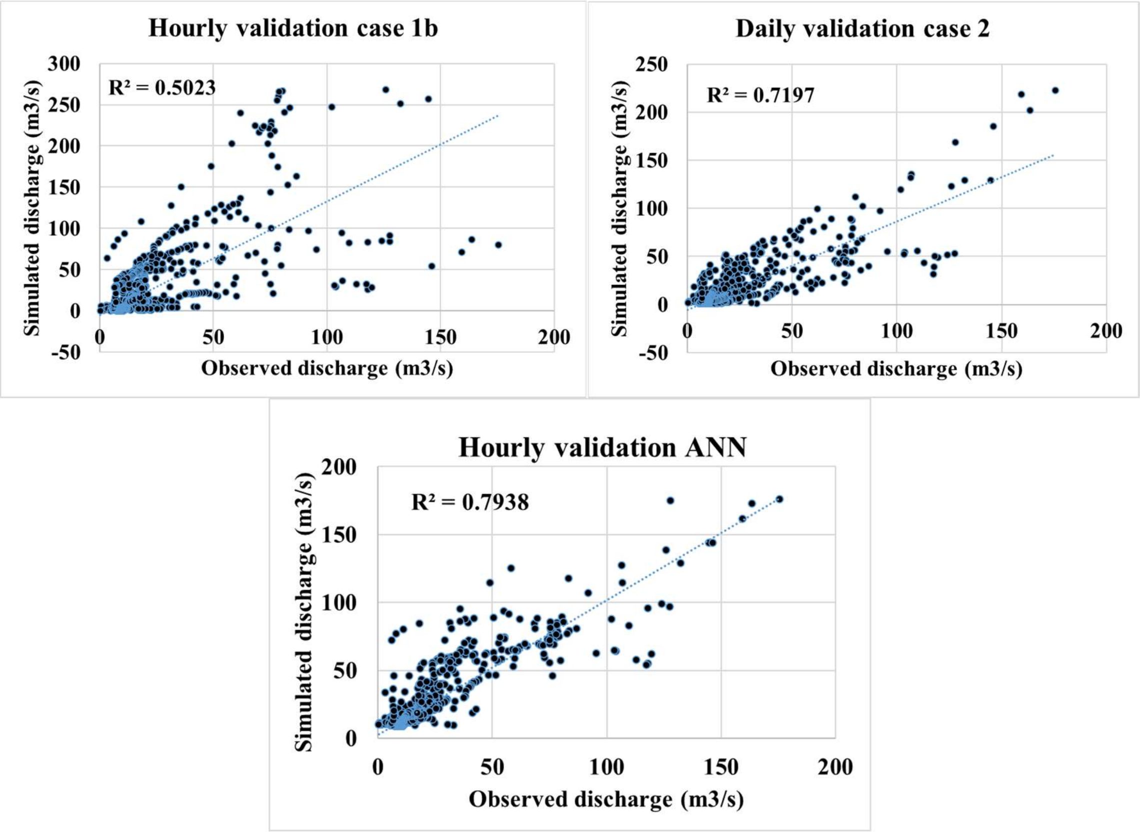

Figure 137 Regression analysis of the hourly validation results at ABA station.

Moreover, the resulting hydrographs of the hourly validation process were presented in Figure 138. In this case as well Case 1b simulate higher discharges than Case 2 and the observed. Both cases reproduced baseflow within the range of observed values. In the November-December 2019 flood period, Case 1b overestimated the first flood in November and underestimate the second flood in December. However, Case 2 captures the trend of the December flood being more intense than the November flood. This situation is more visible in Figure 139. All the flood events in this period were well reproduced by Case 2 and ANN. ANN again performed best.

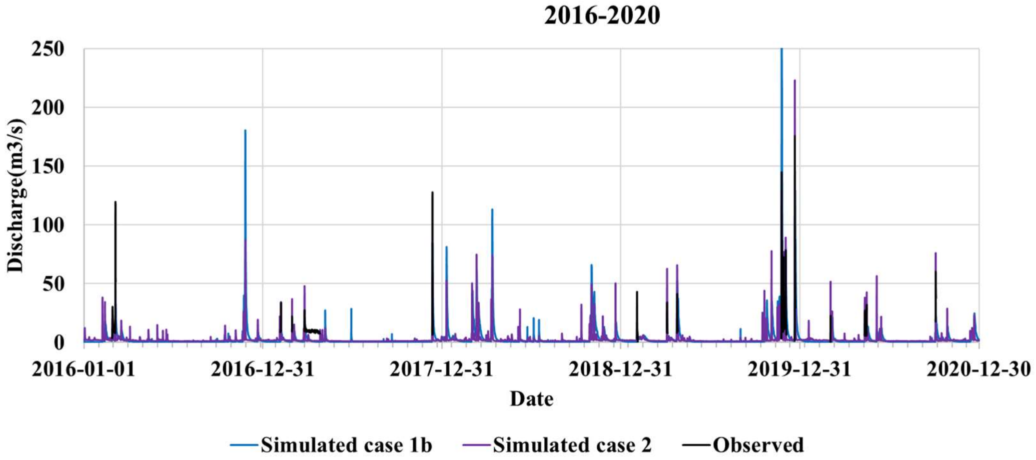

Figure 138 Hourly validation results with MIKE SHE at ABA station over the period 2016-2020.

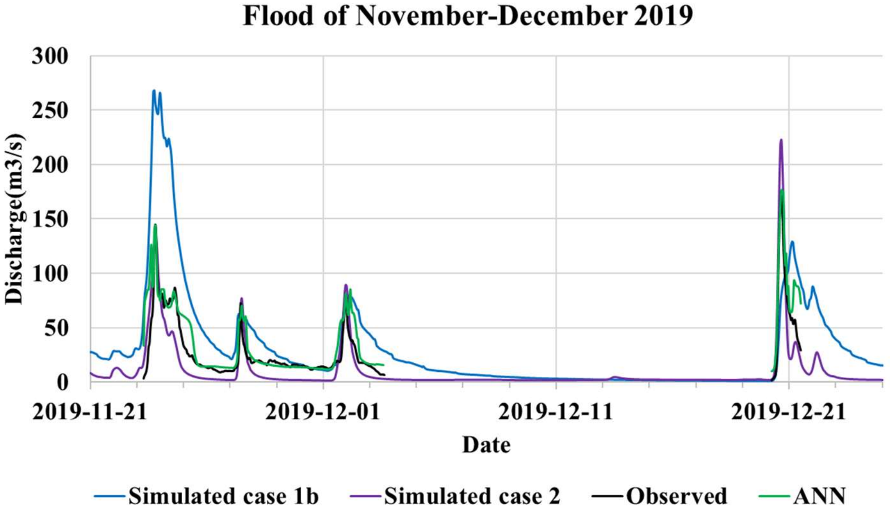

Figure 139 Evaluation of hourly validated and observed hydrographs at ABA station for the flood of November-December 2019.

5.2.3. 6-mn simulations

The 6-mn simulations exposed poor performance for case 1b and case 2, as expected (Table 33). However, case 2 at 6-mn simulations performed better than at daily and hourly simulations. This implies that using higher thickness and lower conductivities for the saturated zone is more advantageous for sub-daily simulations than daily simulations and vice versa for shallower thickness and higher hydraulic conductivities. Since daily or hourly processes are an aggregation of 6-mn processes, it was assumed that using the outputs from daily and hourly ANNs into a second application of ANN will further improve the statistics. Indeed, ANN 2 performed better than the ANN, which used only Case 1b and Case 2 as inputs.

Table 33 Performance statistics of 6-mn calibration in MIKE SHE at ABA station.

6-mn simulations	Calibration			
Indicators	Case 1b	Case 2	ANN (Case 1b+Case 2)	ANN 2 (Case1b+Case2 +ANN daily + ANN hourly)
NSE	-1.77	0.49	0.75	0.89
KGE	-0.08	0.48	0.76	0.89
R	0.44	0.77	0.87	0.94
RMSE	47.10	20.25	14.16	9.40
R^2	0.19	0.59	0.76	0.89
Maximum absolute difference	269.48	110.98	92.73	85.01

A regression analysis plot in Figure 140 shows that Case 2 captured the variations better than Case 1b. In addition Adding more variables into ANN improved the performance statistics.

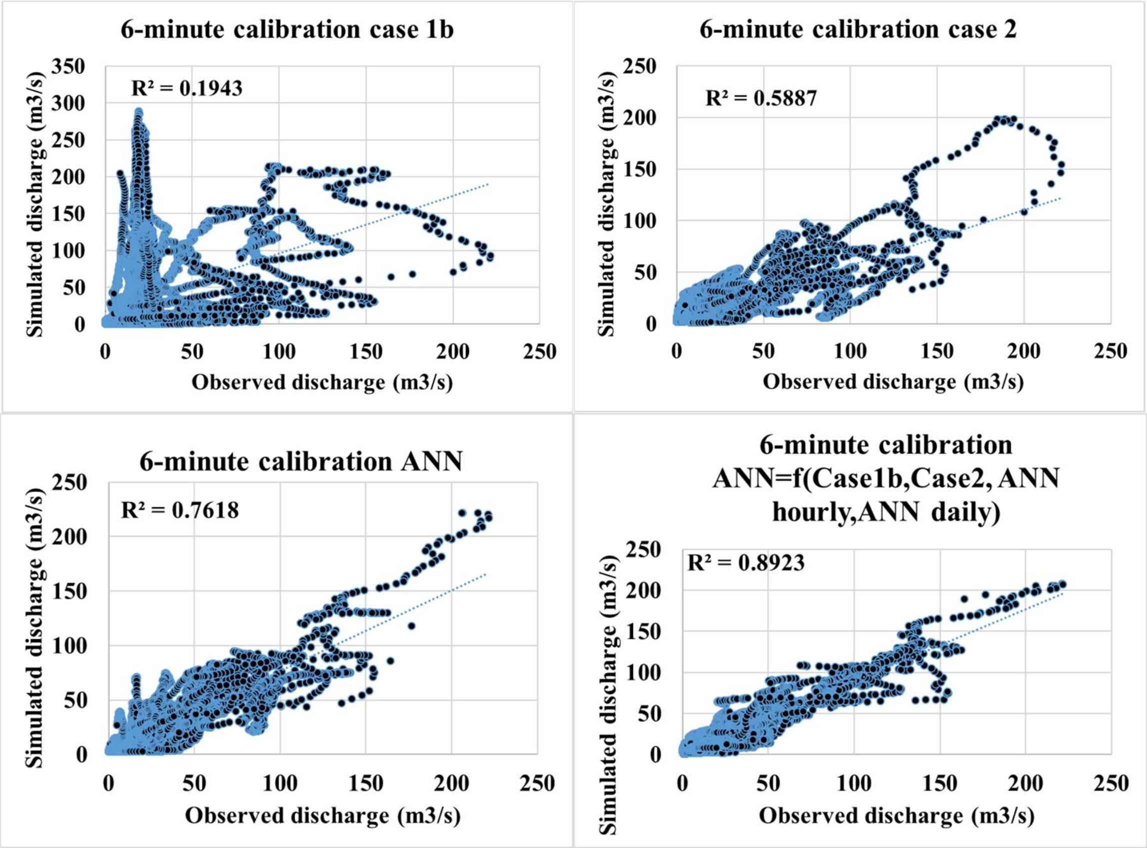

Figure 140 Regression analysis of the 6-mn calibration results at ABA station.

In Figure 141 below, the simulated hydrographs show unrealistic discharges of Case 1b in 2016, and higher peak discharge than observed during the entire calibration period. Case 2 instead represented well the observed hydrographs.

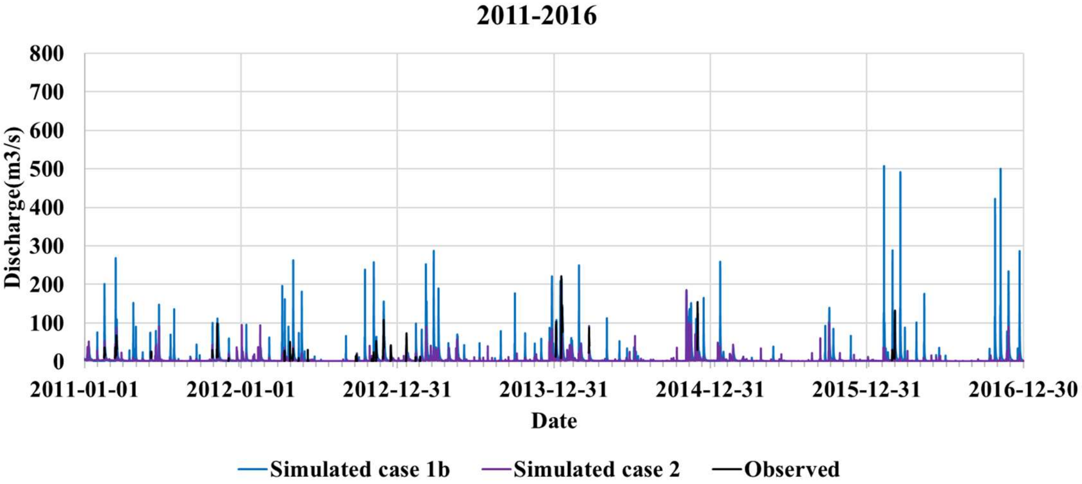

Figure 141 6-mn calibration results with MIKE SHE at ABA station over the period 2011-2016.

A zoom on the flood of January 2014 in Figure 142 highlights the fact that ANN 2 reproduced very well the flood hydrograph. Case 2 and ANN have similar shapes and Case 1b displays a later peak time and larger volume. Using a shallow reservoir with higher conductivities for 6-mn simulations convert most of the infiltrated rainfall to runoff.

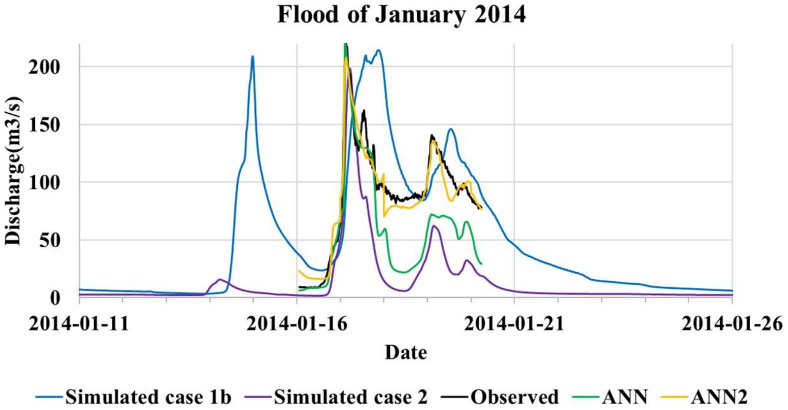

Figure 142 Evaluation of 6-mn calibrated and observed hydrographs at ABA station for the flood of January 2014.

Similar to the other time scales, a validation of 6-mn simulations was performed in 2016-2020. Table 34 presents the performance statistics. Poor performance of Case 1b and Case 2 was observed. ANN (Case 1b+ case 2) did not yield better results either. However, the R^2 of ANN was acceptable. The ANN2 performed well with NSE of 0.67 and KGE of 0.75. It can be noted that the R^2 is similar for the ANNs. The lowest maximum absolute difference was obtained with ANN2. Moreover, the regression analysis in Figure 143 exposes the bad representation of variations at higher values. The variations in lower values are on the other hand well represented in Case 2 and ANNS.

Table 34 Performance statistics of 6-mn validation in MIKE SHE at ABA station.

6-mn simulations	**Validation**			
Indicators	Case 1b	Case 2	ANN (Case 1b+Case 2)	ANN 2 (Case1b+Case2 +ANN daily + ANN hourly)
NSE	-4.02	0.49	0.44	0.67
KGE	-0.71	0.54	0.51	0.75
R	0.54	0.85	0.89	0.87
RMSE	40.72	12.96	13.61	10.45
R^2	0.28	0.72	0.79	0.79
Maximum absolute difference	269.48	83.55	134.93	93.24

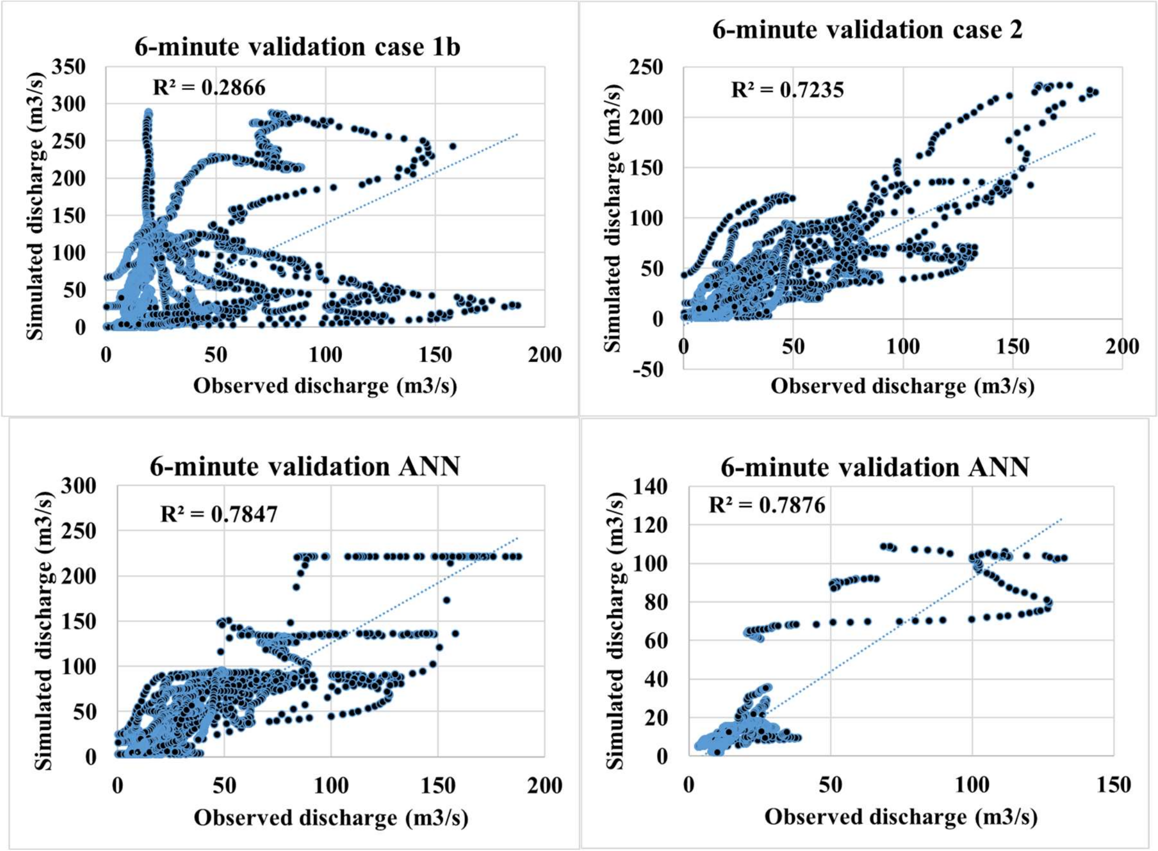

Figure 143 Regression analysis of the 6-mn validation results at ABA station.

Following the performance statistics, the validation hydrographs are presented in Figure 144. Besides the year 2016 where Case 1b reproduce unrealistic behavior probably due to instabilities, all the other parts fall within the range of observed values. The flood of November-December 2019 presented in Figure 145 shows that Case 1b overestimated the discharge. The Case 2 and ANN are in good agreement with the observed values. While ANN2 have good statistics, it does not represent the magnitude of the peak on November 23rd. It underestimated this important flood by almost 100 m^3/s. The remaining flood episodes were well captured by ANN 2.

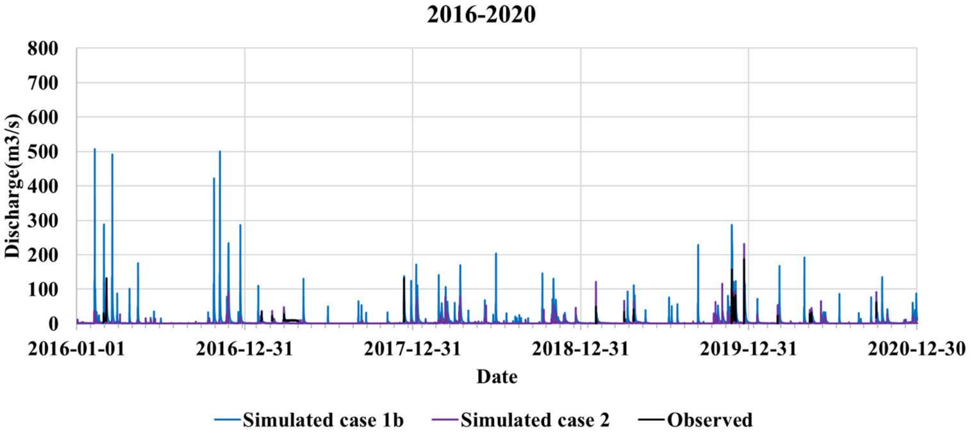

Figure 144 6-mn validation results with MIKE SHE at ABA station over the period 2016-2020.

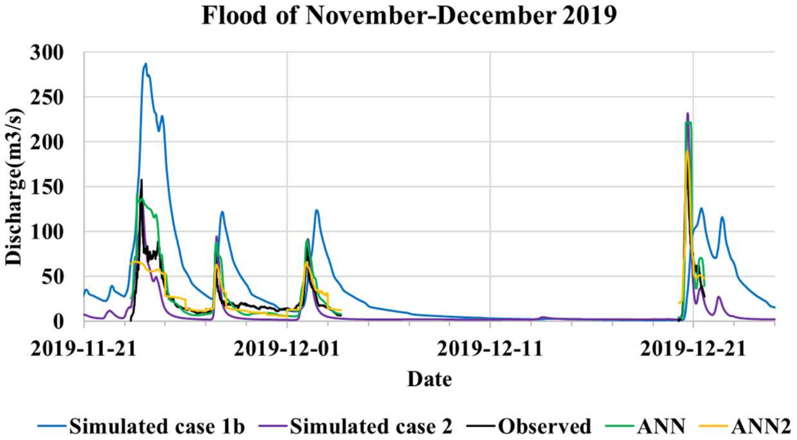

Figure 145 Evaluation of 6-mn validation and observed hydrographs at ABA station for the flood of November-December 2019.

5.2.4. Summary of optimized parameters

The calibrated parameters are summarized in Table 35 and Table 36. Differences are noticeable for hydraulic conductivities, delay parameter, thickness of the saturated zone, initial potential head and neural network parameters.

Table 35 Summary of optimized parameters in MIKE SHE simulations (part A).

Functions	**Parameters**			**Units**	**Daily calibration**					**Hourly calibration**		**6-mn calibration**		
					Case 1a	Case 1b	Case 2	ANN	Case 1b	Case 2	ANN	Case 1b	Case 2	ANN
Domain grid	Resolution	$Grid_{\text{resolution}}$		m	100			-	100		-	100		-
Time Step Control	Max precipitation depth per time step	$P_{\text{Max depth}}$		mm	50				50			50		
	Max infiltration amount per time step	$P_{\text{Max infiltration}}$		mm	50				50			50		
	Input precipitation rate requiring its own time step	$P_{\text{Input rate}}$		mm/h	5				5			5		
Climate	Degree-day Coefficient	$C_{\text{Degree day}}$	Flat	mm/°C/d	4				4			4		
			Northwards		2				2			2		
			Southwards		4				4			4		
Rivers and Lakes	Bed resistance	S_{Bed}		$m^{(1/3)}/s$	20				20			20		
	Leakage coefficient	C_{Leak}		/s	7.50E-05				7.50E-05			7.50E-05		
	Muskingum delay parameter at every 500 m of a river branch	k_{Delay}		mn	0		6		0	6		6	6	
Overland Flow	Manning-Strickler coefficient	S_{Forest}		$m^{(1/3)}/s$	4				4			4		
		S_{Grass}			5				5			5		
		$S_{\text{Open spaces}}$			10				10			10		
		$S_{\text{Artificial}}$			25				25			25		
		$S_{\text{Agricultural areas}}$			20				20			20		

Table 36 Summary of optimized parameters in MIKE SHE simulations (part B).

Functions	Parameters			Units	Daily calibrated value				Hourly calibrated value			6-mn calibrated value		
					Case 1a	Case 1b	Case 2	ANN	Case 1b	Case 2	ANN	Case 1b	Case 2	ANN ANN2
Unsaturated zone	Silt loam		Water content at saturation	-	0.51			-	0.51			0.51		
			Water content at field capacity	-	0.31				0.31			0.31		
			Water content at wilting point	-	0.11				0.11			0.11		
			Saturated hydraulic conductivity	m/s	2.5 x10^{-5}	0.0025	2.5 x10^{-5}		0.005	2.5 x10^{-5}		5 x10^{-5}	2.5 x10^{-5}	
	Loam		Water content at saturation	-	0.48				0.48			0.48		
			Water content at field capacity	-	0.28				0.28			0.28		
			Water content at wilting point	-	0.14				0.14			0.14		
			Saturated hydraulic conductivity	m/s	4 x10^{-6}	0.004	4 x10^{-6}		0.004	4 x10^{-6}		4 x10^{-5}	4 x10^{-6}	
	Clay loam		Water content at saturation	-	0.56				0.56			0.56		
			Water content at field capacity	-	0.36				0.36			0.36		
			Water content at wilting point	-	0.22				0.22			0.22		
			Saturated hydraulic conductivity	m/s	2.5 x10^{-6}	0.005	2.5 x10^{-6}		0.0025	2.5 x10^{-6}		2.5 x10^{-5}	2.5 x10^{-6}	
	Sandy loam		Water content at saturation	-	0.38				0.38			0.38		
			Water content at field capacity	-	0.18				0.18			0.18		
			Water content at wilting point	-	0.08				0.08			0.08		
			Saturated hydraulic conductivity	m/s	0.001	0.006	0.001		0.006	0.001		0.006	0.001	
	Urban impervious		Water content at saturation	-	0.58				0.58			0.58		
			Water content at field capacity	-	0.38				0.38			0.38		
			Water content at wilting point	-	0.24				0.24			0.24		
			Saturated hydraulic conductivity	m/s	10^{-6}	0.001	10^{-6}		0.001	10^{-6}		0.001	10^{-6}	
	ET surface depth		ET $_{depth}$	m	0.1				0.1			0.1		
Saturated zone	Horizontal hydraulic conductivity		$K_{sz\ Horizontal}$	m/s	1 x10^{-6}	8.5 x10^{-3}	1 x10^{-6}		8.5 x10^{-3}	1 x10^{-6}		8.5 x10^{-3}	1 x10^{-6}	
	Vertical hydraulic conductivity		$K_{sz\ vertical}$	m/s	1x10^{-7}	8.5x10^{-4}	1x10^{-7}		8.5x10^{-4}	1x10^{-7}		8.5x10^{-4}	1x10^{-7}	
	Specific yield		Sy	-	0.2				0.2			0.2		
	Thickness of saturated zone	Response Surface slope (°)	0-10	m	-2		-4		-2	-4		-2	-4	
			10-40		-1		-40		-1	-40		-1	-40	
			40-90		0				0			0		
	Initial potential head		Initial head	m	empty		full		empty	full		empty	full	
	Number of layers		N_{Layer}	-	1				1			1		
Neural Network	Number of hidden layers		$N_{Hidden\ Layers}$		-			1	-		1	-		3
	Number of epochs		N_{epochs}					5x10^{+5}			5x10^{+5}			2500

5.2.5. Uncertainty analysis of MIKE SHE simulations in the Paillons catchment

The calibration and validation process have shown that the modeling strategy can generally well represent hydrological processes in the Paillons catchment. In addition, using ANN highly improved the results. This evaluation will not be complete if results at other stream gauges were not analyzed. Thus, the flood of December 2019 was selected for this purpose. It was previously mentioned that gaps and errors exist in the monitoring data. The model is best evaluated by selecting a set of events. In Figure 146, simulated and observed hydrographs are presented at 5 stations. In this case ANN is not yet applied. The figure shows results from Case 1b and Case 2. As expected, Case 2 reproduced well this flood at all locations. However, an overestimation of the peak discharge is observed at TRI and LAC stations. At CON station, an underestimation is observed, instead. Unfortunately, Case 1b performed badly at all locations for this flood.

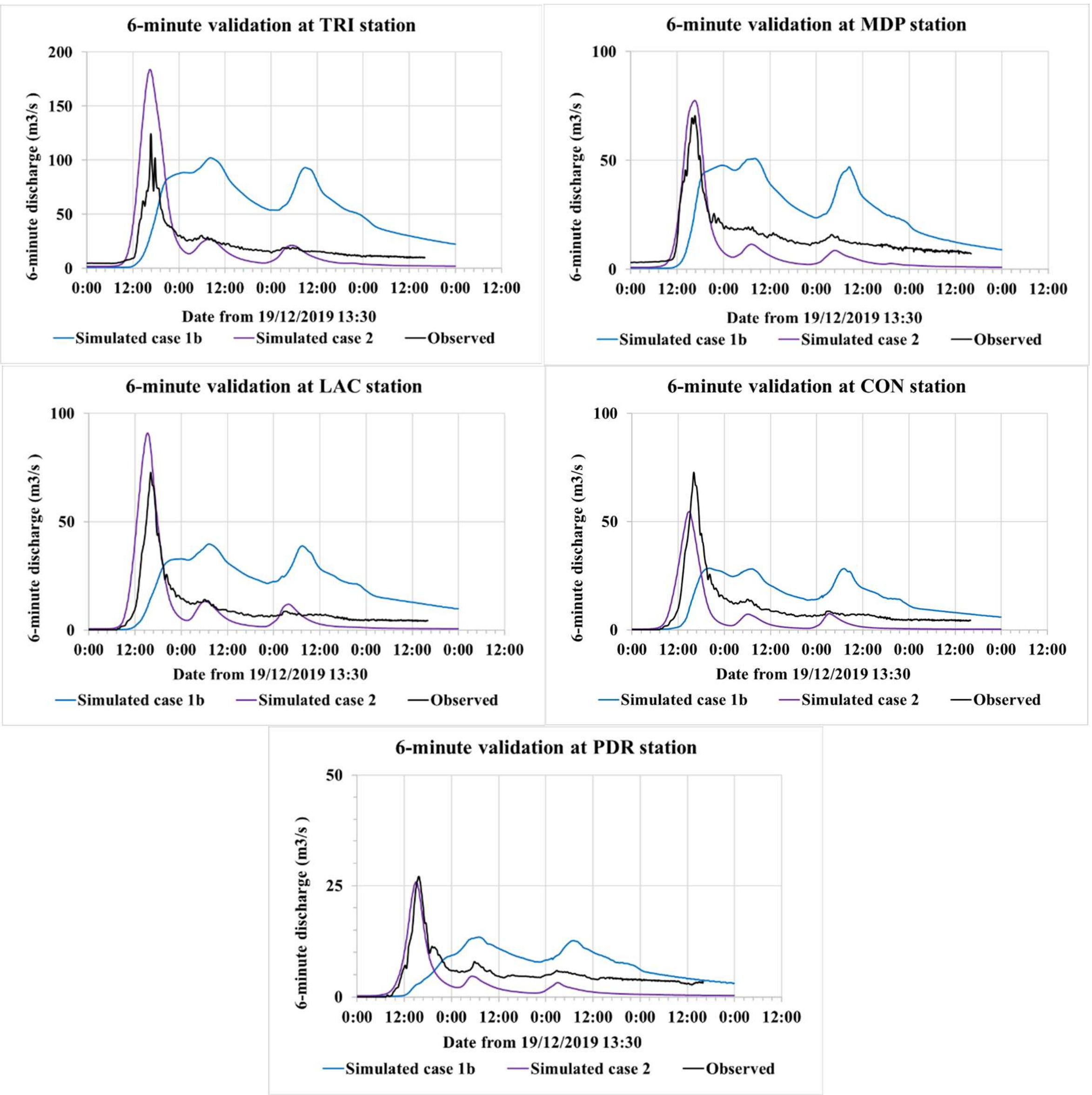

6-minute validation at TRI station

6-minute validation at MDP station

6-minute validation at LAC station

6-minute validation at CON station

6-minute validation at PDR station

Figure 146 Evaluation of 6-mn validation and observed hydrographs at 5 upstream stations for the flood of December 2019.

Consequently, it will be useful to apply ANN at other stations using the outputs from deterministic model simulations to improve the results. However, the observed hydrographs are not free of errors and uncertainties. In fact, previous studies on the Paillons highlighted the fact that discharge estimation among stations within the study area are not in good agreement. These studies suggested updating the rating curves for upstream stations. In addition, data analysis showed that errors and uncertainties propagate through water depths measurements as well.

Additional uncertainties comes from model limitations. In fact, setting up the hydrological model with only one layer in saturated zone is an oversimplification of reality. The Paillons geological is composed of several layers. Some of the layers such as the karst systems and the alluvial zone are known to interacts and absorb an important fraction of infiltration. Using shallower saturated zone led to overestimations of flow discharge because deep seepage is not considered. It can be noted that moving from 1 m to 40 m thickness, the simulated discharges after the flood peak discharge decreased. In fact, for shallower thickness, the soil remains saturated for a long time, yielding higher discharges after the peak time. But the sensitivity analysis showed that lower horizontal hydraulic conductivities reduced that trend along with not reproducing some of the flood events. In short, it will be useful to build and evaluate an integrated hydrological model with all the geological layers defined in Feflow. However, this may cause longer computation time especially during the calibration process. Finding the right balance between model details and the objectives of real-time management of flow processes is challenging.

Moreover, there are uncertainties in rainfall distribution which affects runoff calculations. The use of IDW to map the rainfall may have caused an allocation of intense rainfall over large areas. This accumulation of high volume of water can be the cause of sudden raises in simulated hydrographs seen in the 6-mn simulations. At times when the local stations are missing, the use of national gauges outside the catchment area may be capturing rainfall episodes that are not happening effectively in the Paillons with the same intensity. Finding ways to improve the quality of the local stations is needed.

The use of ANN is a way to absorb uncertainties in input data and catchment description. It is assumed that if ANN can help improve the statistical indicators, this implies that ANN was able to reduce uncertainties by better mimicking the trend in the observed data than each individual deterministic model did. The alternative will be costly field surveys and gauge upgrading to collect more accurate information for hydrogeological modeling. Unfortunately, the model can not solve uncertainties in stream discharges measurements. The image-based assessment of discharge using the available video records will be a useful approach to ensure the robustness of stream gauges measurements whenever possible.

5.3. Sensitivity analysis in Feflow

Due to the lack of long-term monitoring data in the evaluation period, the Feflow model was assessed through sensitivity analysis. Then a comparison of the model's behavior with historical average of 1954-1974 at 4 locations, and 3 points of measurements in October 2010 in groundwater flow in the Paillons catchment was performed. Four parameters were used to assess the flow dynamics: In-transfer rate, Out-transfer rate, specific yield and hydraulic conductivity. Few groundwater extraction points in the alluvial aquifer still exist downstream in the Paillons. They were not included in the assessment.

5.3.1. Recharge, water depths, assessment locations and parameters

The computed total recharge from MIKE SHE was used in Feflow. On average, the recharge varies between 0 and 45 mm/day (Figure 147). MIKE SHE provides a distributed recharge as presented in Figure 148. In this example, the recharge is on average 40 times higher during the selected flood period than during the drought period, which is characterized by high evapotranspiration. The recharge map of the flood period shows two main areas, which are caused by the rainfall distribution on that day.

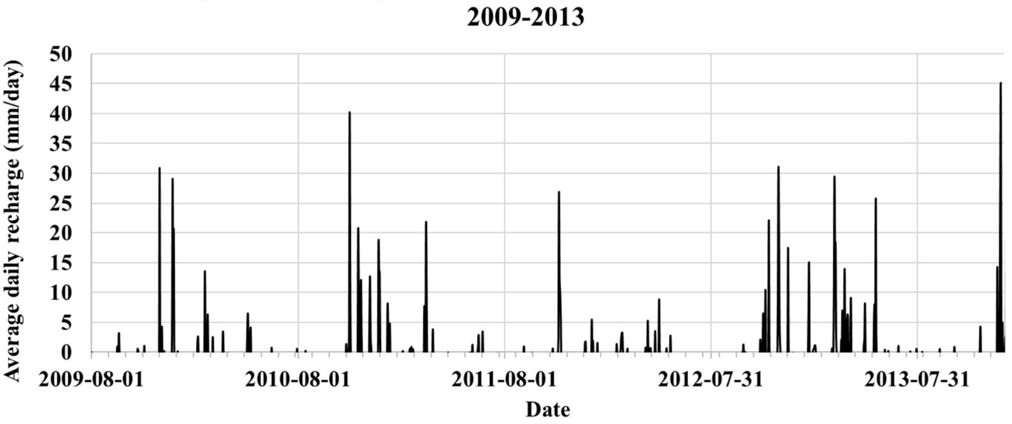

Figure 147 Average estimated recharge from MIKE SHE over the study area.

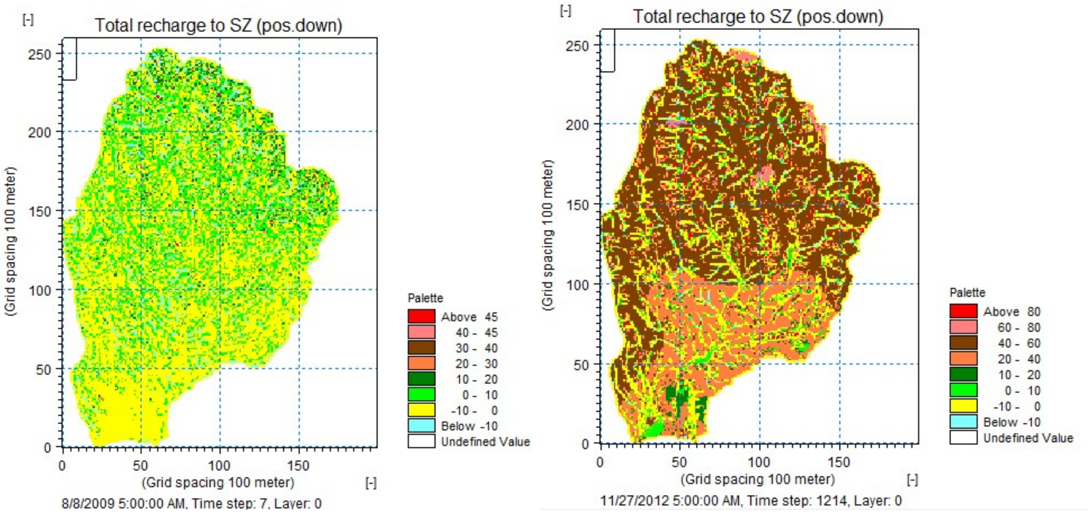

Figure 148 Distribution of estimated recharge (mm/day) from MIKE SHE in drought period (left) and flood period (right).

To account for river-aquifer exchange, the water levels from MIKE SHE coupled with MIKE1D were extracted at 34 points along the streamline and applied to Feflow. Figure 149 show the locations of the extraction points and 4 hydrographs between 2009 and 2013. In Feflow the data is assigned with the Fluid-transfer boundary condition as shown in Figure 150.

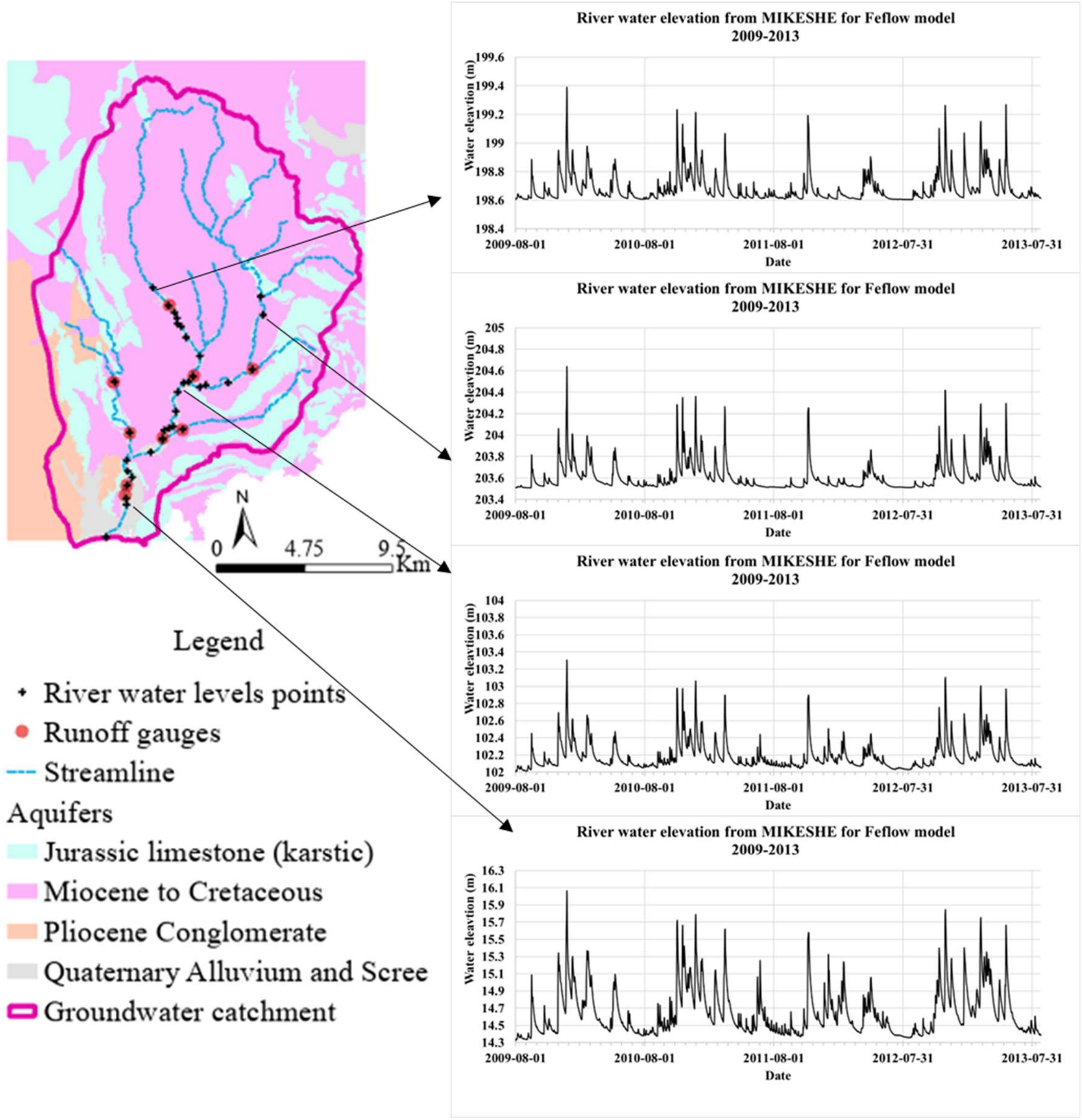

Figure 149 Locations (34 points) of water level extraction from MIKE1D in MIKE SHE for Feflow.

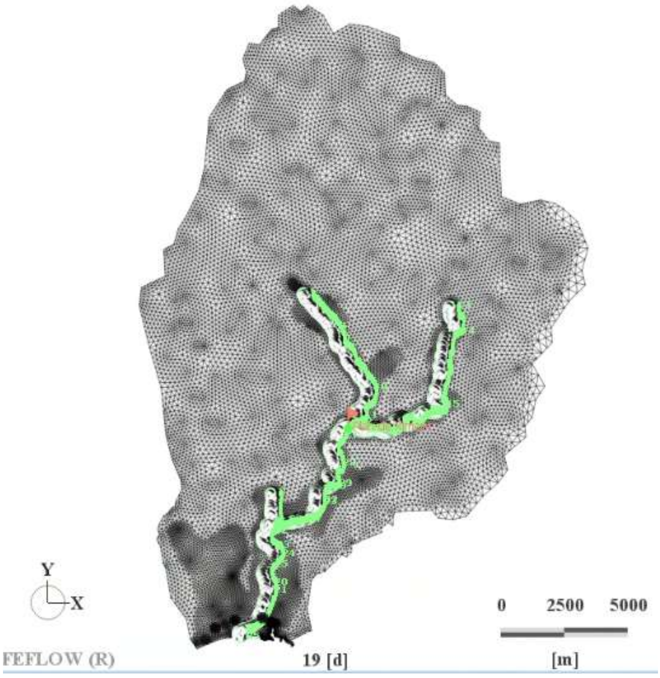

Figure 150 Transfer boundary condition assigned in Feflow model.

The evaluation of points includes: Plant de Rimont, Acropolis, Port, Vieille ville (or Colonna d'Istria) and Nice Centre on the first map (Figure 151). Additional points for further analysis are presented in Figure 152.

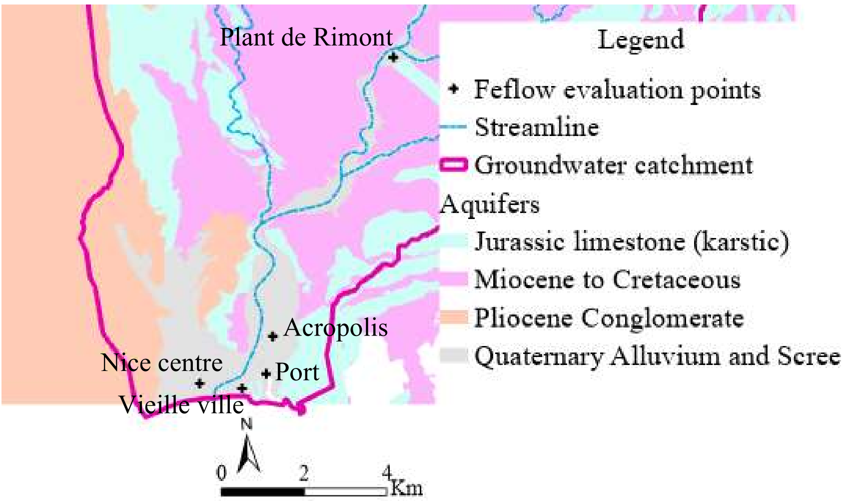

Figure 151 Feflow evaluation points (part a).

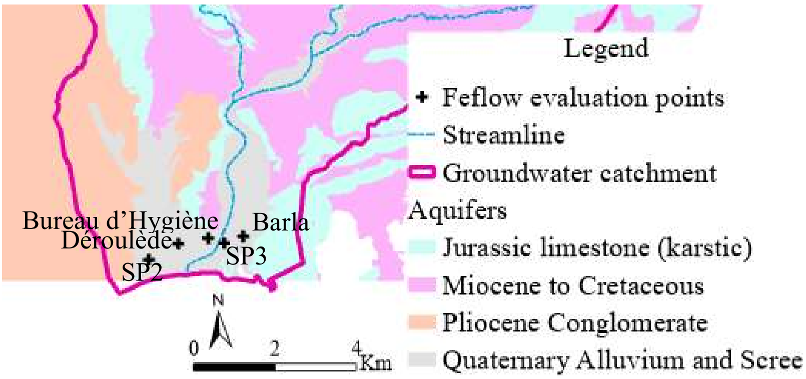

Figure 152 Feflow evaluation points (part b).

The range of values for each parameter is displayed in Table 37. Each parameter is modified at a time to simulate the flow and record the output.

Table 37 Selected parameters for sensitivity analysis.

Parameter	Units	Baseline	Range
In-transfer rate	/s	1.00E-5	1.00E-06 to 1.00E-04
Out-transfer rate	/s	1.00E-4	1.00E-05 to 1.00E-03
Specific yield	-	0.2	0.05 to 0.2
Hydraulic conductivity	m/s	Distributed	1.00E-04 to 2.00E-02

5.3.2. Results of sensitivity analysis and discussions

The results of the sensitivity analysis of In-transfer rate are presented in Table 38 and Figure 153. The highest maximum change of 1.53 m from baseline is found at Plan de Rimont located upstream in an area where the width of the alluvial zone is small and where there is an extraction of groundwater for drinking usage. On the other hand, the lowest maximum change of 0.25 m corresponds to Vieille ville near the sea. The highest mean change is also located at Plan the Rimont, but the lowest mean change is at Nice centre not far from Vieille ville. When In-transfer rate is increased from 1.00E-06 to 1.00E-04, the groundwater baseflow levels are shifted upwards between 0.03 m and 0.63 m, and their peak levels are delayed by 1 day to up to 2 weeks. Plan the Rimont location is closest to the river, which explains its highest sensitivity to In-transfer rate.

Next, the sensitivity of Out-transfer rate in Table 38 and Figure 154 shows higher maximum change than In-transfer rate. In addition, the most sensitive location to changes in Out-transfer rate is Plan de Rimont while the least sensitive is Vieille ville. In fact Vieille ville location is controlled by the downstream boundary of the model which is sea level. From the baseline parameter value to 1.00E-05, there is an upward shift in mean groundwater levels between 0.04 m and 0.38 m, and a slight delay in peak time by 1 day. However, from the baseline parameter to 1.00E-03, in addition to a weaker shift upward of groundwater levels, the delay in peak time varies up to 1 month.

Moreover, the sensitivity analysis of specific yield confirms that the least sensitive location is Vieille ville. However, as presented in Table 38 and Figure 155, the highest maximum change in groundwater levels from baseline is not anymore Plan the Rimont but SP2 and Nice centre locations. Changing specific yield does not shift upward or downward the groundwater table but generates the highest increase in the amplitude of the peaks for lower values of specific yield. In addition, the peak time is delayed 1 to 5 days when Sy is decreased from baseline from 0.2 to 0.05. However, a change in Sy from 0.2 to 0.1 produced peak levels 1 to 5 days earlier in some cases. Higher values of specific yield provoke smoother changes in groundwater levels compared to lower values.

The fourth parameter assessed in the sensitivity analysis is the hydraulic conductivity Kxx. Since the anisotropy relationship Kxx=Kyy=10xKzz was assumed, changes in Kxx was followed by proportional changes in Kzz. The results are presented in Table 38 and Figure 156. In ideal situation, hydraulic conductivity is measured at the boreholes and interpolated. However, the information available in the Paillons is sparse. Therefore, an assessment of this parameter is required. Among the four selected parameter, hydraulic conductivity caused the largest maximum and mean changes in ground water levels at different locations. For example at Déroulède location, the maximum change was 7.17 m and the mean change was 2.36 m. There is no specific trend in changing the hydraulic conductivities. Low or high groundwater levels can be obtained with low or high hydraulic conductivity depending on the location. When the parameter value is decreased from 2.00E-02 to 1.00E-04 m/s, the peaks appeared earlier or are delayed by up to 20 days depending on the location and the date. In addition, the hydraulic conductivity is the only parameter among the selected to influence the groundwater levels below and above the measured values in October 2010.

Table 38 Summary of sensitivity analysis of selected parameters at different locations.

	In-transfer rate									
Location	Plan de Rimont	Acropolis	Ecole Barla	Bureau d'Hygiène	Port	Déroulède	SP3	SP2	Nice centre	Vieille ville
Max change from baseline groundwater level (m)	1.53	0.44	0.46	0.46	0.32	0.51	0.43	0.63	0.59	0.25
Mean change from baseline groundwater level (m)	0.63	0.09	0.08	0.08	0.06	0.06	0.11	0.06	0.03	0.05
	Out-transfer rate									
Max change from baseline groundwater level (m)	1.19	0.64	0.67	0.57	0.40	0.54	0.64	0.65	0.58	0.34
Mean change from baseline groundwater level (m)	0.38	0.11	0.08	0.07	0.06	0.06	0.08	0.06	0.04	0.04
	Specific yield									
Max change from baseline groundwater level (m)	1.00	0.98	1.05	1.06	0.71	1.08	1.20	1.21	1.21	0.50
Mean change from baseline groundwater level (m)	0.15	0.11	0.12	0.12	0.08	0.32	0.08	0.25	0.21	0.05
	Hydraulic conductivity Kxx									
Max change from baseline groundwater level (m)	1.72	3.57	3.15	5.70	2.55	7.17	3.74	5.59	4.52	1.91
Mean change from baseline groundwater level (m)	0.37	1.11	0.77	1.68	1.11	2.36	1.36	1.77	1.43	0.62

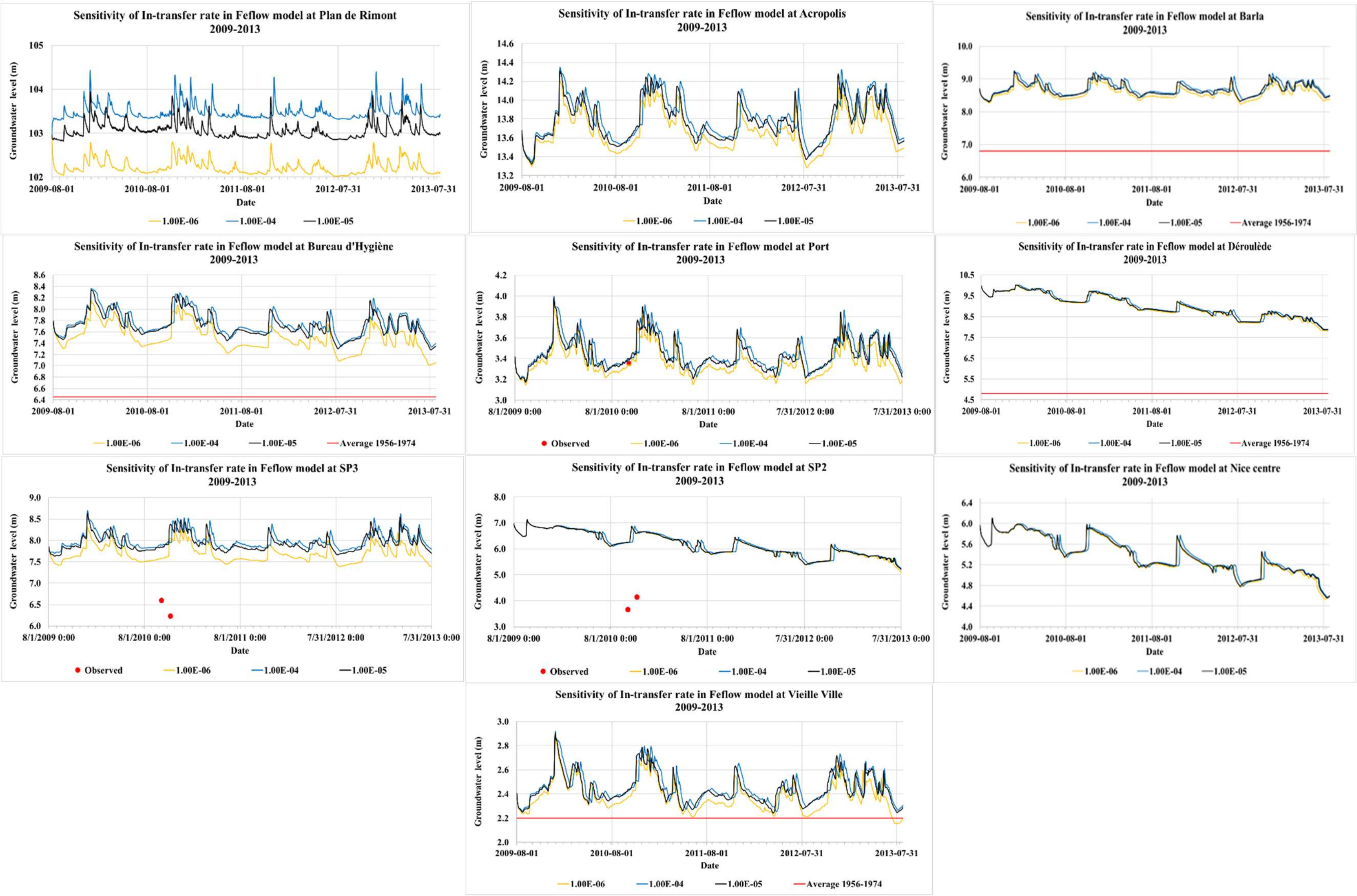

Figure 153 Sensitivity analysis of In-transfer rate at different locations.

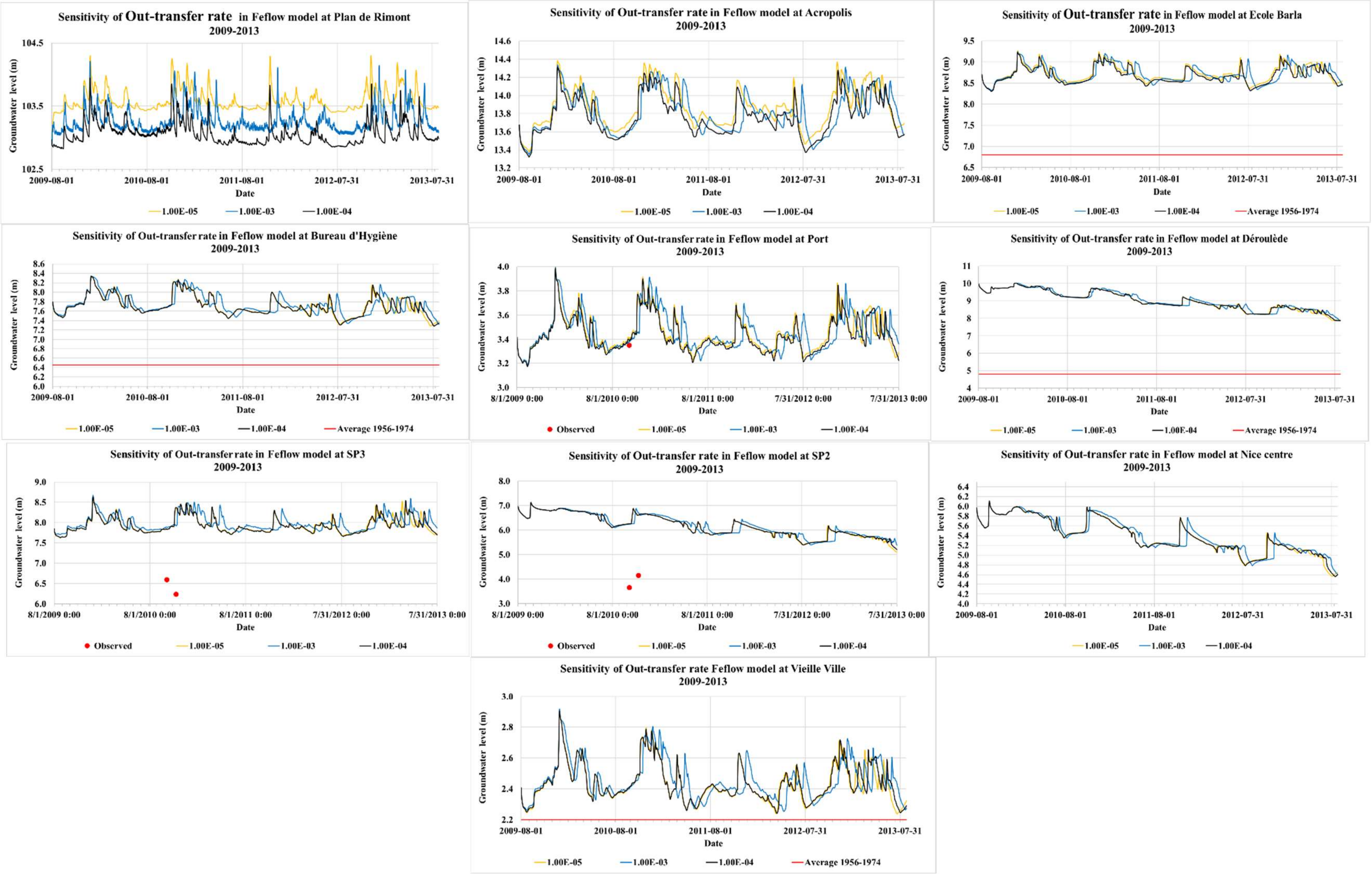
Sensitivity of Out-transfer rate in Feflow model at Plan de Rimont 2009-2013

Sensitivity of Out-transfer rate in Feflow model at Acropolis 2009-2013

Sensitivity of Out-transfer rate in Feflow model at Ecole Barla 2009-2013

Sensitivity of Out-transfer rate in Feflow model at Bureau d'Hygiène 2009-2013

Sensitivity of Out-transfer rate in Feflow model at Port 2009-2013

Sensitivity of Out-transfer rate in Feflow model at Déroulède 2009-2013

Sensitivity of Out-transfer rate in Feflow model at SP3 2009-2013

Sensitivity of Out-transfer rate in Feflow model at SP2 2009-2013

Sensitivity of Out-transfer rate in Feflow model at Nice centre 2009-2013

Sensitivity of Out-transfer rate Feflow model at Vieille Ville 2009-2013

Figure 154 Sensitivity analysis of Out-transfer rate at different locations.

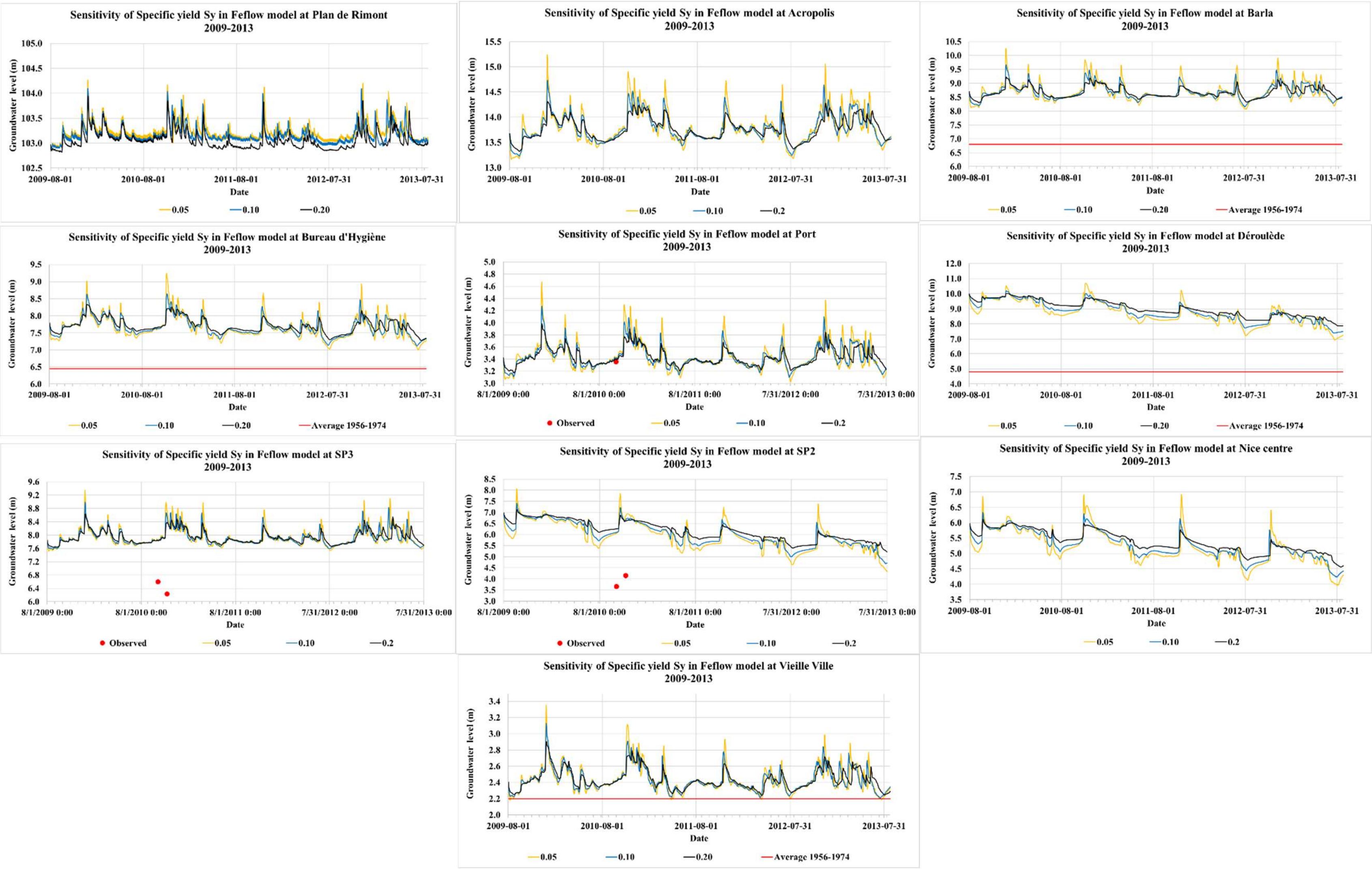

Figure 155 Sensitivity analysis of specific yield at different locations.

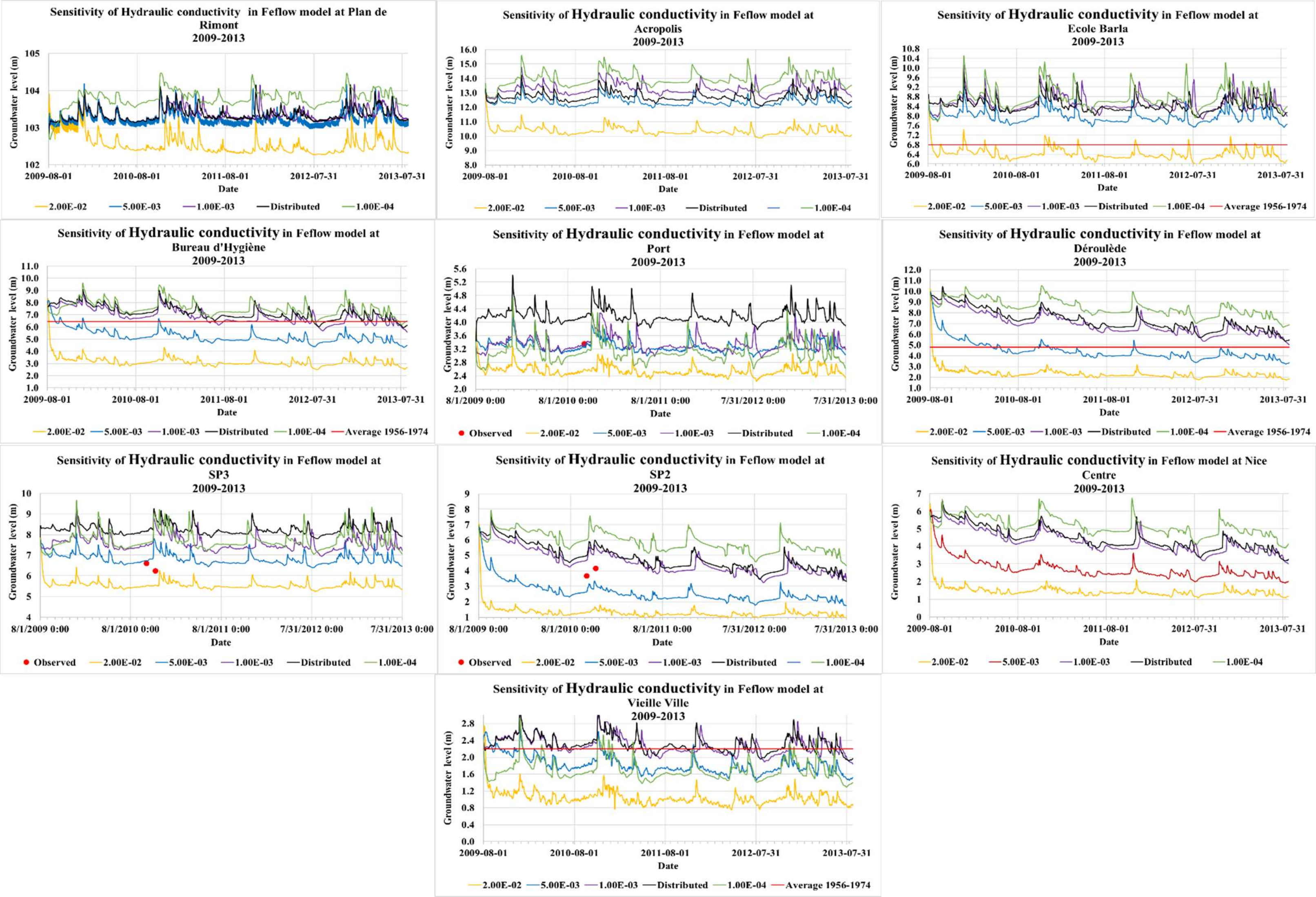
Sensitivity of Hydraulic conductivity in Feflow model at Plan de Rimont 2009-2013

Sensitivity of Hydraulic conductivity in Feflow model at Acropolis 2009-2013

Sensitivity of Hydraulic conductivity in Feflow model at Ecole Barla 2009-2013

Sensitivity of Hydraulic conductivity in Feflow model at Bureau d'Hygiène 2009-2013

Sensitivity of Hydraulic conductivity in Feflow model at Port 2009-2013

Sensitivity of Hydraulic conductivity in Feflow model at Déroulède 2009-2013

Sensitivity of Hydraulic conductivity in Feflow model at SP3 2009-2013

Sensitivity of Hydraulic conductivity in Feflow model at SP2 2009-2013

Sensitivity of Hydraulic conductivity in Feflow model at Nice Centre 2009-2013

Sensitivity of Hydraulic conductivity in Feflow model at Vieille Ville 2009-2013

Figure 156 Sensitivity analysis of hydraulic conductivity Kxx at different locations.

Unfortunately, calibration over a long period is not possible for the groundwater model. Some locations have historical data for which an average was estimated. Notably, Déroulède, Ecole Barla, Bureau d'Hygiène and Vieille ville (or Colonna d'Istria) have records from 1954-1974. But the current state of the water table can divert from these means due to climatic conditions or urbanization. Therefore, it is not a proper calibration to fit toward these mean values. On the other hand, 3 locations (Port, SP3 and SP2) have records on October 5th and November 9th, 2010. The limitation is that the trend around the measured value is not known to build confidence on the calibration at that location. This study recommends making available or producing groundwater levels monitoring information at least at Plan de Rimont, Acropolis (TNL), Port and Nice centre. Two locations, Plan de Rimont and Acropolis (TNL), have boreholes used for groundwater extractions. It is possible to implement piezometers at these locations for groundwater monitoring.

5.4. Calibration and Validation in Feflow

This study assumes the historical mean to be still valid in the period of study. The calibration process is to fit fluctuations of groundwater levels around that mean in addition to match the single measurements in 2010 at different locations. Figure 157 shows the graphical representation of the calibrated Feflow model at different locations. The model was able to fit groundwater levels around the historical means and the few observed value in 2010. Previous studies suggest that the groundwater fluctuates between 1 and 2 m, which is also the case in the model results. In addition the model captured the spatial variability across evaluated locations. These results were obtained with calibrated parameters summarized in Table 39 and Figure 158. The In-transfer and Out-transfer were set uniform, but specific yield and hydraulic conductivity varied at few locations. Unfortunately, lack of data blokes the assessment at this stage. Future production of monitoring information would allow statistical analysis of the performance of the groundwater model.

Looking at the Nodal Darcy flux of groundwater flow during the drought period (left) and flood period (right) in Figure 159, the direction of the flux is generally toward the sea in both drought and flood periods. This does not suggest potential seawater intrusion in these conditions. However, a high resolution assessment is needed to investigate seawater flow processes nearshore. The magnitude of the flux varies between 1.00E-4 and 1.00E-08 m/s. The major part of the area is exposed to fluxes around 1.00E-05 m/s with some location near the port and upstream reaching 1.00E-04 m/s.

Moreover, the contour map of groundwater flow during the drought period (left) and flood period (right) is presented in Figure 160. The two cases correspond to July 24th,2012 and November 5th,2011. In any case, the hydraulic head varied from 200 m upstream to 0.5 m at sea level. The difference is that flood period groundwater levels are on average 1 m above that of drought periods depending on the location.

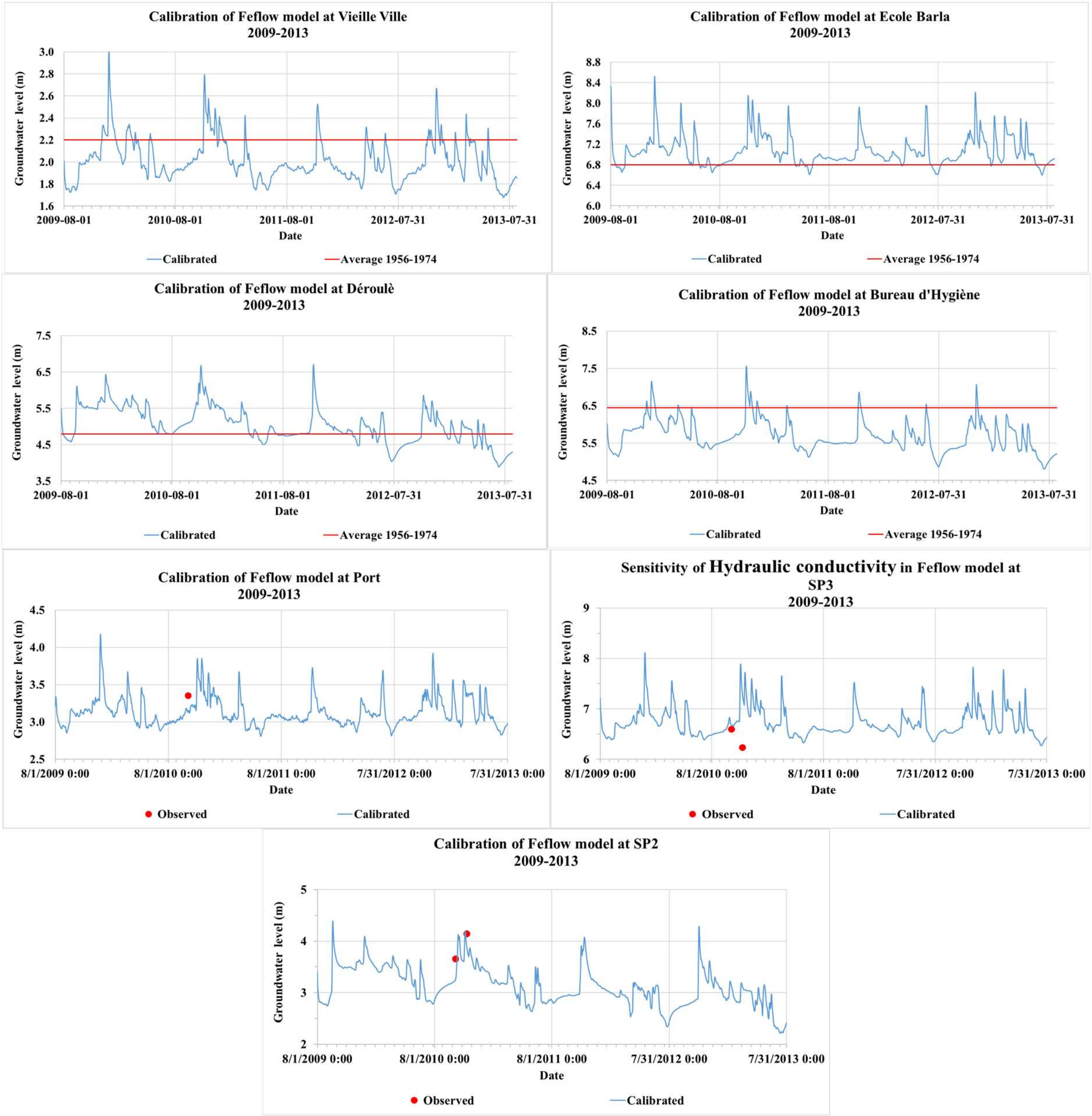

Figure 157 Calibrated groundwater levels at different locations.

Table 39 Calibrated parameters in Feflow model.

Parameter	Units	Calibrated value
In-transfer rate	/s	1.00E-6
Out-transfer rate	/s	1.00E-4
Specific yield	-	0.05
Hydraulic conductivity	m/s	Distributed

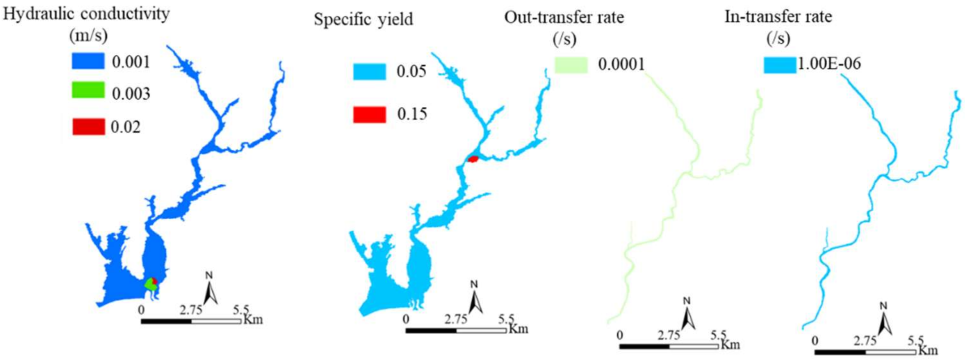

Figure 158 Distribution of calibrated parameters in the Alluvium of the Paillons.

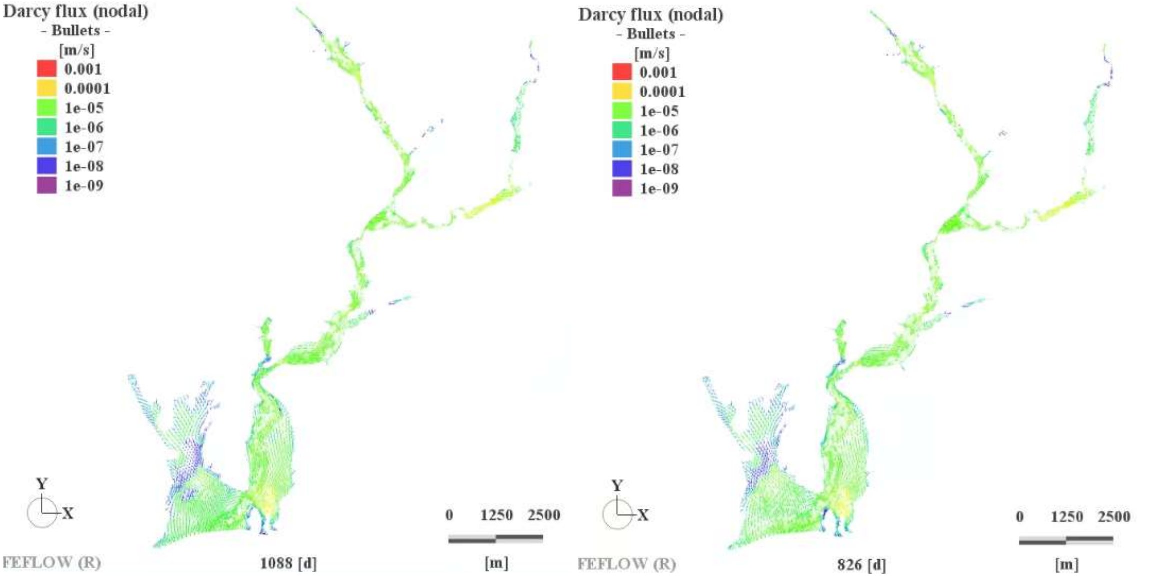

Figure 159 Nodal Darcy flux of groundwater flow during the drought period (left) and flood period (right).

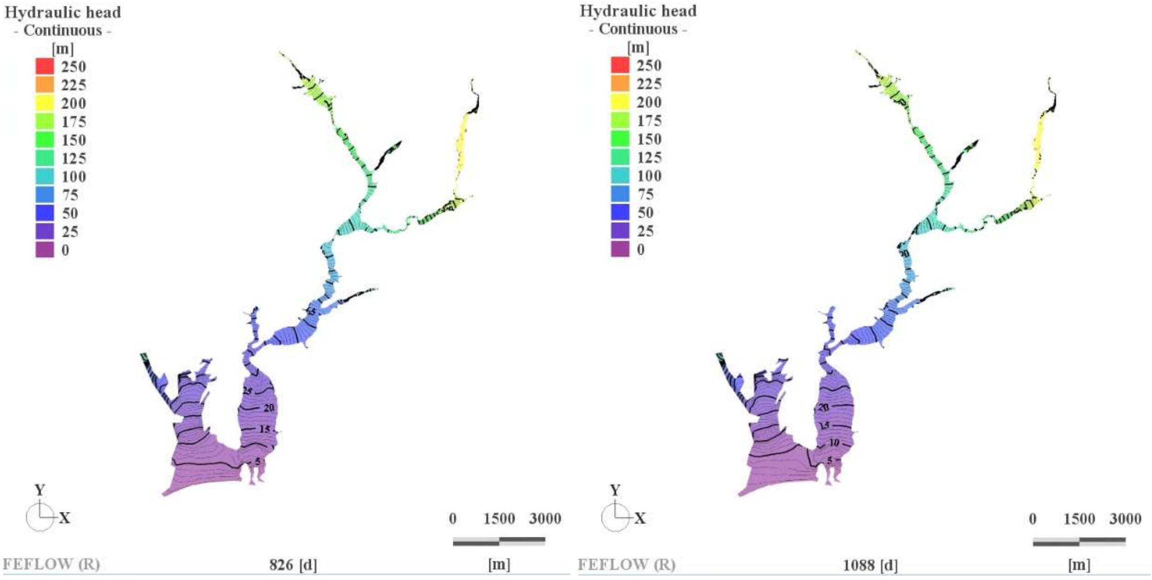

Figure 160 Contour map of groundwater flow during the drought period (left) and flood period (right).

5.5. Assessments of the impacts of groundwater extraction

12 publicly known pumping stations in the alluvium are present and mostly industrial (Table 40). Only 3 of them are used for drinking resources of some communities in the north of Nice city. The

TNL, Port Nicéa and Palais des expositions lack information on groundwater extraction. Therefore, their extraction rates was assumed to be similar to the Palais des Congrès. The calibrated Feflow model did not consider groundwater extraction. It is necessary to assess the impacts of this exaction on groundwater flow dynamics. Additionally, a scenario with a 10 time increase of extraction due to human activity is assessed to identify potential impacts on flow dynamics. The daily rates are assumed constant in the simulation period. However, extraction for drinking may be exposed to some seasonality. The equivalent daily pumping rates varies between 6 m^3/d and 1353 m^3/d with the maximum value at Palais des Arts located near the sea (Figure 161).

Table 40 Groundwater extraction boreholes in the Alluvium of the Paillons.

Borehole	Depth from Surface (m)	Ground elevation (m)	Annual extraction (m^3)	Equivalent daily rate (m^3/d)	Usage
Vicat de Peille 1	15	200	112350	307.81	Industrial
Vicat de Peille 2	13	200	112350	307.81	
Rua	20	210	166044	454.92	Drinking
Fonti	20	230	73880	202.41	
Lafarge de Contes	20	180	101600	278.36	Industrial
SNTA	7.25	80	2200	6.03	
TNL	22.15	12.25	?	273.97	
Palais des Arts	25	5	493800	1352.88	
Port Nicéa	25	15	?	273.97	
Palais des Expositions	40	17	?	273.97	
Palais des congrès	18	10.68	100000	273.97	
Plan de Rimont	20	104	331700	908.77	Drinking

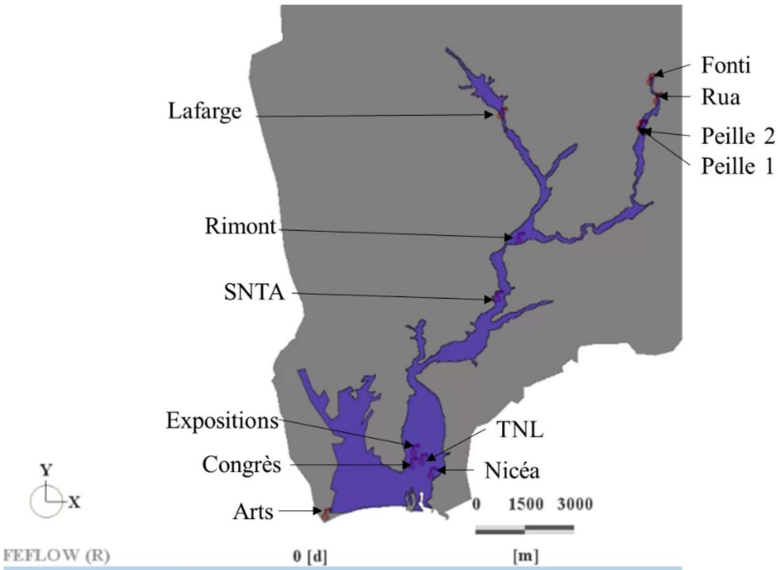

Figure 161 Locations of the groundwater extraction boreholes in the alluvium of the Paillons (violet) within the Feflow modeling domain (grey).

The Figure 162 represents impacts of groundwater extractions on flow dynamics at 8 locations in the alluvium. One of the location is Acropolis (TNL) where there is a borehole for extraction. The other locations have either historical observed mean or measurements in 2010. However, at these locations, groundwater is not extracted anymore. The groundwater level globally decreased with constant extraction over years. The first year is less impacted. At the current pumping rate, the peak levels appeared later than the case without pumping. In the case where the extraction will increase by 10 folds, the impacts will worsen. In fact, the graphs show that ground water levels decreased by more than 2 m at Acropolis (TNL). Areas located far from the extraction boreholes are less impacted. The summary of the impacts of extraction on groundwater flow for two cases in Table 41 highlights the changes of the maximum and the mean values from the calibrated results. Among the 8 locations, Vieille ville is the least impacted by the current extraction at 12 boreholes across the alluvial zone. A 10 time increase in extraction did not result in a decrease in groundwater level at all locations. In fact, areas such as Bureau d'Hygiène, Déroulède, SP2 and Vieille ville experienced smaller changes in maximum and mean values with 10 times the current pumping rates. This situation is explained by the shift in peak time of groundwater levels with the first scenario.

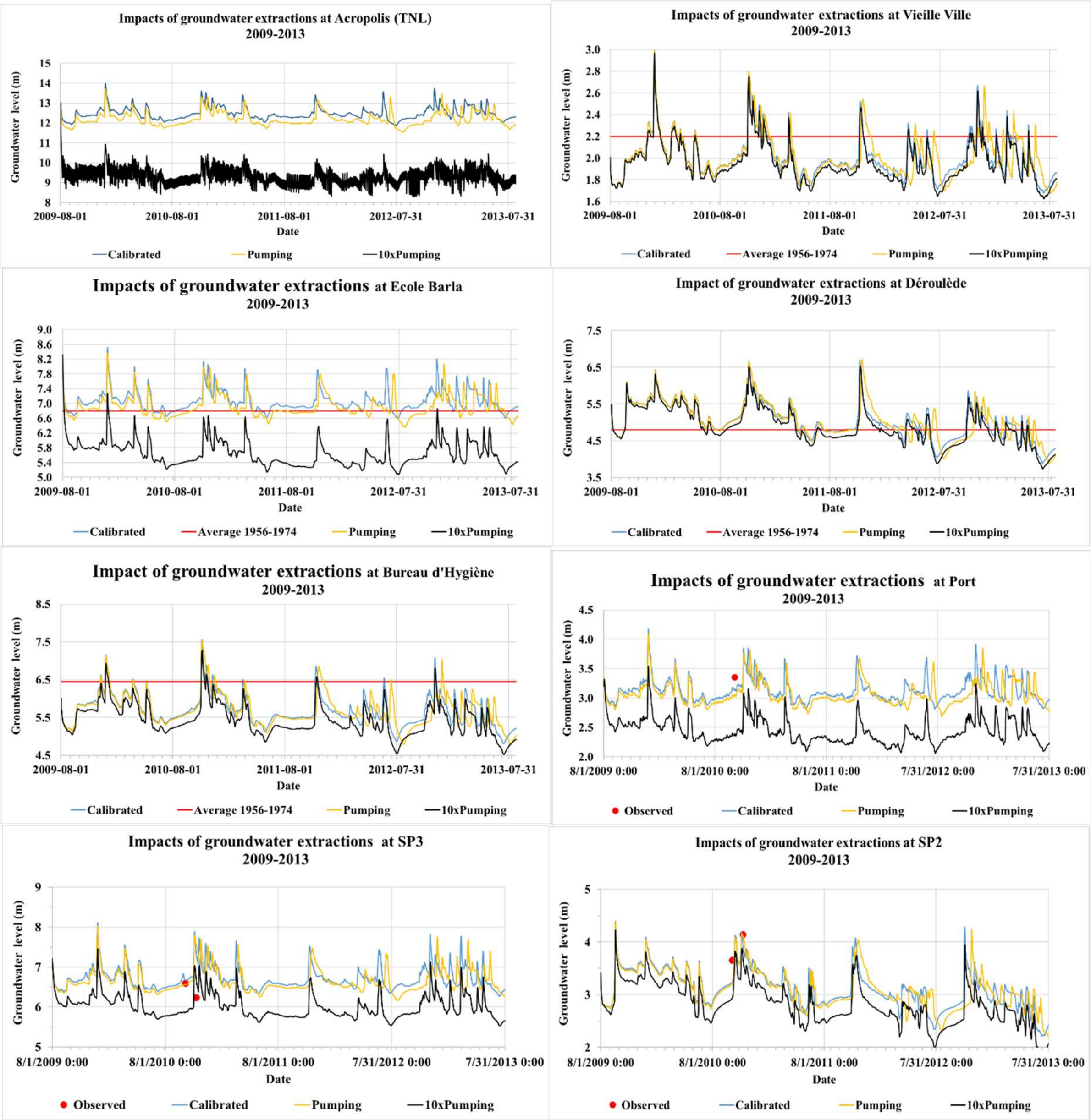

Figure 162 Impacts of groundwater extractions on flow dynamics at different locations in the alluvium.

Table 41 Summary of the impacts of extraction on groundwater flow for two scenarios (current extraction rates and ten times current rates).

Location	**Scenario extraction rate**	**Change from calibrated groundwater level (m)**	
		Maximum	**Mean**
Acropolis (TNL)	Pumping (reference)	1.44	0.33
	10xPumping	4.22	3.14
Ecole Barla	Pumping (reference)	1.11	0.21
	10xPumping	1.92	1.41
Bureau d'Hygiène	Pumping (reference)	1.32	0.19
	10xPumping	0.82	0.26
Port	Pumping (reference)	0.71	0.13
	10xPumping	1.08	0.69
Déroulède	Pumping (reference)	1.53	0.16
	10xPumping	0.77	0.14
SP3	Pumping (reference)	1.22	0.17
	10xPumping	1.25	0.70
SP2	Pumping (reference)	1.52	0.13
	10xPumping	0.97	0.30
Vielle ville	Pumping (reference)	0.56	0.08
	10xPumping	0.31	0.05

This Feflow model of the groundwater dynamics of the Alluvial zone in the Paillons already yielded interesting results. It can be used for impacts assessments of different projects related to groundwater resources and flow dynamics. However, the calibration and validation process are limited by data availability. At this point Feflow can be coupled with MIKEPlus 1D river model to assess the effect of using dynamic river-aquifer exchanges simulations on river water depths and groundwater levels. Since the Paillons is a river which can completely dry out during drought period, the river losing water will be important for baseflow.

Conclusion

In summary, this chapter explored deterministic hydrogeological modeling of runoff and groundwater flow dynamics using MIKE SHE and Feflow tools. Far from being a mere reenactment of the study in the Var catchment, this investigation provided an added value for flow calculation. In MIKE SHE, two cases were assessed and further optimized with the application of ANN. In addition, the modeling strategy resulted in satisfactory results at daily, hourly, and 6-mn time scales. The analysis did not stop at the limitations in using deterministic modeling on areas with limited data. The optimization strategy can absorb uncertainties that are not covered by deterministic models due to weaknesses in data and catchment description. The strategy enabled to construct a hydrological model which provide accurate boundary conditions to the flood model. In fact, flooding is the primary concern in the Lower Paillons River where densely populated communities and sensitive infrastructure have to be protected. The following work will be to reconstruct historical runoff information since 1921 to provide a long-term picture of how runoff processes have been occurring on the Paillons.

In Feflow, an upstream boundary does not exist, which was the case in the Var model. Contrary to the Var, the Paillons lack current groundwater monitoring data. Therefore, an innovative approach is implemented to calibrate and validate the model by comparing with the historical mean. The few studies available of the area suggests that groundwater levels have fluctuated between 1 and 5 m over the time. Two measurements in October 2010 compared to the model results are well reproduced by the model. The main goal of comparing with historical mean is to show that the model can produce flow dynamics around that value. Comparing with historical mean alone is insufficient to qualify the performance of the model. This initial version of the groundwater model suggests that if there were time series of groundwater levels, the model will be able to fit observations after additional calibration. Therefore, an informed recommendation can be made to the local authorities about what is needed in terms of data collection. It should be noted that the impact of river-aquifer exchanges was not evaluated. Future work should investigate this issue to estimate its contribution to baseflow and recharge in the Paillons River.

Conclusions and Future prospects

The primary goal of extending the AquaVar project to the Paillons was to develop a real-time decision support system incorporating multiple deterministic distributed models to comprehensively assess the hydrogeological characteristics of the catchment and predict natural disasters. This system is intended to assist regional water resource management decision-making processes. The scientific question being explored in this study is how to model complex runoff processes and groundwater flow dynamics for real-time decision support system in the context of water hazards and resources management, with a particular emphasis given to strategies for long-term simulations. Long-term simulations are useful to assess the constancy of model performance, and the ability of the tool to also be used to reconstruct past events because the observed data does not give a complete understanding of the past. Different aspects of flow estimation were investigated including monitoring data assessments, image-based estimation of discharge, deterministic hydrological, hydraulic and groundwater modeling and optimization of runoff model results with ANN. This innovative approach ensures to optimize the use of available information in the Paillons for accurate representation of flow processes. Compared to the models of the Var catchment, the hydraulic model is a coupled 1D-2D river-surface model instead of a full 2D surface model as it was done in the Var. In addition, the hydrological model covered 3 time scales and an optimization method was applied which was not the case in the Var. Finally, the Feflow model extends to the whole catchment and did not use an upstream boundary condition like in the Var. However, dynamic river-aquifer exchange was not investigated in this study. It should be implemented in future work to clarify its importance in the context of a dry Paillons River during drought periods and the contribution of the river losing water to groundwater flow.

This study commenced with a discussion regarding the extension of AquaVar’s Environmental Decision Support System (EDSS) architecture to the Paillons catchment. Upon reviewing the characteristics of the EDSS tool and the requirements for incorporating the Paillons, this study introduced an image-based analysis methods as a complementary way to optimize the use of collected flow data in addition to the need for modeling assessments. Subsequently, the three deterministic modeling components were constructed using MIKEPlus, MIKE SHE and Feflow under conditions where data availability was limited. Each model represents distinct hydrological aspects, including hydrological phenomena, surface water movement, groundwater dynamics, and water exchanges between the river and aquifer. After calibration of two cases, MIKE SHE simulations outputs were optimized by applying ANN to two cases at daily and hourly simulations. In addition to apply those two cases in optimizing 6-mn simulations, optimized ANN daily and hourly outputs were integrated in a second optimization of 6-mn model’s outputs.

In comparison to other types of hydrological models such as conceptual models, deterministic distributed hydrological models offer the advantage of providing detailed and accurate representations of the various hydrological processes within the whole catchment. However, they typically demand substantial data inputs during the modeling setup, which can be a limitation in ungauged or poorly gauged catchments with limited field data available. Interestingly, video image analysis provided additional information on flow characteristics to strengthen the modeling outcomes. Moreover, optimization methods such as ANN significantly improved model’s outputs.

In line with the modeling strategy outlined in this study, several hypotheses were formulated during the modeling setup process to bridge the gap between model requirements and available field data:

- River flood is mainly influenced by upstream inflow and can be well represented in 1D;
- Discharge estimation with analysis of video records plays an important role in filling the gap in monitored runoff data;
- Soil depth distribution in the Paillons catchment is strongly influenced by surface slope;
- Limited groundwater enters the catchment from external sources;
- Snowmelt processes are highly influenced by air temperature and sunshine in the Paillons catchment;
- Groundwater flow in the alluvial zone can be simulated without using an upstream boundary condition but with a properly defined initial condition and estimated recharge.

The modeling results demonstrated that, for representing the complex hydraulic and hydrogeological system in the Paillons catchment, the minimum data requirements could be focused on topography, precipitation, air temperature, and geological layers, which are closely linked to the most critical hydrological processes, particularly the rainfall-runoff process. While higher data quality would enhance the accuracy of the simulation for factors such as evapotranspiration and soil conditions, in cases like the Paillons catchment, where few field surveys were available, relationships estimated based on surface slope could be incorporated into the model to produce acceptable results, generally capturing the hydrogeological characteristics of the catchment, and forecasting impending natural disasters. for All the cases are based on slope definition. But case 2, which performed better than case 1 at 6-mn time intervals, suggests to consider deeper depths of the saturated zone. Additionally, in the modeling phase of this study, statistical performance and event assessments during the calibration process helped improve the modeling accuracy during model evaluation. The application of ANN highly improved the simulation results. Nevertheless, in the section discussing uncertainties and limitations, it was noted that further improvements could be expected through future work in the catchment, particularly by conducting more detailed field data surveys to accurately describe soil conditions or using artificial neural networks at simulated outputs from upstream gauging stations.

Hydraulic modeling of groundwater has become a widely used method for managing groundwater resources efficiently. It supplements our understanding of aquifers in the studied regions and offers comprehensive information to aid decision-makers, all at a relatively low cost. However, the accuracy of the model's results hinges on the quality of the input data. In this particular study, a physically based model has been constructed to simulate groundwater flow in the Paillons alluvial zone. In general, the model produces satisfactory results related to the dynamics of flow. Nevertheless, there are no recent monitored time series for model calibration and validation.

The geological layers within the model are represented by digitized versions of hand-drawn maps, which were generated based on geological drilling tests. However, the number of these data is insufficient to create a highly precise numerical model for the entire catchment. More measured data is required, particularly for describing the elevation of the bottom of the alluvium. Additionally, hydraulic conductivity, a critical parameter that significantly influences groundwater flow, varies both horizontally and vertically. Therefore, collecting an extensive dataset of measured data and selecting those that accurately represent specific areas is essential. Furthermore, information regarding the volumes of groundwater extraction from boreholes, especially for industrial purposes, remains unknown. These three types of data should be given top priority for updates, especially in areas where urbanization may have a strong influence on groundwater quality. Another avenue for improvement involves reconsidering the model's structure. The Richards equation, which simulates variably saturated layers, especially in cases of disconnection between the river and the aquifer, was not applied in the current model due to computational time constraints.

Since groundwater is used for drinking and economic activities in the Mediterranean region, the methodology employed in developing the model for the Paillons can be replicated for similar smaller aquifers limited by data availability. With reasonable assumptions, the model can still produce accurate results for long-term simulations. Consequently, this work introduces a novel groundwater management workflow based on a deterministic model. Initially, a numerical model can be developed using available data, and subsequently, the model can be refined by acquiring additional data through field measurements. This approach not only enhances accuracy but also reduces overall investment, as measurements are focused on specific areas and aspects.

This work has contributed to a comprehensive understanding of the Paillons catchment. The Paillons River, as a coastal river, has undergone urbanization in its lower reaches, rendering water quality and quantity vulnerable. In response to this risk, French regulations have proposed various strategies for mitigation. While previous research efforts in this catchment have primarily focused on hydrodynamics, hydrological and hydrogeological aspects of extreme events, the hydrodynamics of the Paillons River for long-term simulations and for real-time decision support systems may have been relatively neglected. Even though there has been a monitoring system since 1987 for river flood management, gap and uncertainties in field measurements pose serious challenge in understanding flow processes and extreme events. This study has addressed this gap in scientific knowledge and flow characteristics. Simulation of extreme events has facilitated the description of overflow dynamics. Furthermore, it has conducted a thorough analysis of the hydrodynamics of the lower Paillons River, considering various factors such as river constructions, river-aquifer interactions, and groundwater flow within the unconfined aquifer. Building upon the insights gained from these three numerical models and the analysis of video records, this modeling system serves the purpose of characterizing the entire spectrum of risks associated with the water system in the Lower Paillons valley.

This doctoral thesis has convincingly demonstrated that a combination of prior studies, field measurements and numerical tools has significantly advanced scientific knowledge pertaining to the Paillons. These methodologies rely on observed and recorded data. To further enhance scientific understanding of the Paillons catchment, it is imperative to maintain the existing monitoring network while reducing measurement uncertainties. Additionally, expanding the measurement network is essential to include additional control points and new indicators for assessing flow characteristics. These recorded data not only aid in comprehending physical behaviors but also serve as valuable inputs for updating numerical tools, thus enhancing our understanding of river behavior during extreme events.

For the extension of AquaVar system to the Paillons, the application of the modeling system, which includes three deterministic models: MIKE SHE, MIKE Plus, and Feflow, holds a promising potential. In addition, image-based analysis of video records and application of ANN to MIKE SHE results reinforce the quality and completeness of the knowledge of flow characteristics in the Paillons. The AquaVar EDSS is expected to integrate meteorological forecast information from external sources, such as Météo-France. Subsequently, through data transformation processes within the system, this estimated dataset will be changed into the standard input data format required for MIKE SHE to enable real-time simulations. The MIKE SHE model will then generate boundary conditions for the other two models, MIKE Plus and Feflow. MIKEPlus is more focused on the lower Paillons valley region within the catchment, but floodplains in upstream parts could be connected to the 1D river model within MIKEPlus to assess flood risk in the upstream parts. All modeling assessment results will be consolidated and provided to the "Operations Center" to support the decision-making process.

It is worth noting that all partners involved in the AquaPaillons research project have played a role in the collecting data and completing this project. The collaborative effort involved the collection of diverse data and knowledge resources, aimed at comprehending the historical context and intricacies of the Paillons. This collective effort has culminated in the creation of the modeling system, which serves as the cornerstone of the AquaPaillons DSS.

The fundamental philosophy underlying this tool is the open sharing of information pertaining to the water cycle within the Paillons. This implies that access to information is freely available to all stakeholders involved in water management within the region. Moreover, it is expected that each stakeholder will actively contribute to the ongoing enhancement and updates of the DSS tool in the future.

References

Abbass, K., Qasim, M. Z., Song, H., Murshed, M., Mahmood, H., & Younis, I. (2022). A review of the global climate change impacts, adaptation, and sustainable mitigation measures. *Environmental Science and Pollution Research*, *29*(28), 42539–42559. https://doi.org/10.1007/s11356-022-19718-6

Abbott, M. B., Bathurst, J. C., Cunge, J. A., O'Connell, P. E., & Rasmussen, J. (1986). An introduction to the European Hydrological System — Systeme Hydrologique Europeen, "SHE", 1: History and philosophy of a physically-based, distributed modelling system. *Journal of Hydrology*, *87*(1), 45–59. https://doi.org/10.1016/0022-1694(86)90114-9

Abily, M., Scarceriaux, C., & Duluc, C.-M. (2015). Ruissellement de surface en milieu urbain: Stratégies d'intégration de données topographiques haute résolution en modélisation hydraulique 2D. *Techniques Sciences Méthodes*, *5*, 31–46. https://doi.org/10.1051/tsm/201505031

Ansari, S., Rennie, C. D., Jamieson, E. C., Seidou, O., & Clark, S. P. (2023). RivQNet: Deep Learning Based River Discharge Estimation Using Close-Range Water Surface Imagery. *Water Resources Research*, *59*(2), e2021WR031841. https://doi.org/10.1029/2021WR031841

Archambaud, J., & Berthet, J. (2021). *Etude des cours d'eau des Alpes-maritimes visant la restauration du fonctionnement morphologique et la prévention des risques d'inondation – Lot 1: Paillons et bassins côtiers du mentonnais Phase 1: Etat des lieux du fonctionnement du bassin versant des Paillons*. Safege-Smiage; Nice Metropolis.

Audra, P., Gilli, É., Mangan, C., & Michelot, N. (2006). *Les traçages karstiques des Alpes-Maritimes*. Université de Nice-Sophia-Antipolis.

Bringas, R. V. (2016). *Deterministic hydrological modeling for flood risk assessment in large urban environments: Application to Mexico City* [Phdthesis, Université Côte d'Azur]. https://theses.hal.science/tel-01488436

Brown, L. C., Bamwell Jr, T. O., & T.O. (1987). *The enhanced stream water quality models QUAL2E and QUAL2E-UNCAS: documentation and user manual. Athens, Ga, USA: US Environmental Protection Agency, Environmental Research Laboratory, 204 pages.*

https://www.researchgate.net/publication/235754236_The_enhanced_stream_water_quality_models_QUAL2E_and_QUAL2E-UNCAS_documentation_and_user_manual

Butts, M. B., Payne, J. T., Kristensen, M., & Madsen, H. (2004). An evaluation of the impact of model structure on hydrological modelling uncertainty for streamflow simulation. *Journal of Hydrology*, *298*(1), 242–266. https://doi.org/10.1016/j.jhydrol.2004.03.042

Carrega, P., & Michelot, N. (2021). Une catastrophe hors norme d'origine météorologique le 2 octobre 2020 dans les montagnes des Alpes-Maritimes. *Physio-Géo. Géographie physique et environnement*, *Volume 16*, Article Volume 16. https://doi.org/10.4000/physio-geo.12370

Chahrour, N., Castaings, W., & Barthélemy, E. (2021). Image-based river discharge estimation by merging heterogeneous data with information entropy theory. *Flow Measurement and Instrumentation*, *81*, 102039. https://doi.org/10.1016/j.flowmeasinst.2021.102039

Chochon, R., Martin, N., Lebourg, T., & Vidal, M. (2022). Analysis of extreme precipitation during the mediterranean event associated with the Alex storm in the Alpes-Maritimes: Atmospheric mechanisms and resulting rainfall. In *Advances in Hydroinformatics* (pp. 397–418). Springer.

Coron, L., Thirel, G., Delaigue, O., Perrin, C., & Andréassian, V. (2017). The suite of lumped GR hydrological models in an R package. *Environmental Modelling & Software*, *94*, 166–171. https://doi.org/10.1016/j.envsoft.2017.05.002

Crawford, N. H., & Linsley, R. (1966). *Digital Simulation in Hydrology: Stanford Watershed Model IV. Technical Report No. 39, Department of Civil and Environmental Engineering, Stanford University, Stanford.* Department of Civil Engineering, Stanford University.

Darwish, M. S., & Moukalled, F. (2003). TVD schemes for unstructured grids. *International Journal of Heat and Mass Transfer*, *46*(4), 599–611. https://doi.org/10.1016/S0017-9310(02)00330-7

Devia, G. K., Ganasri, B. P., & Dwarakish, G. S. (2015). A Review on Hydrological Models. *Aquatic Procedia*, *4*, 1001–1007. https://doi.org/10.1016/j.aqpro.2015.02.126

DHI. (1993). *Danish Hydraulics Institute, 1993. MIKE11, User Guide & Reference Manual. Horsholm, Denmark: Danish Hydraulics Institute, 20 pages.*

DHI. (2023a). *DHI Simulation Engine for 1D river and urban modelling Reference Manual*. DHI. chrome-extension://efaidnbmnnnibpcajpcglclefindmkaj/https://manuals.mikepoweredbydhi.help/latest/Water_Resources/MIKE_1D_reference.pdf

DHI. (2023b). *MIKE+ River Network Modelling User Guide*. chrome-extension://efaidnbmnnnibpcajpcglclefindmkaj/https://manuals.mikepoweredbydhi.help/latest/Cities/MIKE_Plus_River.pdf

DHI. (2023c). *MIKE 21 Flow Model FM Hydrodynamic and Transport Module Scientific Documentation*. 22/03/2023. chrome-extension://efaidnbmnnnibpcajpcglclefindmkaj/https://manuals.mikepoweredbydhi.help/latest/Coast_and_Sea/MIKE_21_Flow_FM_Scientific_Doc.pdf

DHI. (2023d). *MIKE SHE User Guide and Reference Manual*. https://manuals.mikepoweredbydhi.help/latest/MIKE_SHE.htm

Diersch, H.-J. G. (2005). *Feflow Software—Finite Element Subsurface Flow and Transport Simulation System—Reference Manual. WASY GmbH, Berlin.*

Doummar, J., Sauter, M., & Geyer, T. (2012). Simulation of flow processes in a large scale karst system with an integrated catchment model (Mike She) – Identification of relevant parameters influencing spring discharge. *Journal of Hydrology*, *426–427*, 112–123. https://doi.org/10.1016/j.jhydrol.2012.01.021

Downer, C. W., & Ogden, F. L. (2004). GSSHA: Model to simulate diverse stream flow producing processes. *Journal of Hydrologic Engineering*, *9*(3), 161–174.

DRIAS. (2023). *DRIAS, Les futurs du climat—Accueil*. http://www.drias-climat.fr/

Du, M. (2016). *Integrated hydraulic modeling of groundwater flow and river-aquifer exchanges in the lower valley of Var River* [Phdthesis, Université Côte d'Azur]. https://theses.hal.science/tel-01484652

Du, M., Fouché, O., Zavattero, E., Ma, Q., Delestre, O., & Gourbesville, P. (2019). Water planning in a mixed land use Mediterranean area: Point-source abstraction and pollution scenarios by a numerical model of varying stream-aquifer regime. *Environmental Science and Pollution Research*, *26*(3), 2145–2166.

Du, M., Zavattero, E., Ma, Q., Delestre, O., Gourbesville, P., & Fouché, O. (2016). 3D hydraulic modeling of a complex alluvial aquifer for groundwater resource management. *Procedia Engineering*, *154*, 340–347.

Du, M., Zavattero, E., Ma, Q., Delestre, O., Gourbesville, P., & Fouché, O. (2018a). 3D modeling of a complex alluvial aquifer for efficient management – application to the lower valley of Var river, France. *La Houille Blanche*, *1*, Article 1. https://doi.org/10.1051/lhb/2018009

Du, M., Zavattero, E., Ma, Q., Delestre, O., Gourbesville, P., & Fouché, O. (2018b). 3D modeling of a complex alluvial aquifer for efficient management–application to the lower valley of Var river, France. *La Houille Blanche*, *1*, 60–69.

Eltner, A., Sardemann, H., & Grundmann, J. (2020). Technical Note: Flow velocity and discharge measurement in rivers using terrestrial and unmanned-aerial-vehicle imagery. *Hydrology and Earth System Sciences*, *24*(3), 1429–1445. https://doi.org/10.5194/hess-24-1429-2020

Emily, A. (2000a). *Recharge et fonctionnement d'un aquifère karstique tectoniquement compartimenté: Exemple des écailles subalpines de l'arc de Nice (Alpes-Maritimes, France)* [These de doctorat, Besançon]. http://theses.fr/2000BESA2060

Emily, A. (2000b). *Recharge et fonctionnement d'un aquifère karstique tectoniquement compartimenté: Exemple des écailles subalpines de l'arc de Nice (Alpes-Maritimes, France)* [PhD Thesis]. Besançon.

Emily, A., & Tennevin, G. (2009). La source karstique de Sainte-Thècle. Evolution des débits annuels depuis 1940 (Peillon, Alpes-Maritimes). *Ann. Mus. Hist. Nat*, *2*, 1–14.

Ewen, J., Parkin, G., & O'Connell, P. E. (2000). SHETRAN: Distributed River Basin Flow and Transport Modeling System. *Journal of Hydrologic Engineering*, *5*(3), 250–258. https://doi.org/10.1061/(ASCE)1084-0699(2000)5:3(250)

Farnoush, H., & Maghrebi, M. F. (2023). Discharge estimation and rating curve derivation, using satellite geometry data and isovel contours at Karun River, Iran. *Acta Geophysica*. https://doi.org/10.1007/s11600-022-00965-7

Frana, A. S. (2012). *Applicability of MIKE SHE to simulate hydrology in heavily tile drained agricultural land and effects of drainage characteristics on hydrology* [PhD Thesis]. Iowa State University.

Freeze, R. A., & Harlan, R. L. (1969). Blueprint for a physically-based, digitally-simulated hydrologic response model. *Journal of Hydrology*, *9*(3), 237–258. https://doi.org/10.1016/0022-1694(69)90020-1

Frénois, M. (2018). *Nice: Mais d'où viennent les galets de la promenade des Anglais?* [News]. https://www.20minutes.fr/nice/2398315-20181219-nice-o-viennent-galets-promenade-anglais

Game, P., Audra, P., & Gourbesville, P. (2022). Influence of Topography Resolution and Quality on Modeling Hydrological Processes in Paillon River Basin in the South of France. In P. Gourbesville & G. Caignaert (Eds.), *Advances in Hydroinformatics* (pp. 1223–1240). Springer Nature. https://doi.org/10.1007/978-981-19-1600-7_78

Game, P., Wang, M., Audra, P., & Gourbesville, P. (2023a). Challenges & solutions for deterministic hydraulic modelling in Mediterranean coastal catchment. Application to the lower Paillons River, Nice, France. *IOP Conference Series: Earth and Environmental Science*, *1136*(1), 012026. https://doi.org/10.1088/1755-1315/1136/1/012026

Game, P., Wang, M., Audra, P., & Gourbesville, P. (2023b). Flood modelling for a real-time decision support system of the covered Lower Paillons River, Nice, France. *Journal of Hydroinformatics*, jh2023181. https://doi.org/10.2166/hydro.2023.181

Goovaerts, P. (2000). Geostatistical approaches for incorporating elevation into the spatial interpolation of rainfall. *Journal of Hydrology*, *228*(1), 113–129. https://doi.org/10.1016/S0022-1694(00)00144-X

Gourbesville, P., Du, M., Zavattero, E., & Ma, Q. (2016). DSS architecture for water uses management. *Procedia Engineering*, *154*, 928–935.

Gourbesville, P., Du, M., Zavattero, E., Ma, Q., & Gaetano, M. (2018). Decision support system architecture for real-time water management. In *Advances in Hydroinformatics* (pp. 259–272). Springer.

Gourbesville, P., & Ghulami, M. (2022). *Deterministic Modelling for Extreme Flood Events-Application to the storm Alex*.

Gourbesville, P., Tallé, H., Ghulami, M., Andrès, L., & Gaetano, M. (2022). *Challenges for Realtime DSS: Experience from Aquavar System* (pp. 719–735). https://doi.org/10.1007/978-981-19-1600-7_45

Graham, D., & Butts, M. (2005). Flexible, integrated watershed modelling with MIKE SHE. In *Watershed Models* (pp. 245–272). https://doi.org/10.1201/9781420037432.ch10

Grenney, W. J., Wagenet, R. J., & Jurinak, J. J. (1979). An atmospheric—Terrestrial heavy metal transport model. II. Process equations. *Ecological Modelling*, *6*(3), 273–288. https://doi.org/10.1016/0304-3800(79)90016-4

Hauet, A., Jodeau, M., Le Coz, J., Marchand, B., Die Moran, A., Le Boursicaud, R., & Dramais, G. (2013). Application de la méthode LSPIV pour la mesure de champs de vitesse, et de débits de crue sur modèle réduit et en rivière. *Journées de l'hydraulique*, *35*(1), 1–8. https://www.persee.fr/doc/jhydr_0000-0001_2013_act_35_1_1290

Henriksen, H. J., Roberts, M. J., van der Keur, P., Harjanne, A., Egilson, D., & Alfonso, L. (2018). Participatory early warning and monitoring systems: A Nordic framework for web-based flood risk management. *International Journal of Disaster Risk Reduction*, *31*, 1295–1306. https://doi.org/10.1016/j.ijdrr.2018.01.038

Jodeau, M., Hauet, A., Bodart, G., Le Coz, J., & Faure, J.-B. (2022). *Fudaa-LSPIV Version 1.9.2 Manuel utilisateur*. https://forge.irstea.fr/attachments/download/3031/User%20Manual%20Fudaa-LSPIV%201.9.2.pdf

Khakbaz, B., Imam, B., Hsu, K., & Sorooshian, S. (2012). From lumped to distributed via semi-distributed: Calibration strategies for semi-distributed hydrologic models. *Journal of Hydrology*, *418–419*, 61–77. https://doi.org/10.1016/j.jhydrol.2009.02.021

Khan, S., Khan, A. U., Khan, M., Khan, F. A., Khan, S., & Khan, J. (2023). Intercomparison of SWAT and ANN techniques in simulating streamflows in the Astore Basin of the Upper

Indus. *Water Science and Technology*, *88*(7), 1847–1862. https://doi.org/10.2166/wst.2023.299

Kristensen, K. J., & Jensen, S. E. (1975). A model for estimating actual evapotranspiration from potential evapotranspiration. *Hydrology Research*, *6*(3), 170–188. https://doi.org/10.2166/nh.1975.0012

Lanini, S., Ladouche, B., Dewandel, B., Ibba, M., Bailly-Comte, V., & Genevier, M. (2022). *Impact of the Alex storm on the exchanges between the Roya River and its alluvial aquifer*.

Le Bas, C. (2022). *Carte de la profondeur du sol issue de la Base de Données Géographique des Sols de France* [dataset]. Recherche Data Gouv. https://doi.org/10.15454/7ZDND6

Le Coz, J., Hauet, A., Pierrefeu, G., Dramais, G., & Camenen, B. (2010). Performance of image-based velocimetry (LSPIV) applied to flash-flood discharge measurements in Mediterranean rivers. *Journal of Hydrology*, *394*(1), 42–52. https://doi.org/10.1016/j.jhydrol.2010.05.049

Le Gouz de Saint Seine, J. (1995). *Monographie hydrologique et hydraulique du Paillon de Nice en vue de la gestion du risque inondation* [These de doctorat, Grenoble INPG]. http://theses.fr/1995INPG0053

Li, J., Zhang, B., Li, Y., & Li, H. (2018). Simulation of Rain Garden Effects in Urbanized Area Based on Mike Flood. *Water*, *10*, 860. https://doi.org/10.3390/w10070860

Lionello, P., Malanotte-Rizzoli, P., Boscolo, R., Alpert, P., Artale, V., Li, L., Luterbacher, J., May, W., Trigo, R., Tsimplis, M., Ulbrich, U., & Xoplaki, E. (2006). The Mediterranean climate: An overview of the main characteristics and issues. In P. Lionello, P. Malanotte-Rizzoli, & R. Boscolo (Eds.), *Developments in Earth and Environmental Sciences* (Vol. 4, pp. 1–26). Elsevier. https://doi.org/10.1016/S1571-9197(06)80003-0

Liong, S.-Y., Lim, W.-H., & Paudyal, G. N. (2000). River Stage Forecasting in Bangladesh: Neural Network Approach. *Journal of Computing in Civil Engineering*, *14*(1), 1–8. https://doi.org/10.1061/(ASCE)0887-3801(2000)14:1(1)

Liu, J., Liu, T., Bao, A., De Maeyer, P., Feng, X., Miller, S. N., & Chen, X. (2016). Assessment of Different Modelling Studies on the Spatial Hydrological Processes in an Arid Alpine

Catchment. *Water Resources Management*, *30*(5), 1757–1770. https://doi.org/10.1007/s11269-016-1249-2

Lu, J., Yang, X., & Wang, J. (2023). Velocity Vector Estimation of Two-Dimensional Flow Field Based on STIV. *Sensors*, *23*(2), Article 2. https://doi.org/10.3390/s23020955

Ma, Q. (2018). *Modélisation hydrologique déterministe pour les systèmes d'aide à la décision en temps réel: Application au bassin versant Var, France* [These de doctorat, Université Côte d'Azur (ComUE)]. https://www.theses.fr/2018AZUR4015

Ma, Q., Abily, M., Du, M., Gourbesville, P., & Fouché, O. (2020). Integrated Groundwater Resources Management: Spatially-Nested Modelling Approach for Water Cycle Simulation. *Water Resources Management*, *34*(4), 1319–1333. https://doi.org/10.1007/s11269-020-02504-9

Ma, Q., & Gourbesville, P. (2020). *Integration of high resolution models in real time decision support system, application of AquaVar DSS*. https://doi.org/10.3850/38WC092019-0398

Ma, Q., Gourbesville, P., & Gaetano, M. (2020). Aquavar: Decision Support System for Surface and Groundwater Management at the Catchment Scale. In P. Gourbesville & G. Caignaert (Eds.), *Advances in Hydroinformatics* (pp. 19–28). Springer. https://doi.org/10.1007/978-981-15-5436-0_2

Ma, Q., Zavattero, E., Du, M., Vo, N. D., & Gourbesville, P. (2016). Assessment of high resolution topography impacts on deterministic distributed hydrological model in extreme rainfall-runoff simulation. *Procedia Engineering*, *154*, 601–608.

Mair, A., & Fares, A. (2011). Comparison of Rainfall Interpolation Methods in a Mountainous Region of a Tropical Island. *Journal of Hydrologic Engineering*, *16*(4), 371–383. https://doi.org/10.1061/(ASCE)HE.1943-5584.0000330

Mairie de Nice. (2022). Paillon—Nice Ensemble. *https://nice-ensemble.fr/*. https://nice-ensemble.fr/actualites/paillon/

Meteo−France. (2023a). *CLIMAT HD par Météo-France*. https://meteofrance.com/climathd

Meteo−France. (2023b). *Records—6 min à 12 h—Pluies extrêmes en France métropolitaine*. http://pluiesextremes.meteo.fr/france-metropole/Records-6-min-a-12-h.html

Moisan, L., & Stival, B. (2004). A Probabilistic Criterion to Detect Rigid Point Matches Between Two Images and Estimate the Fundamental Matrix. *International Journal of Computer Vision*, *57*, 201–218. https://doi.org/10.1023/B:VISI.0000013094.38752.54

Noori, N., & Kalin, L. (2016). Coupling SWAT and ANN models for enhanced daily streamflow prediction. *Journal of Hydrology*, *533*, 141–151. https://doi.org/10.1016/j.jhydrol.2015.11.050

Observatoire des Territoires, F. (2021). *Nombre d'Arrêtés de Catastrophes Naturelles publiés au J.O. | L'Observatoire des Territoires* [Public]. https://www.observatoire-des-territoires.gouv.fr/nombre-darretes-de-catastrophes-naturelles-publies-au-jo

Oyallon, E., & Rabin, J. (2015). An Analysis of the SURF Method. *Image Processing On Line*, *5*, 176–218. https://doi.org/10.5201/ipol.2015.69

Payrastre, O., Nicolle, P., Bonnifait, L., Brigode, P., Astagneau, P., Baise, A., Belleville, A., Bouamara, N., Bourgin, F., & Breil, P. (2022). *The 2 October 2020 Alex storm in south-eastern France: A contribution of the scientific community to the flood peak discharges estimation*.

Pietri, A. (1955). Le Paillon, torrent de Nice. Essai d'étude d'un cours d'eau des Préalpes méditerranéennes. Première partie: Étude physique. L'édifice structural du bassin da Paillon. *Thèse Soutenue En 1955 Devant La Faculté Des Lettres Et Des Sciences D'aix-En-Provence*, 12. https://www.departement06.fr/documents/Import/decouvrir-les-am/recherchesregionales5_01.pdf

Pline, C. (1991a). *Contribution à l'étude géologique, hydrogéologique et géotechnique de la basse-plaine alluviale du Paillon (Alpes-Maritimes, France)* [These de doctorat, Nice]. http://www.theses.fr/1991NICE4471

Pline, C. (1991b). Contribution à l'étude géologique, hydrogéologique et géotechnique de la basse-plaine alluviale du Paillon (Alpes-Maritimes, France) [Thesis, Nice]. In *Http://www.theses.fr*. http://www.theses.fr/1991NICE4471

Pons, F., Bonnifait, L., Criado, D., Payrastre, O., Billaud, F., Brigode, P., Fouchier, C., Gourbesville, P., Kuss, D., & Le Nouveau, N. (2022). *Towards a hydrological consensus about the 2nd–3rd*

October 2020 ALEX storm event in the French "Alpes Maritimes" region. Copernicus Meetings.

Refsgaard, J. C. (1997). Parameterisation, calibration and validation of distributed hydrological models. *Journal of Hydrology*, *198*(1), 69–97. https://doi.org/10.1016/S0022-1694(96)03329-X

Ribes, A., Thao, S., Vautard, R., Dubuisson, B., Somot, S., Colin, J., Planton, S., & Soubeyroux, J.-M. (2019). Observed increase in extreme daily rainfall in the French Mediterranean. *Climate Dynamics*, *52*. https://doi.org/10.1007/s00382-018-4179-2

Rind, D., Goldberg, R., Hansen, J., Rosenzweig, C., & Ruedy, R. (1990). Potential evapotranspiration and the likelihood of future drought. *Journal of Geophysical Research: Atmospheres*, *95*(D7), 9983–10004. https://doi.org/10.1029/JD095iD07p09983

Roe, P. L. (1981). Approximate Riemann solvers, parameter vectors, and difference schemes. *Journal of Computational Physics*, *43*(2), 357–372. https://doi.org/10.1016/0021-9991(81)90128-5

Sabbion, P. (2016). Paillon River, France–Opportunities and Policies. *Urban Sustainability and River Restoration: Green and Blue Infrastructure*, 235.

Safege. (2009). *Le Contrat de Rivière des Paillons*. https://www.gesteau.fr/sites/default/files/contratrivierepaillons_dossierdefinitif_2009.pdf

Safege. (2012). *Mise à jour du modèle hydraulique et hydrologique seconde phase*. MNCA; MNCA.

Safege. (2013). *Mise à jour du modèle hydrologique et hydraulique de Nice. Phase 3: Modélisation 2D du risque de ruissellement urbain*. MNCA; MNCA.

Safege. (2015). *Etude hydraulique de modélisation des écoulements de temps de pluie sur le parcours de la ligne 2 projetée du tramway de Nice. Etat actuel et incidences. Modélisation de l'état actuel sur les secteurs de Cassin/Carras, Nikaia et Grosso/Magnan.* MNCA; MNCA.

Salvan, L. (2017). *Connaissances et modélisations pour la gestion du pluvial en zone urbaine: Application à la ville de Nice* [These de doctorat, Université Côte d'Azur (ComUE)]. https://www.theses.fr/2017AZUR4124

Salvan, L., Abily, M., Gourbesville, P., & Schoorens, J. (2016). Drainage System and Detailed Urban Topography: Towards Operational 1D-2D Modelling for Stormwater Management. *Procedia Engineering*, *154*, 890–897. https://doi.org/10.1016/j.proeng.2016.07.469

Salvan, L., Zavattero, E., Delestre, O., & Gourbesville, P. (2018). Analysis of Flood and Dry Threshold Definition in Two-Dimensional Hydrodynamic Flood Modeling Tools. In *Advances in Hydroinformatics* (pp. 675–687). Springer.

Schwarz, V., & Soubeyroux, J.-M. (2022). Quel climat en France en 2050 et 2100 ? *Annales des Mines - Responsabilité et environnement*, *106*(2), 27–31. https://doi.org/10.3917/re1.106.0027

Sekulić, G., Ivković, M., & Ćipranić, I. (2017). Modelling of hydrological processes in the catchment area of lake Skadar. *Tehnički Vjesnik*, *24*(Supplement 2), 427–434. https://doi.org/10.17559/TV-20151120230958

Shepard, D. (1968). A two-dimensional interpolation function for irregularly-spaced data. *Proceedings of the 1968 23rd ACM National Conference*, 517–524. https://doi.org/10.1145/800186.810616

Shivhare, N., Dikshit, P. K. S., & Dwivedi, S. B. (2018). A Comparison of SWAT Model Calibration Techniques for Hydrological Modeling in the Ganga River Watershed. *Engineering*, *4*(5), 643–652. https://doi.org/10.1016/j.eng.2018.08.012

Shuttleworth, W. J., & Wallace, J. S. (1985). Evaporation from sparse crops-an energy combination theory. *Quarterly Journal of the Royal Meteorological Society*, *111*(469), 839–855. https://doi.org/10.1002/qj.49711146910

SIP, AERMEC, ANTEAGROUP, IDEALP, & REGION PACA. (2016). *Etude de restauration de la continuité écologique des Paillons—Phase 1: Diagnostic des enjeux—Phase 2: Diagnostic des obstacles. Syndicat intercommunal des Paillons*. Agence de l'eau Rhône Méditerranée Corse. https://www.documentation.eauetbiodiversite.fr/notice/etude-de-restauration-de-la-continuite-ecologique-des-paillons-phase-1-diagnostic-des-enjeux-phase-20

Stojković, M., Kostić, S., Plavšić, J., & Prohaska, S. (2017). A joint stochastic-deterministic approach for long-term and short-term modelling of monthly flow rates. *Journal of Hydrology*, *544*, 555–566. https://doi.org/10.1016/j.jhydrol.2016.11.025

Sun, G., Wei, X., Hao, L., Sanchis, M. G., Hou, Y., Yousefpour, R., Tang, R., & Zhang, Z. (2023). Forest hydrology modeling tools for watershed management: A review. *Forest Ecology and Management*, *530*, 120755. https://doi.org/10.1016/j.foreco.2022.120755

Tauro, F., Piscopia, R., & Grimaldi, S. (2019). PTV-Stream: A simplified particle tracking velocimetry framework for stream surface flow monitoring. *CATENA*, *172*, 378–386. https://doi.org/10.1016/j.catena.2018.09.009

Tennevin, G., Emily, A., & Mangan, C. (2017). *Etude hydrogéologique des ressources en eau stratégiques superficielles et souterraines du bassin-versant des Paillons—Rapport de phase I H2EA*. https://www.rhone-mediterranee.eaufrance.fr/eau-potable-et-assainissement/eau-potable/ressources-strategiques-pour-laep

Tennevin, G., Emily, A., & Mangan, C. (2018). *Etude hydrogéologique des ressources en eau stratégiques superficielles et souterraines du bassin-versant des Paillons—Rapport de phase II H2EA*. https://www.rhone-mediterranee.eaufrance.fr/eau-potable-et-assainissement/eau-potable/ressources-strategiques-pour-laep

Tennevin, G., Emily, A., & Mangan, C. (2019a). *Etude hydrogéologique des ressources en eau stratégiques superficielles et souterraines du bassin-versant des Paillons—Annexes H2EA*. https://www.rhone-mediterranee.eaufrance.fr/eau-potable-et-assainissement/eau-potable/ressources-strategiques-pour-laep

Tennevin, G., Emily, A., & Mangan, C. (2019b). *Etude hydrogéologique des ressources en eau stratégiques superficielles et souterraines du bassin-versant des Paillons—Rapport de phase III H2EA*. https://www.rhone-mediterranee.eaufrance.fr/eau-potable-et-assainissement/eau-potable/ressources-strategiques-pour-laep

Verruijt, A. (1970). *Theory of groundwater flow. Macmillan Education UK (Ed.), 182 pages.*

Vo, N. D. (2015). *Deterministic hydrological modelling for flood risk assessment and climate change in large catchment. Application to Vu Gia Thu Bon catchment, Vietnam* [Phdthesis, Université Nice Sophia Antipolis]. https://theses.hal.science/tel-01245061

Wacheux, C. (2022). *Ensemble strategy for decision-support tool: A case study of the Alex storm in 2020 in la Roya and la Vésubie valleys*. Copernicus Meetings.

Wang, Q., Li, S., Jia, P., Qi, C., & Ding, F. (2013). A Review of Surface Water Quality Models. *The Scientific World Journal*, *2013*, e231768. https://doi.org/10.1155/2013/231768

Wardropper, C., & Brookfield, A. (2022). Decision-support systems for water management. *Journal of Hydrology*, *610*, 127928. https://doi.org/10.1016/j.jhydrol.2022.127928

Wool, T., Ambrose, R. B., Martin, J. L., & Comer, A. (2020). WASP 8: The Next Generation in the 50-year Evolution of USEPA's Water Quality Model. *Water*, *12*(5), Article 5. https://doi.org/10.3390/w12051398

Yan, J., & Smith, K. R. (1994). Simulation of Integrated Surface Water and Ground Water Systems—Model Formulation1. *JAWRA Journal of the American Water Resources Association*, *30*(5), 879–890. https://doi.org/10.1111/j.1752-1688.1994.tb03336.x

Yazdani, M., Zarate, P., Coulibaly, A., & Zavadskas, E. K. (2017). A group decision making support system in logistics and supply chain management. *Expert Systems with Applications*, *88*, 376–392. https://doi.org/10.1016/j.eswa.2017.07.014

Zavattero, E. (2019). *Intégration de modélisation à surface libre dans un système d'aide à la décision: Application à la Basse Vallée du Var, France* [PhD Thesis]. Université Côte d'Azur (ComUE).

Zavattero, E., Du, M., Ma, Q., Delestre, O., & Gourbesville, P. (2016). 2d sediment transport modelling in high energy river–application to var river, France. *Procedia Engineering*, *154*, 536–543.

Zavattero, E., Zhai, Y., Qin, M., Du, M., Gourbesville, P., & Delestre, O. (2018). 2D Surface Water Quality Model: A Forecasting Tool for Accidental Pollution in Urban River—Application to the Var River, France. In *Advances in Hydroinformatics* (pp. 285–299). Springer.

Zhai, Z., Martínez, J. F., Beltran, V., & Martínez, N. L. (2020). Decision support systems for agriculture 4.0: Survey and challenges. *Computers and Electronics in Agriculture*, *170*, 105256. https://doi.org/10.1016/j.compag.2020.105256

Appendix

List of appendices

Appendix 1 6-mn rainfall correlation among different stations (2010-2021)

	6033002	**6059003**	**6074005**	**6077006**	**6088001**	**6091003**	**6136005**	**6075007**	**6088007**	**ABA**	**PDR**	**LAG**	**MDP**	**CON**	**BAI**	**ESC**	**COA**	**LUC**
6033002	1.00																	
6059003	0.33	1.00																
6074005	0.33	0.26	1.00															
6077006	0.37	0.30	0.52	1.00														
6088001	0.32	0.34	0.21	0.22	1.00													
6091003	0.32	0.57	0.30	0.38	0.26	1.00												
6136005	0.36	0.40	0.38	0.44	0.27	0.50	1.00											
6075007	0.56	0.31	0.38	0.41	0.28	0.32	0.37	1.00										
6088007	0.43	0.51	0.25	0.29	0.41	0.42	0.37	0.35	1.00									
ABA	0.17	0.23	0.14	0.16	0.18	0.23	0.20	0.16	0.27	1.00								
PDR	0.23	0.25	0.19	0.21	0.17	0.28	0.27	0.22	0.28	0.30	1.00							
LAG	0.19	0.35	0.17	0.20	0.16	0.34	0.26	0.19	0.24	0.26	0.29	1.00						
MDP	0.22	0.33	0.21	0.23	0.17	0.37	0.31	0.23	0.28	0.27	0.52	0.47	1.00					
CON	0.27	0.30	0.24	0.27	0.20	0.34	0.35	0.28	0.29	0.30	0.47	0.38	0.47	1.00				
BAI	0.24	0.27	0.23	0.25	0.17	0.33	0.37	0.25	0.24	0.22	0.31	0.34	0.45	0.45	1.00			
ESC	0.24	0.26	0.23	0.27	0.17	0.29	0.33	0.26	0.23	0.23	0.33	0.32	0.43	0.53	0.51	1.00		
COA	0.28	0.24	0.29	0.32	0.19	0.28	0.34	0.31	0.24	0.21	0.31	0.26	0.31	0.43	0.35	0.44	1.00	
LUC	0.26	0.25	0.27	0.32	0.17	0.29	0.35	0.27	0.24	0.19	0.27	0.28	0.34	0.40	0.39	0.49	0.47	1.00

Appendix 2 Hourly rainfall correlation among different stations (2010-2021)

	6033002	**6059003**	**6074005**	**6077006**	**6088001**	**6091003**	**6136005**	**6075007**	**6088007**	**ABA**	**PDR**	**LAG**	**MDP**	**CON**	**BAI**	**ESC**	**COA**	**LUC**
6033002	1.00																	
6059003	0.60	1.00																
6074005	0.60	0.46	1.00															
6077006	0.65	0.51	0.80	1.00														
6088001	0.54	0.64	0.37	0.40	1.00													
6091003	0.59	0.79	0.51	0.59	0.54	1.00												
6136005	0.65	0.64	0.64	0.69	0.48	0.73	1.00											
6075007	0.80	0.55	0.68	0.71	0.48	0.57	0.64	1.00										
6088007	0.68	0.80	0.46	0.50	0.67	0.71	0.63	0.58	1.00									
ABA	0.38	0.51	0.32	0.35	0.39	0.48	0.44	0.35	0.51	1.00								
PDR	0.41	0.46	0.35	0.39	0.32	0.49	0.48	0.39	0.47	0.50	1.00							
LAG	0.39	0.57	0.35	0.40	0.34	0.59	0.50	0.38	0.48	0.54	0.49	1.00						
MDP	0.39	0.54	0.37	0.41	0.32	0.58	0.52	0.40	0.48	0.51	0.79	0.61	1.00					
CON	0.50	0.57	0.47	0.52	0.39	0.62	0.63	0.51	0.54	0.56	0.65	0.59	0.64	1.00				
BAI	0.46	0.52	0.46	0.50	0.35	0.60	0.64	0.48	0.48	0.49	0.54	0.58	0.64	0.73	1.00			
ESC	0.47	0.50	0.46	0.51	0.33	0.55	0.61	0.48	0.46	0.47	0.55	0.54	0.60	0.77	0.74	1.00		
COA	0.53	0.47	0.55	0.60	0.35	0.53	0.61	0.56	0.46	0.42	0.50	0.47	0.50	0.69	0.62	0.70	1.00	
LUC	0.49	0.46	0.52	0.58	0.33	0.52	0.61	0.51	0.43	0.42	0.47	0.48	0.51	0.66	0.65	0.70	0.72	1.00

Appendix 3 Daily rainfall correlation among different stations (2010-2021)

	6033002	**6059003**	**6074005**	**6077006**	**6088001**	**6091003**	**6136005**	**6075007**	**6088007**	**ABA**	**PDR**	**LAG**	**MDP**	**CON**	**BAI**	**ESC**	**COA**	**LUC**
6033002	1.00																	
6059003	0.85	1.00																
6074005	0.79	0.72	1.00															
6077006	0.85	0.75	0.93	1.00														
6088001	0.81	0.89	0.66	0.70	1.00													
6091003	0.86	0.89	0.80	0.85	0.78	1.00												
6136005	0.87	0.86	0.89	0.90	0.76	0.90	1.00											
6075007	0.93	0.84	0.88	0.90	0.79	0.85	0.90	1.00										
6088007	0.88	0.93	0.72	0.75	0.89	0.86	0.84	0.84	1.00									
ABA	0.74	0.79	0.63	0.67	0.76	0.75	0.74	0.72	0.80	1.00								
PDR	0.72	0.70	0.62	0.66	0.65	0.71	0.70	0.69	0.74	0.63	1.00							
LAG	0.81	0.89	0.73	0.77	0.79	0.90	0.86	0.81	0.86	0.77	0.70	1.00						
MDP	0.72	0.76	0.67	0.69	0.67	0.78	0.76	0.73	0.75	0.65	0.92	0.76	1.00					
CON	0.89	0.86	0.82	0.87	0.80	0.91	0.90	0.88	0.88	0.76	0.74	0.86	0.77	1.00				
BAI	0.82	0.80	0.81	0.82	0.71	0.85	0.90	0.84	0.80	0.70	0.67	0.85	0.76	0.87	1.00			
ESC	0.88	0.84	0.80	0.84	0.77	0.86	0.89	0.88	0.84	0.72	0.71	0.84	0.75	0.90	0.85	1.00		
COA	0.88	0.78	0.88	0.92	0.71	0.85	0.89	0.91	0.78	0.68	0.68	0.80	0.72	0.88	0.85	0.87	1.00	
LUC	0.88	0.79	0.86	0.90	0.73	0.85	0.91	0.89	0.80	0.70	0.68	0.80	0.72	0.88	0.87	0.88	0.91	1.00

Appendix 4 Monthly rainfall correlation among different stations (2010-2021)

	6033002	**6059003**	**6074005**	**6077006**	**6088001**	**6091003**	**6136005**	**6075007**	**6088007**	**ABA**	**PDR**	**LAG**	**MDP**	**CON**	**BAI**	**ESC**	**COA**	**LUC**
6033002	1.00																	
6059003	0.95	1.00																
6074005	0.87	0.84	1.00															
6077006	0.92	0.87	0.95	1.00														
6088001	0.93	0.95	0.83	0.87	1.00													
6091003	0.95	0.95	0.89	0.92	0.92	1.00												
6136005	0.95	0.94	0.92	0.94	0.91	0.95	1.00											
6075007	0.97	0.94	0.91	0.92	0.91	0.94	0.95	1.00										
6088007	0.96	0.96	0.85	0.88	0.96	0.93	0.93	0.95	1.00									
ABA	0.64	0.68	0.54	0.59	0.61	0.64	0.63	0.62	0.64	1.00								
PDR	0.58	0.57	0.53	0.54	0.54	0.56	0.53	0.56	0.57	0.48	1.00							
LAG	0.77	0.84	0.69	0.74	0.74	0.82	0.78	0.76	0.76	0.73	0.61	1.00						
MDP	0.64	0.67	0.59	0.60	0.61	0.66	0.62	0.64	0.63	0.57	0.92	0.75	1.00					
CON	0.81	0.82	0.76	0.81	0.75	0.85	0.81	0.79	0.78	0.68	0.66	0.89	0.76	1.00				
BAI	0.72	0.75	0.72	0.72	0.64	0.77	0.76	0.74	0.70	0.65	0.57	0.87	0.74	0.88	1.00			
ESC	0.81	0.82	0.74	0.78	0.72	0.80	0.80	0.83	0.77	0.71	0.67	0.89	0.77	0.90	0.86	1.00		
COA	0.76	0.74	0.77	0.80	0.65	0.78	0.77	0.79	0.70	0.65	0.65	0.87	0.75	0.90	0.89	0.92	1.00	
LUC	0.79	0.77	0.76	0.79	0.67	0.80	0.79	0.79	0.73	0.69	0.62	0.86	0.72	0.91	0.90	0.92	0.95	1.00

Appendix 5 Different types of aquifers in the Quaternary alluvium in Nice (Pline, 1991)

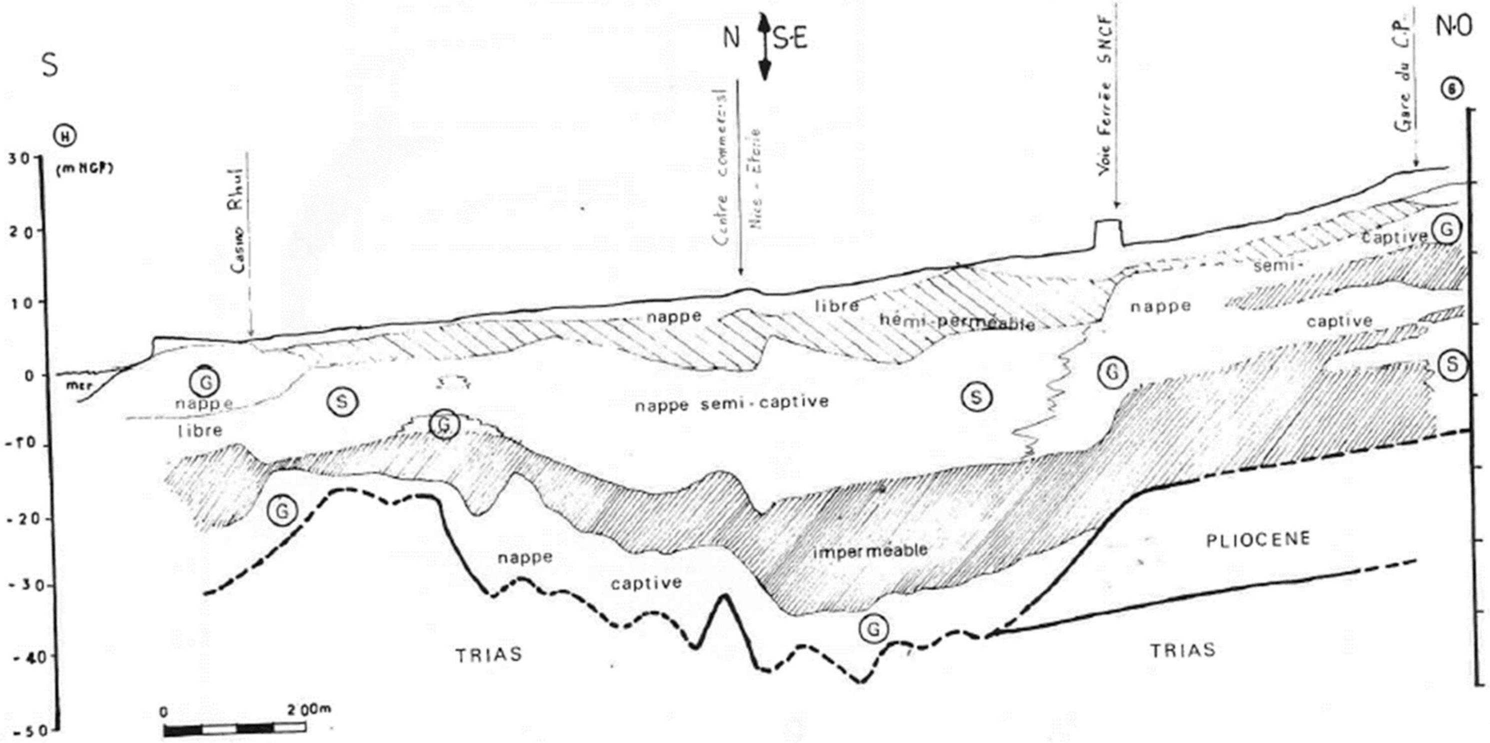

AQUIFERES ET TYPES DE NAPPES DES TERRAINS QUATERNAIRES / SECTEUR NICE - CENTRE

— **Figure 3.3** —

Appendix 6 Map of tracings of drainage network in the Karst layers of the Paillons catchment (Tennevin et al., 2017)

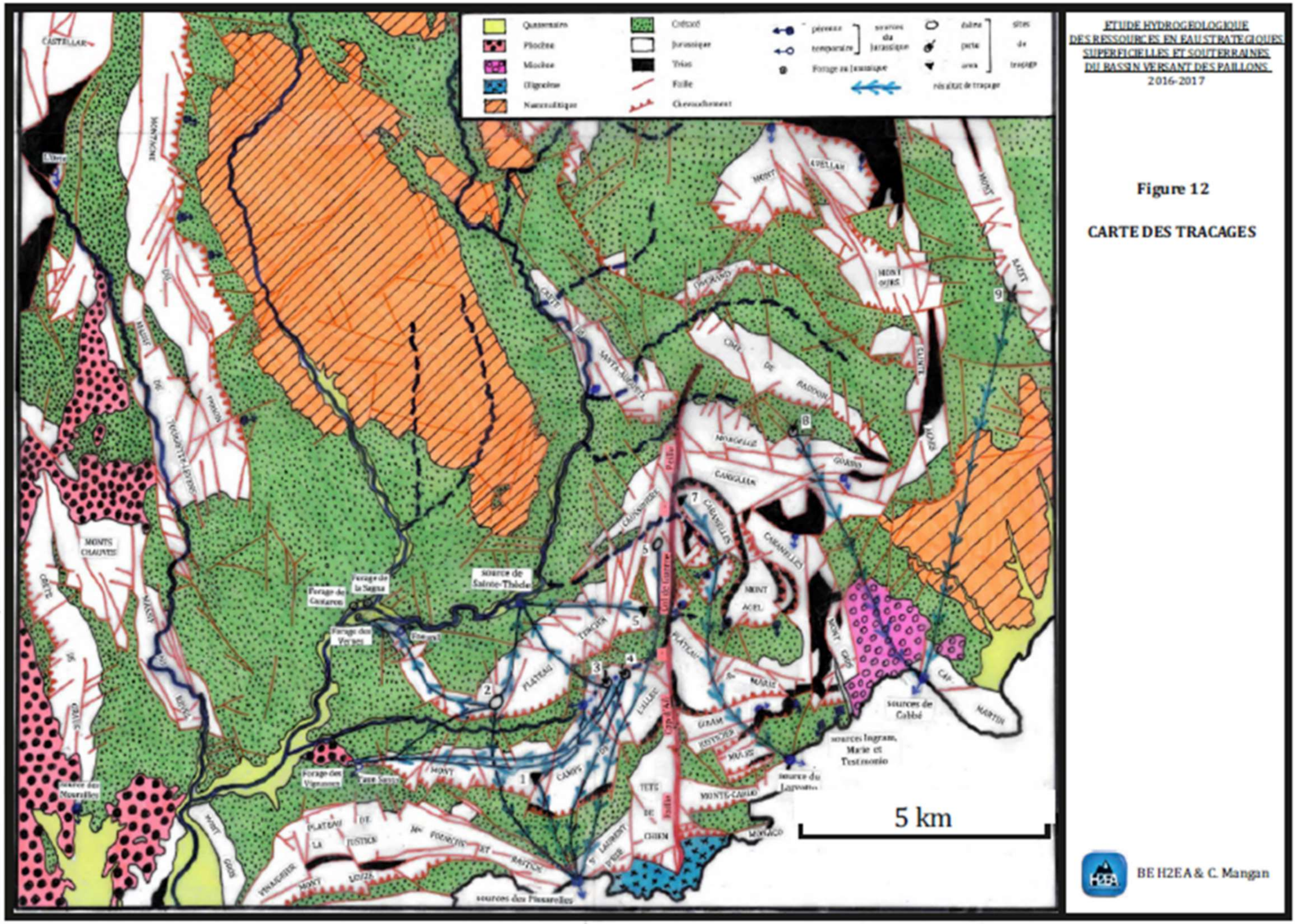

Appendix 7 Geological map and groundwater natural outlets and extraction points in the Paillons catchment (Tennevin et al., 2017)

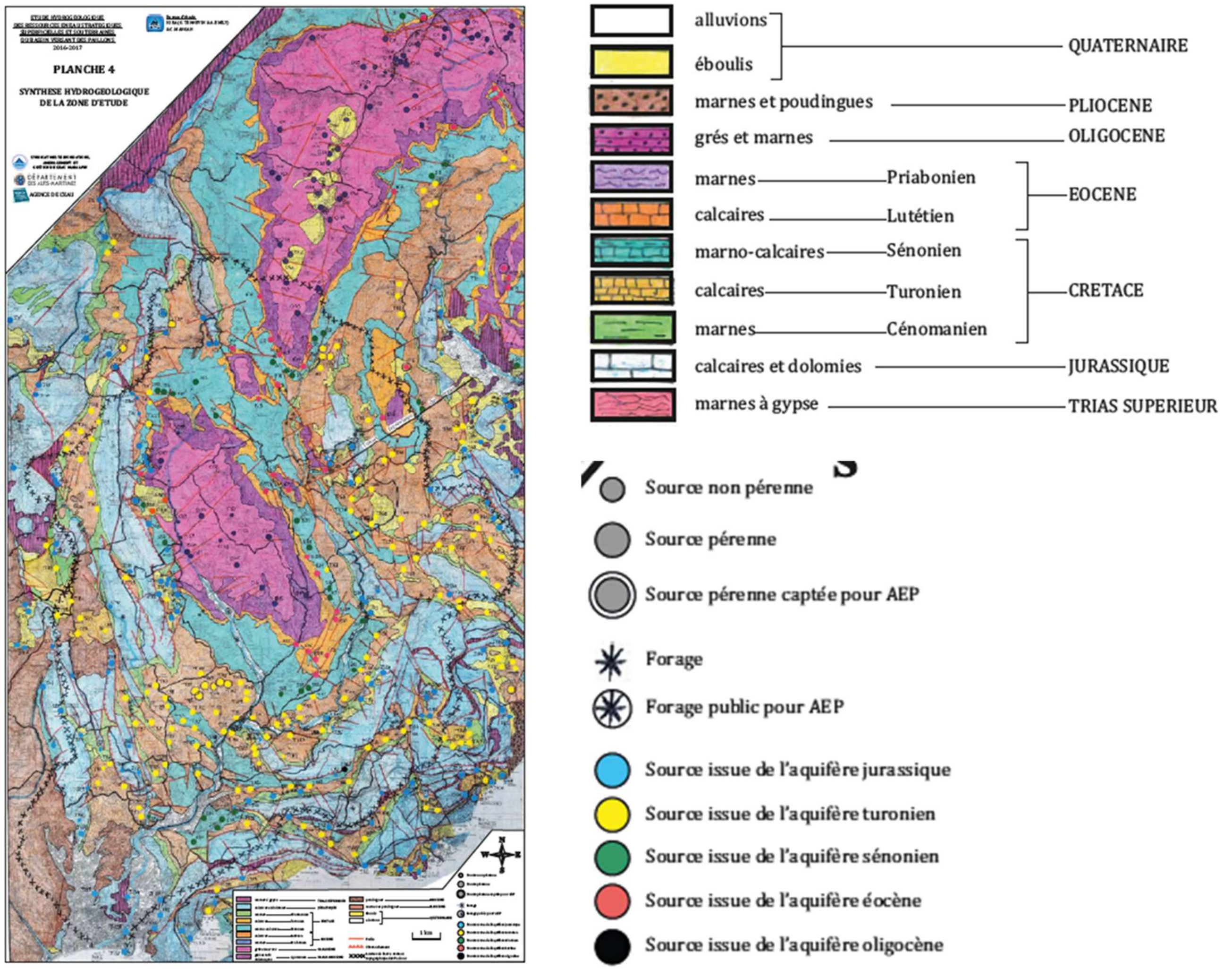

Appendix 8 NeuroShell 2 Set up (https://neuroshell-2.software.informer.com/1.5/)

NeuroShell 2 is the neural network product targeted towards computer science.

Open the software and define a new problem in the file tab

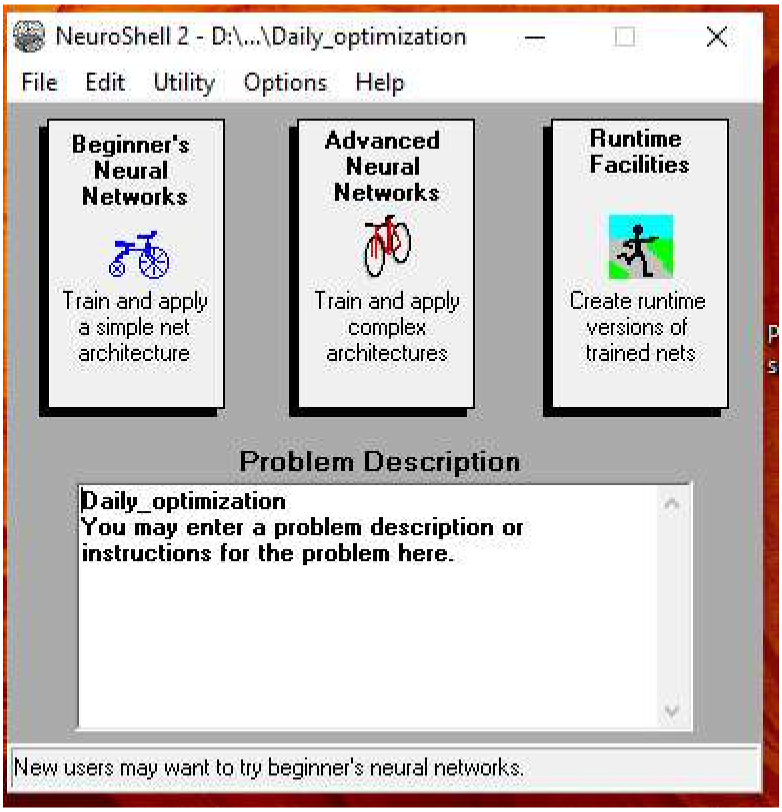

Daily_optimization
You may enter a problem description or instructions for the problem here.

New users may want to try beginner's neural networks.

Select Advanced Neural Networks

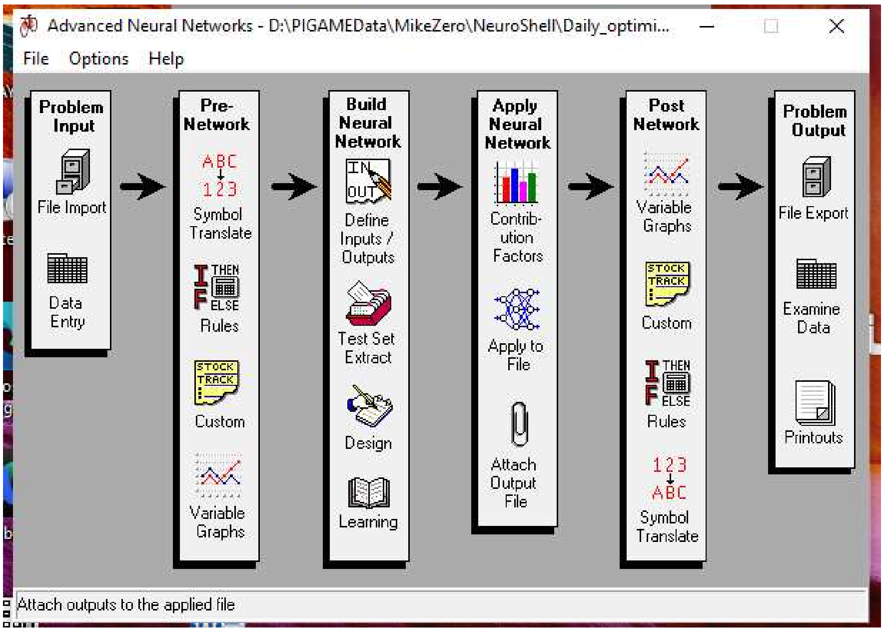

Attach outputs to the applied file

In problem Input use File import or Data entry to add the data table containing model results and observed data:

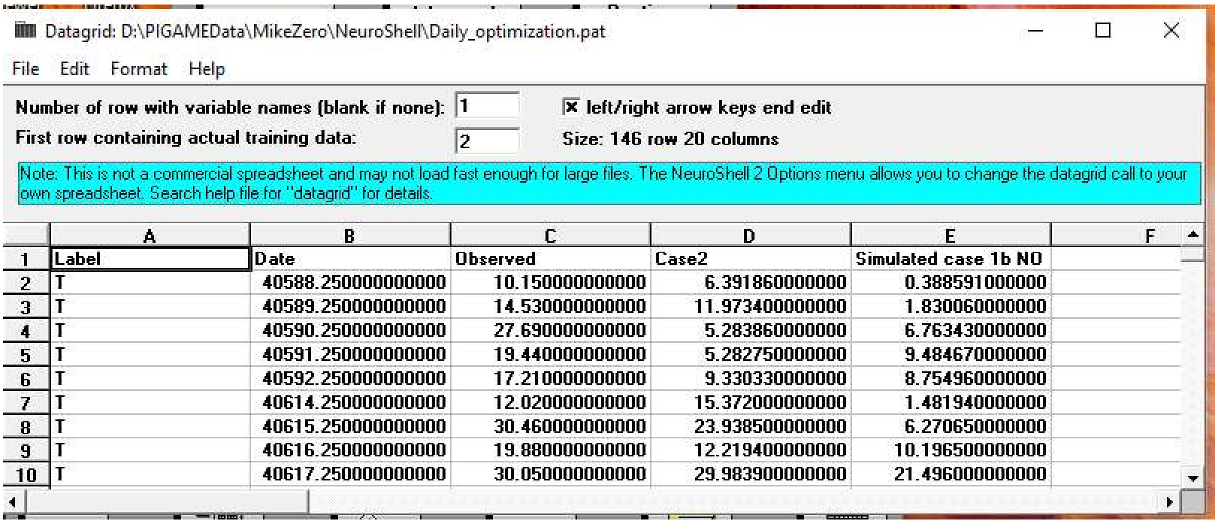

Number of row with variable names (blank if none): 1

First row containing actual training data: 2

☒ left/right arrow keys end edit

Size: 146 row 20 columns

Note: This is not a commercial spreadsheet and may not load fast enough for large files. The NeuroShell 2 Options menu allows you to change the datagrid call to your own spreadsheet. Search help file for "datagrid" for details.

	A	B	C	D	E	F
1	Label	Date	Observed	Case2	Simulated case 1b NO	
2	T	40588.250000000000	10.150000000000	6.391860000000	0.388591000000	
3	T	40589.250000000000	14.530000000000	11.973400000000	1.830060000000	
4	T	40590.250000000000	27.690000000000	5.283860000000	6.763430000000	
5	T	40591.250000000000	19.440000000000	5.282750000000	9.484670000000	
6	T	40592.250000000000	17.210000000000	9.330330000000	8.754960000000	
7	T	40614.250000000000	12.020000000000	15.372000000000	1.481940000000	
8	T	40615.250000000000	30.460000000000	23.938500000000	6.270650000000	
9	T	40616.250000000000	19.880000000000	12.219400000000	10.196500000000	
10	T	40617.250000000000	30.050000000000	29.983900000000	21.496000000000	

Define inputs/Outputs in Build Neural Network:

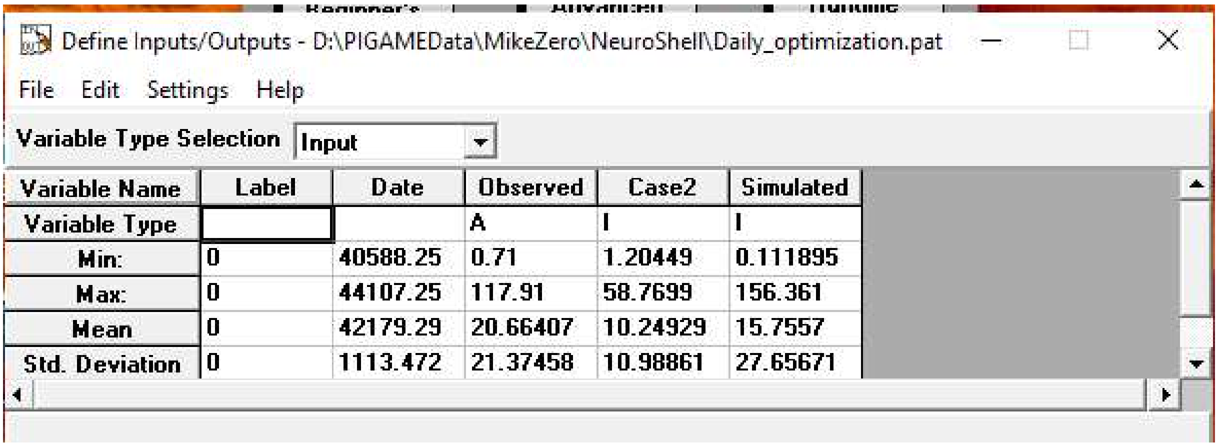

Variable Type Selection: Input

Variable Name	Label	Date	Observed	Case2	Simulated
Variable Type			A	I	I
Min:	0	40588.25	0.71	1.20449	0.111895
Max:	0	44107.25	117.91	58.7699	156.361
Mean	0	42179.29	20.66407	10.24929	15.7557
Std. Deviation	0	1113.472	21.37458	10.98861	27.65671

In test set extract by row marker the Training and Production sets:

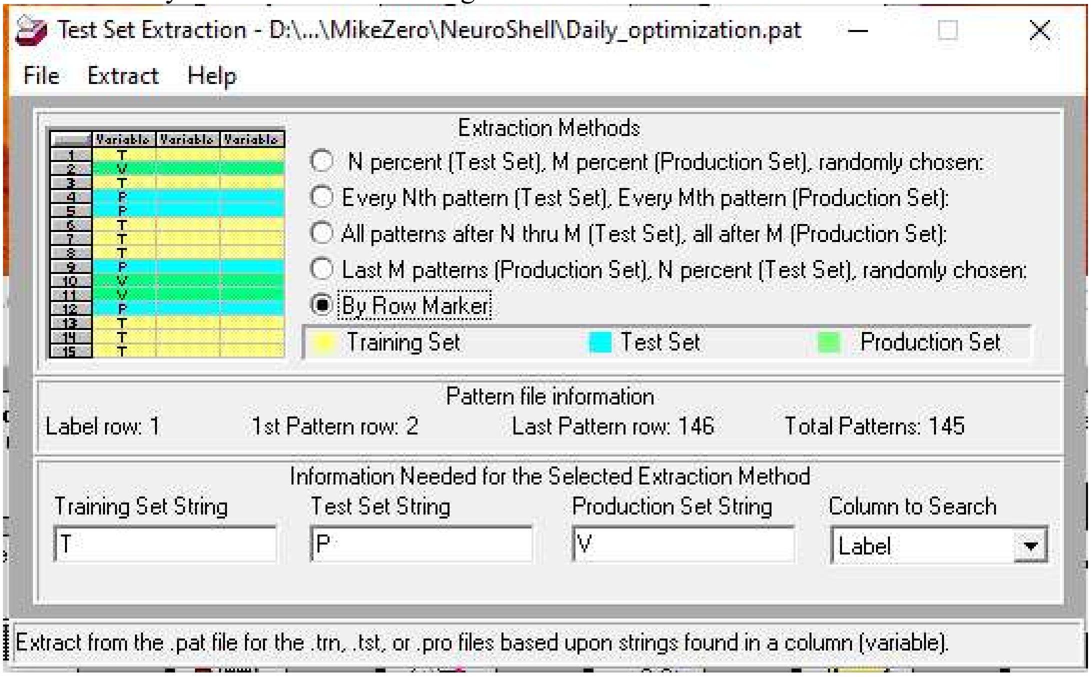

Extraction Methods

○ N percent (Test Set), M percent (Production Set), randomly chosen:

○ Every Nth pattern (Test Set), Every Mth pattern (Production Set):

○ All patterns after N thru M (Test Set), all after M (Production Set):

○ Last M patterns (Production Set), N percent (Test Set), randomly chosen:

● By Row Marker

🟨 Training Set 🟦 Test Set 🟩 Production Set

Pattern file information

Label row: 1 1st Pattern row: 2 Last Pattern row: 146 Total Patterns: 145

Information Needed for the Selected Extraction Method

Training Set String	Test Set String	Production Set String	Column to Search
T	P	V	Label

Extract from the .pat file for the .trn, .tst, or .pro files based upon strings found in a column (variable).

In Design select the architecture (standard nets: first for daily and hourly data, third for six-mn data)

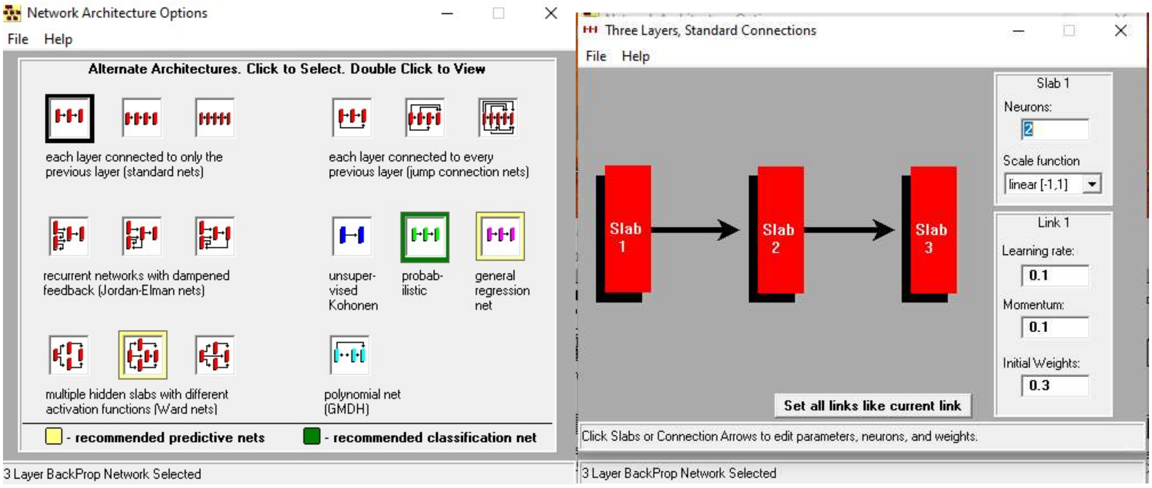

3 Layer BackProp Network Selected

Slab 1
Neurons: 2
Scale function: linear [-1,1]

Link 1
Learning rate: 0.1
Momentum: 0.1
Initial Weights: 0.3

Click Slabs or Connection Arrows to edit parameters, neurons, and weights.

3 Layer BackProp Network Selected

And Training and Stop Training Criteria: > 20000 epochs for daily and hourly data, and 2500 epochs for six-mn data

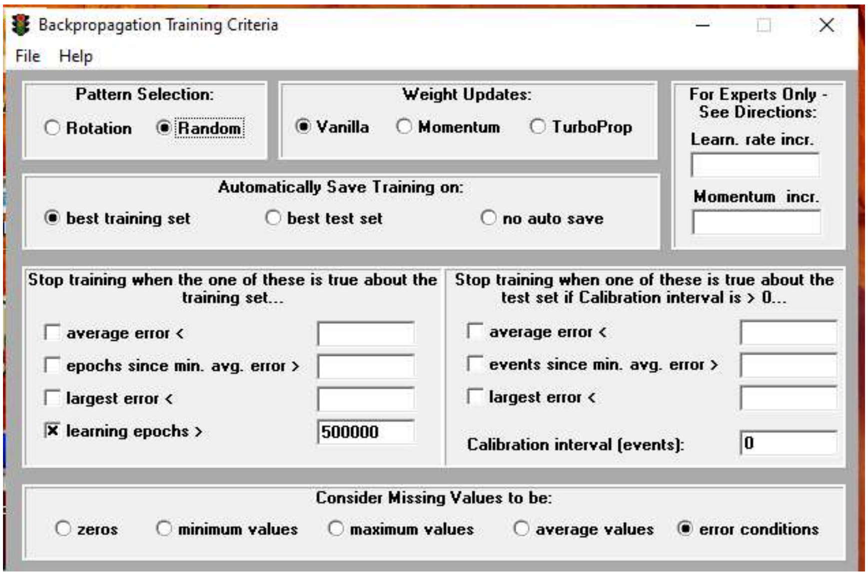

Pattern Selection: ○ Rotation ● Random

Weight Updates: ● Vanilla ○ Momentum ○ TurboProp

For Experts Only - See Directions:
Learn. rate incr.
Momentum incr.

Automatically Save Training on: ● best training set ○ best test set ○ no auto save

Stop training when the one of these is true about the training set...
☐ average error <
☐ epochs since min. avg. error >
☐ largest error <
☒ learning epochs > 500000

Stop training when one of these is true about the test set if Calibration interval is > 0...
☐ average error <
☐ events since min. avg. error >
☐ largest error <
Calibration interval (events): 0

Consider Missing Values to be: ○ zeros ○ minimum values ○ maximum values ○ average values ● error conditions

In Learning, select to automatically save training on best training set and run to start training the ANN model:

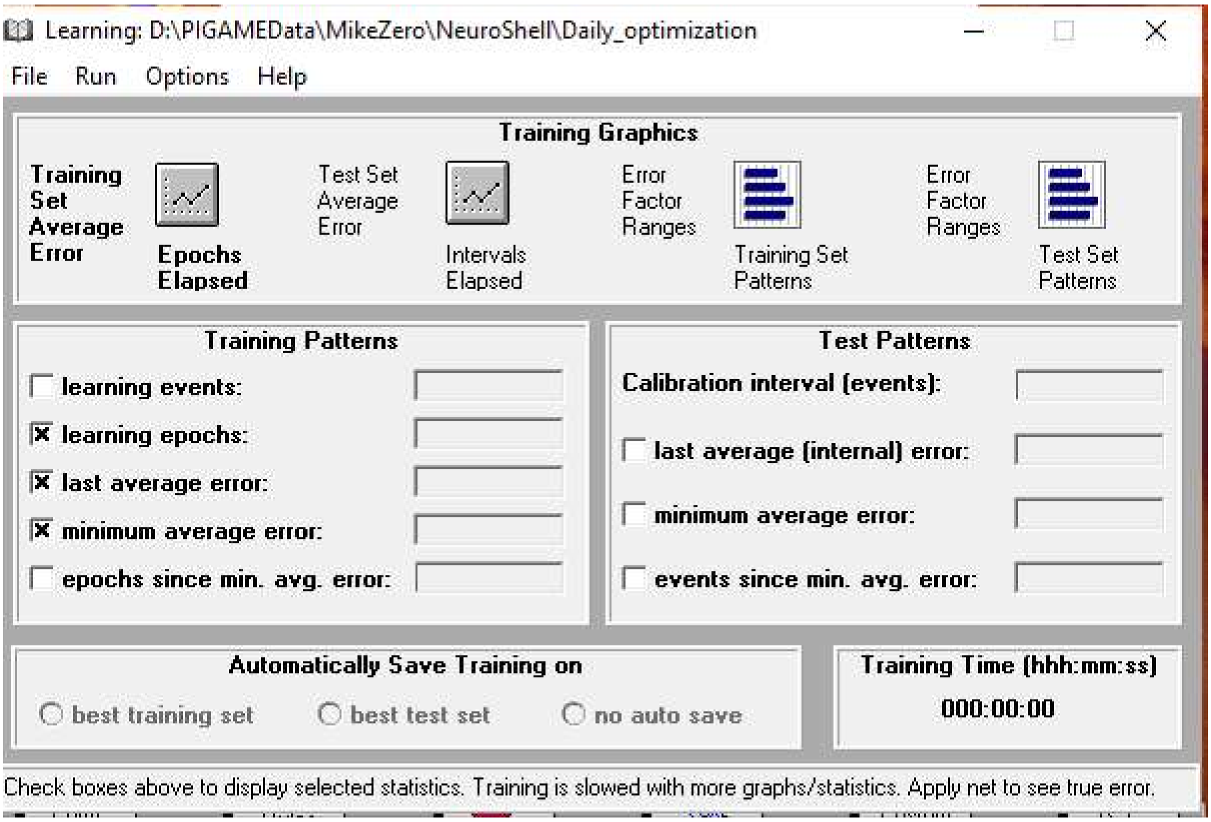

Training Patterns
☐ learning events:
☒ learning epochs:
☒ last average error:
☒ minimum average error:
☐ epochs since min. avg. error:

Test Patterns
Calibration interval (events):
☐ last average (internal) error:
☐ minimum average error:
☐ events since min. avg. error:

Automatically Save Training on
○ best training set ○ best test set ○ no auto save

Training Time (hhh:mm:ss)
000:00:00

Check boxes above to display selected statistics. Training is slowed with more graphs/statistics. Apply net to see true error.

In Apply Neural Network contribution factors, click on Apply to file:

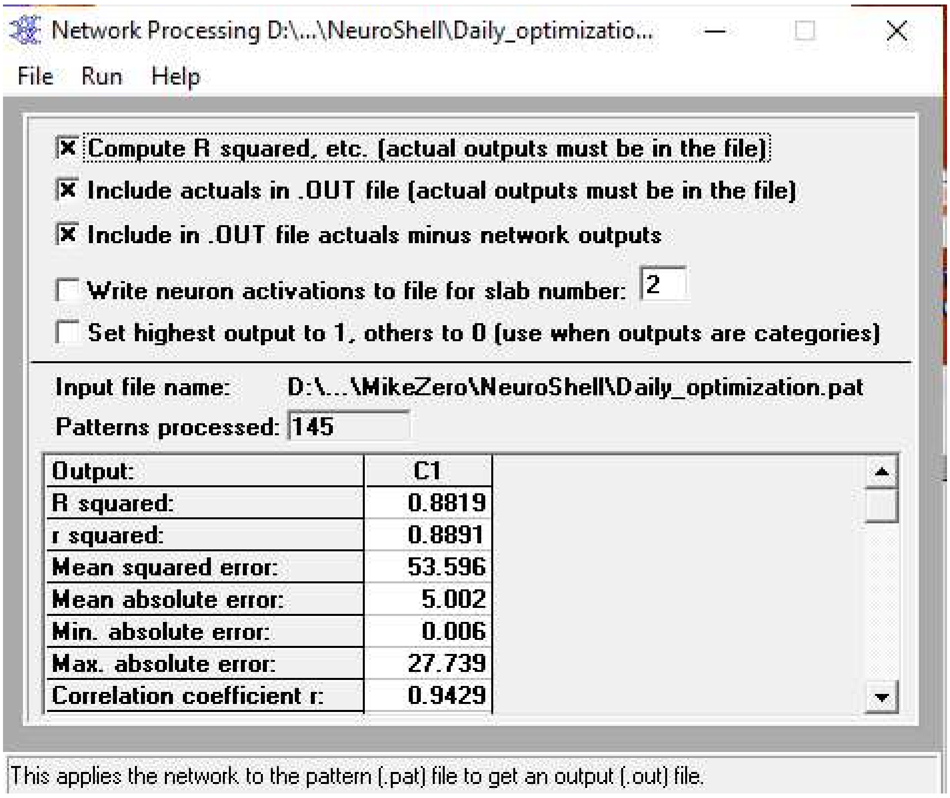

☒ Compute R squared, etc. (actual outputs must be in the file)
☒ Include actuals in .OUT file (actual outputs must be in the file)
☒ Include in .OUT file actuals minus network outputs
☐ Write neuron activations to file for slab number: 2
☐ Set highest output to 1, others to 0 (use when outputs are categories)

Input file name: D:\...\MikeZero\NeuroShell\Daily_optimization.pat
Patterns processed: 145

Output:	C1
R squared:	0.8819
r squared:	0.8891
Mean squared error:	53.596
Mean absolute error:	5.002
Min. absolute error:	0.006
Max. absolute error:	27.739
Correlation coefficient r:	0.9429

This applies the network to the pattern (.pat) file to get an output (.out) file.

Update the Design and repeat the process until satisfactory statistics are obtained (e.g. R squared close to 1)

Then, export output file for post processing: